

6717

NATIONAL LIBRARY
OTTAWA



BIBLIOTHÈQUE NATIONALE
OTTAWA

NAME OF AUTHOR....*Guang-Jyh Hwang*.....
TITLE OF THESIS...*Thermal Instability and*.....
 ...*Finite Amplitude Convection*.....
 ...*with Secondary Flow*.....
UNIVERSITY....*University of Alberta*.....
DEGREE FOR WHICH THESIS WAS PRESENTED.....~~Ph.D.~~...*Ph.D.*..
YEAR THIS DEGREE GRANTED.....*Fall 1970*.....

Permission is hereby granted to THE NATIONAL LIBRARY
OF CANADA to microfilm this thesis and to lend or sell copies
of the film.

The author reserves other publication rights, and
neither the thesis nor extensive extracts from it may be
printed or otherwise reproduced without the author's
written permission.

(Signed)...*Guang-Jyh Hwang*

PERMANENT ADDRESS:

...*9731-83 Ave*...
...*Edmonton, Alberta*...
...*Canada*.....

DATED...*Oct 5*.....19 *70*

THE UNIVERSITY OF ALBERTA

THERMAL INSTABILITY AND FINITE AMPLITUDE CONVECTION
WITH SECONDARY FLOW

by



GUANG-JYH HWANG

A THESIS

SUBMITTED TO THE FACULTY OF GRADUATE STUDIES
IN PARTIAL FULFILMENT OF THE REQUIREMENTS FOR THE DEGREE
OF DOCTOR OF PHILOSOPHY

DEPARTMENT OF MECHANICAL ENGINEERING

EDMONTON, ALBERTA

FALL, 1970

UNIVERSITY OF ALBERTA

FACULTY OF GRADUATE STUDIES

The undersigned certify that they have read, and recommend to the Faculty of Graduate Studies for acceptance, a thesis entitled "THERMAL INSTABILITY AND FINITE AMPLITUDE CONVECTION WITH SECONDARY FLOW" submitted by Guang-Jyh Hwang in partial fulfilment of the requirements for the degree of Doctor of Philosophy.

..... *K. C. Cheng*
Supervisor

..... *L. S. Hock*

..... *A. R. Riddle*

..... *H. Seyer*

..... *Donald Quon*

..... *E. M. Sparrow*
External Examiner

Sept. 21, 1970
Date

ABSTRACT

The boundary vorticity method is developed to overcome the extremely slow convergence of the existing numerical methods of solution for the biharmonic equation in polar coordinates. This method determines numerically the vorticity function at the boundary and has the advantage that two second order partial differential equations are solved instead of a single fourth order biharmonic equation. The distinctive features of the new method are simplicity, computational stability and a significant saving in computing time as compared with the conventional method.

As an application of the boundary vorticity method to a class of forced convective heat transfer problems where the secondary flow is set up immediately with the appearance of body forces normal to the main flow in a channel, a well-known problem of fully developed combined free and forced laminar convection in uniformly heated horizontal tubes is solved numerically.

In another class of forced convective heat transfer problems where the density (or temperature) gradient is parallel to the body force direction, thermal instability of free convection flows appears. As an example, the onset of buoyancy-generated longitudinal vortex rolls is studied both theoretically and experimentally for fully developed laminar forced convection between two infinite horizontal plates where

each wall is subjected to identical uniform axial temperature gradient but maintained at temperatures T_1 and T_2 ($T_1 > T_2$, $T_1 < T_2$ and $T_1 = T_2$) at lower and upper surfaces, respectively. The onset of longitudinal vortex rolls is verified for air by a direct flow visualization technique using cigarette smoke and is confirmed also by transverse temperature profile measurement. The experimental results for the critical Rayleigh number are compared with theory and the agreement is found to be good.

After studying the thermal instability in plane Poiseuille flow, finite amplitude thermal convection considering the non-linear effect in the post-critical regime is studied numerically by using the boundary vorticity method and its improved (or modified) iterative scheme based on the assumption that the wave number does not deviate from that predicted by the linear stability analysis.

A study of the Prandtl number effect for the forced convective heat transfer with secondary flow reveals that all the heat transfer results for $Pr \geq 0(1)$ approach the asymptotic result for $Pr \rightarrow \infty$ by using a suitable parameter.

The results of the present investigation indicate that the boundary vorticity method can be considered as a general procedure for the numerical solution of forced convective heat transfer problem with secondary flow.

ACKNOWLEDGEMENTS

The author wishes to extend his appreciation to

- Dr. K.C. Cheng for his supervision of this thesis and also throughout the four years' graduate studies,
- Dr. G.S.H. Lock for his instruction in a series of graduate courses on convection heat transfer,
- Dr. W. Nakayama for his assistance and discussion in the formulation of the thermal instability problem,
- Mr. M. Akiyama for his contributions to the work described in Chapter V by designing the testing apparatus and carrying out the preliminary experimental work including the development of the flow visualization technique,
- The staff members of the computing center at the University of Alberta for their operation of the IBM 360/67 digital computer in connection with the present numerical work,
- The National Research Council of Canada for postgraduate scholarship (1967-1970) and financial support for the construction of experimental facilities through Grant NRC A-1655,
- Miss Susan Schultz for her patience in typing this thesis,
- Messrs. T.M. Hrudehy, A. Semeniuk and S.W. Hong for their editorial checking on part of the thesis.
- His parents and wife for their constant encouragement.

TABLE OF CONTENTS

	<u>Page</u>
CHAPTER I <u>INTRODUCTION</u>	1
CHAPTER II <u>BOUNDARY VORTICITY METHOD</u>	9
2.1 Introduction	9
2.2 New Numerical Method for the Computa- tion of Boundary Vorticity	13
2.3 Concluding Remarks	24
References	30
Appendix 2.1 Gaussian Elimination Method	32
CHAPTER III <u>BOUNDARY VORTICITY METHOD FOR</u> <u>CONVECTIVE HEAT TRANSFER WITH</u> <u>SECONDARY FLOW IN HORIZONTAL TUBES..</u>	34
3.1 Introduction	34
3.2 Theoretical Analysis	37
3.3 Finite-Difference Approximations	45
3.3.1 Properties of Matrices and the Relaxation Factor	48
3.3.2 The Application of the Boundary Vorticity Method	50
3.3.3 Errors and Mesh Sizes	54
3.3.4 Iterative Procedure	58
3.4 Flow and Heat Transfer Results	60
3.5 Concluding Remarks	75
References	77
Appendix 3.1 Numerical Results	79
CHAPTER IV <u>THERMAL INSTABILITY IN PLANE</u> <u>POISEUILLE FLOW</u>	83
4.1 Introduction	83
4.2 Theoretical Analysis	87
4.3 A Power Series Solution	98
4.4 Results and Discussion	102
4.5 Concluding Remarks	115
References	118
Appendix 4.1 The Elements of Matrix $[C_{ij}]$...	120
Appendix 4.2 Numerical Results	123

	<u>Page</u>
CHAPTER V <u>AN EXPERIMENTAL INVESTIGATION OF</u> <u>THERMAL INSTABILITY IN PLANE</u> <u>POISEUILLE FLOW</u>	126
5.1 Introduction	126
5.2 Experimental Apparatus and Procedure	130
5.3 Experimental Results and Discussion	134
5.4 Concluding Remarks	154
References	156
CHAPTER VI <u>FINITE AMPLITUDE CONVECTION IN</u> <u>PLANE POISEUILLE FLOW</u>	157
6.1 Introduction	157
6.2 Theoretical Analysis	163
6.3 Finite-Difference Approximations	172
6.3.1 Properties of Matrices and the Relaxation Factor	173
6.3.2 The Application of the Boundary Vorticity Method and Its Improved Iterative Scheme	175
6.3.3 Errors and Mesh Sizes	175
6.3.4 A Comparison of the Method of Unsteady State Solution, Boundary Vorticity Method and Its Improved Iterative Scheme	178
6.4 Results and Discussion	181
6.5 Concluding Remarks	216
References	219
Appendix 6.1 Order of Magnitude Analysis for Governing Equations	221
Appendix 6.2 Numerical Results	225
CHAPTER VII - <u>GENERAL CONCLUDING REMARKS</u>	231
LIST OF FORTRAN IV PROGRAMMING	237
ADDENDUM.....	264

LIST OF TABLES

<u>Table</u>		<u>Page</u>
2.1	The relation between the number of boundary vorticity values to be determined and the repeated number of computations required	23
3.1	The boundary conditions for the governing equations	43
3.2	Values of w and θ at the center without secondary flow	46
4.1	Critical values of $Ri(\Delta T > 0)$ below which longitudinal vortex rolls have priority of appearance over the T-S waves ($Pr = 0.7$)	113
6.1	A comparison of the method of unsteady state solution, boundary vorticity method and its improved iterative scheme for the case of $\mu = 0$ and $Ra/Ra^* = 4.69$	179

LIST OF FIGURES

<u>Figure</u>		<u>Page</u>
1.1	Structure of the thesis	8
2.1	Coordinate system for a physical model with boundary conditions	14
3.1	Coordinate system and numerical grid	38
3.2	The linear relation between ξ_b and ψ_b	53
3.3	Convergence of numerical solution for heat transfer results	56
3.4	Comparison of velocity and temperature distributions along central vertical line from the present study with experi- mental and theoretical results from Mori et al.	62
3.5	Comparison of velocity and temperature distributions along central vertical line from the present study with experimental data from Mori et al.	64
3.6	Comparison of velocity and temperature distributions along central vertical line from the present study with experimental data from Mori et al.	65
3.7	Streamlines and isothermals	67
3.8	Distributions of secondary flow velocity components u , v	68
3.9	$fRe/(fRe)_0$ versus $ReRa$	70
3.10	$Nu/(Nu)_0$ versus $ReRa$	72
3.11	New correlation based on $Nu/(Nu)_0$ versus $PrReRa$	73
4.1	System of coordinates	88
4.2	Thermal boundary conditions on the bottom and top plates	89

<u>Figure</u>		<u>Page</u>
4.3	Fully developed velocity and temperature distributions in the unperturbed state	89
4.4	Neutral stability curves for longitudinal vortex rolls	103
4.5	Neutral stability curve for the case $ \mu \rightarrow \infty$	104
4.6	Critical wave number versus $ \mu $	106
4.7	Second critical eigenvalues of Ra	107
4.8	Secondary flow streamlines and isothermals of perturbation temperature	109
4.9	Perturbations of axial velocity component	111
4.10	Comparison of thermal instability with hydrodynamic instability	112
5.1	Configuration and coordinate system	128
5.2	Schematic diagram of experimental apparatus (unit inch)	131
5.3	Comparison of experimental data with theoretical velocity distribution at $y' = 0$ with $h = 1$ inch and $Re = 160$	135
5.4	Comparison of experimental data with theoretical velocity distribution along transverse direction y' at $z'/h = 0.5$ with $h = 1$ inch and $Re = 160$	136
5.5	Comparison of experimental data with theoretical temperature distribution at $y' = 0$ with $Re = 140$, $h = 1$ inch, $\tau = 1.85^\circ\text{F/in.}$ and $T_w = 85.6^\circ\text{F}$ at $x' = 62$ inches	138
5.6	Secondary flow patterns for the case $\mu = 0$ and $h = 1$ inch	141
5.7	Comparison of experimental data with theoretical stability curves for longitudinal vortex rolls.....	143

<u>Figure</u>		<u>Page</u>
5.8	Formation of secondary flow patterns with free convection effect for the case of negative μ and $h = 1$ inch	145
5.9	Comparison of experimental data with critical $ReRa_{\tau}$ for the case $ \mu \rightarrow \infty$	148
5.10	Formation of secondary flow patterns with free convection effect for the case $ \mu \rightarrow \infty$ and $h = 1$ inch	149
5.11	Transverse temperature measurement data for $ \mu \rightarrow \infty$	150
5.12	Comparison of critical wave number versus $ \mu $ from theory with experimental data from post-critical regime	152
6.1	Coordinate system and numerical grid	164
6.2	Effect of grid size on the convergence of the flow and heat transfer results for the case of $Pr = 0.7$, $\mu = 0$ and $Ra = 8010.52$	176
6.3	Comparison of velocity profiles from this investigation with the approximate analytical results of Mori and Uchida and their experimental data for the case of $Pr = 0.7$, $\mu = 0$ and $Ra = 8010.52$	183
6.4	Comparison of temperature profiles from this investigation with the approximate analytical results of Mori and Uchida and their experimental data for the case of $Pr = 0.7$, $\mu = 0$ and $Ra = 8010.52$	184
6.5	Lines of constant axial velocity for the case of $Pr = 0.7$ and $\mu = 0$	187
6.6	Isotherms for the case of $Pr = 0.7$ and $\mu = 0$	189
6.7	Lines of constant vorticity for the case of $Pr = 0.7$ and $\mu = 0$	191
6.8	Secondary flow streamlines for the case of $Pr = 0.7$ and $\mu = 0$	193

<u>Figure</u>		<u>Page</u>
6.9	Secondary flow streamlines for the case Pr = 0.7 and $\mu = -30$	195
6.10	Secondary flow streamlines for the case of Pr = 0.7 and $ \mu \rightarrow \infty$	197
6.11	Axial velocity distributions for the case of Pr = 0.7 and $\mu = -30$	200
6.12	Temperature distributions for the case of Pr = 0.7 and $\mu = -30$	201
6.13	$(fRe)_3/(fRe)_0$ versus Ra for the case of $\mu = 0$ and $\mu = \text{finite}$ with Pr = 0.7	206
6.14	$(fRe)_3/(fRe)_0$ versus $PrReRa_\tau$ for the case of $ \mu \rightarrow \infty$	207
6.15	$(Nu)_1$ versus Ra for the case of $\mu = 0$	210
6.16	$(Nu)_i/(Pr\mu)$ ($i=1,2,3$) versus Ra with $\mu (= \text{finite})$ as a parameter for Pr = 0.7 ..	213
6.17	$(Nu)_i/(Nu)_0$ ($i=1,2,3$) versus $PrReRa_\tau$ for the case of $ \mu \rightarrow \infty$	215

NOMENCLATURE

A_n	=coefficient of a power series
a	=radius of a tube or wave number, $2\pi h/\lambda$
a_{ij}	=element of a matrix
C	$=-C_1 a^3/4\nu\mu$, defined in equation (3.8)
C_1	=axial pressure gradient, $\partial P/\partial Z$
C_2	=axial temperature gradient, $\partial T/\partial Z$
c	=complex wave speed
C_{ij}	=element of a matrix
D	=differentiation with respect to z , d/dz
f	=friction factor, defined in equations (3.27), (6.25), (6.26) and (5.27) or a function
f'	=a function
G	=a function defined by equation (4.9)
Gr	=Grashof number, defined in equations (4.5) and (6.9)
g	=gravitational acceleration
h	=grid size or distance between two parallel plates
\bar{h}	=average heat transfer coefficient
i	=imaginary unit
\underline{I}	=unit matrix
k	=thermal conductivity
k_i	=element of a vector
L	=linear operator
M, m	=integers
$\max(x_i)$	=maximum value of x_i , $i=1,2,\dots$

N	=integer
Nu	=Nusselt number defined in equation (3.27), (6.28) to (6.30) and (6.32) to (6.34)
$O(x)$	=order of x
P	=pressure
Pr	=Prandtl number, ν/κ
p	=dimensionless pressure disturbance
p'	=pressure disturbance
R	=radial coordinate
Ra	=Rayleigh number, $PrGr$ defined in equations (3.8) and (6.9)
Re	=Reynolds number defined in equations (3.8), (4.5) and (6.2)
Ri	=Richardson number, $-Ra/64 PrRe^2$
r	=dimensionless radial coordinate, R/a
T	=temperature
t'	=time
t	=dimensionless time, $t'\nu/h^2$
U, V, W	=velocity components in R , ϕ and Z directions or x' , y' and z' directions
u, v, w	=dimensionless velocity components in R , ϕ and Z directions or dimensionless velocity disturbance in x' , y' and z' directions
u', v', w'	=velocity disturbances in x', y' and z' directions
X, Y	=Cartesian coordinates
x, y, z	=dimensionless Cartesian coordinates
x', y', z'	=Cartesian coordinates
\underline{x}	=unknown vector
Z	=axial coordinate

∇^2	=dimensionless Laplacian operator, $\partial^2/\partial r^2 + \partial/(r\partial r) + \partial^2/r^2\partial\phi^2$ or $\partial^2/\partial y^2 + \partial^2/\partial z^2$
∇^4	$=\nabla^2\nabla^2$
∇_1^2	=Laplacian operator, $\partial^2/\partial R^2 + \partial/(R\partial R) + \partial^2/R^2\partial\phi^2$ or $\partial^2/\partial y'^2 + \partial^2/\partial z'^2$
$\nabla_{x,y,z}^2$	=dimensionless Laplacian operator in x, y and z directions, $\partial^2/\partial x^2 + \partial^2/\partial y^2 + \partial^2/\partial z^2$
	=absolute value or determinant
[]	=matrix
\sum	=summation
β	=coefficient of thermal expansion
Δ	=difference
ΔT	=temperature difference between two plates, $T_1 - T_2$
ϵ	=small quantity
θ	=dimensionless temperature difference, $(T - T_w)/CC_2 aPr$, defined in equation (3.8) or dimensionless temperature disturbance
θ'	=temperature disturbance
κ	=thermal diffusivity
λ	=wavelength of vortex rolls
μ	=viscosity or parameter, $Re\eta h/\Delta T$, defined in equations (4.3) and (6.9)
ν	=kinematic viscosity
ξ	=dimensionless vorticity function
ξ'	=vorticity function
ρ	=density
σ	=constant
τ	=shear stress or temperature gradient along x'direction, $\partial T/\partial x'$

ϕ	=polar angle
ϕ_u	=basic velocity profile function, $8(z-z^2)$
ϕ_θ	=basic temperature profile function, $2/3 \cdot (z-2z^3+z^4)$
ψ	=dimensionless stream function
ψ'	=stream function
ω	=relaxation factor

Superscripts

-1	=inversion of matrix
(n)	=nth number of iteration
$'$	=perturbation quantity, dimensional quantity or other specified quantity
$-$	=mean value
$*$	=critical value or function of z only
o	=value at previous iteration step

Subscripts

b	=boundary point or basic quantity in the unperturbed state
c	=characteristic quantity
i,j	=space subscripts of grid point
j,k	=space subscripts of grid point
M	=mixed mean temperature
0	=condition for pure forced convection or maximum quantity

w =value at wall

x,y =in corresponding directions

τ =quantity based on axial temperature gradient

— =vector or matrix

1. =value obtained from average gradient at lower plate

2 =value obtained from average gradient at upper plate

3 =value obtained from overall balance

I =value obtained from average gradient along pipe wall

II =value obtained from overall balance

CHAPTER I

GENERAL INTRODUCTION

When body forces (buoyancy, Coriolis and centrifugal forces) act in a direction normal to the main flow for fully developed laminar forced convection in channels of various shapes, a secondary motion will be set up after the dimensionless characteristic parameter determined by the given body force and the flow field reaches a critical value. This secondary motion is known to modify the axial velocity profile and temperature field with subsequent increase in the friction factor and the Nusselt number. For the familiar cases of uniformly heated horizontal tubes, tubes rotating about an axis perpendicular or parallel to the axis of the tube and curved pipes, the secondary motion will be set up with the appearance of the body forces and the critical value of the characteristic parameter governing the onset of secondary flow can be considered as 0. On the other hand, under certain circumstances the body forces acting on the fluid element may not be large enough to overcome the stabilizing effects of viscous and thermal diffusion leading to a thermal instability problem.

The secondary flow pattern will depend on a particular combination of the kind of body forces and the geometrical shape of the flow passage but is known to be qualitatively

similar for different body forces with the same geometrical shape of the channel. Although various noncircular channels may be encountered in practical design configurations, consideration is given here to only two important geometrical shapes, namely, circular tube and rectangular channel.

In order to put the scope of the present work into proper perspective, the possible combinations of the body force (buoyancy, Coriolis or centrifugal force) with circular tube or rectangular channel for the convective heat transfer problems will be considered next:

(a) For a combination of circular tube with buoyancy force, we can mention the familiar problems of uniformly heated horizontal tube and uniformly heated tube rotating about an axis parallel to the axis of the tube. The former deals with body force due to temperature variation in the gravitational force field and the latter deals with the body force due to acceleration in the rotating field.

(b) A combination of buoyancy force in the gravitational field or accelerating rotating field with the rectangular channel leads to several interesting cases. For the horizontal rectangular channel, secondary flow can arise when the walls are uniformly heated or either the side wall or the bottom wall is maintained at higher temperature. For the limiting case of a flat rectangular duct or a parallel-plate channel, a secondary flow in the form of an infinite pairs of vortex rolls may appear at a certain critical

value of the characteristic parameter depending on the hydrodynamic and thermal conditions. The thermal instability problem for the fully developed laminar forced convection between two infinite horizontal plates will be studied extensively in this thesis. For a fully developed laminar flow in uniformly heated horizontal rectangular channel with a large aspect ratio (width/height), a boundary-value problem for the free convection exists near the side walls and thermal instability problem may exist in the central region.

(c) A combination of centrifugal force and circular tube can be found in forced convective heat transfer in curved pipes. Curved pipes and spiral pipes are used extensively in various heat exchanger equipments.

(d) A similar combination of centrifugal force and rectangular channel can be found in the form of curved rectangular channels in various heating and cooling equipments. In particular, a curved rectangular channel with large aspect ratio (height/width) may lead to a limiting case of tangential flow between two concentric cylinders giving rise again to a stability problem.

(e) A combination of Coriolis force and circular tube can be found in the form of a heated straight tube rotating about an axis perpendicular to the axis of the tube for the cooling of gas turbine blades.

(f) A combination of Coriolis force and rectangular channel with various aspect ratios can arise in the form of

uniformly heated rectangular channel rotating about an axis perpendicular to the axis of the channel. It is interesting to note that the limiting case of a parallel-plate channel with infinite plates parallel to the rotating axis also leads to a stability problem.

It is noted that more than one kind of body forces may coexist in a given forced convection problem. For example, for the uniformly heated helical tubes with small radius of curvature, buoyancy and Coriolis forces may have to be considered in addition to the centrifugal forces under certain circumstances. Furthermore, the inclined tube effect may be of importance. After considering possible combinations of the body force and the geometrical shape, the methods of theoretical analysis available in the literature for forced convective heat transfer with secondary flow will be reviewed briefly.

For the low characteristic parameter region near the critical value (zero or finite), the intensity of the secondary flow is rather weak and a perturbation method is known to be applicable. However, it is also known that Morton's perturbation method diverges quickly with the increase of the characteristic parameter and fails to yield solution for the practically important range of characteristic parameter. Morton's perturbation approach is also limited to the secondary flow problem involving circular tube and cannot be readily applied to the noncircular channel such as square channel problem. On the other hand, for the post-critical

regime near the critical characteristic parameter, a perturbation theory based on Stuart's energy-balance method is known to be applicable to the fully developed laminar forced convection with secondary flow between two infinite parallel plates which is a limiting case of a rectangular channel with large aspect ratio. However, an appreciable error is found for flow and heat transfer results at a characteristic parameter say ten times the critical value. At this point, it may be of interest to note that in the case of buoyancy forces, the momentum and energy equations are coupled. For the case of centrifugal forces, the momentum and energy equations are uncoupled within the assumption of constant physical properties. However, the methods of analysis for various convective heat transfer problems with secondary flow are similar.

For the high characteristic parameter regime, the intensity of the secondary flow is strong and the flow field may be divided into a core region and a boundary layer near the wall. In the core region the viscosity and heat conduction can be neglected and the body force is approximately balanced by a pressure gradient across the cross-section. Consequently, the secondary flow in the direction of body force can be considered as approximately uniform in the core region. On the other hand, inside the boundary layer near the wall, the body force is small and the secondary flow is driven by a pressure gradient. Although the boundary-layer technique proves to be very useful for the prediction of flow and heat transfer

results in high parameter regime, the assumption of uniform boundary layer thickness along the entire wall does lead to some error and the method must be considered as an approximate one. For the convective heat transfer in the circular tube with strong secondary flow, the analysis involves the solutions of the governing equations for continuity, momentum and energy for the flows in both the core region and the boundary layer such that the two solutions match at the edge of the boundary layer. The above method using basic equations cannot be readily applied to the noncircular channel and the extension of the Stuart's energy-balance method considering the balances of kinetic energy and entropy production for the boundary layers is found to be more convenient.

The above brief review on the analytical methods of solution for forced convective heat transfer with secondary flow reveals clearly that no analytical method is available for the approximate solution in the intermediate range of the characteristic parameter. One of the purposes of this investigation is to bridge the gap between the perturbation method for the relatively low parameter range and the boundary-layer technique for the high parameter region by the numerical solution using the newly developed algorithm called boundary vorticity method. The new numerical method of analysis is believed to have wide applicability to various forced convective heat transfer problems with secondary flow. In order to demonstrate the applicability of the newly deve-

veloped numerical technique, combined free and forced laminar convection for fully developed flow in uniformly heated horizontal tubes is studied numerically in this thesis. After studying the thermal instability problem in plane Poiseuille flow, the boundary vorticity method is again employed to solve the finite amplitude thermal convection problem in the post-critical regime for the plane Poiseuille flow. The onset of thermal instability in plane Poiseuille flow is also verified experimentally by using air as a working fluid.

The following schematic diagram serves to demonstrate the general structure of the thesis, the topics treated and the interrelationships among them.

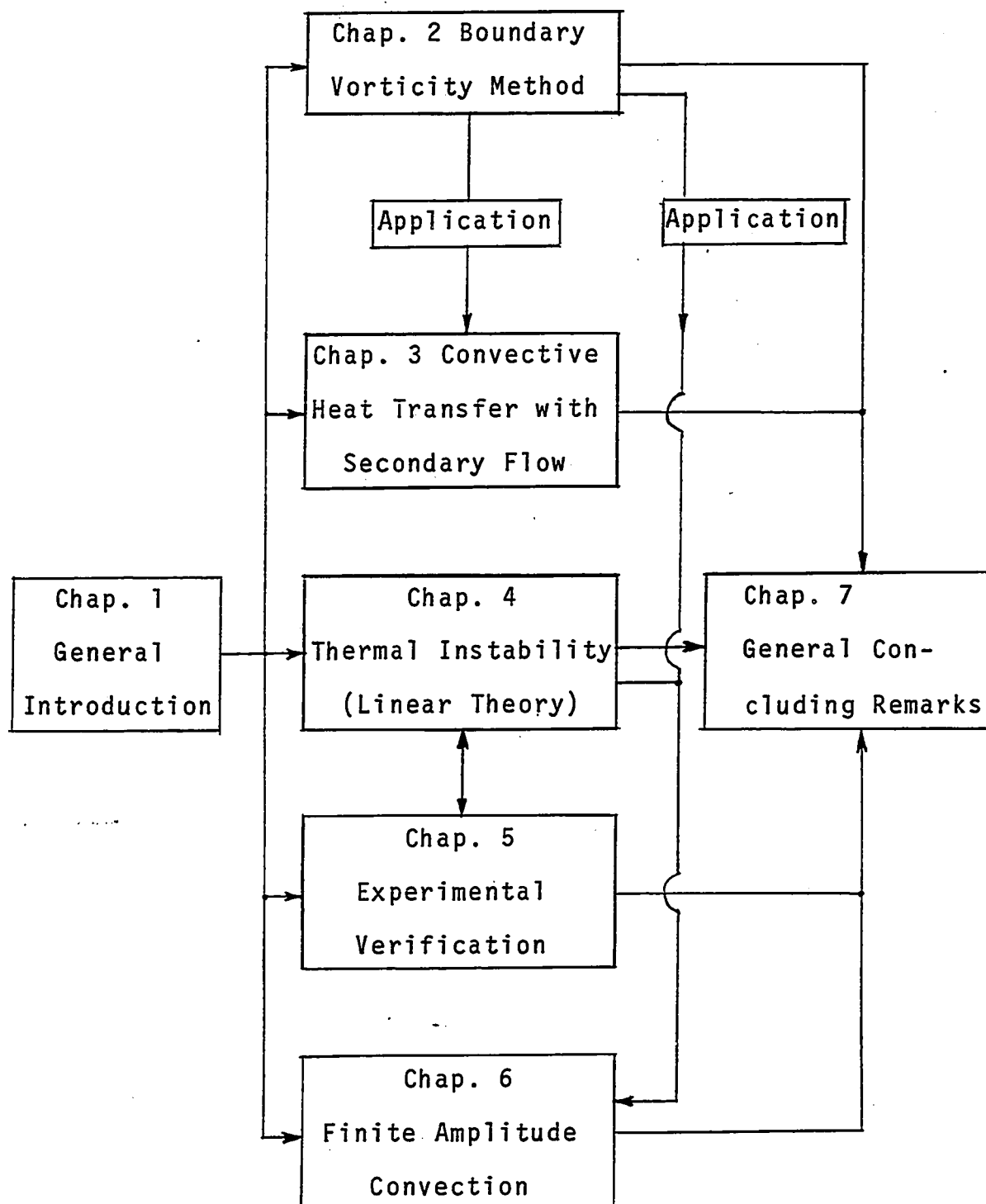


Fig. 1.1 Structure of the thesis

CHAPTER II

BOUNDARY VORTICITY METHOD

2.1 Introduction

In steady state two-dimensional fluid mechanics problems, we often encounter the solution of a quasi-linear partial differential equation involving a biharmonic operator, namely, the following vorticity transport equation:

$$\frac{\partial \psi'}{\partial y'} \frac{\partial \nabla_1^2 \psi'}{\partial x'} - \frac{\partial \psi'}{\partial x'} \frac{\partial \nabla_1^2 \psi'}{\partial y'} = \nu \nabla_1^2 \nabla_1^2 \psi' - f' \quad (2.1)$$

or alternatively,

$$\frac{\partial \psi'}{\partial y'} \frac{\partial \xi'}{\partial x'} - \frac{\partial \psi'}{\partial x'} \frac{\partial \xi'}{\partial y'} = \nu \nabla_1^2 \xi' - f' \quad (2.2)$$

$$\xi' = \nabla_1^2 \psi' \quad (2.3)$$

where $\nabla_1^2 = \frac{\partial^2}{\partial x'^2} + \frac{\partial^2}{\partial y'^2}$ and f' is a known function.

Analytical solution of the above fourth order quasi-linear elliptic partial differential equation (2.1) is in general very difficult and the finite-difference method is used most

commonly in recent years for the solution of various engineering problems.

The numerical solution of the biharmonic equation without the nonlinear terms in equation (2.1) has been studied for many years. In 1954, Cornock [2.1] showed a rather tedious conventional finite difference approximation to the biharmonic equation formulated in Cartesian coordinate system. He also suggested that it is probably advantageous to use two second order equations instead of a fourth order one. In 1958, Conte and Dames [2.2] successfully solved the biharmonic equation by an Alternating Direction Method. With the symmetry property of the iterative matrix, they derived an iteration parameter which leads to a quite fast convergence rate. However, for a problem formulated in polar coordinate system, with or without nonlinear terms, the iteration parameter cannot be found. In 1960, Keller [2.3] proved that the "best" biharmonic numerical scheme converges much slower than the "best" Laplace scheme. Recently, Newell and Bergles [2.4] solved combined free and forced convection problem in horizontal circular tubes similar to the one which will be discussed in Chapter III by using point successive over-relaxation or underrelaxation method. Their results show that it requires considerable computing time which is considered to be impractical (11 hours on IBM 7040 to obtain a solution for an intermediate parameter).

Summarizing the above brief literature survey, we can

conclude that the existing finite-difference iterative method is too inefficient and impractical for solving the fourth order partial differential equation involving biharmonic operator particularly for the problem formulated in polar coordinate system. The slow convergence rate and the rather involved algebraic expression for the biharmonic operator as compared with a harmonic operator may discourage us from further attempt in the numerical solution. Before the reference [2.4] appeared, an attempt had been made to solve the combined free and forced convection problem in horizontal circular tubes using the technique employed in my earlier work [2.5]. The numerical methods used in references [2.4, 2.5] are similar. However, the technique used in [2.5] was found to be too inefficient for the problem formulated in polar coordinates. Consequently, the boundary vorticity method was developed where the undefined vorticity function on solid boundaries can be determined numerically. Because of this development, the fourth order partial differential equation (2.1) can now be reduced to a Poisson's equation (2.3) and a quasi-linear second order partial differential equation for vorticity function (2.2). As pointed out in references [2.1] and [2.3], it is not difficult to see the advantages of the present method. The number of iterations required for a convergent solution will be much less than the point successive overrelaxation or underrelaxation method employed by Newell and Bergles [2.4]. Besides the fluid mechanics problems, we

can cite many problems in solid mechanics where this simple and yet efficient numerical method can be applied. It will be seen that the method can be applied to the problems which will be discussed in Chapters III and VI with considerable success.

2.2 New Numerical Method for the Computation of Boundary Vorticity

In order to demonstrate the method clearly without any loss of generality, the nonlinear terms in the equations (2.1) and (2.2) will be omitted for the present discussion. For the numerical solution of the problem which will be considered in Chapters III and VI, the nonlinear terms in equations (2.1) and (2.2) are linearized by taking the values of $\frac{\partial \psi'}{\partial y'}$ and $\frac{\partial \psi'}{\partial x'}$ obtained from the previous iteration step. Neglecting the nonlinear terms, equations (2.1), (2.2) and (2.3) can be put in the following dimensionless forms, respectively:

$$\frac{\partial^4 \psi}{\partial x^4} + 2 \frac{\partial^4 \psi}{\partial x^2 \partial y^2} + \frac{\partial^4 \psi}{\partial y^4} = f \quad (2.4)$$

or alternatively,

$$\frac{\partial^2 \xi}{\partial x^2} + \frac{\partial^2 \xi}{\partial y^2} = f \quad (2.5)$$

$$\frac{\partial^2 \psi}{\partial x^2} + \frac{\partial^2 \psi}{\partial y^2} = \xi \quad (2.6)$$

For simplicity, we consider the solution of equations (2.5) and (2.6) for a region of unit square (see Fig. 2.1) with boundary conditions identical to the ones which will be used

in Chapter VI. The number of meshes considered is $3 \times 3 = 9$. Usually, for the problems studied in this thesis, it will require about 500 to 1600 meshes to obtain a numerical solution with a truncation error of the order of 10^{-3} . The coordinate system, boundary conditions and nodal points are shown in Fig. 2.1.

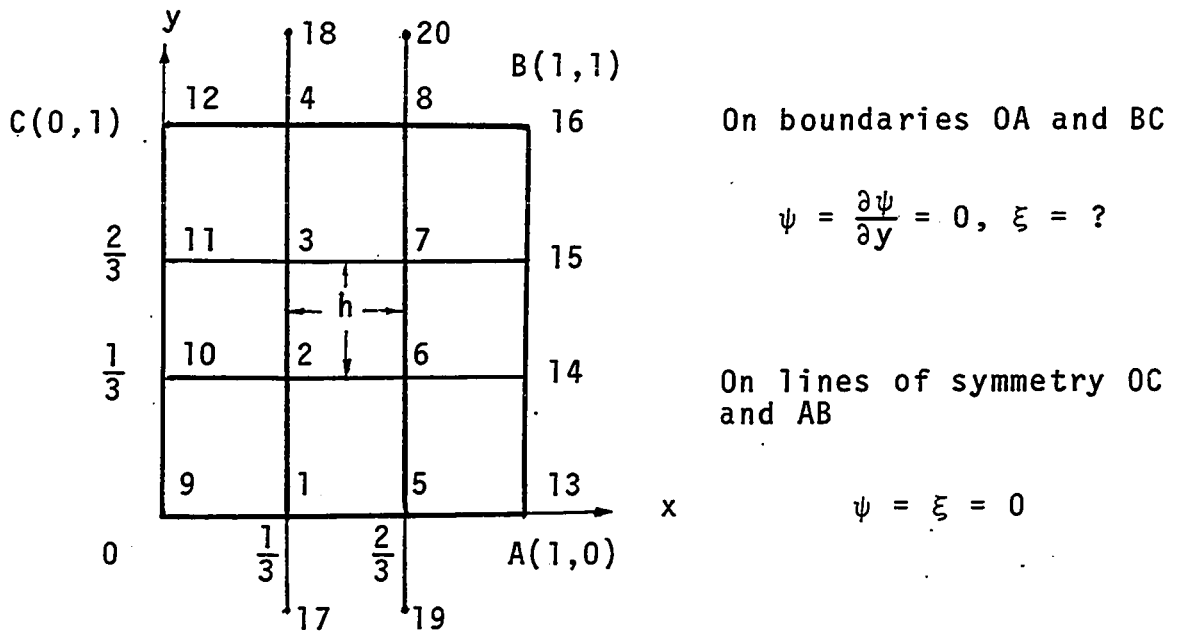


Fig. 2.1 Coordinate system for a physical model with boundary conditions

Physically, the lines OA and BC represent parts of two infinite horizontal plates and lines OC and AB represent lines of symmetry. For the problem which will be studied in Chapter VI, there is an infinite number of vortex rolls appearing between the two infinite horizontal plates. By the symmetry,

only the region OABC needs consideration for the study of a vortex roll.

The significance of the boundary vorticity method is to determine the boundary vorticity numerically on the boundary lines OA and BC and propose to use equations (2.5) and (2.6) instead of equation (2.4) for obtaining a greater convergence rate and simpler algebraic expressions. Two methods are available for the determination of the boundary vorticity and these will be discussed next.

Method (a): Referring to Fig. 2.1, the equations and the boundary conditions are

	On boundaries OA and BC	On lines of symmetry AB and OC
$\frac{\partial^2 \psi}{\partial x^2} + \frac{\partial^2 \psi}{\partial y^2} = \xi$	$\frac{\partial \psi}{\partial y} = 0$	$\psi = 0$
$\frac{\partial^2 \xi}{\partial x^2} + \frac{\partial^2 \xi}{\partial y^2} = f$	$\xi = ?$	$\xi = 0$

(2.7)

It is seen that we must determine the vorticity ξ on the boundaries OA and BC such that the stream function $\psi = 0$ on the same lines.

Using a five-point finite-difference approximation and considering the boundary conditions in (2.7), the system of linear algebraic equations to be solved after discretizing the equation in (2.7) is shown below as

$$\begin{bmatrix} -4 & 2 & 0 & 0 & 1 & 0 & 0 & 0 \\ 1 & -4 & 1 & 0 & 0 & 1 & 0 & 0 \\ 0 & 1 & -4 & 1 & 0 & 0 & 1 & 0 \\ 0 & 0 & 2 & -4 & 0 & 0 & 0 & 1 \\ 1 & 0 & 0 & 0 & -4 & 2 & 0 & 0 \\ 0 & 1 & 0 & 0 & 1 & -4 & 1 & 0 \\ 0 & 0 & 1 & 0 & 0 & 1 & -4 & 1 \\ 0 & 0 & 0 & 1 & 0 & 0 & 2 & -4 \end{bmatrix} \begin{bmatrix} \psi_1 \\ \psi_2 \\ \psi_3 \\ \psi_4 \\ \psi_5 \\ \psi_6 \\ \psi_7 \\ \psi_8 \end{bmatrix} = h^2 \begin{bmatrix} \xi_1 \\ \xi_2 \\ \xi_3 \\ \xi_4 \\ \xi_5 \\ \xi_6 \\ \xi_7 \\ \xi_8 \end{bmatrix} \quad (2.8)$$

$$\begin{bmatrix} -4 & 1 & 1 & 0 \\ 1 & -4 & 0 & 1 \\ 1 & 0 & -4 & 1 \\ 0 & 1 & 1 & -4 \end{bmatrix} \begin{bmatrix} \xi_2 \\ \xi_3 \\ \xi_6 \\ \xi_7 \end{bmatrix} = h^2 \begin{bmatrix} f_2 \\ f_3 \\ f_6 \\ f_7 \end{bmatrix} - \begin{bmatrix} \xi_1 \\ \xi_4 \\ \xi_5 \\ \xi_8 \end{bmatrix} \quad (2.9)$$

It is noted that the elements ξ_1 , ξ_4 , ξ_5 and ξ_8 shown on the right-hand side of equation (2.8) and the last column vector of equation (2.9) are the unknown boundary vorticities to be determined. We further note that a total of 12 algebraic equations for 16 unknowns are obtained. Theoretically, we can eliminate 8 unknowns at the interior points 2, 3, 6 and 7 with the following four equations remaining for the 8 unknowns at the boundary points 1, 4, 5 and 8,

$$\begin{bmatrix} \psi_1 \\ \psi_4 \\ \psi_5 \\ \psi_8 \end{bmatrix} = \begin{bmatrix} a_{11} & a_{12} & a_{13} & a_{14} \\ a_{21} & a_{22} & a_{23} & a_{24} \\ a_{31} & a_{32} & a_{33} & a_{34} \\ a_{41} & a_{42} & a_{43} & a_{44} \end{bmatrix} \begin{bmatrix} \xi_1 \\ \xi_4 \\ \xi_5 \\ \xi_8 \end{bmatrix} + \begin{bmatrix} k_1 \\ k_4 \\ k_5 \\ k_8 \end{bmatrix} \quad (2.10)$$

or in a vector form,

$$\underline{\psi}_b = \underline{A} \underline{\xi}_b + \underline{k} \quad (2.11)$$

where subscript b refers to the boundary points. Using the remaining boundary condition $\psi = 0$ on boundaries OA and BC, the boundary vorticity can be obtained as

$$\underline{\xi}_b = - \underline{A}^{-1} \underline{k} . \quad (2.12)$$

The above elimination method is impractical for a system with say 10 unknowns since the matrix \underline{A} cannot be found readily.

The following numerical technique may be suggested to evaluate the matrix \underline{A} and the vector \underline{k} . We note that there are a total of 20 unknowns for the elements of the matrix \underline{A} and the vector \underline{k} . By assuming 5 different vectors for $\underline{\xi}_b$ and solving the equations (2.8) and (2.9), 5 different vectors $\underline{\psi}_b$ can be obtained and 20 equations exist for the 20 unknown elements of the matrix \underline{A} and the vector \underline{k} . This procedure is also impractical for a large system with say 100 unknowns.

It will be shown that the most significant point of the boundary vorticity method is the fact that we do not need to solve for all the boundary vorticities simultaneously. It is possible to apply a line iterative scheme to obtain a convergent solution. We note that a very efficient numerical technique called Gaussian elimination method (see Appendix 2.1) can be applied to solve a system of algebraic equations with a tridiagonal matrix. Then, the system of algebraic equations on each vertical line (see Fig. 2.1) with a tridiagonal matrix can be solved simultaneously. Employing the line iterative method, we are able to solve the boundary vorticity exactly (on each line separately) together with the other unknowns on each line and iterate until the solution converges.

For example, consider the first line at $x = \frac{1}{3}$; the algebraic equations for this line can be written as follows:

$$\begin{bmatrix} -4 & 1 \\ 1 & -4 \end{bmatrix} \begin{bmatrix} \xi_2 \\ \xi_3 \end{bmatrix} = \begin{bmatrix} h^2 f_2 - \xi_1 - \xi_6 \\ h^2 f_3 - \xi_4 - \xi_7 \end{bmatrix} \quad (2.13)$$

$$\begin{bmatrix} -4 & 2 & 0 & 0 \\ 1 & -4 & 1 & 0 \\ 0 & 1 & -4 & 1 \\ 0 & 0 & 2 & -4 \end{bmatrix} \begin{bmatrix} \psi_1 \\ \psi_2 \\ \psi_3 \\ \psi_4 \end{bmatrix} = \begin{bmatrix} h^2 \xi_1 - \psi_5 \\ h^2 \xi_2 - \psi_6 \\ h^2 \xi_3 - \psi_7 \\ h^2 \xi_4 - \psi_8 \end{bmatrix} \quad (2.14)$$

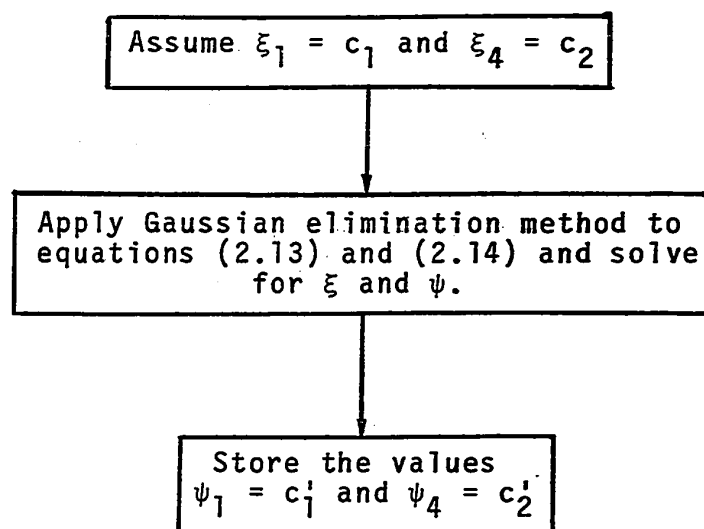
It is noted that the values on the line $x = \frac{2}{3}$ from the latest iteration step are to be used in the above equations (2.13) and (2.14). After eliminating the unknowns at points 2 and 3, we obtain the following linear relation between ψ_1 , ψ_4 and ξ_1 , ξ_4 .

$$\begin{bmatrix} \psi_1 \\ \psi_4 \end{bmatrix} = \begin{bmatrix} a_{11} & a_{12} \\ a_{21} & a_{22} \end{bmatrix} \begin{bmatrix} \xi_1 \\ \xi_4 \end{bmatrix} + \begin{bmatrix} k_1 \\ k_2 \end{bmatrix} \quad (2.15)$$

The discovery of the linear relation (2.15) is the key to the success of the boundary vorticity method. We can easily obtain the boundary vorticities (ξ_1 and ξ_4) by using the boundary conditions $\psi_1 = \psi_4 = 0$. The result is

$$\begin{bmatrix} \xi_1 \\ \xi_4 \end{bmatrix} = - \begin{bmatrix} a_{11} & a_{12} \\ a_{21} & a_{22} \end{bmatrix}^{-1} \begin{bmatrix} k_1 \\ k_2 \end{bmatrix} . \quad (2.16)$$

The procedure of finding the elements a_{11} , a_{12} , a_{21} , a_{22} , k_1 and k_2 is shown schematically below:



Similarly, we may further assume $\xi_1 = c_3$, $\xi_4 = c_4$ and $\xi_1 = c_5$, $\xi_4 = c_6$ and obtain the corresponding values $\psi_1 = c_3'$, $\psi_4 = c_4'$ and $\psi_1 = c_5'$, $\psi_4 = c_6'$, respectively. Using the values c_i and c_i' ($i=1,2,\dots,6$) and equation (2.15), we have the following 6 linear algebraic equations for a_{ij} and k_i ($i,j=1,2$).

$$\begin{bmatrix} c_1 & c_2 & 0 & 0 & 1 & 0 \\ 0 & 0 & c_1 & c_2 & 0 & 1 \\ c_3 & c_4 & 0 & 0 & 1 & 0 \\ 0 & 0 & c_3 & c_4 & 0 & 1 \\ c_5 & c_6 & 0 & 0 & 1 & 0 \\ 0 & 0 & c_5 & c_6 & 0 & 1 \end{bmatrix} \begin{bmatrix} a_{11} \\ a_{12} \\ a_{21} \\ a_{22} \\ k_1 \\ k_2 \end{bmatrix} = \begin{bmatrix} c_1' \\ c_2' \\ c_3' \\ c_4' \\ c_5' \\ c_6' \end{bmatrix} \quad (2.17)$$

The elements a_{ij} and k_i ($i,j=1,2$) can now be found provided

that the matrix is not singular. By using equation (2.16), the boundary vorticities ξ_1 and ξ_4 can then be determined. Now, on the line $x = \frac{1}{3}$, six equations (see equations (2.13) and (2.14)) with six unknowns are solved. We note that the obtained values for ψ_1 and ψ_4 must be zero theoretically but numerically they are found to be the order of 10^{-7} as compared with the maximum value inside the region. Next we may move to the line $x = \frac{2}{3}$, and iterate using the same procedure until the errors are within a prescribed limit given by

$$\max(\epsilon_1, \epsilon_2) < \epsilon = 0(10^{-5}) \quad (2.18)$$

where

$$\epsilon_1 = \sum_i \frac{|\xi_i^{(n)} - \xi_i^{(n-1)}|}{|\xi_i^{(n)}|}$$

$$\epsilon_2 = \sum_i \frac{|\psi_i^{(n)} - \psi_i^{(n-1)}|}{|\psi_i^{(n)}|}$$

Method (b): Alternatively, we may formulate the problem as

	On boundaries OA and BC	On line of symmetry AB and OC
$\frac{\partial^2 \psi}{\partial x^2} + \frac{\partial^2 \psi}{\partial y^2} = \xi$	$\psi = 0$	$\psi = 0$
		(2.19)
$\frac{\partial^2 \xi}{\partial x^2} + \frac{\partial^2 \xi}{\partial y^2} = f$	$\xi = ?$	$\xi = 0$

In contrast to method (a) the values of ξ on the boundaries OA and BC are to be determined such that $\frac{\partial \psi}{\partial y} = 0$ on these lines. The procedure described in Method (a) can now be applied except that the following equation should be used instead of equation (2.14).

$$\begin{bmatrix} -1 & 2 & 0 & 0 \\ 1 & -4 & 1 & 0 \\ 0 & 1 & -4 & 1 \\ 0 & 0 & 2 & 1 \end{bmatrix} \begin{bmatrix} \Delta\psi_1 \\ \psi_2 \\ \psi_3 \\ \Delta\psi_4 \end{bmatrix} = \begin{bmatrix} h^2 \xi_1 \\ h^2 \xi_2 - \psi_6 \\ h^2 \xi_3 - \psi_7 \\ h^2 \xi_4 \end{bmatrix} \quad (2.20)$$

where $\Delta\psi_1 = \psi_2 - \psi_{17}$ and $\Delta\psi_4 = \psi_{18} - \psi_3$.

The boundary vorticity ξ_1 and ξ_4 must now be determined such that $\Delta\psi_1 = \Delta\psi_4 = 0$.

Finally, we note that the technique developed here can also be extended to the case where the number of boundary vorticity values to be determined is either less or greater

than two on each line or block. Table 2.1 shows the relation between the number of boundary vorticity values to be determined and the corresponding repeated number of computations required.

Table 2.1 The relation between the number of boundary vorticity values to be determined and the repeated number of computations required

Number of boundary vorticity values	1	2	3	4	.	.	.	N
Number of elements for matrix <u>A</u> and vector <u>k</u>	2	6	12	20	.	.	.	$N(N+1)$
Number of Computations required to determine <u>ξ_b</u>	2	3	4	5	.	.	.	$N+1$
Total number of computations on each line or block	3	4	5	6	.	.	.	$N+2$

2.3 Concluding Remarks

(a) Because of the extremely slow convergence of the biharmonic equation, the boundary vorticity method is very effective particularly for a problem formulated in polar coordinate system. For example, for the combined free and forced convection problem in horizontal circular tubes which will be considered in Chapter III, the line iterative technique using the boundary vorticity method converges in approximately 5 minutes on IBM 360/67 for an intermediate parameter in comparison with 11 hours on IBM 7040 required by using the conventional method [2.4]. According to the above comparison, the new method is estimated to be about ten times faster than the conventional method employed in [2.4].

(b) Considering the boundary conditions $\psi_1 = \psi_4 = \psi_5 = \psi_8 = 0$ and combining equation (2.8) and (2.9), we have the following system of linear algebraic equations:

$$\begin{bmatrix} -4 & 1 & -h^2 & 0 & 1 & 0 & 0 & 0 \\ 1 & -4 & 0 & -h^2 & 0 & 1 & 0 & 0 \\ 2/h^2 & 0 & -4 & 1 & 0 & 0 & 1 & 0 \\ 0 & 2/h^2 & 1 & -4 & 0 & 0 & 0 & 1 \\ 1 & 0 & 0 & 0 & -4 & 1 & -h^2 & 0 \\ 0 & 1 & 0 & 0 & 1 & -4 & 0 & -h^2 \\ 0 & 0 & 1 & 0 & 2/h^2 & 0 & -4 & 1 \\ 0 & 0 & 0 & 1 & 0 & 2/h^2 & 1 & -4 \end{bmatrix} \begin{bmatrix} \psi_2 \\ \psi_3 \\ \xi_2 \\ \xi_3 \\ \psi_6 \\ \psi_7 \\ \xi_6 \\ \xi_7 \end{bmatrix} = \begin{bmatrix} 0 \\ 0 \\ h^2 f_2 \\ h^2 f_3 \\ 0 \\ 0 \\ h^2 f_6 \\ h^2 f_7 \end{bmatrix} \quad (2.21)$$

The boundary vorticity method can be considered essentially the same as the procedure to determine the unknowns on each vertical line ($\psi_2, \psi_3, \xi_2, \xi_3$ on line $x = \frac{1}{3}$ and $\psi_6, \psi_7, \xi_6, \xi_7$ on line $x = \frac{2}{3}$) simultaneously. If we put equation (2.21) in the vector form, we have

$$\underline{A} \underline{x} = \underline{k} . \quad (2.22)$$

Letting,

$$\underline{A} = \underline{D} - \underline{E} - \underline{F} \quad (2.23)$$

where

$$\underline{D} = \begin{bmatrix} \underline{B} & 0 \\ 0 & \underline{B} \end{bmatrix} , \quad \underline{E} = \begin{bmatrix} 0 & -\underline{I} \\ 0 & 0 \end{bmatrix} , \quad \underline{F} = \begin{bmatrix} 0 & 0 \\ -\underline{I} & 0 \end{bmatrix} ,$$

$$\underline{B} = \begin{bmatrix} -4 & 1 & -h^2 & 0 \\ 1 & -4 & 0 & -h^2 \\ 2/h^2 & 0 & -4 & 1 \\ 0 & 2/h^2 & 1 & -4 \end{bmatrix} \quad \text{and} \quad \underline{I} = \begin{bmatrix} 1 & 0 & 0 & 0 \\ 0 & 1 & 0 & 0 \\ 0 & 0 & 1 & 0 \\ 0 & 0 & 0 & 1 \end{bmatrix} = \text{an unit matrix,}$$

the line successive relaxation procedure is (see reference [2.6])

$$\begin{aligned} \underline{x}^{(n+1)} = & (\underline{D} - \omega \underline{E})^{-1} \{ (1 - \omega) \underline{D} + \omega \underline{F} \} \underline{x}^{(n)} \\ & + \omega (\underline{D} - \omega \underline{E})^{-1} \underline{k} \end{aligned} \quad (2.24)$$

where ω is the relaxation factor.

It is noted that a method using the direct inversion of the submatrix \underline{B} converges as well as the boundary vorticity method does. The repeated computations for finding the elements a_{ij} and k_i in equation (2.17) can be avoided. However, an efficient technique for the direct inversion of the submatrix \underline{B} or generally the following submatrix is required.

$$\underline{B} = \begin{bmatrix} \underline{C} & \underline{H} \\ \underline{G} & \underline{C} \end{bmatrix} \quad (2.25)$$

where

$$\underline{C} = \begin{bmatrix} -4 & 1 & 0 & \dots & 0 \\ 1 & -4 & 1 & \dots & 0 \\ \vdots & & & & \vdots \\ 0 & \dots & 1 & -4 & 1 \\ 0 & \dots & 0 & 1 & -4 \end{bmatrix}, \quad \underline{H} = -h^2 \underline{I}$$

and

$$\underline{G} = \begin{bmatrix} 2/h^2 & 0 & 0 & . & . & 0 \\ 0 & 0 & 0 & . & . & 0 \\ . & & & & & . \\ . & & & & & . \\ 0 & . & . & 0 & 0 & 0 \\ 0 & . & . & 0 & 0 & 2/h^2 \end{bmatrix}$$

(c) By carefully examining the system of linear algebraic equations (2.21), another new iterative scheme may be suggested. Following equations (2.21) and (2.22) and letting,

$$\underline{A} = \underline{D}' - \underline{E}' - \underline{F}' \quad (2.26)$$

where

$$\underline{D}' = \begin{bmatrix} \underline{B}' & \underline{0} & \underline{0} & \underline{0} \\ \underline{0} & \underline{B}' & \underline{0} & \underline{0} \\ \underline{0} & \underline{0} & \underline{B}' & \underline{0} \\ \underline{0} & \underline{0} & \underline{0} & \underline{B}' \end{bmatrix}, \quad \underline{E}' = \begin{bmatrix} \underline{0} & \underline{0} & \underline{0} & \underline{0} \\ \underline{H} & \underline{0} & \underline{0} & \underline{0} \\ \underline{I} & \underline{0} & \underline{0} & \underline{0} \\ \underline{0} & \underline{I} & \underline{H} & \underline{0} \end{bmatrix},$$

$$\underline{F}' = \begin{bmatrix} \underline{0} & \underline{H}' & \underline{I} & \underline{0} \\ \underline{0} & \underline{0} & \underline{0} & \underline{I} \\ \underline{0} & \underline{0} & \underline{0} & \underline{H}' \\ \underline{0} & \underline{0} & \underline{0} & \underline{0} \end{bmatrix}, \quad \underline{B}' = \begin{bmatrix} -4 & 1 \\ 1 & -4 \end{bmatrix},$$

$$\underline{H} = \begin{bmatrix} 2/h^2 & 0 \\ 0 & 2/h^2 \end{bmatrix}, \quad \underline{H}' = \begin{bmatrix} -h^2 & 0 \\ 0 & -h^2 \end{bmatrix}$$

$$\text{and } \underline{I} = \begin{bmatrix} 1 & 0 \\ 0 & 1 \end{bmatrix} = \text{an unit matrix,}$$

the line successive relaxation procedure [2.6] this time is

$$\begin{aligned} \underline{x}^{(n+1)} &= (\underline{D}' - \omega \underline{E}')^{-1} \{ (1 - \omega) \underline{D}' + \omega \underline{E}' \} \underline{x}^{(n)} \\ &+ \omega (\underline{D}' - \omega \underline{E}')^{-1} \underline{k}. \end{aligned} \quad (2.27)$$

Now the Gaussian elimination method (see Appendix 2.1) can be readily applied here for the direct inversion of the submatrix \underline{B}' or generally the following submatrix.

$$\underline{B}' = \begin{bmatrix} -4 & 1 & & & & \\ 1 & -4 & 1 & & & 0 \\ & 1 & -4 & 1 & & \\ & & \ddots & \ddots & \ddots & \\ & & & \ddots & \ddots & \\ & & & & 1 & -4 & 1 \\ 0 & & & & 1 & -4 & 1 \\ & & & & & 1 & -4 \end{bmatrix} \quad (2.28)$$

By comparing equation (2.24) with equation (2.27), we note that the latter iterative scheme avoids the difficulty of using the direct inversion of the submatrix \underline{B} (see equation (2.25)). Consequently, computing time for finding the elements a_{ij} and k_i in equation (2.17) can be saved. This improved iterative scheme is employed in Chapter VI with approximately one-quarter of computing time being saved as compared with the boundary vorticity method for a problem formulated in Cartesian coordinates.

(d) A further systematic numerical experiment is necessary to compare all the conventional techniques with the newly developed boundary vorticity method and the improved iterative scheme discussed in part (c) for various engineering problems so that a designer may choose a simple and yet efficient procedure for a particular problem.

References

- 2.1 Cornock, A.F., "The Numerical Solution of Poisson's and the Biharmonic Equations by Matrices," Proceedings, Cambridge Philosophical Society, Vol. 50, 1954, pp. 524-535.
- 2.2 Conte, S.D., and Dames, R.T., "An Alternating Direction Method for Solving the Biharmonic Equation," Mathematical Tables and Other Aids to Computations, Vol. 12, 1958, pp. 198-205.
- 2.3 Keller, H.B., "Special Block Iterations with Applications to Laplace and Biharmonic Difference Equations," SIAM Review, Vol. 2, No. 4, 1960, pp. 277-287.
- 2.4 Newell, P.H., Jr., and Bergles, A.E., "Analysis of Combined Free and Forced Convection for Fully Developed Laminar Flow in Horizontal Tubes," Journal of Heat Transfer, Trans. ASME, Series C, Vol. 92, 1970, pp. 83-93.
- 2.5 Cheng, K.C., and Hwang, G.J., "Numerical Solution for Combined Free and Forced Laminar Convection in Horizontal Rectangular Channels," Journal of Heat Transfer, Trans. ASME, Series C, Vol. 19, 1969, pp. 59-66.
- 2.6 Varga, R.S., Matrix Iterative Analysis, Prentice-Hall, New Jersey, 1965.

- 2.7 Wachspress, E.L., Iterative Solution of Elliptic Systems and Applications to the Neutron Diffusion Equations of Reactor Physics, Prentice-Hall, New Jersey, 1966.

Appendix 2.1 Gaussian Elimination Method [2.7]

If we have a system of linear algebraic equations

$$\underline{A} \underline{x} = \underline{k}$$

with a tridiagonal matrix \underline{A} ,

$$\underline{A} = \begin{bmatrix} b_1 & -c_1 & & & & \\ -a_2 & b_2 & -c_2 & & & 0 \\ & -a_3 & b_3 & -c_3 & & \\ & & \ddots & \ddots & \ddots & \\ & & & -a_{n-2} & b_{n-2} & -c_{n-2} \\ 0 & & & -a_{n-1} & b_{n-1} & -c_{n-1} \\ & & & & -a_n & b_n \end{bmatrix},$$

then a numerical procedure called Gaussian elimination method or Crout's (or Cholesky's) method may be used to solve for \underline{x} . The procedure is carried out by using forward elimination and then backward substitution as described below:

$$h_1 = c_1/b_1 ; \quad h_m = c_m/(b_m - a_m h_{m-1}) , \quad m=2,3,\dots,n-1$$

$$p_1 = k_1 ; \quad p_m = (k_m + a_m p_{m-1}) / (b_m - a_m h_{m-1}), \quad m=2,3,\dots,n$$

and

$$x_n = p_n$$

$$x_m = p_m + h_m x_{m+1}, \quad m=n-1, n-2, \dots, 1$$

CHAPTER III

BOUNDARY VORTICITY METHOD FOR CONVECTIVE HEAT TRANSFER WITH SECONDARY FLOW IN HORIZONTAL TUBES*

3.1 Introduction

The effects of the double helix secondary flow caused by unbalanced buoyancy forces in heated horizontal tubes on such important design parameters as friction factor and Nusselt number have been studied both theoretically and experimentally by several investigators in recent years. Trefethen [3.2] pointed out that the secondary flow patterns caused by buoyancy forces in heated horizontal tubes, centrifugal forces in curved pipes and Coriolis forces in radial rotating tubes for fully developed laminar flow are at least qualitatively similar, and compared the flow and heat transfer data from the three types of tubes. Morton's analysis [3.3] on the free convection effects for fully developed laminar forced convection in uniformly heated horizontal tubes by a perturbation method is applicable only for rather small parameter ($ReRa$) region. del Casal and Gill [3.4] analysed the same problem by the same method considering the variation of density in the axial direction and throughout the cross-section without the usual assumption of a constant

* A somewhat condensed earlier version of this work is reported in [3.1].

pressure gradient. Mori and Futagami [3.5] presented a theoretical investigation for the problem considered by Morton [3.3] dealing with high $ReRa$ region by a boundary-layer approximation. The high $ReRa$ regime is characterized by strong secondary flow, and the flow field may be divided into a core region and a boundary layer near the wall. Mathematically, the core region is governed by a hyperbolic type equation and the boundary layer is governed by a parabolic equation. It is of interest to note that the solution in the neighborhood of top and bottom stagnation points may be improved, if the regions are described by elliptic equations. Recently, Newell and Bergles [2.4] presented correlations for the effects of free convection on water for the so-called glass tube and infinite conductivity thermal boundary conditions. It is noted that their correlation curves are considerably below the experimental data for air obtained by Mori et al. [3.6]. Furthermore, the convergence rate of the iterative technique used by them is extremely slow and not practical from the viewpoint of computing time. Faris and Viskanta [3.7] further extended Morton's perturbation approach by expanding the dependent variable in ascending power of Gr/Re^2 . Recently, Siegwarth et al. [3.8] extended the boundary layer approximation employed in [3.5] to the problem with relatively small core velocity for the cases of $Pr = 1$ and $Pr \rightarrow \infty$. Their correlation curve predicts nearly the same result as the one obtained by Mori and Futagami [3.5].

The purpose of this chapter is to present a numerical solution for a steady fully developed laminar forced convection with buoyancy effects in uniformly heated horizontal tubes with an aim to bridge the gap between the perturbation solution [3.3] for small parameter ($ReRa$) and the boundary-layer approximation [3.5] for large parameter ($ReRa$) by using line iterative over- (or under-) relaxation coupled with the newly developed boundary vorticity method. It will be seen later that the gap has now been successfully closed and the numerical technique employed can save the computing time greatly as compared with the one used by Newell and Bergles [2.4]. The effect of Prandtl number on flow and heat transfer results is also studied.

3.2 Theoretical Analysis

Consider a steady hydrodynamically and thermally fully developed Newtonian laminar flow in a horizontal circular tube under axially uniform wall heat flux and peripherally uniform wall temperature at any axial position. The flow will be referred to cylindrical coordinates (R, ϕ, Z) as shown in Fig. 3.1.

The following assumptions are made in this analysis:

- (a) Viscous dissipation and compression work are negligible.
- (b) The axial direction derivatives are zero except that pressure and temperature gradients are constant, namely $\partial P / \partial Z = C_1$ and $\partial T / \partial Z = C_2$.
- (c) The variations of physical properties are small. The density is considered to be constant except for its variation in the R - and ϕ - directions buoyancy terms.

Referring to the value at the wall, the equation of state for negligibly small variation of static pressure may be written as,

$$\frac{\rho_w}{\rho} - 1 = \frac{1}{T_w} (T - T_w) = \beta(T - T_w) . \quad (3.1)$$

This expression is exact for an ideal gas, and represents a reasonable approximation for real gases. For liquids, the above equation (3.1) is valid only for the case when the

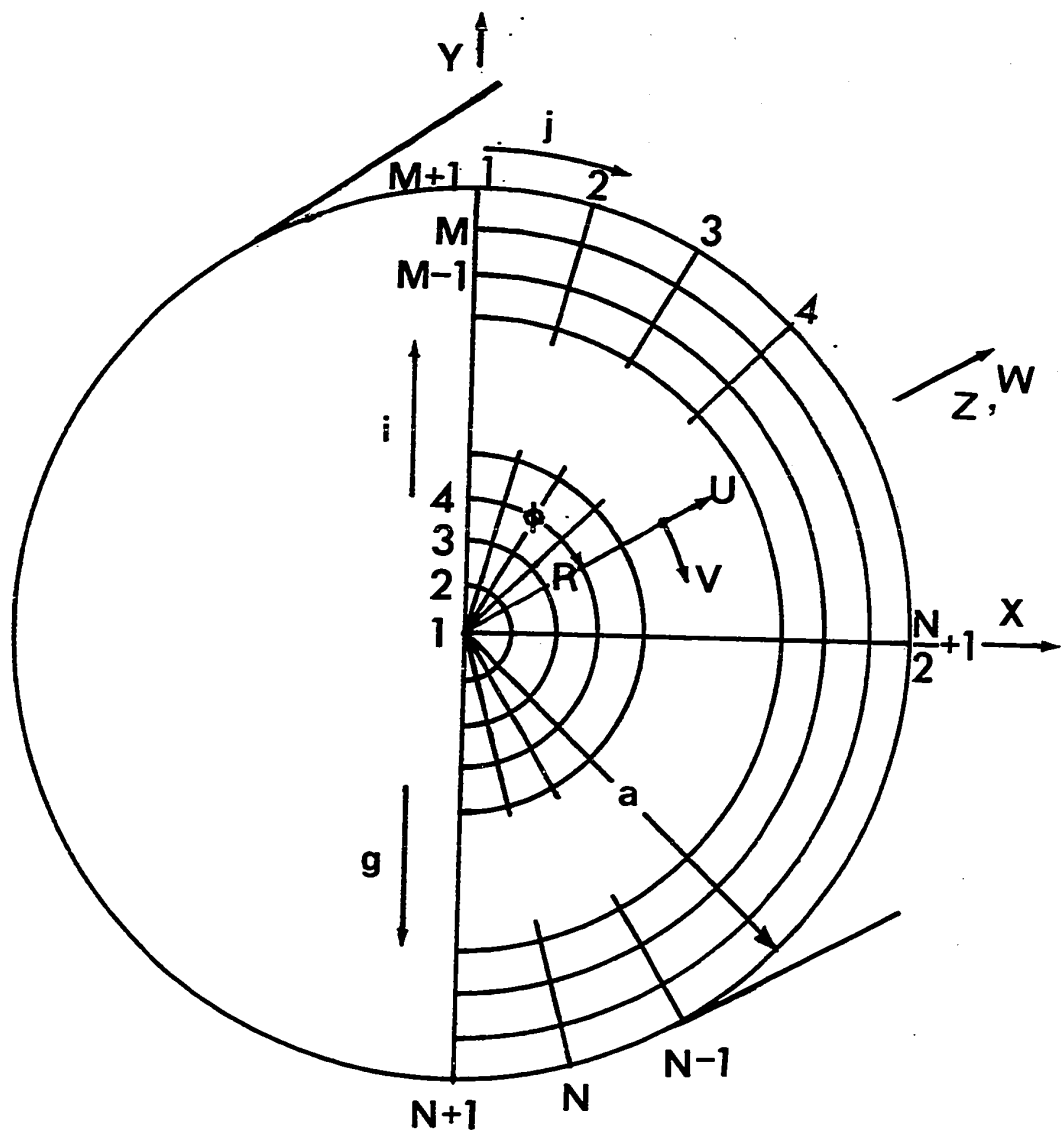


Fig. 3.1 Coordinate system and numerical grid

temperature difference is small. A different formulation for the equation of state considering the temperature dependency of density is required for a fluid with large temperature difference.

With the foregoing assumptions, the governing equations for fully developed laminar flow are:

Continuity equation

$$\frac{\partial(RU)}{\partial R} + \frac{\partial V}{\partial \phi} = 0 \quad (3.2)$$

Momentum equations

$$\begin{aligned} U \frac{\partial U}{\partial R} + \frac{V}{R} \frac{\partial U}{\partial \phi} - \frac{V^2}{R} = & - \frac{1}{\rho} \frac{\partial P}{\partial R} + \nu \left(\nabla_1^2 U - \frac{U}{R^2} - \frac{2}{R^2} \frac{\partial V}{\partial \phi} \right) \\ & - \beta g (T_w - T) \cos \phi \end{aligned} \quad (3.3)$$

$$\begin{aligned} U \frac{\partial V}{\partial R} + \frac{V}{R} \frac{\partial V}{\partial \phi} + \frac{UV}{R} = & - \frac{1}{\rho R} \frac{\partial P}{\partial \phi} + \nu \left(\nabla_1^2 V + \frac{2}{R^2} \frac{\partial U}{\partial \phi} - \frac{V}{R^2} \right) \\ & + \beta g (T_w - T) \sin \phi \end{aligned} \quad (3.4)$$

$$U \frac{\partial W}{\partial R} + \frac{V}{R} \frac{\partial W}{\partial \phi} = - \frac{1}{\rho} \frac{\partial P}{\partial Z} + \nu \nabla_1^2 W \quad (3.5)$$

Energy equation

$$U \frac{\partial T}{\partial R} + \frac{V}{R} \frac{\partial T}{\partial \phi} + W \frac{\partial T}{\partial Z} = \kappa \nabla_1^2 T \quad (3.6)$$

where

$$\nabla_1^2 = \frac{\partial^2}{\partial R^2} + \frac{1}{R} \frac{\partial}{\partial R} + \frac{1}{R^2} \frac{\partial^2}{\partial \phi^2}$$

The momentum equations (3.3), (3.4), and (3.5) and the energy equation (3.6) are quasi-linear, second order partial differential equations of elliptic type.

Because of symmetry with respect to vertical center line, it is only required to consider the right (or left) half of the circular region. The boundary conditions are:

$$U = V = W = T_w - T = 0 \text{ at pipe wall}$$

$$\frac{\partial U}{\partial \phi} = V = \frac{\partial W}{\partial \phi} = \frac{\partial T}{\partial \phi} = 0 \text{ at vertical center line} \\ \text{excluding the center point} \quad (3.7)$$

$$\frac{\partial V}{\partial X} = U = \frac{\partial W}{\partial X} = \frac{\partial T}{\partial X} = 0 \text{ at the center}$$

First derivatives with respect to X are introduced to satisfy the symmetry property at the center.

Introducing the following non-dimensional transformations,

$$(X, Y, R) = a(x, y, r), (U, V, W) = (u, v, Cw)v/a,$$

$$C_1 = \partial P / \partial Z, C_2 = \partial T / \partial Z, C = -C_1 a^3 / 4\nu\mu = Re / (2\bar{w}), \quad (3.8)$$

$$T_w - T = C C_2 a Pr \theta, Pr = \nu/\kappa, Re = 2a\bar{w}\rho/\mu,$$

$$Ra = \beta g C_2 a^4 / \nu\kappa,$$

and a dimensionless stream function ψ ,

$$u = \frac{1}{r} \frac{\partial \psi}{\partial \phi}, \quad v = -\frac{\partial \psi}{\partial r}, \quad (3.9)$$

the momentum and energy equations (3.3) to (3.6) can be restated in the following dimensionless form after eliminating pressure terms between equations (3.3) and (3.4) and using the continuity equation (3.2).

Vorticity transport equation for secondary flow:

$$u \frac{\partial \xi}{\partial r} + \frac{v}{r} \frac{\partial \xi}{\partial \phi} = \nabla^2 \xi - RaC \left(\frac{\partial \theta}{\partial r} \sin \phi + \frac{1}{r} \frac{\partial \theta}{\partial \phi} \cos \phi \right) \quad (3.10)$$

where the vorticity function is defined by

$$\xi = \nabla^2 \psi = \frac{\partial^2 \psi}{\partial r^2} + \frac{1}{r} \frac{\partial \psi}{\partial r} + \frac{1}{r^2} \frac{\partial^2 \psi}{\partial \phi^2} \quad (3.11)$$

Axial momentum equation:

$$u \frac{\partial w}{\partial r} + \frac{v}{r} \frac{\partial w}{\partial \phi} = \nabla^2 w + 4 \quad (3.12)$$

Energy equation:

$$\text{Pr} \left(u \frac{\partial \theta}{\partial r} + \frac{v}{r} \frac{\partial \theta}{\partial \phi} \right) = \nabla^2 \theta + w \quad (3.13)$$

We should note that the vorticity function is introduced to apply the boundary vorticity method and avoid using biharmonic operator $\nabla^4 \psi$ in the equation (3.10). The boundary conditions corresponding to the governing equations are tabulated in Table 3.1 for easy reference.

The boundary conditions can be employed directly in the numerical computation except those marked as *1, *2, *3 and *4. For the conditions *1, *2 at the center, it is usual to avoid it by an extrapolation or other approximation to obtain one more algebraic equation for the value at the center. In this study, it is proposed to circumvent the difficulty by transforming equations (3.12) and (3.13) into Cartesian coordinate system and use the center point and the adjacent four points for the finite-difference formulation. By doing so, the boundary conditions $\frac{\partial w}{\partial x}$ and $\frac{\partial \theta}{\partial x} = 0$ can be posed naturally without introducing any artificial error. For the conditions *3 and *4, the boundary vorticity method

Table 3.1 The boundary conditions for the governing equations

Governing equation	Highest derivative and the number of boundary conditions required		Available boundary conditions			
	r-direction	ϕ -direction	$r = 0$	$r = 1$	$r \neq 0$ $\phi = 0$	$r \neq 0$ $\phi = \pi$
(3.10)	2	2	$\xi = 0$	$\xi = ?^{*3}$	$\xi = 0$	$\xi = 0$
(3.11)	2	2	$\psi = 0$	$\frac{\partial \psi}{\partial r} = \psi = 0^{*4}$	$\psi = 0$	$\psi = 0$
(3.12)	2	2	$\frac{\partial w}{\partial x} = 0^{*1}$	$w = 0$	$\frac{\partial w}{\partial \phi} = 0$	$\frac{\partial w}{\partial \phi} = 0$
(3.13)	2	2	$\frac{\partial \theta}{\partial x} = 0^{*2}$	$\theta = 0$	$\frac{\partial \theta}{\partial \phi} = 0$	$\frac{\partial \theta}{\partial \phi} = 0$

discussed in Chapter II is found to be particularly effective. Referring to Table 2.1 in Chapter II, the number of unknown boundary vorticity to be determined on each radial line is found to be one for the present problem. Thus it requires three repeated computation on each line. The detailed algebraic equations and procedure will be discussed in the next section.

3.3 Finite-Difference Approximations

Referring to Fig. 3.1, the axial momentum and energy equations (3.12) and (3.13) can be approximated in the following finite-difference form.

$$\begin{aligned}
 \sigma(u_{i,j}^0) & \frac{f_{i+1,j} - f_{i-1,j}}{2(\Delta r)} + \frac{v_{i,j}^0}{r_i} \frac{f_{i,j+1} - f_{i,j-1}}{2(\Delta \phi)} \\
 & = \frac{f_{i+1,j} - 2f_{i,j} + f_{i-1,j}}{(\Delta r)^2} \\
 & + \frac{1}{r_i} \frac{f_{i+1,j} - f_{i-1,j}}{2(\Delta r)} \\
 & + \frac{1}{r_i^2} \frac{f_{i,j+1} - 2f_{i,j} + f_{i,j-1}}{(\Delta \phi)^2} + G_{i,j}
 \end{aligned} \tag{3.14}$$

where

$$\sigma = 1, G_{i,j} = 4 \quad \text{when } f_{i,j} = w_{i,j},$$

$$\sigma = Pr, G_{i,j} = w_{i,j} \quad \text{when } f_{i,j} = \theta_{i,j},$$

Superscript 0 signifies the values at previous iteration step,

and $i=2,3,\dots,M, j=1,2,\dots,N+1$.

The above equation (3.14) cannot be readily applied to the center point ($i=1$) since the original equations (3.12) and (3.13) are singular at the center. However, the difficulty can be overcome by writing the equations in Cartesian coordinates using the boundary conditions *1 and *2 in Table 3.1. The result is given as,

$$\sigma v_{i,j}^0 \frac{f_{2,1} - f_{2,N+1}}{2(\Delta r)} = \frac{f_{2,1} + 2f_{2,N/2+1} + f_{2,N+1} - 4f_{1,j}}{(\Delta r)^2} + G_{1,j} \quad (3.15)$$

A numerical experiment was performed to check the adequacy of the treatment of the singularity at the center. The following table demonstrates that the procedure is very satisfactory.

Table 3.2 Values of w and θ at the center without secondary motion

w	θ	
0.9999	0.1877	($M=20, N=10$)
1.0000	0.1875	(exact solution)

It is believed that the treatment of the singularity at the center point is quite general and can be applied equally to the other problems formulated in polar coordinates to avoid unnecessary errors.

The vorticity transport equation (3.10) and the equation for stream function (3.11) can also be approximated in the finite-difference form with the following substitutions.

$$\sigma = 1, G_{i,j} = -RaC\left(\frac{\partial \theta}{\partial r} \sin \phi + \frac{1}{r} \frac{\partial \theta}{\partial \phi} \cos \phi\right)_{i,j} \text{ when } f_{i,j} = \xi_{i,j},$$

$$\sigma = 0, G_{i,j} = -\xi_{i,j} \text{ when } f_{i,j} = \psi_{i,j}$$

$$i=2,3,\dots,M+1, \quad j=2,3,\dots,N$$

The first derivatives $\frac{\partial \theta}{\partial r}$, $\frac{\partial \theta}{\partial \phi}$ and $\frac{\partial \psi}{\partial r}$ are to be approximated by using five-point finite-difference formula.

$$\begin{aligned} \frac{\partial f_{i,j}}{\partial r} &= (f_{5,j} - 6f_{4,j} + 18f_{3,j} - 10f_{2,j} - 3f_{i,j})/(12\Delta r), \quad i=2 \\ &= (f_{i-2,j} - 8f_{i-1,j} + 8f_{i+1,j} - f_{i+2,j})/(12\Delta r), \quad i=3,4,\dots,M-1 \\ &= - (f_{M-3,j} - 6f_{M-2,j} + 18f_{M-1,j} - 10f_{M,j} \\ &\quad - 3f_{M+1,j})/(12\Delta r), \quad i=M \end{aligned} \quad (3.16)$$

The expression for $\frac{\partial f_{i,j}}{\partial \phi}$ is similar. In the computation of $\frac{\partial \psi}{\partial \phi}$, the following approximations are used noting that $\frac{\partial^2 \psi}{\partial \phi^2} = 0$ at $\phi = 0$ and $\phi = \pi$.

$$\begin{aligned}
 \frac{\partial f_{i,j}}{\partial \phi} &= (8f_{i,2} - f_{i,3})/(6\Delta\phi), \quad j=1 \\
 &= (-f_{i,2} + 8f_{i,3} - f_{i,4})/(12\Delta\phi), \quad j=2 \\
 &= (f_{i,j-2} - 8f_{i,j-1} + 8f_{i,j+1} - f_{i,j+2})/(12\Delta\phi), \quad j=3,4,\dots,N-1 \\
 &= (f_{i,N-2} - 8f_{i,N-1} + f_{i,N})/(12\Delta\phi), \quad j=N \\
 &= (f_{i,N-1} - 8f_{i,N})/(6\Delta\phi), \quad j=N+1
 \end{aligned} \tag{3.17}$$

3.3.1 Properties of Matrices and the Relaxation Factor

Rearranging equations (3.14) and (3.15), we obtain

$$\begin{aligned}
 &(1 - \frac{\Delta r}{2r_i} + \sigma \frac{\Delta r}{2} u_{i,j}^0) f_{i-1,j} - 2[1 + (\frac{\Delta r}{r_i \Delta \phi})^2] f_{i,j} \\
 &+ (1 + \frac{\Delta r}{2r_i} - \sigma \frac{\Delta r}{2} u_{i,j}^0) f_{i+1,j} \\
 &= - (\frac{\Delta r}{r_i \Delta \phi})^2 [(1 + \sigma \frac{r_i \Delta \phi}{2} v_{i,j}^0) f_{i,j-1} \\
 &+ (1 - \sigma \frac{r_i \Delta \phi}{2} v_{i,j}^0) f_{i,j+1}] - G_{i,j} (\Delta r)^2
 \end{aligned} \tag{3.18}$$

and

$$\begin{aligned}
 -4f_{1,j} + (1 - \sigma \frac{\Delta r}{2} v_{1,j}^0) f_{2,1} &= - (1 + \sigma \frac{\Delta r}{2} v_{1,j}^0) f_{2,N+1} \\
 -2f_{2,N/2+1} - G_{1,j} (\Delta r)^2 & \quad (3.19)
 \end{aligned}$$

Because of the nonlinear terms, the properties of the coefficient matrices of equations (3.18) and (3.19) are;

- (a) real,
- (b) non-symmetric,
- (c) diagonally dominant if and only if

$$\begin{aligned}
 \left| \frac{\Delta r}{2r_i} - \sigma \frac{\Delta r}{2} u_{i,j}^0 \right| &\leq 1, \\
 \left| \sigma \frac{r_i \Delta \phi}{2} v_{i,j}^0 \right| &\leq 1 \quad \text{for all } i,j \text{ except} \\
 &\quad \text{at the center point} \quad (3.20)
 \end{aligned}$$

and

$$\left| \sigma \frac{\Delta r}{2} v_{i,j}^0 \right| \leq 1 \quad \text{at the center.}$$

Since the matrices are not symmetric and their eigenvalues change from step to step (due to the corrections of $u_{i,j}^0$ and $v_{i,j}^0$), the determination of optimal relaxation factor is very difficult. But fortunately, as long as the property (c) is held, the numerical computation is always stable and a conver-

gent solution can be obtained with an over-relaxation factor of near unity. For the case when the property (c) is not held at all the points, an under-relaxation factor ranging from 0.2 to 1.0 may be used to stabilize the numerical computation. Numerical solution may be extended further to higher parameter by using the under-relaxation factor but only at the expense of considerable computing time.

3.3.2 The Application of the Boundary Vorticity Method

As pointed out in Chapter II, the numerical computation of a fourth order elliptic partial differential equation requires a tremendously large computing time, particularly, for the present problem formulated in polar coordinates. Consequently, the boundary vorticity method was developed to solve the present problem. The detailed procedure will be shown next.

Replacing the dummy function $f_{i,j}$ in equation (3.14) by $\xi_{i,j}$ and $\psi_{i,j}$, respectively, we have

$$\begin{aligned}
 & \left(1 - \frac{\Delta r}{2r_i} + \frac{\Delta r}{2} u_{i,j}^0\right) \xi_{i-1,j} - 2\left[1 + \left(\frac{\Delta r}{r_i \Delta \phi}\right)^2\right] \xi_{i,j} \\
 & + \left(1 + \frac{\Delta r}{2r_i} - \frac{\Delta r}{2} u_{i,j}^0\right) \xi_{i+1,j} \\
 & = - \left(\frac{\Delta r}{r_i \Delta \phi}\right)^2 \left[\left(1 + \frac{r_i \Delta \phi}{2} v_{i,j}^0\right) \xi_{i,j-1} \right. \\
 & \left. + \left(1 - \frac{r_i \Delta \phi}{2} v_{i,j}^0\right) \xi_{i,j+1}\right] - G_{i,j} (\Delta r)^2
 \end{aligned} \tag{3.21}$$

and

$$\begin{aligned}
 & (1 - \frac{\Delta r}{2r_i})\psi_{i-1,j} - 2[1 + (\frac{\Delta r}{r_i \Delta \phi})^2]\psi_{i,j} + (1 + \frac{\Delta r}{2r_i})\psi_{i+1,j} \\
 & = - (\frac{\Delta r}{r_i \Delta \phi})^2 [\psi_{i,j-1} + \psi_{i,j+1}] - (\Delta r)^2 \xi_{i,j} \quad (3.22)
 \end{aligned}$$

Using the boundary conditions $\xi_{i,1} = \xi_{i,N+1} = \xi_{1,j} = 0$, for equation (3.21), $\psi_{i,1} = \psi_{i,N+1} = \psi_{1,j} = 0$ and $\frac{\partial \psi_{M+1,j}}{\partial r} = 0$ (or $\psi_{M,j} = \psi_{M+2,j}$), for equation (3.22), and considering the radial line $j=2$, we have the following linear algebraic equations in matrix forms.

$$\begin{bmatrix}
 B_2 & C_2 & & & & & & & & \\
 A_3 & B_3 & C_3 & & & & & & & 0 \\
 & A_4 & B_4 & C_4 & & & & & & \\
 & & \cdot & \cdot & \cdot & & & & & \\
 & & & \cdot & \cdot & \cdot & & & & \\
 & & & & \cdot & \cdot & \cdot & & & \\
 & & & & & A_{M-2} & B_{M-2} & C_{M-2} & & \\
 & & & & & & A_{M-1} & B_{M-1} & C_{M-1} & \\
 & & & & & & & A_M & B_M & \\
 & & & & & & & & 0 &
 \end{bmatrix}
 \begin{bmatrix}
 \xi_{2,2} \\
 \xi_{3,2} \\
 \xi_{4,2} \\
 \vdots \\
 \vdots \\
 \xi_{M-2,2} \\
 \xi_{M-1,2} \\
 \xi_{M,2}
 \end{bmatrix}
 =
 \begin{bmatrix}
 K_2 \\
 K_3 \\
 K_4 \\
 \vdots \\
 \vdots \\
 K_{M-2} \\
 K_{M-1} \\
 K_M - C_M \xi_{M+1,2}
 \end{bmatrix} \quad (3.23)$$

and

$$\begin{bmatrix}
 B'_2 & C'_2 & & & & & \\
 A'_3 & B'_3 & C'_3 & & & & 0 \\
 & A'_4 & B'_4 & C'_4 & & & \\
 & & \cdot & \cdot & \cdot & & \\
 & & & \cdot & \cdot & \cdot & \\
 & & & & A'_{M-1} & B'_{M-1} & C'_{M-1} \\
 & & & & & A'_M & B'_M & C'_M \\
 0 & & & & & & (A'_{M+1} + C'_{M+1}) & B'_{M+1}
 \end{bmatrix}
 \begin{bmatrix}
 \psi_{2,2} \\
 \psi_{3,2} \\
 \psi_{4,2} \\
 \vdots \\
 \psi_{M-1,2} \\
 \psi_{M,2} \\
 \psi_{M+1,2}
 \end{bmatrix}
 =
 \begin{bmatrix}
 K'_2 - (\Delta r)^2 \xi_{2,2} \\
 K'_3 - (\Delta r)^2 \xi_{3,2} \\
 K'_4 - (\Delta r)^2 \xi_{4,2} \\
 \vdots \\
 K'_{M-1} - (\Delta r)^2 \xi_{M-1,2} \\
 K'_M - (\Delta r)^2 \xi_{M,2} \\
 K'_{M+1} - (\Delta r)^2 \xi_{M+1,2}
 \end{bmatrix}$$

(3.24)

where,

$$A_i = 1 - \frac{\Delta r}{2r_i} + \frac{\Delta r}{2} u_{i,2}^0$$

$$B_i = -2 \left[1 + \left(\frac{\Delta r}{r_i \Delta \phi} \right)^2 \right]$$

$$C_i = 1 + \frac{\Delta r}{2r_i} - \frac{\Delta r}{2} u_{i,2}^0$$

$$K_i = - \left(\frac{\Delta r}{r_i \Delta \phi} \right)^2 \left(1 - \frac{r_i \Delta \phi}{2} v_{i,2}^0 \right) \xi_{i,3} - G_{i,2} (\Delta r)^2$$

$$A'_i = 1 - \frac{\Delta r}{2r_i}$$

$$B'_i = B_i$$

$$C_i' = 1 + \frac{\Delta r}{2r_i}$$

$$K_i' = - \left(\frac{\Delta r}{r_i \Delta \phi} \right)^2 \psi_{i,3}$$

First of all, we assume $\xi_{M+1,2} = \xi_b^{(1)}$ in the above equations (3.23) and (3.24). Using the Gaussian elimination method, we are able to solve equation (3.23) simultaneously for $\xi_{i,2}$, $i=2,3,\dots,M$. Substituting the obtained vorticity function into the right-hand side of equation (3.24) and again applying the Gaussian elimination method, the values for stream function can be found. Then, we store the value $\psi_{M+1,2} = \psi_b^{(1)}$. Secondly, we assume $\xi_{M+1,2} = \xi_b^{(2)}$ and follow the same procedure to obtain $\psi_{M+1,2} = \psi_b^{(2)}$ but observing the linear relation between ξ_b and ψ_b , we can obtain ξ_b such that $\psi_b = 0$.

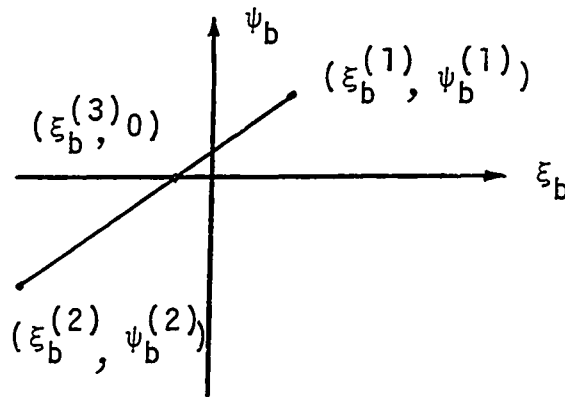


Fig. 3.2 The linear relation between ξ_b and ψ_b

The expression for $\xi_b^{(3)}$ is

$$\xi_b^{(3)} = - \frac{\xi_b^{(1)} - \xi_b^{(2)}}{\psi_b^{(1)} - \psi_b^{(2)}} (0 - \psi_b^{(2)}) + \xi_b^{(2)} \quad (3.25)$$

Using $\xi_b^{(3)}$ and solving equations (3.23) and (3.24) again, we obtain $\xi_{i,2}$ and $\psi_{i,2}$, $i=2,3,\dots,M$ which are the numerical solutions on the radial line $j=2$. Then we move on to the next lines, $j=3,4,\dots$ etc. and iterate them. By this method, we find that the values of the stream function on the boundary $r = 1$ are numerically around the order of 10^{-7} as compared with the largest value at interior points. Theoretically, of course, the stream function must vanish on the boundary. The error of the above magnitude may be caused by a round-off error using a single precision.

3.3.3 Errors and Mesh Sizes

The accuracy of the results and computing time required are important factors in the numerical calculation. The order of magnitude of errors and the computing time required should be estimated so that within an allowable computing time, a satisfactory result with errors less than a prescribed limit can be obtained. The analysis of all possible errors and a numerical experiment on mesh sizes are necessary before the numerical solution.

In the process of solving the system of partial differential equations (3.9) to (3.13) and associated boundary conditions, errors may come from the following sources:

- (a) inherent error resulting from the finite-difference approximations for the governing partial differential equations and the related boundary conditions,
- (b) the convergence of each partial differential equation and the nonlinear terms,
- (c) round-off errors.

In the usual computation, the error source (a) may have the largest magnitude of error as compared with the other two sources. The inherent error is closely related to the mesh size, the magnitude of secondary velocity in the nonlinear terms and the second, third and higher derivatives in the finite-difference approximation. In this study, both central difference and two-point non-central difference are used as the approximations for the nonlinear terms. Although the latter always assures that the matrices would be diagonally dominant, the accuracy is very poor as shown in Fig. 3.3. Two alternative methods of determining the same flow and heat transfer parameters are used to check the accuracy of the numerical results. Initially, non-central difference for the nonlinear terms with 20×10 grids is used in the computation to accelerate the convergence. Central difference with 40×20 grids is finally used to complete all the numerical computation. It is noted that central difference with 32×32 grids

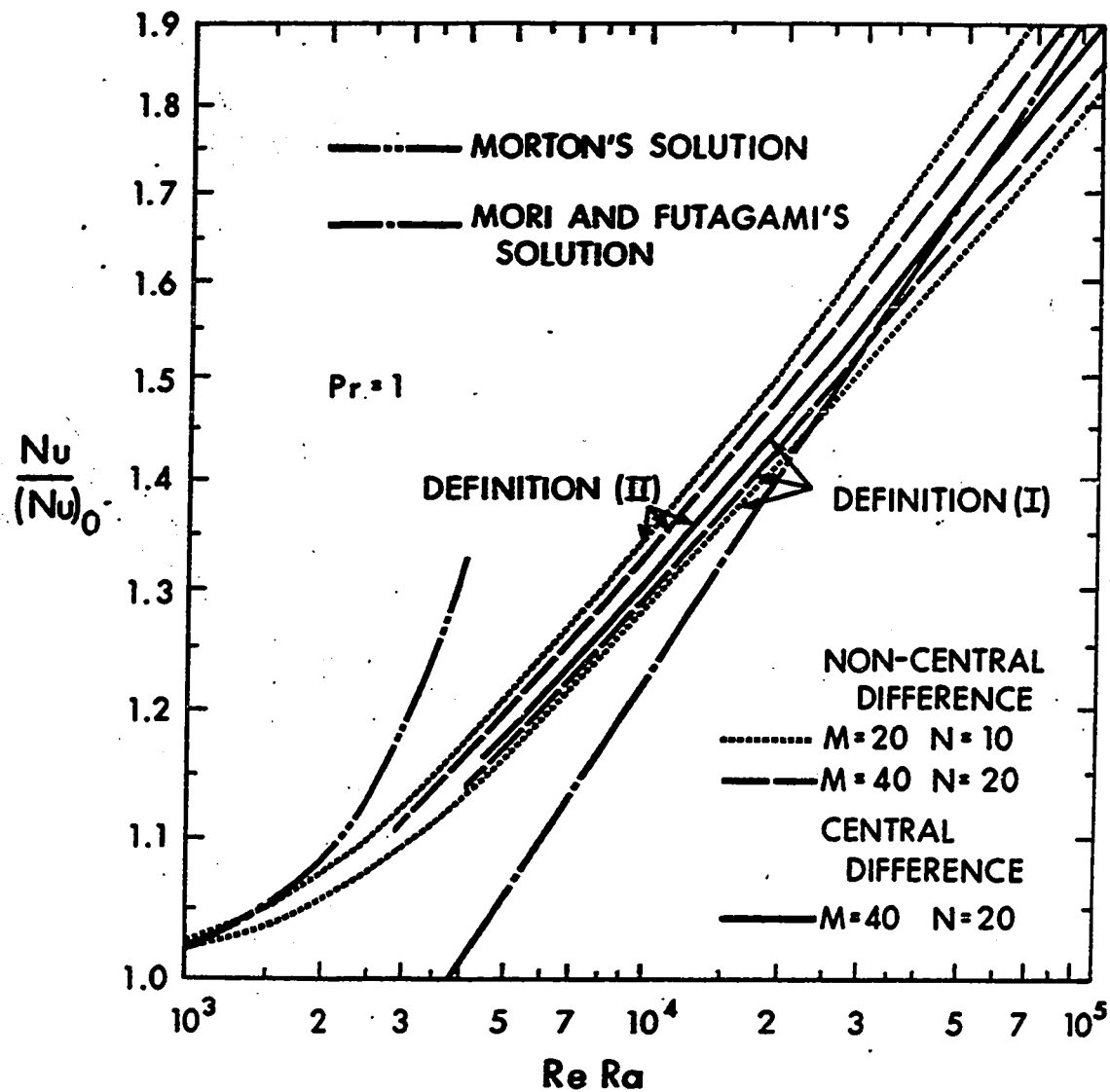


Fig. 3.3 Convergence of numerical solution for heat transfer result

is also used to extend the solution to the higher parameter region for the case of $Pr = 0.72$. Error source (b) is controlled such that the order of error is two orders less than the inherent error. The inherent error in this study is of $O(10^{-3})$. Thus a prescribed error for all the dependent variables are set as

$$\epsilon = \frac{\sum_{i,j} |f_{i,j}^{(n+1)} - f_{i,j}^{(n)}|}{\sum_{i,j} |f_{i,j}^{(n+1)}|} \leq O(10^{-5}) \quad (3.26)$$

Regarding error source (c), we note that the round-off error should not grow as long as the matrices are diagonally dominant. There is another way of checking the round-off error in the Gaussian elimination method and the boundary vorticity method applied here. The computed numerical values of the stream function on the boundary can be interpreted as the order of round-off error which is found to be of $O(10^{-7})$ in comparison with the largest value of the stream function at interior points for all grid sizes, namely, 20×10 , 40×20 and 32×32 . For each RaC , it requires 1 ~ 2 minutes using 20×10 grids for initial computation and 2 ~ 3 minutes for 40×20 grids in final calculation. It requires much larger computing time for higher Nusselt number ratio region. On the other hand, we cannot obtain convergent solution using

central difference for the present grid size of 40×20 when the Nusselt number ratio is greater than approximately 2.5.

It is significant to note that the computing time required by Newell and Bergles [2.4] for the numerical solution of similar problem with biharmonic operator is about 11 hours on IBM 7040 to obtain a complete solution for one RaC in the intermediate region with a grid size of 20×20 and about 2.5 hours on IBM 7094. In contrast, the present numerical method requires only about 5 minutes using 40×20 grids on IBM 360/67 which is estimated to be about one-tenth of the computing time required by them for the comparable situations.

3.3.4 Iterative Procedure

In this study, the line successive over- (or under-) relaxation method [2.6] and the boundary vorticity method are employed to solve the system of nonlinear algebraic equations. The equations are linearized by taking $u_{i,j}^0$ and $v_{i,j}^0$ equal to their previous values. That is, the system of nonlinear equations are replaced by another system of linear equations. Referring to equations (3.9) to (3.13), the procedure for numerical solution is:

- (a) Assign values for Pr , RaC , M and N .
- (b) The value of $w_{i,j}$ at each node point is obtained by solving equation (3.12) in finite-difference form and satisfying the boundary conditions using the assumption

that $u_{i,j}^0$ and $v_{i,j}^0$ being equal to the previous values of an assumed flow pattern at the beginning.

- (c) The calculated values of $w_{i,j}$ and still the same values for $u_{i,j}^0$ and $v_{i,j}^0$ are substituted into the finite-difference form of equation (3.13) to compute $\theta_{i,j}$ satisfying the corresponding boundary conditions.
- (d) Substituting the obtained $\theta_{i,j}$ into the finite-difference form of equation (3.10) and still using the same $u_{i,j}^0$ and $v_{i,j}^0$, the values for $\xi_{i,j}$ and $\psi_{i,j}$ are solved by applying the boundary vorticity method.
- (e) The new values for $u_{i,j}^0$ and $v_{i,j}^0$ are computed from the finite-difference form of equation (3.9).
- (f) Using the new $u_{i,j}^0$ and $v_{i,j}^0$, outer iteration from steps (b) to (e) is repeated until equation (3.26) is satisfied.
- (g) The obtained $w_{i,j}$ and $\theta_{i,j}$ are used to calculate the flow and heat transfer characteristics.

The expression for the parameter $ReRa$ can be obtained from equation (3.8) as

$$ReRa = 2\bar{w} RaC .$$

The number of inner iterations in steps (b), (c) and (d) is not very restrictive. In this study, it is set to be less than 30.

3.4 Flow and Heat Transfer Results

The product of friction factor and Reynolds number (fRe) and the Nusselt number (Nu) can be obtained by considering either the average values for velocity and temperature gradients, respectively, along the pipe wall, or the overall force and energy balances, respectively for the axial length dZ . The results are

$$\begin{aligned}
 (fRe)_I &= \frac{2\bar{\tau}_w}{\rho\bar{W}^2} \cdot \frac{2a\bar{W}\rho}{\mu} = 4 \frac{\bar{W} \left| \frac{\partial \bar{W}}{\partial r} \right|_w}{\bar{W}} \\
 (fRe)_{II} &= \frac{8}{\bar{W}} \\
 (Nu)_I &= \frac{\bar{h}(2a)}{k} = 2 \cdot \frac{\bar{W} \left| \frac{\partial \bar{\theta}}{\partial r} \right|_w}{\left| \bar{W}\bar{\theta} \right|} \\
 (Nu)_{II} &= \frac{\bar{W}^2}{\left| \bar{W}\bar{\theta} \right|}
 \end{aligned} \tag{3.27}$$

where subscript I denotes the value of the parameter obtained from the average gradient along the pipe wall and subscript II denotes the value of the parameter obtained from the overall balance. Simpson's rule is used to obtain the average quantities indicated above.

In order to show the convergence of the numerical solu-

tion, the ratio of the Nusselt numbers $Nu/(Nu)_0$ is plotted against the parameter $ReRa$ in Fig. 3.3 for two different mesh sizes $M = 20, N = 10$ and $M = 40, N = 20$, using central and two point non-central differences for the nonlinear terms. It is seen that the heat transfer results obtained from the above two definitions coincide, using central difference with mesh size $M = 40$ and $N = 20$, indicating the accuracy of the numerical solution.

For comparison, the heat transfer results from Morton's analysis [3.3] using perturbation method and Mori and Futagami's boundary-layer approximation [3.5] are also shown in Fig. 3.3 for the case $Pr = 1$. It is seen clearly that for the values of the parameter $ReRa$ ranging approximately from 2×10^3 to 4×10^4 , neither the perturbation method nor the boundary-layer approximation is effective. In contrast, the numerical solution clearly bridges the gap between the perturbation solution and the boundary-layer approximation. Relative merits of these three methods are of interest.

In order to further assess the accuracy of the numerical solution, the axial velocity and temperature profiles along the central vertical line from this analysis are compared against the experimental data given in [3.6] and theoretical curves given in [3.5] for $Pr = 0.72$ and $ReRa = 0.89 \times 10^5$ in Fig. 3.4. A good agreement is observed between the numerical solution and the experimental data for the velocity distribution. Numerical solution predicts higher value than

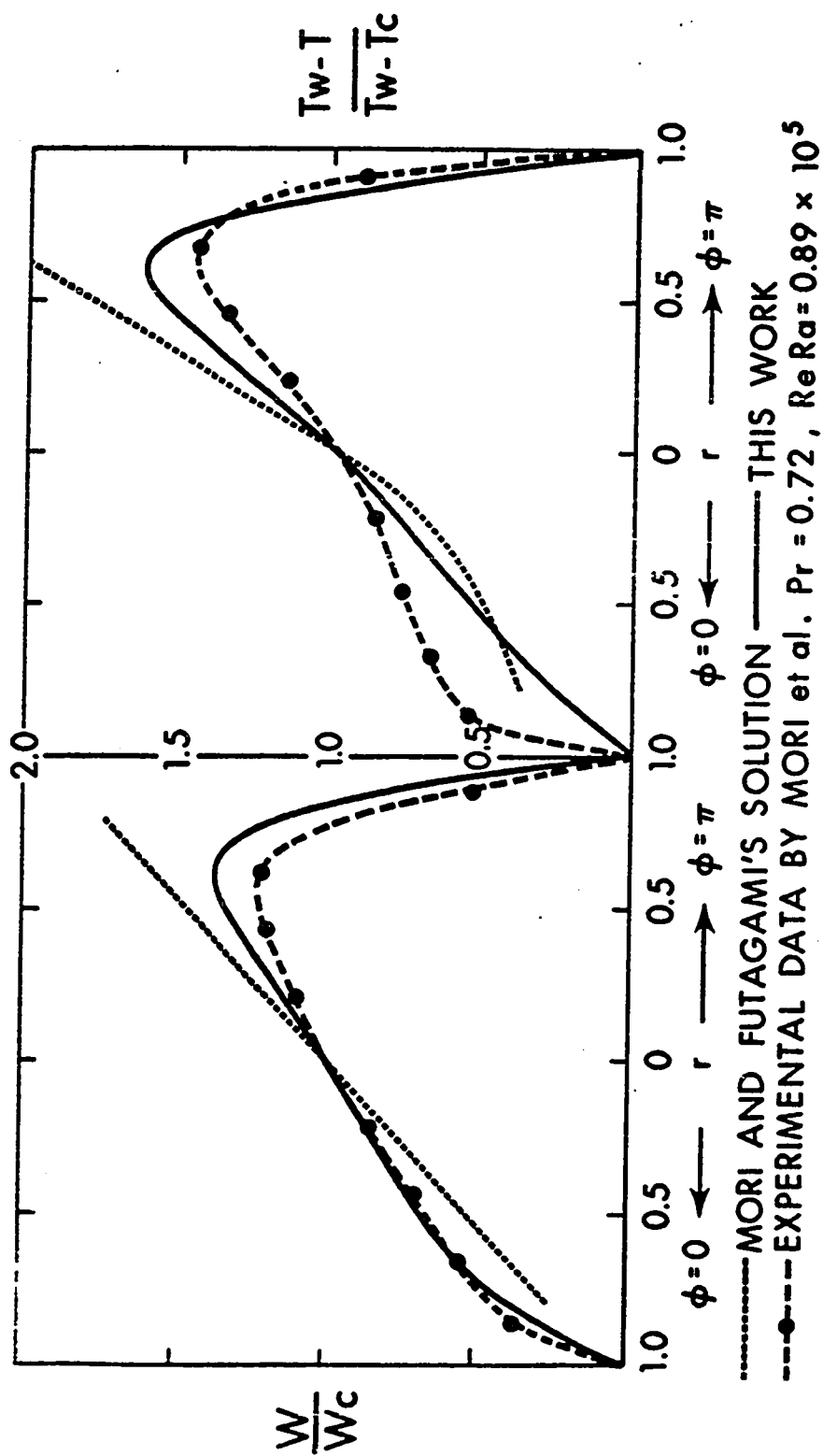


Fig. 3.4 Comparison of velocity and temperature distributions along central vertical line from the present study with experimental and theoretical results from Mori et al.

experimental data near the bottom and slightly lower value near the top ($\phi = 0$). Similar remarks also apply to the temperature profiles with the exception that rather substantial discrepancy exists between numerical solution and experimental data near the top ($\phi = 0$). In Fig. 3.5, the experimental data [3.6] are further compared with the numerical results for the same value of $Nu/(Nu)_0 = 1.62$ but at different $ReRa (= 5.04 \times 10^4)$. The general trend is similar but the discrepancy reduces somewhat. One further comparison at higher value of $Nu/(Nu)_0 = 2.0$ is shown in Fig. 3.6. A rather good agreement is found for velocity profiles. For temperature profiles, experimental and numerical data check quite well near the bottom part ($\phi = \pi$) and an improved agreement is observed near the top part ($\phi = 0$) as compared with those shown in Figs. 3.4 and 3.5.

Summarizing the above comparisons, it can be said that the agreement for velocity profile is quite good and the agreement for temperature profile is reasonable near the bottom part but rather poor near the top part ($\phi = 0$). This inconsistency in temperature distribution needs further consideration. For the region in question, $r = 0 \sim 1.0$ and $\phi = 0$, it is clear that the temperature distributions from the experimental data and numerical solution are definitely on the opposite side of the temperature distribution for the case of pure forced convection without secondary flow. Focusing our attention on temperature distribution along the vertical

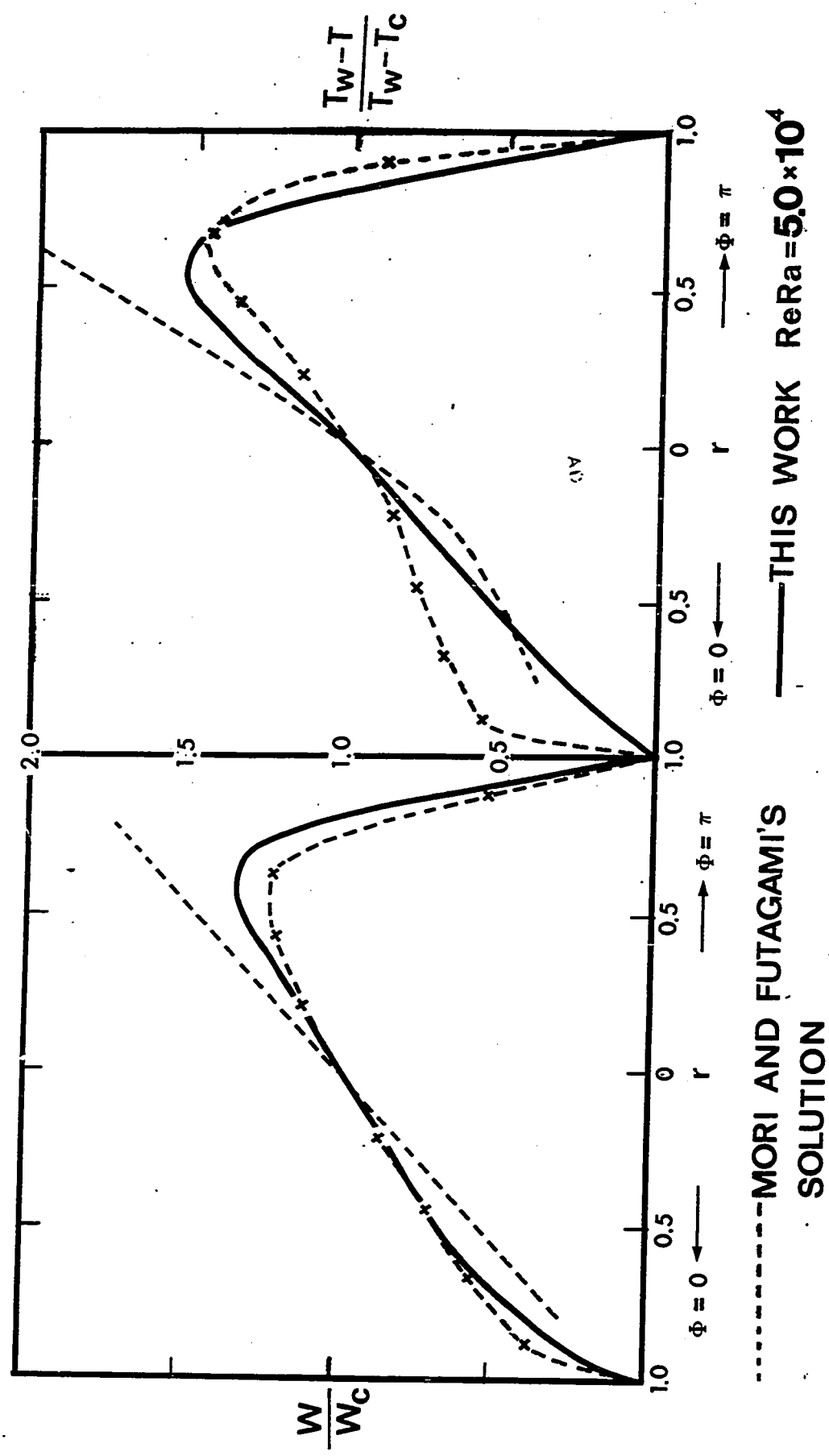


Fig. 3.5 Comparison of velocity and temperature distributions along central vertical line from the present study with experimental data from Mori et al.

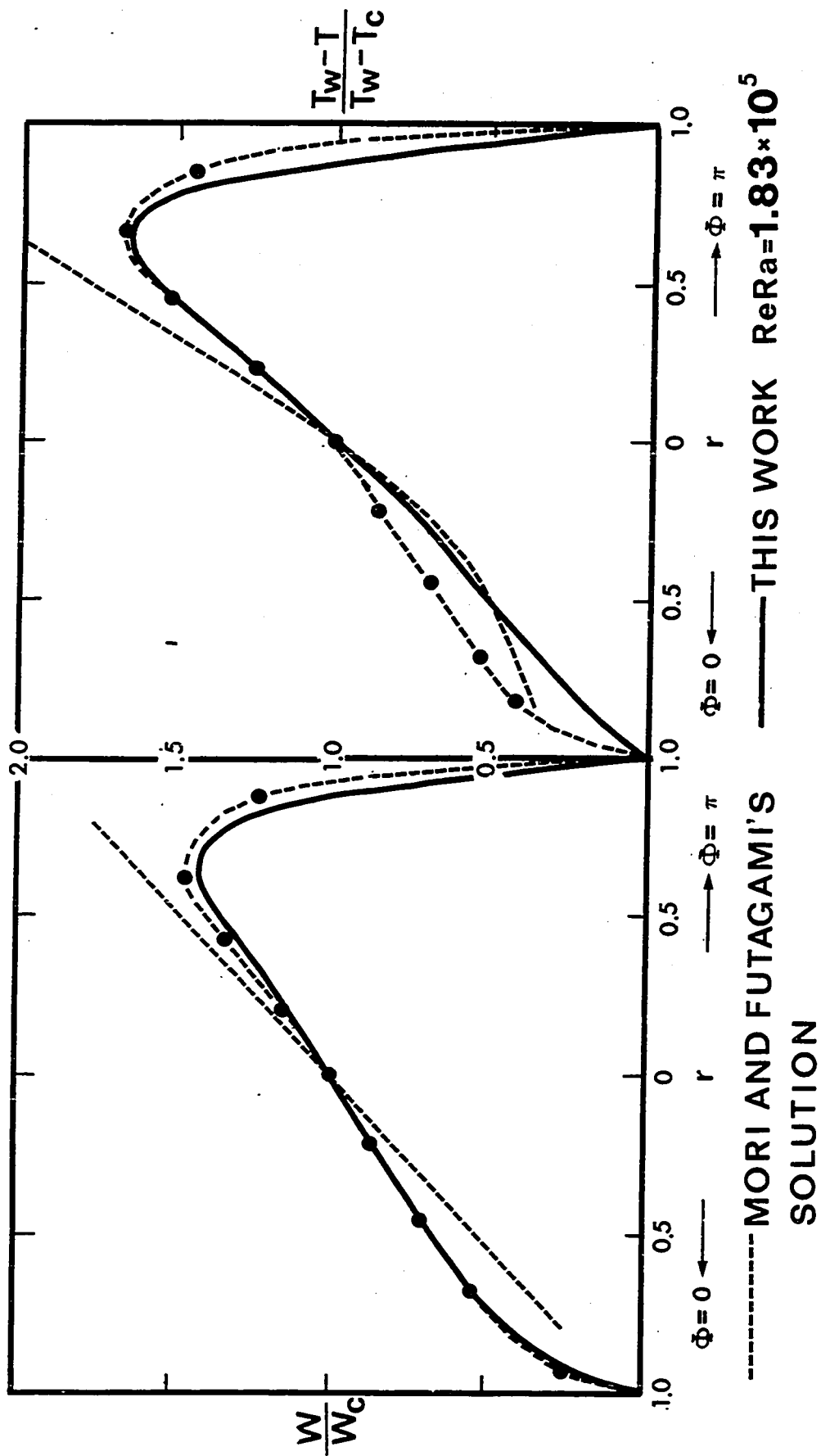


Fig. 3.6 Comparison of velocity and temperature distributions along central vertical line from the present study with experimental data from Mori et al.

center line, it is well known that the effect of the buoyancy force is to shift the location of the maximum value toward the bottom wall and decrease the magnitude of the value near the top wall. The discrepancy may be caused by the difference between the assumption of uniform circumferential wall temperature in the theoretical analysis and the probable non-uniform distribution of wall temperature in the experiment. The theoretical curves given by Mori and Futagami [3.5] are seen to be inadequate for $ReRa = 0.89 \times 10^5$ as shown in Fig. 3.4. The above discrepancy between experimental data and numerical solution is also reflected in the heat transfer result which will be discussed later. We also note that the assumption of uniform boundary-layer thickness along the circumference in the boundary-layer approximation may also lead to some errors near the top and bottom walls.

The streamlines and isothermals for $Pr = 0.72$ and $ReRa = 0.8976 \times 10^5$ are shown in Fig. 3.7. The temperature drops very gradually from the top to the center. This behavior clearly contradicts the experimental data. As the parameter $ReRa$ increases, the centers of circulation move toward the side walls.

The distributions of secondary velocity components u , v for representative values of $ReRa$ with $Pr = 0.72$ are shown in Fig. 3.8. It is seen that the downward velocity component v becomes more uniformly distributed in the core region as $ReRa$ increases. This trend confirms the asymptotic

center line, it is well known that the effect of the buoyancy force is to shift the location of the maximum value toward the bottom wall and decrease the magnitude of the value near the top wall. The discrepancy may be caused by the difference between the assumption of uniform circumferential wall temperature in the theoretical analysis and the probable non-uniform distribution of wall temperature in the experiment. The theoretical curves given by Mori and Futagami [3.5] are seen to be inadequate for $ReRa = 0.89 \times 10^5$ as shown in Fig. 3.4. The above discrepancy between experimental data and numerical solution is also reflected in the heat transfer result which will be discussed later. We also note that the assumption of uniform boundary-layer thickness along the circumference in the boundary-layer approximation may also lead to some errors near the top and bottom walls.

The streamlines and isothermals for $Pr = 0.72$ and $ReRa = 0.8976 \times 10^5$ are shown in Fig. 3.7. The temperature drops very gradually from the top to the center. This behavior clearly contradicts the experimental data. As the parameter $ReRa$ increases, the centers of circulation move toward the side walls.

The distributions of secondary velocity components u , v for representative values of $ReRa$ with $Pr = 0.72$ are shown in Fig. 3.8. It is seen that the downward velocity component v becomes more uniformly distributed in the core region as $ReRa$ increases. This trend confirms the asymptotic

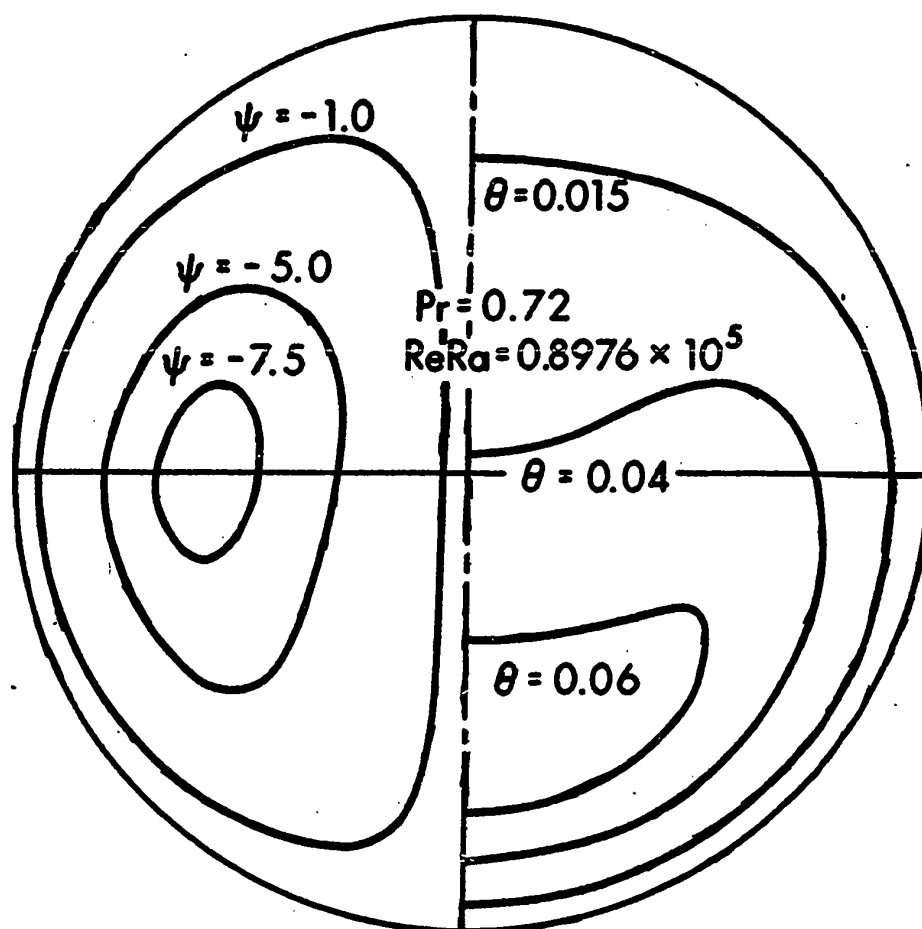


Fig. 3.7 Streamlines and isothermals

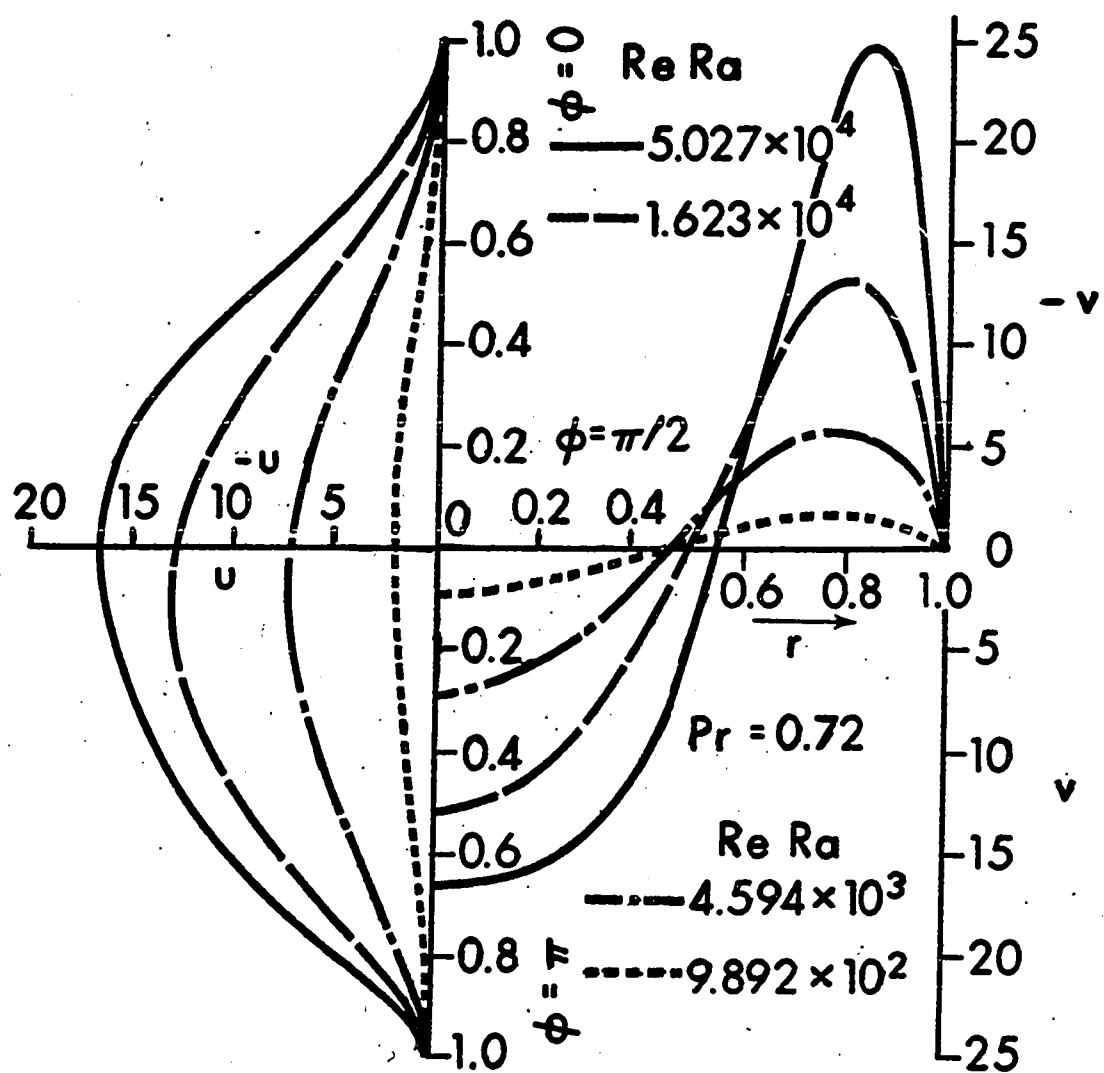


Fig. 3.8 Distributions of secondary flow velocity components u , v

behavior of Mori and Futagami's boundary-layer approximation [3.5]. But the distribution of radial velocity u along the vertical central axis is not symmetric with respect to the horizontal central axis. This contradicts with Mori and Futagami's assumption [3.5].

The effect of Prandtl number on flow result is shown in Fig. 3.9 where $fRe/(fRe)_0$ is plotted against $ReRa$. This figure serves to show the range of applicability in terms of the parameter $ReRa$ for both boundary-layer approximation and numerical solution. It is seen that for the range considered, considerable discrepancy exists between the two predictions. However, it appears that at higher value of the parameter the two predictions approach each other. It is noted that the effect of Prandtl number on friction factor is negligible for large Prandtl number.

The effect of Prandtl number on heat transfer result is shown in Fig. 3.10 where $Nu/(Nu)_0$ is plotted against $ReRa$ with Prandtl number as a parameter. For $Pr = 1$, the two curves from boundary-layer approximation and numerical solution approach each other at around $ReRa = 4 \times 10^4$ indicating good agreement thereon. However, for the case $Pr = 0.72$ considerable difference exists between the two results aside from the fact that boundary-layer approximation cannot be applied to the low $ReRa$ region. It is also seen that the effect of Prandtl number on $Nu/(Nu)_0$ is similar to the effect of $ReRa$ on the ratio $Nu/(Nu)_0$.

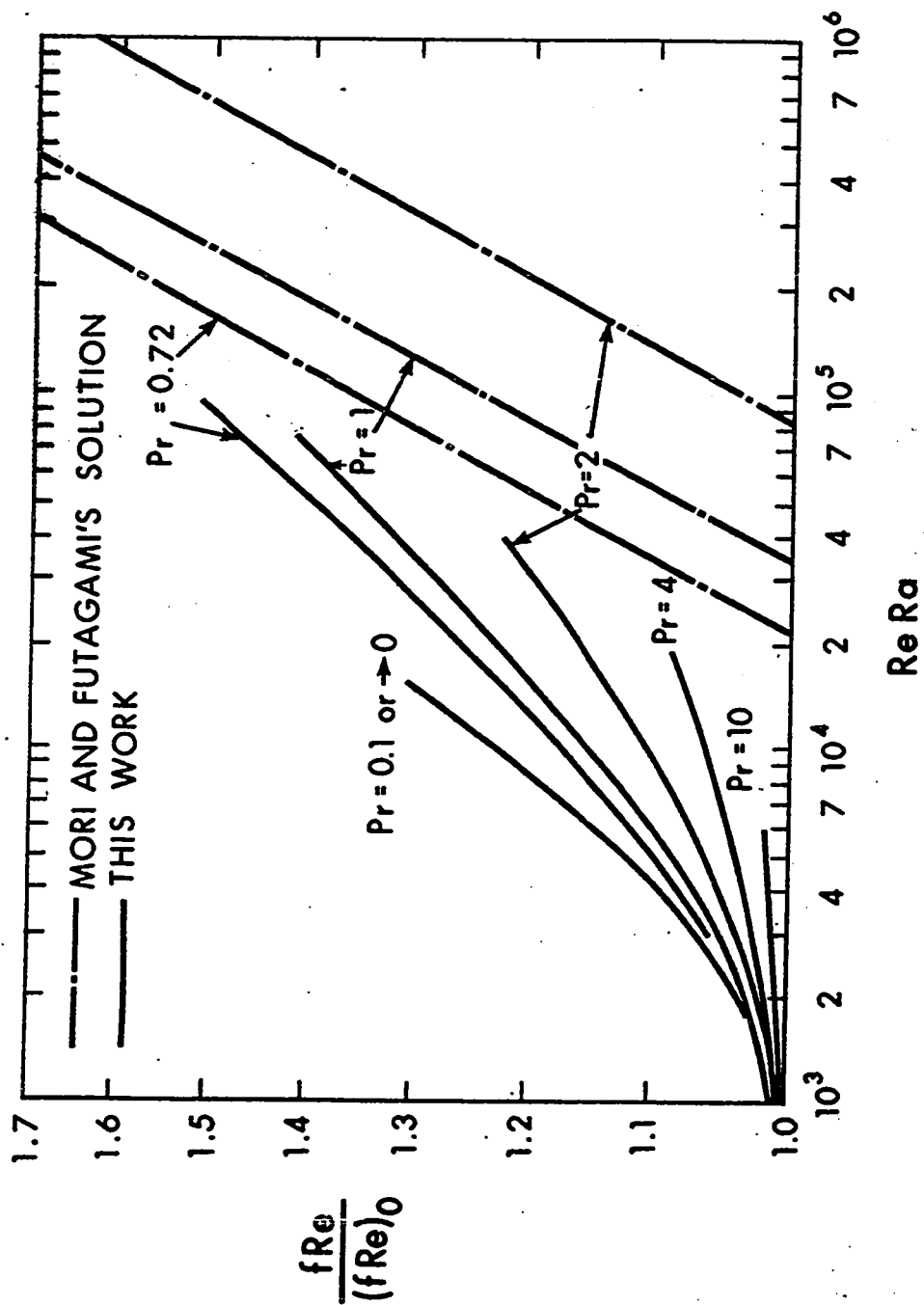


Fig. 3.9 $fRe/(fRe)_0$ versus $ReRa$

The result of numerical solution for heat transfer shows clearly that an asymptotic line exists for each Prandtl number. Consequently, for $Nu/(Nu)_0 > 1.75$, an estimate for heat transfer result may be made by extending the existing curves linearly in Fig. 3.10. Fig. 3.10 also shows clearly the respective range of applicability for the perturbation method, numerical method, and boundary-layer approximation.

In Fig. 3.10, it is of interest to observe that the distance between the curves $Pr = 1$ and $Pr = 10$ almost equals to the distance between the curves $Pr = 10$ and $Pr = 100$ for a given value of $Nu/(Nu)_0$. This observation enables us to study the asymptotic behavior for $Pr \rightarrow \infty$. For the case when $Pr \rightarrow \infty$ and the secondary motion is weak, the nonlinear terms in momentum equations (3.10) and (3.12) are negligible. On the contrary, the advective terms in the energy equation (3.13) should be retained in view of the large Prandtl number effect. Based on the above observation, the two parameters Pr and RaC can be combined into one parameter $PrRaC$ characterizing the asymptotic solution for $Pr \rightarrow \infty$. The parameter $PrRaC$ also can be transformed into $PrReRa$ by using the relation $C = Re/(2\bar{w})$ in equation (3.8). The curves for $Nu/(Nu)_0$ versus the new coordinate $PrReRa$ with Pr as a parameter are shown in Fig. 3.11. The curve corresponding to $N = 0.471 (GP)^{1/4}$ given by Siegwarth et al. [3.8] is also shown after transforming into $Nu/(Nu)_0 = 0.190 (PrReRa)^{1/5}$ by using the relation $GP = PrReRa/(2Nu)$. As pointed out in the Introduction (Section 3.1),

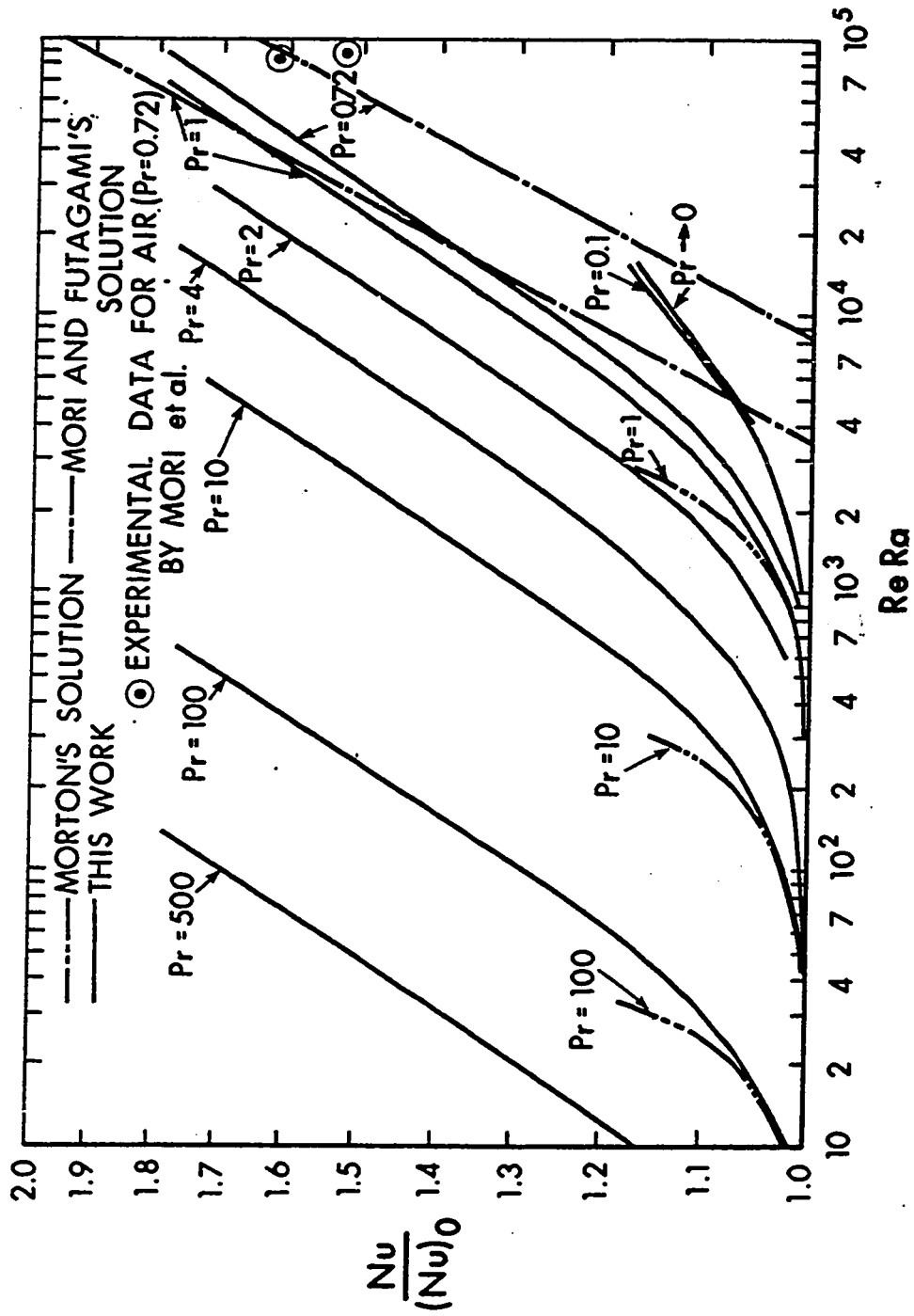


Fig. 3.10 $Nu/(Nu)_0$ versus $Re Ra$

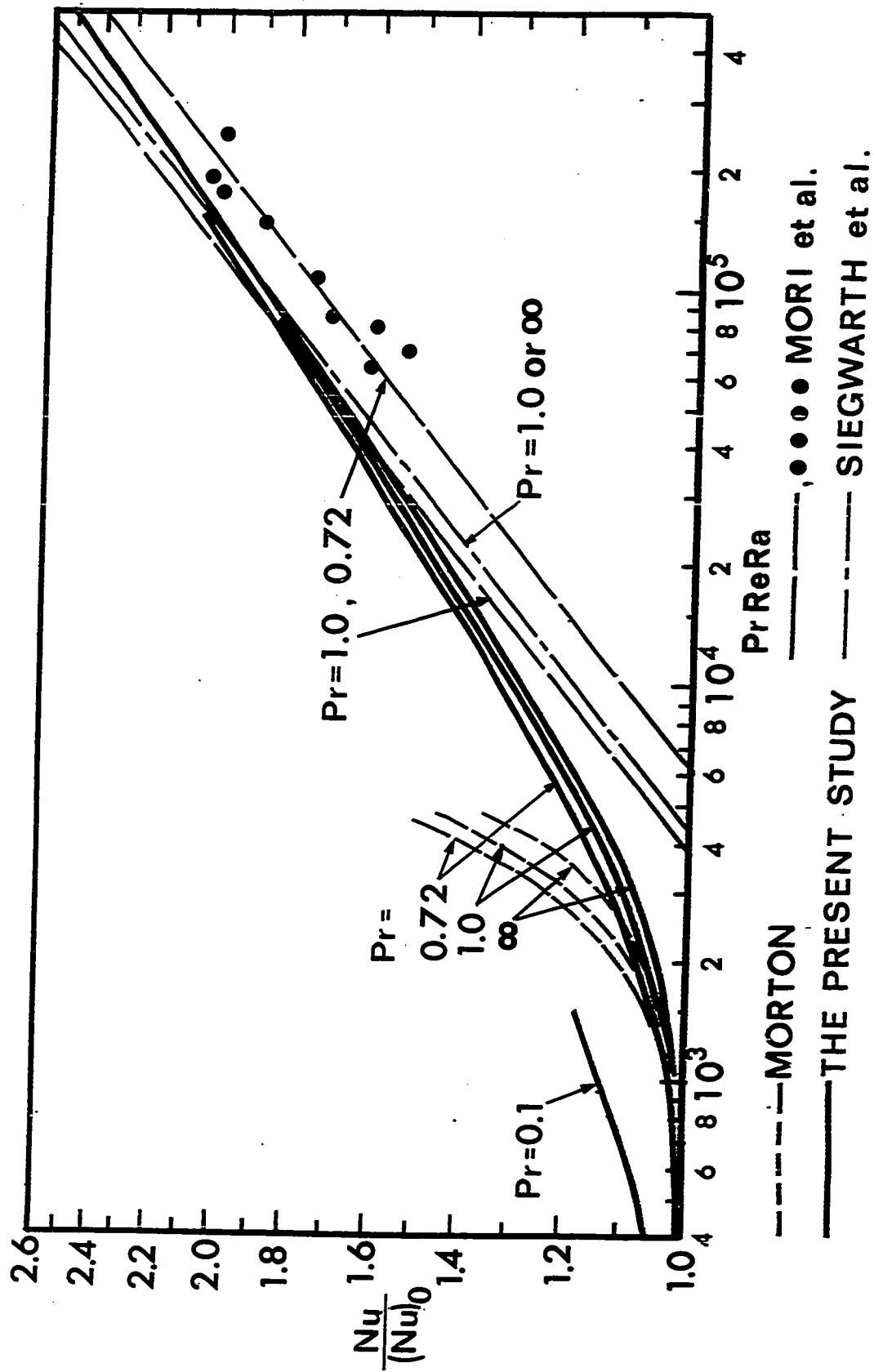


Fig. 3.11 New correlation based on $Nu/(Nu)_0$ versus $Pr Re Ra$

this curve deviates from Mori and Futagami's solution for $Pr = 1$ [3.5] by only about 1.5%. It is noted that for the case of $Pr = 0.72$, the curve obtained by Mori and Futagami [3.5] contradicts with both the present numerical solution and the perturbation method [3.3]. For the same value of $PrReRa$, the numerical and perturbation solutions predict higher heat transfer rate in the case of smaller Prandtl number. It is significant to note that with the present new correlation the numerical solution for $Pr = 0(1)$ already approaches the asymptotic solution for $Pr \rightarrow \infty$. Furthermore, Siegwirth et al. [3.8] also show that the curves for $Pr = 1$ and $Pr \rightarrow \infty$ are identical. In other words, with Prandtl numbers ranging from $0(1)$ to ∞ , a simple correlation for heat transfer results exists for various Prandtl numbers ($Pr = 0(1) \sim \infty$). For example, the heat transfer result is identical for a given value of $PrReRa$ regardless of the value of Pr within the range of $Pr = 0(1) \sim \infty$. This observation is believed to be significant since separate numerical solution is not required for various Prandtl numbers ranging from $0(1)$ to ∞ . The numerical results for flow and heat transfer are listed in the Appendix for possible future reference.

3.5 Concluding Remarks

(a) The application of the boundary vorticity method in this numerical study is very successful with tremendous improvement in computing efficiency. It is believed to have wide applicability in solving the related similar problems.

(b) A combination of using Cartesian coordinates at the center and cylindrical coordinates elsewhere proves to be quite satisfactory to overcome the singularity at the center. The treatment is quite general and can be readily applied to the numerical computation of the other engineering problems formulated in polar coordinates.

(c) The numerical solution is effective up to a reasonably high value of the parameter and clearly fills the gap between the perturbation method and the boundary-layer approximation. The above observation is important since the same remark applies also to a class of broadly similar secondary flow problems.

(d) Plotting of all the numerical results for various Prandtl numbers based on $Nu/(Nu)_0$ versus $PrReRa$ reveals that the Nusselt number for Prandtl number of order one already approaches the asymptotic solution for the case of $Pr \rightarrow \infty$. This observation is significant since it suggests that we need not carry out separate numerical solution for various Prandtl numbers ranging from order one to infinity in order to study the Prandtl number effect. This aspect of Prandtl number effect points out the possibility of solving

Graetz problem with buoyancy effect in the thermal entrance region.

(e) The results of the numerical analysis presented are valid within the Boussinesq approximation. The dependency of physical properties on temperature can also be readily accommodated.

References

- 3.1 Hwang, G.J., and Cheng, K.C., "Boundary Vorticity Method for Convective Heat Transfer with Secondary Flow - Application to the Combined Free and Forced Laminar Convection in Horizontal Tubes," Proceedings, Fourth International Heat Transfer Conference, Vol. 4, Paris-Versailles, 1970, NC 3.5.
- 3.2 Trefethen, L., "Fluid Flow in Radial Rotating Tubes," IX^e Congr s International de M canique Appliqu e, Universit  de Bruxelles, Vol. 2, 1957, pp. 341-351.
- 3.3 Morton, B.R., "Laminar Convection in Uniformly Heated Horizontal Pipes at Low Rayleigh Numbers", Quarterly Journal of Mechanics and Applied Mathematics, Vol. 12, Pt. 4, 1959, pp. 410-420.
- 3.4 del Casal, E., and Gill, W.N., "A Note on Natural Convection Effects in Fully Developed Horizontal Tube Flow," AIChE Journal, Vol. 8, No. 4, 1962, pp. 570-574.
- 3.5 Mori, Y., and Futagami, K., "Forced Convective Heat Transfer in Uniformly Heated Horizontal Tubes (2nd Report, Theoretical Study)," International Journal of Heat and Mass Transfer, Vol. 10, No. 12, 1967, pp. 1801-1813.

- 3.6 Mori, Y., et al., "Forced Convective Heat Transfer in Uniformly Heated Horizontal Tubes, 1st Report - Experimental Study on the Effect of Buoyancy," International Journal of Heat and Mass Transfer, Vol. 9, No. 5, 1966, pp. 453-463.
- 3.7 Faris, G.N., and Viskanta, R., "An Analysis of Laminar Combined Forced and Free Convection Heat Transfer in A Horizontal Tube," International Journal of Heat and Mass Transfer, Vol. 12, 1969, pp. 1295-1309.
- 3.8 Siegwarth, D.P., et al., "Effect of Secondary Flow on the Temperature Field and Primary Flow in a Heated Horizontal Tube," International Journal of Heat and Mass Transfer, Vol. 12, No. 12, 1969, pp. 1535-1552.

Appendix 3.1 Numerical Results

$$fRe = [(fRe)_I + (fRe)_{II}]/2, \quad Nu = [(Nu)_I + (Nu)_{II}]/2$$

RaC	$\bar{w} \times 10$	$\overline{w\theta} \times 10^2$	$(fRe)_0$	$(Nu)_0$
0	5.0	5.729	16.0	4.364

Pr = 0

RaC $\times 10^{-4}$	$\bar{w} \times 10$	$\overline{w\theta} \times 10^2$	fRe	Nu
0.1	4.944	5.563	16.17	4.392
0.3	4.719	4.943	16.95	4.503
0.5	4.508	4.394	17.75	4.622
0.7	4.338	3.981	18.45	4.725
1.0	4.153	3.557	19.27	4.845
2.0	3.813	2.867	20.95	5.083

Pr = 0.1

RaC $\times 10^{-4}$	$\bar{w} \times 10$	$w\theta \times 10^2$	fRe	Nu
0.1	4.944	5.560	16.17	4.394
0.2	4.840	5.265	16.52	4.445
0.3	4.722	4.944	16.94	4.507
0.5	4.514	4.401	17.73	4.629
0.7	4.348	3.989	18.40	4.736
1.0	4.166	3.565	19.21	4.864
2.0	3.834	2.859	20.87	5.138

Pr = 0.72

$RaC \times 10^{-4}$	$\bar{w} \times 10$	$\bar{w\theta} \times 10^2$	fRe	Nu
0.1	4.946	5.525	16.17	4.425
0.2	4.854	5.183	16.48	4.542
0.3	4.756	4.836	16.81	4.674
0.5	4.594	4.288	17.41	4.919
0.7	4.471	3.902	17.90	5.122
1.0	4.331	3.495	18.48	5.369
2.0	4.058	2.782	19.72	5.921
4.0	3.795	2.204	21.07	6.535
7.0	3.591	1.823	22.28	7.072
10.0	3.439	1.611	23.24	7.399
20.0	3.199	1.263	25.05	8.196
30.0	3.049	1.074	26.30	8.742
35.0	2.988	1.002	26.81	8.981
40.0	2.945	0.9571	27.25	9.160
42.0	2.927	0.9377	27.41	9.233

Pr = 1

$RaC \times 10^{-4}$	$\bar{w} \times 10$	$\bar{w\theta} \times 10^2$	fRe	Nu
0.03	4.988	5.678	16.03	4.379
0.06	4.974	5.616	16.08	4.404
0.1	4.947	5.493	16.16	4.452
0.2	4.861	5.117	16.45	4.615
0.3	4.773	4.758	16.75	4.786
0.5	4.630	4.220	17.28	5.079
1.0	4.395	3.459	18.20	5.587
2.0	4.142	2.774	19.31	6.184

Pr = 1

$RaC \times 10^{-4}$	$\bar{w} \times 10$	$\bar{w\theta} \times 10^2$	fRe	Nu
5.0	3.807	2.051	21.01	7.067
10.0	3.551	1.607	22.53	7.847
15.0	3.397	1.378	23.54	8.366
20.0	3.287	1.232	24.33	8.764
25.0	3.182	1.109	25.06	9.102
70.0	2.795	0.7187	28.48	10.80

Pr = 2

$RaC \times 10^{-4}$	$\bar{w} \times 10$	$\bar{w\theta} \times 10^2$	fRe	Nu
0.06	4.975	5.539	16.07	4.465
0.1	4.952	5.343	16.15	4.587
0.3	4.826	4.504	16.57	5.170
0.6	4.685	3.833	17.07	5.724
1.0	4.556	3.354	17.55	6.187
3.0	4.236	2.447	18.88	7.331
5.0	4.072	2.085	19.64	7.953

Pr = 4

$RaC \times 10^{-4}$	$\bar{w} \times 10$	$\bar{w\theta} \times 10^2$	fRe	Nu
0.06	4.977	5.331	16.07	4.645
0.1	4.961	5.024	16.12	4.897
0.2	4.921	4.490	16.25	5.391
0.4	4.855	3.923	16.47	6.006
0.7	4.781	3.479	16.72	6.568
1.0	4.724	3.207	16.92	6.957
2.0	4.596	2.707	17.40	7.799

Pr = 10

$RaC \times 10^{-3}$	$\bar{w} \times 10$	$\overline{w\theta} \times 10^2$	fRe	Nu
0.03	4.996	5.703	16.01	4.375
0.06	4.996	5.679	16.01	4.394
0.1	4.996	5.626	16.01	4.434
0.2	4.994	5.445	16.02	4.578
0.4	4.988	5.076	16.03	4.898
0.7	4.982	4.686	16.05	5.293
1.0	4.976	4.422	16.07	5.595
2.0	4.958	3.923	16.13	6.264
3.0	4.945	3.647	16.17	6.701
4.0	4.933	3.459	16.21	7.033
6.0	4.913	3.201	16.28	7.537

Pr = 100

$RaC \times 10^{-2}$	$\bar{w} \times 10$	$\overline{w\theta} \times 10^2$	fRe	Nu
0.1	4.997	5.628	16.01	4.434
0.2	4.998	5.453	16.01	4.578
0.5	4.998	4.946	16.01	5.047
1.0	4.998	4.450	16.01	5.610
2.0	4.997	3.965	16.01	6.295
3.0	4.997	3.701	16.01	6.744
5.0	4.997	3.388	16.01	7.366
6.0	4.996	3.281	16.01	7.606

Pr = 500

$RaC \times 10^{-1}$	$\bar{w} \times 10$	$\overline{w\theta} \times 10^2$	fRe	Nu
1.0	4.998	4.945	16.01	5.048
3.0	4.998	4.161	16.00	6.000
6.0	4.999	3.701	16.00	6.748

CHAPTER IV

THERMAL INSTABILITY IN PLANE POISEUILLE FLOW*

4.1 Introduction

In order to predict flow and heat transfer characteristics for forced convection under the effect of body forces, it is necessary under certain conditions to investigate the onset of secondary motion and determine the most probable flow pattern. Body forces acting in a direction normal to the main flow can cause a pair of helical vortex rolls, for examples, in a heated horizontal rectangular Channel [2.5] or a curved rectangular Channel [4.2]. In these cases, the secondary flow appears as soon as the fluid is brought into motion in the axial direction. However, when the aspect ratio ((side length in a direction normal to the body force)/(side length in a direction parallel to the body force)) of the rectangular channel approaches infinity, the body forces may leave no effect on the main flow with small body force parameter and provides merely a potential of instability. As the parameter increases beyond a certain value, the flow can no longer maintain its original pattern and the secondary motion results. The well-known examples are the Taylor vortices [4.3] developed between rotating concentric cylinders

* The work reported in [4.1] is based on this part of the dissertation.

and Bénard cell [4.4] formed in a thin fluid layer heated from below. Gill and del Casal [4.5] analysed the effect of buoyancy and variable viscosity on two-dimensional velocity profiles and gave a qualitative discussion on the instability of the flow in view of Tollmien-Schlichting theory. However, they did not consider stationary vortex-type secondary flow. Recently, Mori and Uchida [4.6] examined forced convective heat transfer between horizontal flat plates. The instability of the flow in their problem is caused by a linear basic temperature distribution only. Thus, the critical Rayleigh number 1708 is exactly the same as the one observed in the classical Bénard's problem [4.7]. Sparrow, Goldstein and Jonsson [4.8] studied the thermal instability in a horizontal fluid layer considering the effect of boundary conditions and nonlinear temperature profile caused by uniform internal heat generation. Their results show that parabolic part of the basic temperature profile destabilizes the flow and changes the wavelength of the vortex rolls.

The purpose of this chapter is to investigate the possibility of the onset of longitudinal vortex rolls for fully developed laminar forced convection between two infinite horizontal parallel plates with a constant axial temperature gradient and at different or identical temperature levels at the upper and lower plates. For the present problem, the uniform temperature gradient along the main flow direction also yields a nonlinear temperature profile. The convective

motion of the main flow disturbance also affects the critical Rayleigh number and changes the wavelength of the vortex rolls. Thus, the instability of the flow can be considered to depend on the following four factors:

- (a) the wave number, $a = 2\pi h/(\text{wavelength})$, which characterizes the mode of disturbance,
- (b) the linear part of the basic temperature profile,
- (c) the nonlinear part of the basic temperature profile,
- (d) the convective motion of the main flow direction disturbance.

We note that the factors (a) and (b) constitute the problem studied by Mori and Uchida [4.6] and the factors (a), (b) and (c) govern the problem studied by Sparrow, Goldstein and Jonsson [4.8]. It is evident that one additional factor is brought into consideration in the present study. Furthermore, from the physical point of view, this problem can be considered to be more general as compared with the two earlier works [4.6, 4.8]. It is worthwhile to point out an interesting limiting case. If the vertical gradient of the linear basic temperature profile is negligibly small in comparison with that of the nonlinear part, then the factors (a), (c) and (d) determine the flow. This situation corresponds to the limiting case of axially uniformly heated horizontal rectangular channel [2.5] where the aspect ratio (width/height) approaches infinity.

An eighth order ordinary differential equation with

eigenvalue R_a will be derived for the present problem and solved by employing a power series similar to that used in [4.8].

4.2 Theoretical Analysis

Consider a fully developed laminar flow between two horizontal parallel plates with a constant axial temperature gradient τ and a temperature difference ΔT between the upper and lower plates at any axial position. The system of coordinates is shown in Fig. 4.1 where two infinite horizontal flat plates are located at $z' = 0$ and h , respectively. Under certain conditions, an infinite number of pairs of vortex rolls with alternating flow direction may appear between the upper and lower plates. The wall temperatures on the bottom and top plates are shown in Fig. 4.2 and can be expressed as

$$T_1 = T_0 + \tau x', \quad T_2 = T_1 - \Delta T = T_0 - \Delta T + \tau x' \quad (4.1)$$

where ΔT is the temperature difference between the two plates which may be negative, zero and positive depending on the relative magnitude of T_1 and T_2 . Each case has its own significance in the practical problem. The constant τ is the axial temperature gradient. The fully developed basic velocity and temperature distributions are illustrated in Fig. 4.3 and the expressions for the unperturbed state are

$$\frac{U_b}{U_0} = 4\left(\frac{z'}{h}\right) \left[1 - \left(\frac{z'}{h}\right)\right] = \frac{\phi_u}{2} \quad (4.2)$$

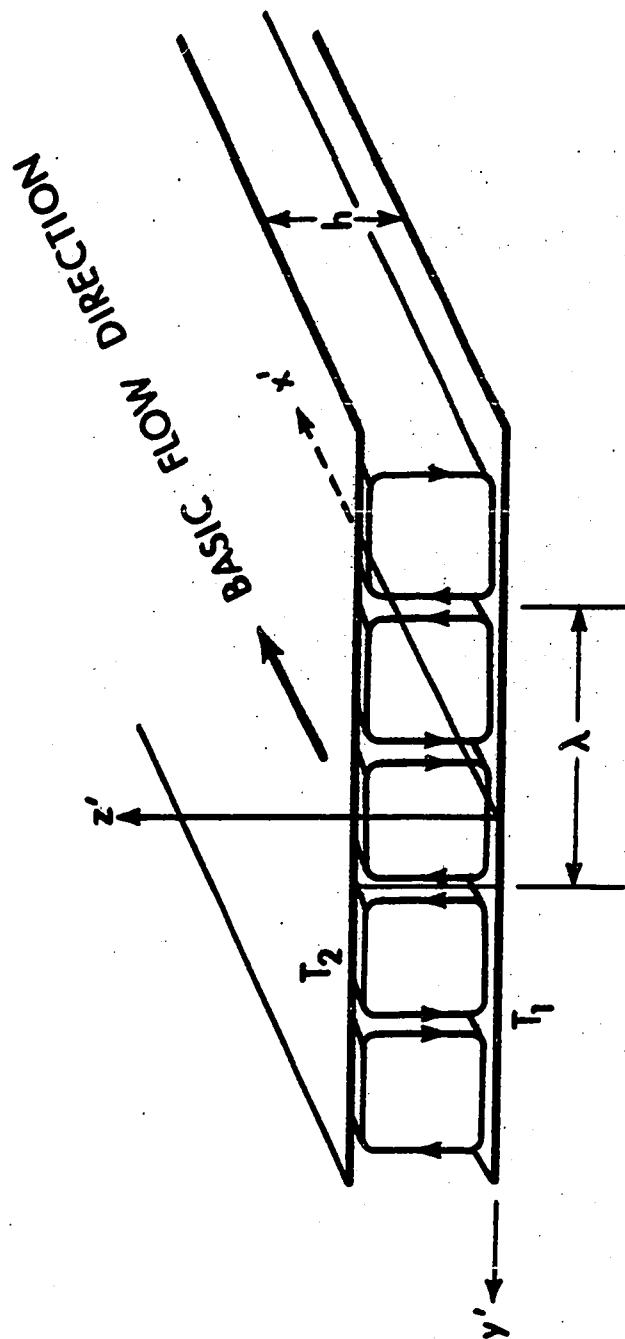


Fig. 4.1 System of coordinates

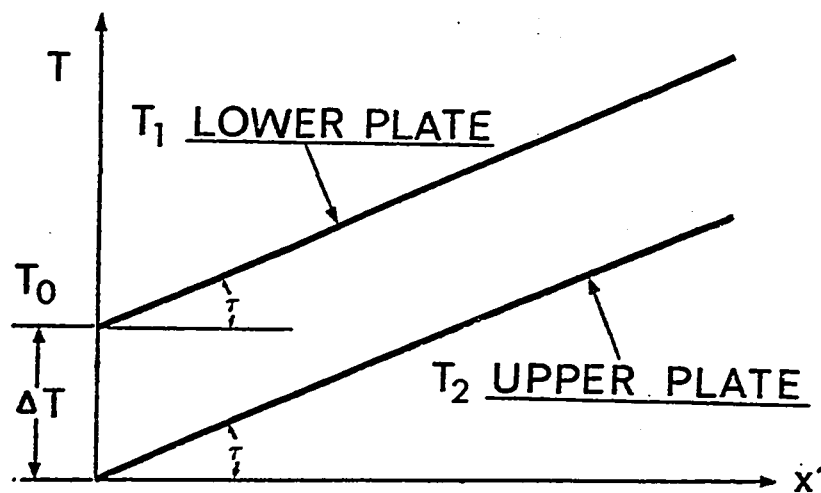


Fig. 4.2 Thermal boundary conditions on the bottom and top plates

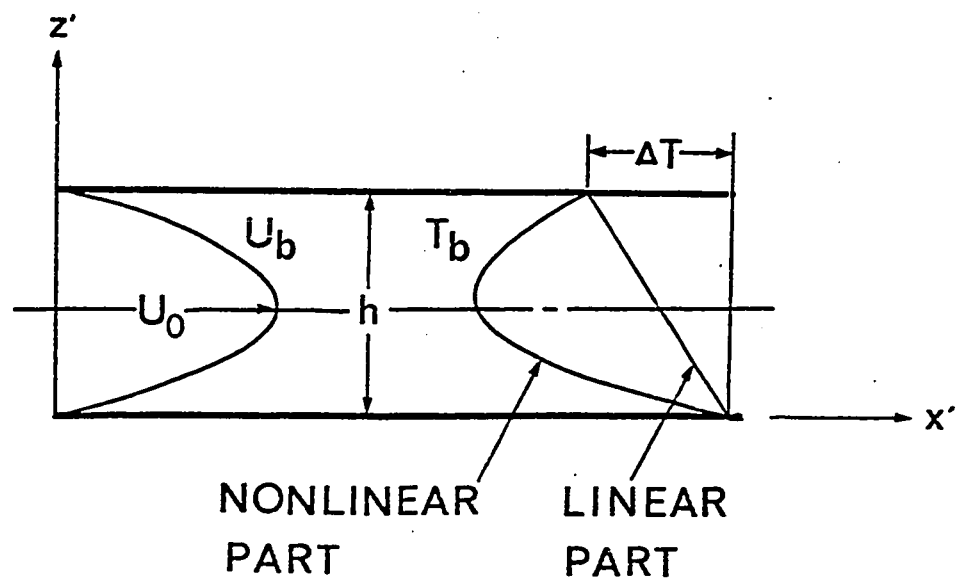


Fig. 4.3 Fully developed velocity and temperature distributions in the unperturbed state

$$\begin{aligned} \frac{T_b - T_1}{\Delta T} &= -\frac{2}{3} \text{Pr} \mu \left(\frac{z'}{h}\right) \left[1 - 2\left(\frac{z'}{h}\right)^2 + \left(\frac{z'}{h}\right)^3\right] - \left(\frac{z'}{h}\right) \\ &= -\text{Pr} \mu \phi_\theta(z) - z \end{aligned} \quad (4.3)$$

where U_0 is the maximum velocity in the unperturbed state, Pr is Prandtl number and $\mu = \text{Re} h / \Delta T$. It is noted that the characteristic parameter μ represents the effect of longitudinal wall temperature gradient for the present problem, and $\text{Pr} \mu$ the magnitude of departure of T_b from the linear distribution.

The following assumptions are made to facilitate the analysis:

- (a) Boussinesq approximation is valid,
- (b) physical properties are constant,
- (c) disturbance quantities and their derivatives are taken to be sufficiently small for their products to be neglected, i.e., the equations are linearized following a procedure commonly employed in linear stability analysis.

In order to investigate the conditions under which the steady fully developed laminar convection is stable against small disturbances, we superimpose the perturbations on the basic flow quantities as

$$U = U_b + u', \quad V = v', \quad W = w', \quad T = T_b + \theta' \quad \text{and} \quad P = P_b + p' \quad (4.4)$$

where U , V and W are velocity components in the x' , y' and z'

directions, respectively. Introducing the non-dimensional quantities,

$$(x,y,z) = (x', y', z')/h, (u,v,w) = (u',v',w')h/\nu, \\ \theta = \theta'/\Delta T, p = p'h^2/\rho\nu^2, t = t'\nu/h^2, \quad (4.5)$$

Grashof number $Gr = g\beta\Delta Th^3/\nu^2$ and Reynolds number $Re = U_0 h/(2\nu)$ and considering the equations expressing conservation of mass, momentum and energy, the linearized equations for perturbation components are obtained in the following dimensionless form after eliminating pressure terms.

$$\left(\frac{\partial}{\partial t} + Re\phi_u \frac{\partial}{\partial x} - \nabla_{x,y,z}^2\right) u = -\frac{\partial p}{\partial x} - Re w D\phi_u \quad (4.6)$$

$$\left[\left(\frac{\partial}{\partial t} + Re\phi_u \frac{\partial}{\partial x} - \nabla_{x,y,z}^2\right) \nabla_{x,y,z}^2 - Re(D^2\phi_u \frac{\partial}{\partial x} + D\phi_u \frac{\partial^2}{\partial x \partial z})\right] w \\ = Gr \nabla^2 \theta \quad (4.7)$$

$$\left(\frac{\partial}{\partial t} + Re\phi_u \frac{\partial}{\partial x} - \frac{1}{Pr} \nabla_{x,y,z}^2\right) \theta = (1 + Pr\mu D\phi_\theta) w - (\mu/Re)u \quad (4.8)$$

where $\nabla^2 = \partial^2/\partial x^2 + \partial^2/\partial y^2$, $\nabla_{x,y,z}^2 = \partial^2/\partial x^2 + \partial^2/\partial y^2 + \partial^2/\partial z^2$,

$$\phi_u = 8z(1-z),$$

$$\phi_\theta = (2z/3)(1 - 2z^2 + z^3),$$

and $D = d/dz$.

There are 4 unknowns u , w , p and θ for 3 equations (4.6) to (4.8). Since $\partial p/\partial x$ in equation (4.6) will be identically zero in later discussion, equations (4.6) to (4.8) represent a consistent set of equations.

In order to show the region of interest, we consider the following general form of disturbance.

$$\begin{aligned} u &= u^*(z) G(x,y,t) \\ w &= w^*(z) G(x,y,t) \\ \theta &= \theta^*(z) G(x,y,t) \\ p &= p^*(z) G(x,y,t) \end{aligned} \tag{4.9}$$

where $G(x,y,t) = \exp[i(a_x x - ct) + i a_y y]$,

$$a_x = 2\pi h/(\text{wavelength in } x \text{ direction}),$$

$$a_y = 2\pi h/(\text{wavelength in } y \text{ direction}),$$

$$c = c_r + i c_i, \text{ a complex quantity where}$$

c_r is the circular frequency of the oscillation and

c_i is the amplification factor.

For the present longitudinal vortex rolls, the wavelength in x direction can be considered as infinitely long, and thus the wave number can be set as $a_x = 0$. Substituting equation (4.9) with $a_x = 0$ into equations (4.6) to (4.8), we have

$$[(D^2 - a^2) + ic]u^* = Re w^* D\phi_u \quad (4.10)$$

$$[(D^2 - a^2) + ic] (D^2 - a^2)w^* = Gr a^2 \theta^* \quad (4.11)$$

$$\left[\frac{1}{Pr} (D^2 - a^2) + ic\right]\theta^* = - (1 + Pr\mu D\phi_\theta)w^* + (\mu/Re)u \quad (4.12)$$

where $a = \sqrt{a_x^2 + a_y^2}$ in general but $a = a_y$ in this case and $\partial p/\partial x$ is neglected in equation (4.10). For marginal stability $c = 0$ and we have

$$(D^2 - a^2)u^* = Re w^* D\phi_u \quad (4.13)$$

$$(D^2 - a^2)^2 w^* = Gr a^2 \theta^* \quad (4.14)$$

$$\frac{1}{Pr} (D^2 - a^2)\theta^* = - (1 + Pr\mu D\phi_\theta)w^* + (\mu/Re)u^* \quad (4.15)$$

Boundary conditions are

$$w^* = Dw^* = \theta^* = u^* = 0 \text{ at } z = 0 \text{ and } 1 \quad (4.16)$$

The axial perturbation momentum is supplied by the main flow through the product of w^* and $ReD\phi_u$ on the right-hand side of equation (4.13) and is balanced by the viscous force on the left-hand side of the equation (4.13). The normal direction momentum is supplied by the buoyant force term on the right-hand side of equation (4.14) and is balanced by the viscous force term on the left-hand side of the equation (4.14). The thermal energy comes from two sources; one is due to the vertical temperature gradient through the product of $(1 + Pr\mu D\phi_\theta)$ and w^* and the other is due to the axial temperature gradient through the product of (μ/Re) and u^* on the right-hand side of equation (4.15). These two contributions are balanced by the conduction term on the left-hand side of equation (4.15). For the limiting case when $Re = 0$ and $\mu = Re\eta/\Delta T = 0$, equation (4.13) and the terms $Pr\mu D\phi_\theta w^*$ and $(\mu/Re)u^*$ on the right-hand side of equation (4.15) vanish identically. This corresponds to the horizontal thin fluid layer problem heated from below [4.7] and gives us a critical $Ra^* = 1707.8$ with wave number $a = 3.116$. For the case when $\mu = 0$ but $Re \neq 0$, equation (4.13) is retained but is seen to be uncoupled with equation (4.15). This implies that the main flow velocity distribution does not affect the stability of

of the flow. This is a limiting case of the present problem and was treated analytically and theoretically by Mori and Uchida [4.6]. Let us focus our attention on equation (4.15) now; if $Pr \rightarrow 0$, the critical Ra^* is affected by the term $(\mu/Re)u^*$ only. On the other hand, if $Pr\mu$ is large the flow is strongly affected by the main temperature distribution and is seen to be almost linearly proportional to Pr or μ . In the limit as $|\mu| \rightarrow \infty$, a different characteristic temperature based on the axial temperature gradient is used and the first term $-w^*$ on the right-hand side of equation (4.15) can be neglected. The governing equations for this case will be formulated later.

Eliminating u^* and θ^* among equations (4.13), (4.14) and (4.15) and denoting $Ra = PrGr$, we have the following governing equation for w^* .

$$(D^2 - a^2)^4 w^* = -a^2 Ra [(D^2 - a^2) + \mu L] w^* \quad (4.17)$$

where

$$\begin{aligned} L &= Pr(D^2 - a^2)D\phi_\theta - D\phi_u \\ &= 2[4(1 + Pr)(2z - 1) - 8Prz(1 - z)D \\ &\quad + \frac{1}{3} Pr(1 - 6z^2 + 4z^3)(D^2 - a^2)] \end{aligned} \quad (4.18)$$

The boundary conditions corresponding to equation (4.16) are now rewritten as,

$$w^* = Dw^* = (D^2 - a^2)^2 w^* = (D^2 - a^2)^3 w^* = 0 \quad \text{at } z = 0 \text{ and } 1 \quad (4.19)$$

The third boundary condition, $(D^2 - a^2)^2 w^* = 0$, is obtained by setting $\theta^* = 0$ in equation (4.14) and the fourth boundary condition is derived by considering both equations (4.14) and (4.15) and setting $w^* = u^* = 0$.

When $|\mu| = |\text{Re}\tau h / \Delta T| \rightarrow \infty$, ΔT can no longer be taken as a characteristic quantity. The quantity τh is used instead of ΔT for this case. Equations (4.14) and (4.15) are now rewritten as

$$(D^2 - a^2)^2 w^* = \text{Gr}_\tau a^2 \theta^* \quad (4.20)$$

$$\frac{1}{\text{Pr}} (D^2 - a^2) \theta^* = - \text{PrRe} D\phi_\theta w^* + u^* \quad (4.21)$$

Similarly, corresponding to equations (4.17) and (4.18), we have

$$(D^2 - a^2)^4 w^* = - a^2 \text{ReRa}_\tau [\text{Pr}(D^2 - a^2) D\phi_\theta - D\phi_u] w^* \quad (4.22)$$

where subscript τ signifies that the characteristic quantity

th is used instead of ΔT for defining Ra . Upon comparing the equation (4.22) with equations (4.17) and (4.18) we note that the effect of linear temperature profile term $a^2 Ra (D^2 - a^2) w^*$ vanishes and the parameter $Ra\mu$ is now replaced by $ReRa_\tau$. The boundary conditions posed for equation (4.22) remain identical to those given by equation (4.19).

In equation (4.22), if the effect of nonlinear temperature profile is much larger than the effect of main flow direction disturbance, then the last term on the right-hand side of equation (4.22) can be neglected, and equation (4.22) becomes

$$(D^2 - a^2)^3 w^* = - a^2 Pr Re Ra_\tau D\phi_\theta w^* \quad (4.23)$$

It is noted that the critical value of $Pr Re Ra_\tau$ and wave number a can also be obtained from the solution of equation (4.22) as the asymptotic case.

4.3 A Power Series Solution

In view of the considerable complexity of equations (4.17), (4.18) and (4.22), the numerical technique employed by Sparrow, et al. [4.8] seems to be most effective for the present problem. The unknown function w^* in equation (4.17) is expressed in the following power series

$$w^* = \sum_{n=0}^{\infty} \frac{A_n}{n!} z^n \quad (4.24)$$

where A 's are constant coefficients. Applying the boundary conditions (4.19) at $z = 0$, we have

$$A_0 = A_1 = 0, \quad A_4 = 2a^2 A_2, \quad A_6 = 3a^4 A_4 \quad (4.25)$$

Substituting the power series (4.24) into equation (4.17) and after equating the coefficients of z^n on both sides of the equation, the following recursion formula for A_n ($n \geq 8$) is obtained.

$$\begin{aligned}
A_{m+8} = & 4a^2 A_{m+6} - 6a^4 A_{m+4} + [4a^6 - a^2 Ra(1 + 2Pr \mu/3)] A_{m+2} \\
& - [a^8 - a^4 Ra + 8Pr \mu a^2 Ra \{ - (1 + 1/Pr) - 2m - a^2/12 \\
& - m(m-1)/2 \}] A_m \\
& - 16Pr \mu a^2 Ra [(1 + 1/Pr)m + m(m-1) + m(m-1)(m-2)/6] A_{m-1} \\
& - 4m(m-1)Pr \mu a^4 Ra A_{m-2} \\
& + (8m/3)(m-1)(m-2)Pr \mu a^4 Ra A_{m-3}
\end{aligned} \tag{4.26}$$

For the sake of brevity, the recursion formula for equation (4.22) is omitted here. Now, the remaining four coefficients A_2 , A_3 , A_5 and A_7 in the series (4.24) still remain unknown. The boundary conditions (4.19) at $z=1$ provide the following homogeneous algebraic equations for these coefficients.

$$\begin{bmatrix} c_{11} & c_{12} & c_{13} & c_{14} \\ c_{21} & c_{22} & c_{23} & c_{24} \\ c_{31} & c_{32} & c_{33} & c_{34} \\ c_{41} & c_{42} & c_{43} & c_{44} \end{bmatrix} \begin{bmatrix} A_2 \\ A_3 \\ A_5 \\ A_7 \end{bmatrix} = 0 \tag{4.27}$$

where C_{ij} ($i, j=1,2,3,4$) are functions of Pr , μ , a and Ra as indicated in Appendix 4.1. But for equation (4.22), the coefficients C_{ij} 's are functions of Pr , a and $ReRa_\tau$ only.

The determinant of the coefficient matrix $[C_{ij}]$ must be zero in order that a nontrivial solution exists; thus

$$|C_{ij}| = 0 . \quad (4.28)$$

In seeking a set of parameters Pr , μ , a and Ra (or Pr , a and $ReRa_\tau$) satisfying the condition (4.28), the values for Pr and μ (or Pr only when $|\mu| \rightarrow \infty$) are preassigned, and the relation between a and Ra (or $ReRa_\tau$) is sought. The set of minimum Rayleigh number Ra (or $ReRa_\tau$) and the corresponding wave number a is the solution of the problem with the preassigned Pr and μ (or Pr). All computations are performed by IBM 360/67 at the Computing Center of the University of Alberta insuring accuracy for the first eigenvalues of Ra such that

$$\epsilon = \frac{|C_{ij}|^{n+5} - |C_{ij}|^n}{|C_{ij}|^{n+5}} < 10^{-5} \quad (4.29)$$

and for the second eigenvalues $\epsilon < 10^{-4}$. The values of the wave number a and Rayleigh number Ra (or $ReRa_\tau$) are considered to be accurate up to four and five significant figures,

respectively.

In addition to obtaining the numerical results for neutral stability curves, secondary flow streamlines, perturbations of the axial velocity and temperature distributions are also computed. Secondary flow stream function ψ is defined by $v = \partial\psi/\partial z$ and $w = -\partial\psi/\partial y$.

4.4 Results and Discussion

The results for neutral stability curves are shown in Fig. 4.4. The effects of adverse linear temperature distribution, main flow direction disturbance and nonlinear temperature profile (see the corresponding factors (b), (d) and (c) in Section 4.1) will be explained clearly using this figure. First of all, if the flow is destabilized by the adverse linear temperature distribution alone, then we obtain a critical $Ra^* = 1707.8$ and wave number $a = 3.116$ which are exactly the same as those found in the classical Bénard problem. For the case when the top plate is kept at higher temperature level ($T_2 > T_1$), the flow is theoretically always stable.

With $Pr \rightarrow 0$ and $\mu \neq 0$, the effect of main flow direction disturbance also destabilizes the flow, and the critical Rayleigh number decreases from 1707.8 for the case $T_1 > T_2$ and from infinity for the case $T_2 > T_1$, respectively, as $|\mu|$ increases. Both solid and dashed curves representing positive and negative Ra , respectively, approach to a definite value which will be discussed in the next figure.

Similarly, for $Pr \neq 0$ and $\mu \neq 0$, the effect of nonlinear temperature profile also destabilizes the flow and the two curves for positive and negative Ra approach to each other. It is interesting to note the asymptotic behaviour for the case of $|\mu| \rightarrow \infty$ where the instability of the flow depends on Pr and $ReRa_T$ only (see Fig. 4.5).

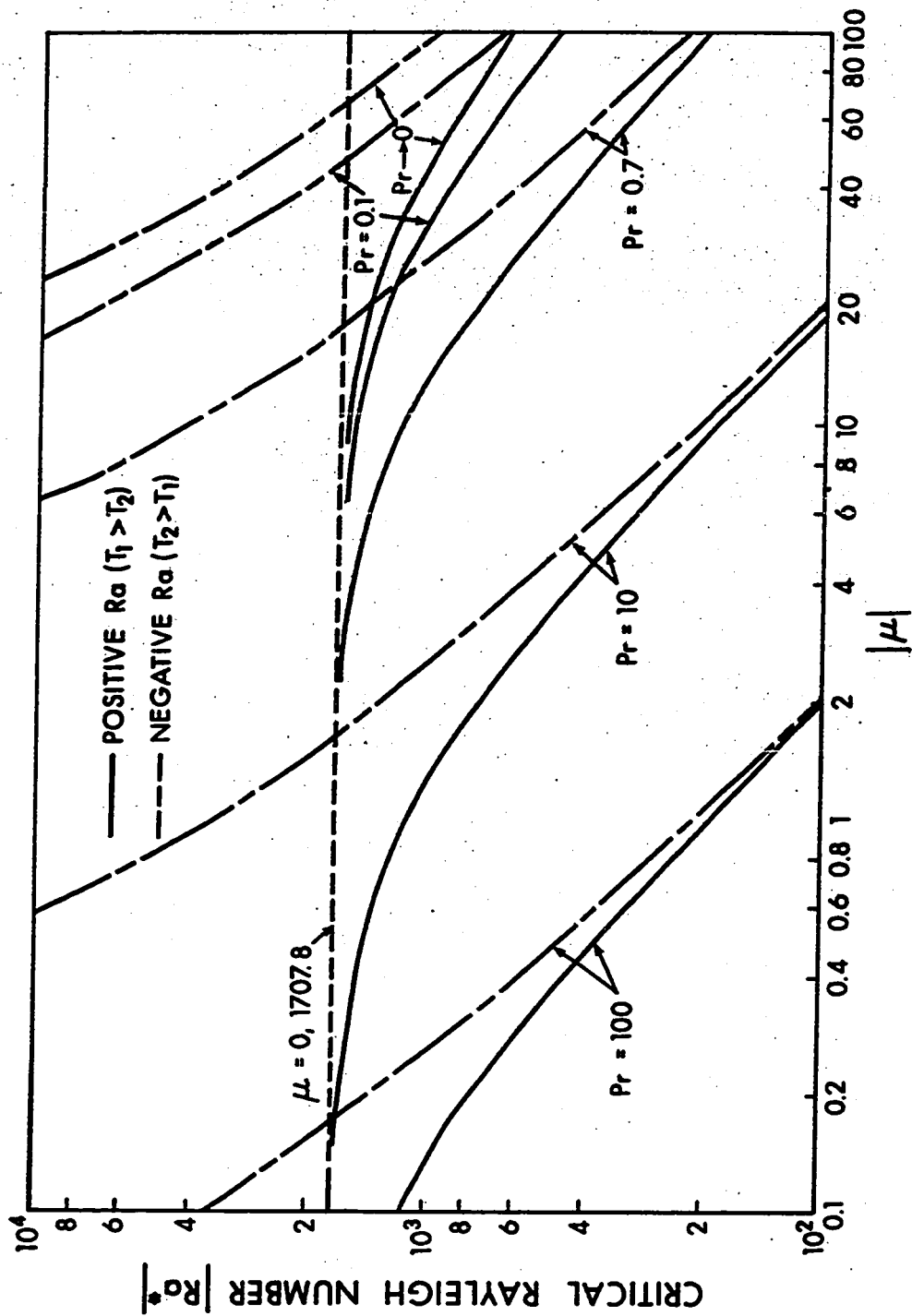


Fig. 4.4 Neutral stability curves for longitudinal vortex rolls

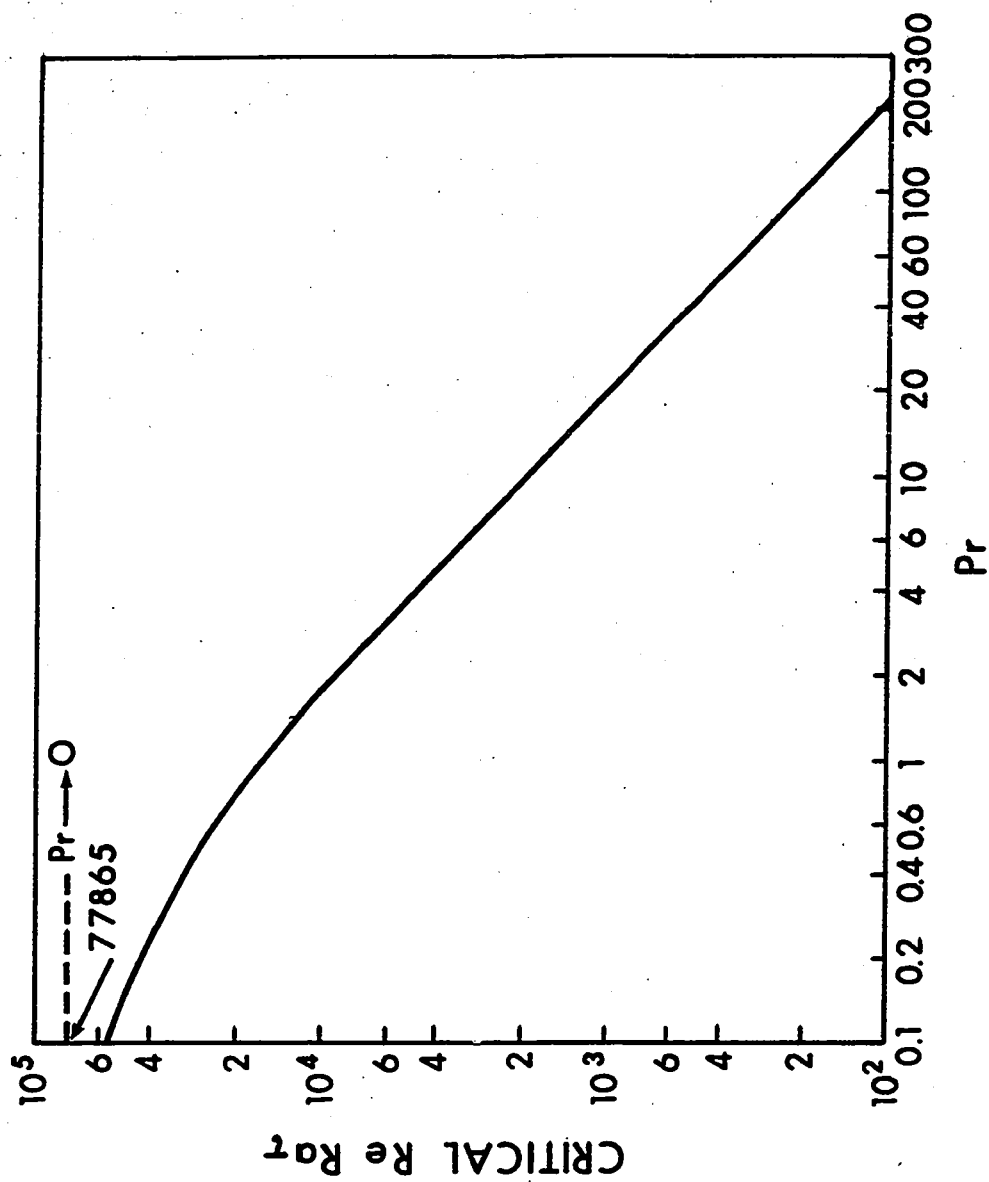
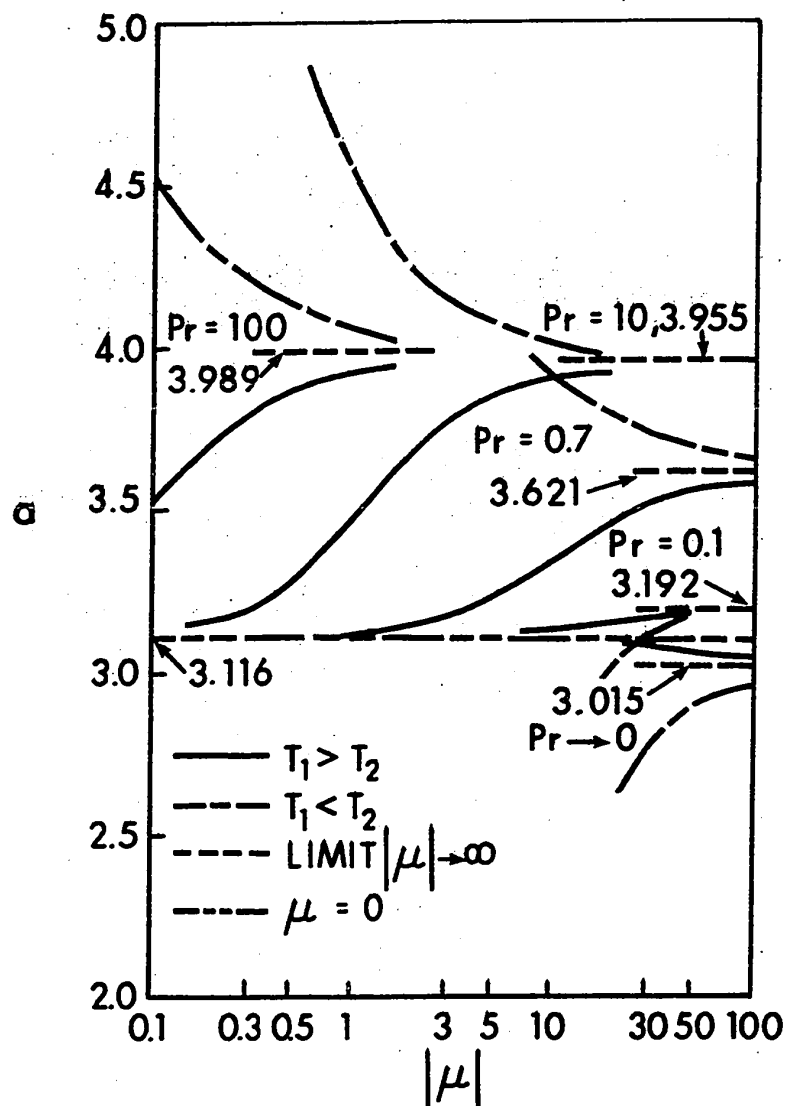


Fig. 4.5 Neutral stability curve for the case $|\mu| \rightarrow \infty$

Fig. 4.5 shows an important and interesting limiting case for Fig. 4.4. The solution for this case can be obtained from equation (4.22) for the case when $|\mu| \rightarrow \infty$. When $Pr \rightarrow 0$, the secondary flow is caused merely by the main flow direction disturbance, and the critical value is $ReRa_{\tau} = 77865$. On the other hand, when $Pr \geq 2$ the value of the parameter $PrReRa_{\tau}$ approaches asymptotically to 20355 and the wave number a approaches to 4.000. At $Pr = 2$ the value of $PrReRa_{\tau}$ deviates only 2% and the wave number a deviates only 5% from the limiting values of 20355 and 4.000, respectively.

With Pr as a parameter, the relation between critical wave number a and the characteristic parameter μ is shown in Fig. 4.6. For the case $T_1 > T_2$, all the solid curves start with the value of 3.116 and approach asymptotically to the values for the limiting case $|\mu| \rightarrow \infty$. For the case $T_1 < T_2$, all the dashed curves also approach to the limiting values for the case $|\mu| \rightarrow \infty$. As $Pr \rightarrow 0$, the trend of the curves for the cases of $T_1 \gtrless T_2$ is seen to be opposite to that for a higher Prandtl number. This is due to the effect of main flow direction disturbance. As pointed out earlier in connection with Fig. 4.5, the wave number for the limiting case $|\mu| \rightarrow \infty$ is also seen to approach the value of 4.000 as Pr increases.

Second critical Rayleigh numbers for the case $T_1 > T_2$ are shown in Fig. 4.7. The values represented by the upper curves are seen to be one order of magnitude higher than the

Fig. 4.6 Critical wave number versus $|\mu|$

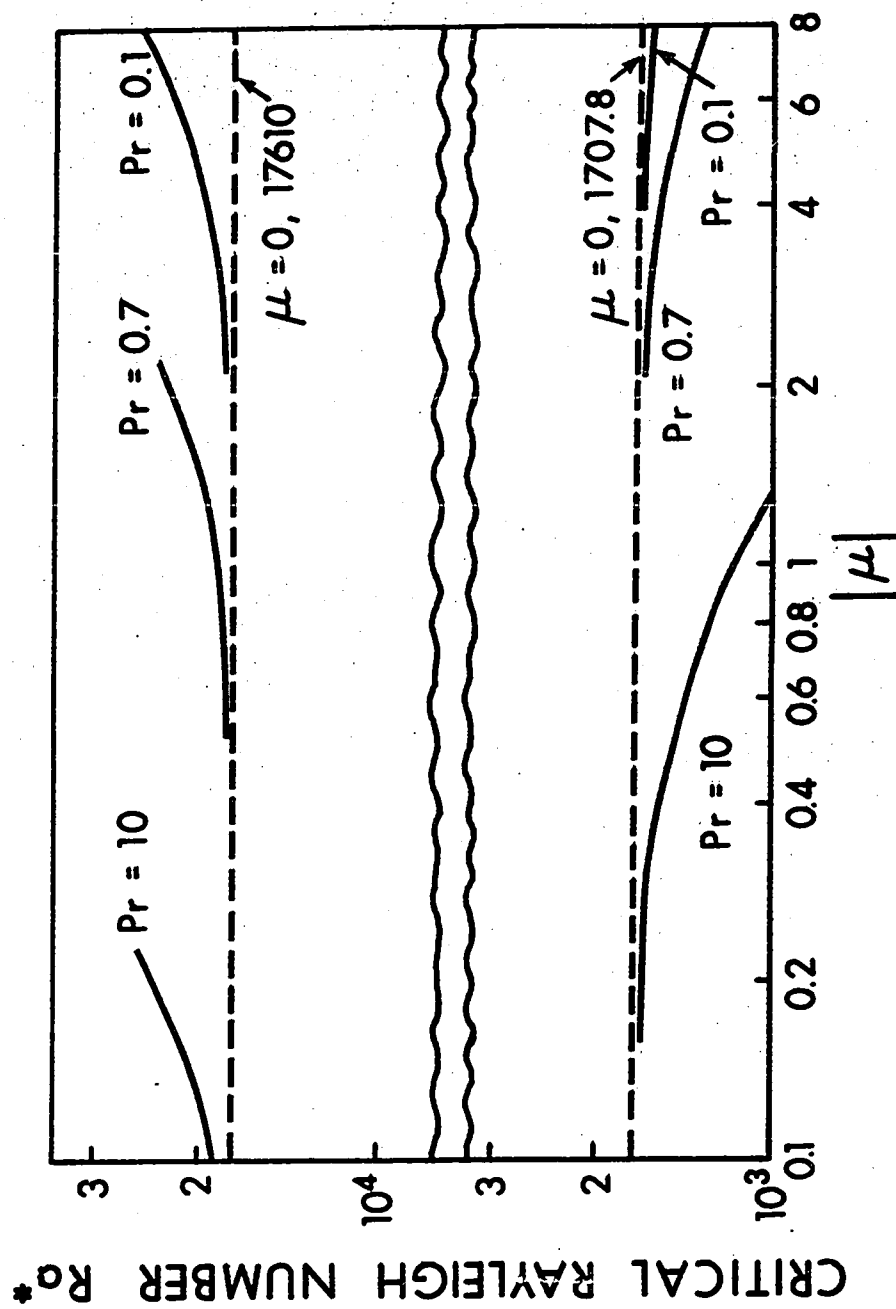


Fig. 4.7 Second critical eigenvalues of Ra

first critical eigenvalues. The difference becomes even more pronounced as μ increases. The second critical values may have no practical significance because they are computed on the assumption of Poiseuille flow. The basic flow and temperature fields may differ considerably from the Poiseuille flow profiles at a Rayleigh number which is one order of magnitude higher than the first critical value. However, the results indicate that we may expect a flow pattern, determined solely from the first eigenfunction, to exist in some regions of Ra near the first critical values, though non-linear terms may play a role in the governing equations at high Rayleigh number.

Figs. 4.8 (a, b and c) show secondary flow streamlines and isothermals of perturbation temperature for three typical cases. The values of ψ and θ are those obtained by setting $-A_2/a = 1$. For case (a), the isothermals have only one eye since there is no maximum (or minimum) basic temperature in the fluid, otherwise, two eyes exist such as shown in cases (b) and (c). The horizontal zero perturbation line ($\theta = 0$) and the center of vortex move downward as μ increases for the case $T_1 > T_2$. For the case $T_2 > T_1$, the movement is opposite. Case (c) in Fig. 4.8 also shows a double vortex structure, but the strength of the upper vortex is seen to be about two orders of magnitude less than that of the main vortex. These figures also indicate the location of the maximum temperature disturbance. This information can be utilized

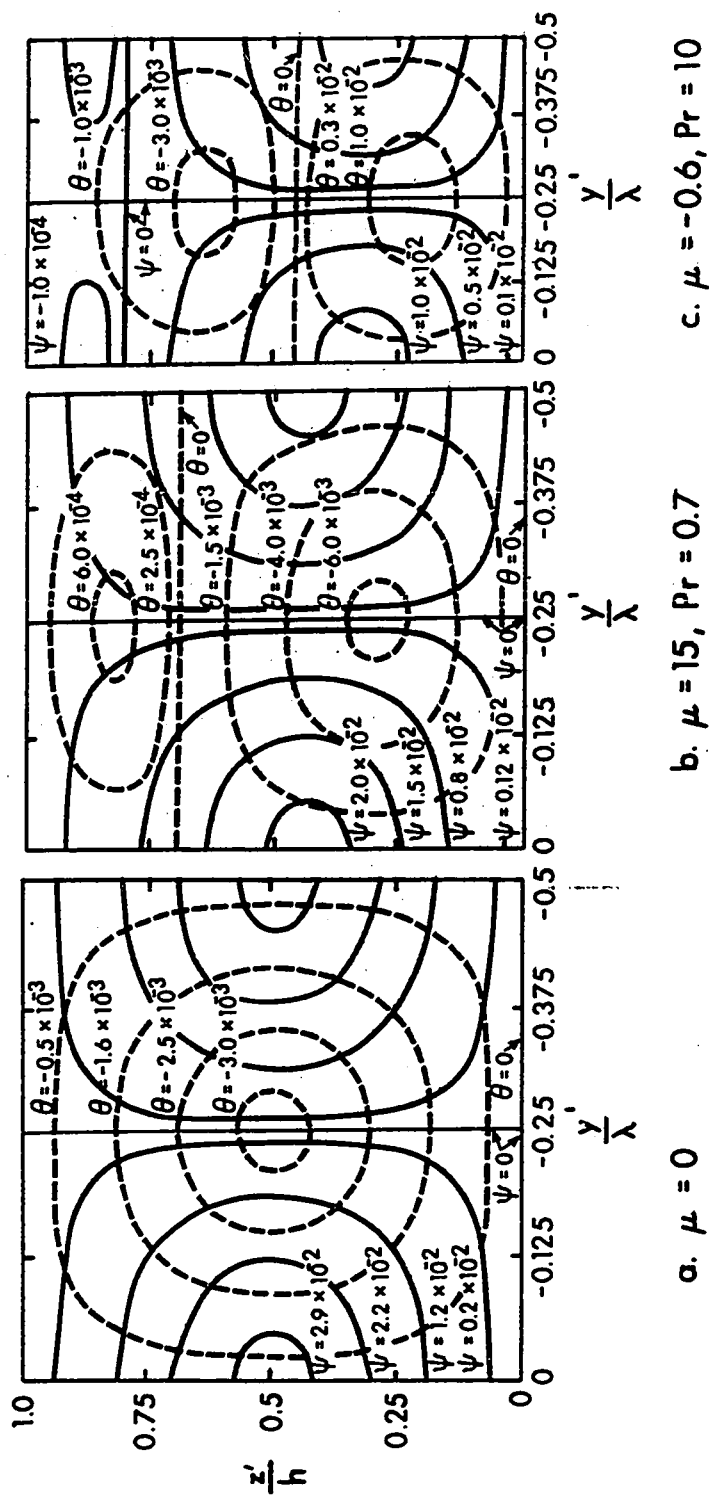


Fig. 4.8 Secondary flow streamlines and isothermals of perturbation temperature

to detect the onset of instability as will be discussed in the next chapter.

In Fig. 4.9, the perturbations of the axial velocity component on line A-A (see the figure) are shown for several combinations of Pr and μ . In most cases, the minimum (or maximum) perturbation velocity is located at approximately $z = 1/4$ or $3/4$.

Finally, for the completeness of the present study, it is necessary to show the region of parameters (Re , Ra_τ , Ra) where the longitudinal vortex rolls may have priority of appearance. In Fig 4.10, the critical Re ($= 5400$) for two-dimensional Tollmien-Schlichting waves is compared with the thermal instability for $Pr = 0.7$. When the flow has a value of Re less than 5400 but the values of Ra and Ra_τ are above the slant straight lines indicated in the figure for a given value of $\mu = ReRa_\tau/Ra$, then this flow is considered to be unstable predominantly for the vortex rolls. Gage and Reid [4.9] pointed out that the critical Re for the T-S waves is also influenced by the thermal structure of the flow. Thus, the comparison shown in Fig. 4.10 must be considered as tentative. A more convenient comparison can be made by using Richardson number, $Ri = - Ra/64 PrRe^2$. According to the analysis in reference [4.9] for the case $T_1 > T_2$, $Pr = 1$ and $\mu = 0$, in the region $Ri < - 0.92 \times 10^{-6}$ the vortex rolls are more probable than T-S waves. The criterion is clearly affected by the presence of μ as shown in Table 4.1 for

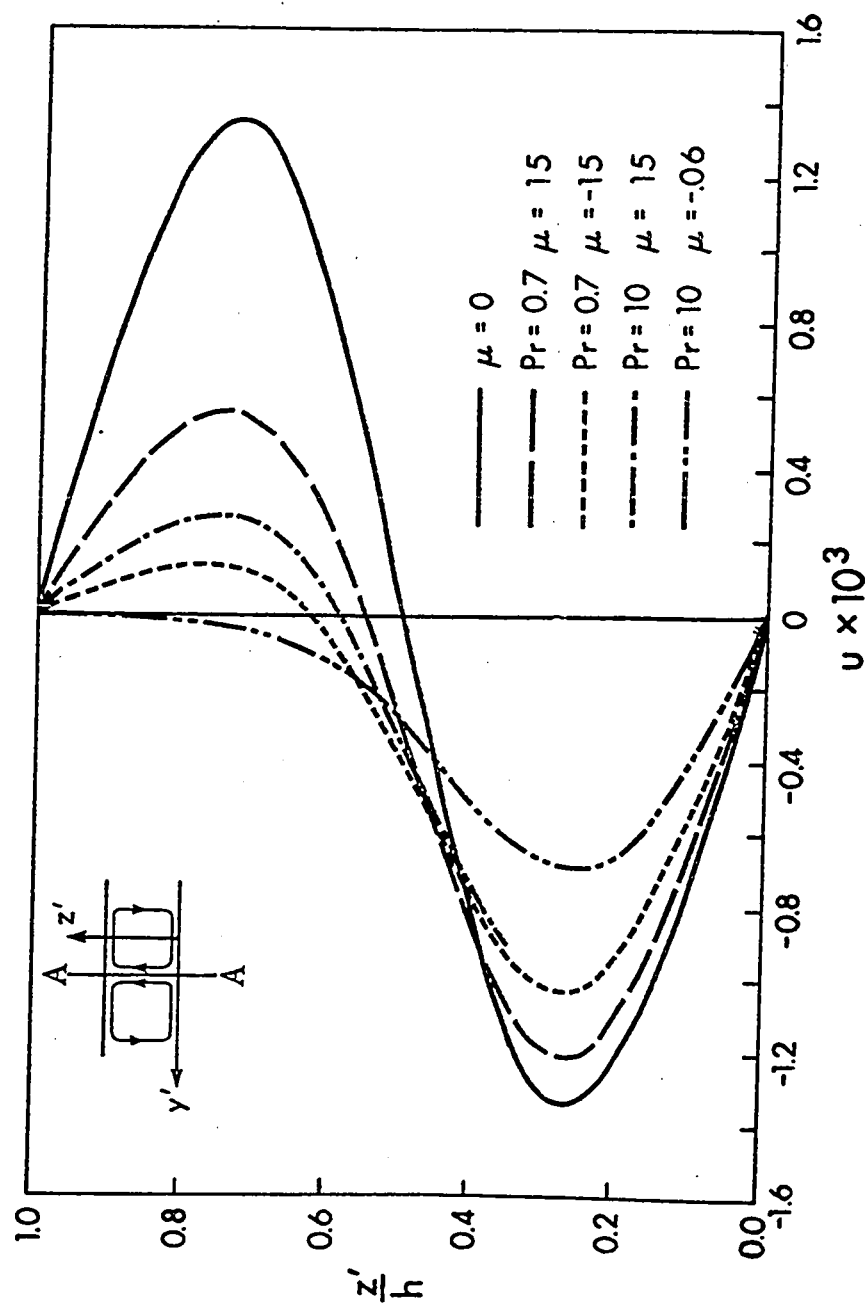


Fig. 4.9 Perturbations of axial velocity component

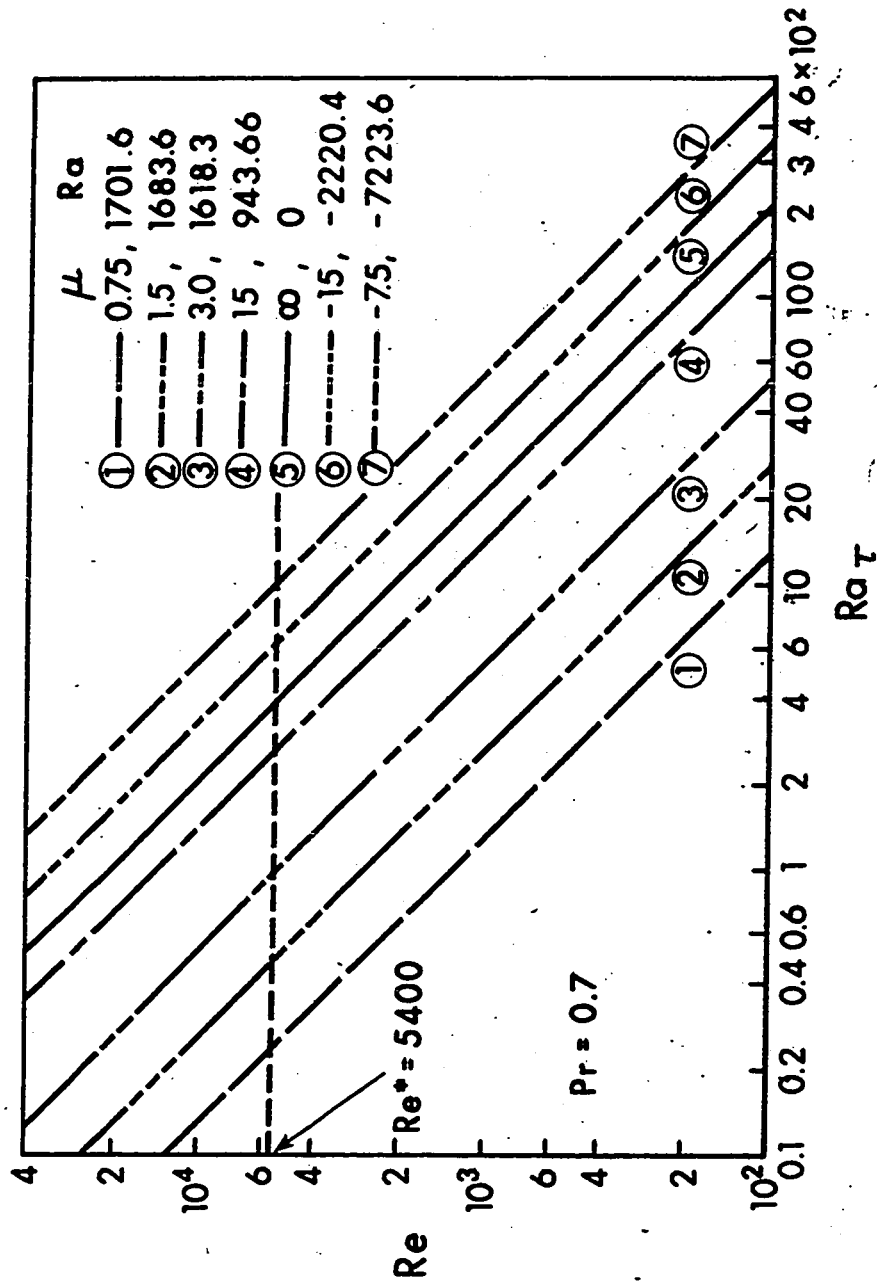


Fig. 4.10 Comparison of thermal instability with hydrodynamic instability

$Pr = 0.7$. It is also seen that at extremely low Re there is a possibility of transverse or three dimensional vortex rolls.

Table 4.1 Critical values of Ri ($\Delta T > 0$) below which longitudinal vortex rolls have priority of appearance over the T-S waves ($Pr = 0.7$)

μ	0	10	100	∞
$Ri^* \times 10^6$	-1.3	-0.91	-0.15	0

The assumption of fully developed laminar flow should also be examined carefully since instability in the entrance region might be significant under certain circumstances. To the best of the author's knowledge, the literature in this area is not available. There are at least two factors which may be important in the entrance region.

(a) Due to the thinner thermal boundary layer in the entrance region, the flow may be more stable.

(b) Due to the steeper temperature gradient in the entrance region, the flow may be more unstable.

The effects of the above two conditions are seen to be opposite with each other. For condition (a), the present study is still valid. For condition (b), we note that when

the influence of the secondary motion on the fully developed basic velocity and temperature fields is negligibly small, and the growth or decay of the motion depends on the flow and thermal structure of the fully developed region only, the present results are still considered to be valid. Therefore, the validity of the present analysis depends on the stability of the flow in the entrance region. A further study is required to explore the instability problem in the entrance region. The numerical results are tabulated in the Appendix 4.2 for reference.

4.5 Concluding Remarks

(a) The linearized stability analysis is carried out for the fully developed laminar forced convection between two infinite horizontal flat plates subjected to identical uniform axial temperature gradient but maintained at temperatures T_1 and T_2 ($T_1 > T_2$, $T_1 < T_2$ and $T_1 = T_2$) at lower and upper surfaces, respectively. The limiting case of vanishing axial temperature gradient and heating from below ($T_1 > T_2$) reduces to the problem studied by Mori and Uchida [4.6] and also to the classical Bénard convection problem (Roll-type convection) [4.7] mathematically. In addition to the two destabilizing effects such as the adverse vertical temperature gradient [4.7] and the nonlinear temperature profile [4.8] considered in the literature, the present study considers one additional destabilizing effect in the form of the convective motion of the main flow direction disturbance. Consequently, from the viewpoint of destabilizing effects, the present work can be considered as more general than the earlier works [4.6, 4.7, 4.8]. The effect of Prandtl number on thermal instability is also studied comprehensively.

(b) The forced convection between two horizontal flat plates considered in the present chapter is destabilized by linear and nonlinear parts of the basic temperature distribution and also by the convective motion of the main flow direction disturbance. For the case of $|\mu| \rightarrow 0$ (see equations (4.3) and (4.15)), the linear part of the basic temperature

distribution dominates the instability of the flow. For the case of $Pr|\mu| \rightarrow \infty$ (see again equations (4.3) and (4.15)), the nonlinear part of the basic temperature distribution destabilizes the flow. Furthermore, for the case of $Pr \rightarrow 0$ and $|\mu| \rightarrow \infty$ the convective motion of the main flow direction disturbance plays an important role in destabilizing the flow. It is interesting to note that when $Pr \geq 0(1)$, the neutral stability curves shown in Figs. 4.4 and 4.5 already approach to their respective asymptotic values for $Pr \rightarrow \infty$.

(c) The critical wave number a depends on the values of Pr and μ . For example, for positive Ra , as μ is increased from 0, the wave number a starts deviation from 3.116 and approaches to a limiting value at a certain value of μ for a given Prandtl number.

(d) Most recently, Kurzweg [4.10] studied stability of natural convection within an inclined channel. He found that the critical Grashof number for the onset of longitudinal vortex rolls between inclined parallel plates with an angle ϕ with respect to the vertical is

$$Gr^* = (\text{const}/Pr)\csc \phi \quad (4.30)$$

or

$$Ra^* \sin \phi = 1707.8 \quad (4.31)$$

The problem treated by Kurzweg corresponds to the limiting

case $\mu = 0$ for the present problem if a plane channel is inclined at the angle ϕ with respect to the vertical. It is noted that the stability curves shown in Figs. 4.4 and 4.5 can also be applied to the inclined plane channel by simply replacing Ra^* and $ReRa_\tau^*$ by $Ra^* \sin \phi$ and $ReRa_\tau^* \sin \phi$, respectively, for the inclination angle effect provided that the basic velocity and temperature profiles are still given by equations (4.2) and (4.3), respectively.

References

- 4.1 Nakayama, W., Hwang, G.J., and Cheng, K.C., "Thermal Instability in Plane Poiseuille Flow," Journal of Heat Transfer, Trans. ASME, Series C, Vol. 92, 1970, pp. 61-68.
- 4.2 Cheng, K.C., and Akiyama, Mitsunobu, "Laminar Forced Convection Heat Transfer in Curved Rectangular Channels," International Journal of Heat and Mass Transfer, Vol. 13, No. 3, 1970, pp. 471-490.
- 4.3 Taylor, G.I., "Stability of a Viscous Liquid Contained Between Two Rotating Cylinders," Philosophical Transactions, Series A, Vol. 223, 1923, pp. 289-343.
- 4.4 Bénard, H., and Avsec, D., "Travau récents sur les tourbillons cellulaires et les tourbillons en bandes applications a l'astrophysique et a la météorologie," Journal de Physique, No. 11, 1930, pp. 486-500.
- 4.5 Gill, W.N., and del Casal, E., "A Theoretical Investigation of Natural Convection Effects in Forced Horizontal Flow," AIChE Journal, Vol. 8, 1962, pp. 513-518.
- 4.6 Mori, Y., and Uchida, Y., "Forced Convective Heat Transfer Between Horizontal Flat Plates," International Journal of Heat and Mass Transfer, Vol. 9, 1966, pp. 803-817.

- 4.7 Pellew, A., and Southwell, R.V., "On Maintained Convective Motion in a Fluid Heated from Below," Proceedings of the Royal Society, London, Series A, Vol. 176, 1940, pp. 312-343.
- 4.8 Sparrow, E.M., Goldstein, R.J., and Jonsson, V.K., "Thermal Instability in a Horizontal Fluid Layer: Effect of Boundary Conditions and Nonlinear Temperature Profile," Journal of Fluid Mechanics, Vol. 18, 1964, pp. 513-528.
- 4.9 Gage, K.S., and Reid, W.H., "The Stability of Thermally Stratified Plane Poiseuille Flow," Journal of Fluid Mechanics, Vol. 33, 1968, pp. 21-32.
- 4.10 Kurzweg, U.H., "Stability of Natural Convection Within an Inclined Channel," Journal of Heat Transfer, Trans. ASME, Series C, Vol. 92, 1970, pp. 190-191.

Appendix 4.1 The Elements of Matrix $[C_{ij}]$

$$C_{11} = \frac{1}{2} + \frac{2a^2}{4!} + \frac{3a^4}{6!} + K_{1,2}$$

$$C_{12} = \frac{1}{3!} + K_{1,3}$$

$$C_{13} = \frac{1}{5!} + K_{1,5}$$

$$C_{14} = \frac{1}{7!} + K_{1,7}$$

$$C_{21} = 1 + \frac{2a^2}{3!} + \frac{3a^4}{5!} + K_{2,2}$$

$$C_{22} = \frac{1}{2} + K_{2,3}$$

$$C_{23} = \frac{1}{4!} + K_{2,5}$$

$$C_{24} = \frac{1}{6!} + K_{2,7}$$

$$C_{31} = -2a^2 + 2a^2(1-a^2) + 3a^4\left(\frac{1}{2} - \frac{a^2}{12}\right) + K_{3,2}$$

$$C_{32} = -2a^2 + K_{3,3}$$

$$C_{33} = 1 - \frac{a^2}{3} + K_{3,5}$$

$$C_{34} = \frac{1}{3!} - \frac{a^2}{60} + K_{3,7}$$

$$C_{41} = 3a^4 + 6a^4 \left(\frac{a^2}{2} - 1 \right) + 3a^4 \left(1 - \frac{3a^2}{2} + \frac{a^4}{8} \right) + K_{4,2}$$

$$C_{42} = 3a^4 + K_{4,3}$$

$$C_{43} = -3a^2 + \frac{a^4}{2} + K_{4,5}$$

$$C_{44} = 1 - \frac{a^2}{2} + \frac{a^4}{40} + K_{4,7}$$

$$\text{where } K_{1,j} = \sum_{n=8}^m \frac{B_{n,j}}{n!}$$

$$K_{2,j} = \sum_{n=8}^m \frac{B_{n,j}}{(n-1)!}$$

$$K_{3,j} = \sum_{n=8}^m \left[\frac{1}{(n-4)!} - \frac{2a^2}{(n-2)!} \right] B_{n,j}$$

$$K_{4,j} = \sum_{n=8}^m \left[\frac{1}{(n-6)!} - \frac{3a^2}{(n-4)!} + \frac{3a^4}{(n-2)!} \right] B_{n,j}$$

$$j = 2, 3, 5, 7,$$

and B's are the coefficients in the following equation for $A_n (n \geq 8)$ [c.f. equation (4.26)].

$$A_n = B_{n,2}A_2 + B_{n,3}A_3 + B_{n,5}A_5 + B_{n,7}A_7$$

Infinite series for K's were terminated when the desired convergence was obtained.

Appendix 4.2 Numerical Results

Pr = 100

μ	a	Ra*
0	3.116	1707.8
0.075	3.399	1322.3
0.225	3.738	699.80
0.525	3.878	346.70
0.75	3.911	250.85
1.5	3.950	130.38
-1.875	4.021	-111.87
-1.125	4.043	-190.38
-0.75	4.069	-293.13
-0.525	4.104	-433.09
-0.225	4.256	-1174.8
-0.15	4.387	-2013.3
-0.075	4.761	-6094.9

Pr \rightarrow 0

μ	a	Ra*
0	3.116	1707.8
7.5	3.113	1661.2
15	3.105	1547.1
26.25	3.091	1341.0
45	3.073	1051.9
75	3.056	762.02
-75	2.947	-1445.9
-52.5	2.907	-2390.4
-37.5	2.844	-4077.9
-30	2.777	-6078.2
-22.5	2.645	-10965.

Pr = 0.1

μ	a	Ra*
0	3.116	1707.8
3	3.118	1693.0
7.5	3.127	1623.0
15	3.145	1441.9
22.5	3.159	1256.5
30	3.169	1098.4
45	3.179	864.97
60	3.184	708.49
75	3.186	598.43
-75	3.184	-954.09
-52.5	3.173	-1514.8
-37.5	3.151	-2447.0
-26.25	3.098	-4355.3
-18.75	2.988	-8273.1

Pr = 10

μ	a	Ra*
0	3.116	1707.8
0.375	3.221	1568.0
0.75	3.397	1309.3
1.5	3.616	913.62
3	3.775	548.47
4.5	3.830	389.25
7.5	3.881	245.65
11.25	3.906	167.97
15	3.918	127.59
-18.75	3.986	-109.36
-11.25	4.006	-186.05
-7.5	4.031	-286.34
-5.25	4.064	-422.83
-3.75	4.107	-618.79
-3	4.145	-804.18
-2.25	4.208	-1144.4
-1.5	4.331	-1957.7
-1.125	4.451	-2982.7
-0.75	4.683	-5894.1
-0.675	4.760	-7205.5
-0.6	4.858	-9164.4

Pr = 0.7

μ	a	Ra*
0	3.116	1707.8
1.5	3.128	1683.6
3	3.160	1618.3
5.25	3.223	1478.6
7.5	3.284	1329.0
15	3.415	943.66
30	3.510	575.38
45	3.546	410.98
60	3.564	319.20
75	3.576	260.81
-75	3.667	-309.83
-52.5	3.687	-459.59
-37.5	3.712	-676.76
-30	3.735	-884.47
-22.5	3.770	-1271.0
-18.75	3.798	-1620.4
-15	3.836	-2220.4
-11.25	3.891	-3462.0
-7.5	3.962	-7223.6
-6.75	3.973	-9022.1

Pr = 0.7

μ	a	Ra* _{II}
0	5.365	17610
0.15	5.366	17636
0.3	5.369	17712
0.45	5.374	17839
0.75	5.392	18252
1.125	5.432	19077
1.5	5.498	20267
2.25	5.741	23703

Pr = 0.1

μ	a	Ra* _{II}
0	5.365	17610
0.75	5.374	17677
1.5	5.404	17877
3	5.521	18685
5.25	5.840	20941
7.5	6.279	24315

Second Critical Eigenvalues

Pr = 10

μ	a	Ra* _{II}
0	5.365	17610
0.075	5.359	18444
0.1125	5.364	19519
0.1875	5.471	23050
0.225	5.597	25328

Critical ReRa_τ for the case of $|\mu| \rightarrow \infty$

Pr	a	ReRa_τ^*
0	3.015	77864
0.1	3.192	56319
0.2	3.317	44212
0.4	3.481	30931
0.7	3.621	21305
1	3.702	16238
2	3.826	9047.3
3	3.876	6267.9
5	3.920	3881.7
7	3.940	2811.2
10	3.955	1988.5
20	3.974	1006.6
40	3.984	506.40
60	3.987	338.30
100	3.989	203.32
150	3.990	135.66
250	4.000	81.449

CHAPTER V

AN EXPERIMENTAL INVESTIGATION OF THERMAL INSTABILITY IN PLANE POISEUILLE FLOW*

5.1 Introduction

The effects of buoyancy forces on fully developed laminar forced convection in horizontal rectangular channels under the thermal boundary conditions of axially uniform wall heat flux and peripherally uniform wall temperature were studied by Cheng and Hwang [2.5] for various aspect ratios. It was found that as the aspect ratio (width/height) increases, the eyes of the vortices move further toward the shorter vertical side walls. Consequently, the effect of buoyancy forces is negligible as the aspect ratio approaches infinity. However, in reality, another type of secondary flow may arise leading to a thermal instability problem discussed in Chapter IV. The thermal instability of a horizontal fluid layer subjected to various boundary conditions has been studied very extensively, both theoretically and experimentally in the past. For the horizontal fluid layer subjected to an adverse temperature gradient (with the lower surface temperature T_1 higher than the upper surface temperature T_2),

* More complete results of this work are reported in [5.1]. The contribution of Mr. M. Akiyama to the work described here is clearly stated in the Acknowledgement.

the system is potentially unstable because of its top-heavy situation and the onset of secondary motion is marked by a critical Rayleigh number. For a horizontal fluid layer without forced flow, the system is always stable theoretically if the upper surface is maintained at higher temperature than the lower surface, namely $T_2 > T_1$. However, with the main flow in the horizontal direction and the fluid temperature less than both T_1 and T_2 , the region near the lower surface will again be subjected to an adverse temperature gradient and the system is now potentially unstable. We can easily see that the critical Rayleigh number would be higher when $T_2 > T_1$ than when $T_1 > T_2$. In other words, with the main flow in the horizontal direction, the onset of convection is always possible with either $T_1 > T_2$ or $T_2 > T_1$.

A theoretical investigation of the thermal instability was carried out in Chapter IV to determine the conditions marking the onset of longitudinal columnar vortices due to buoyant forces in a fully developed laminar flow between two infinite horizontal parallel plates (see Figs. 4.1 and 5.1). The thermal boundary conditions of uniform axial temperature gradient and temperatures T_1 and T_2 at the lower and upper surfaces, respectively, were considered. The theoretical results in Chapter IV show that for the case of $T_1 \neq T_2$, the critical Rayleigh number depends on the dimensionless parameter μ characterizing the effect of the uniform axial temperature gradient, and also Prandtl number. On the other hand, for

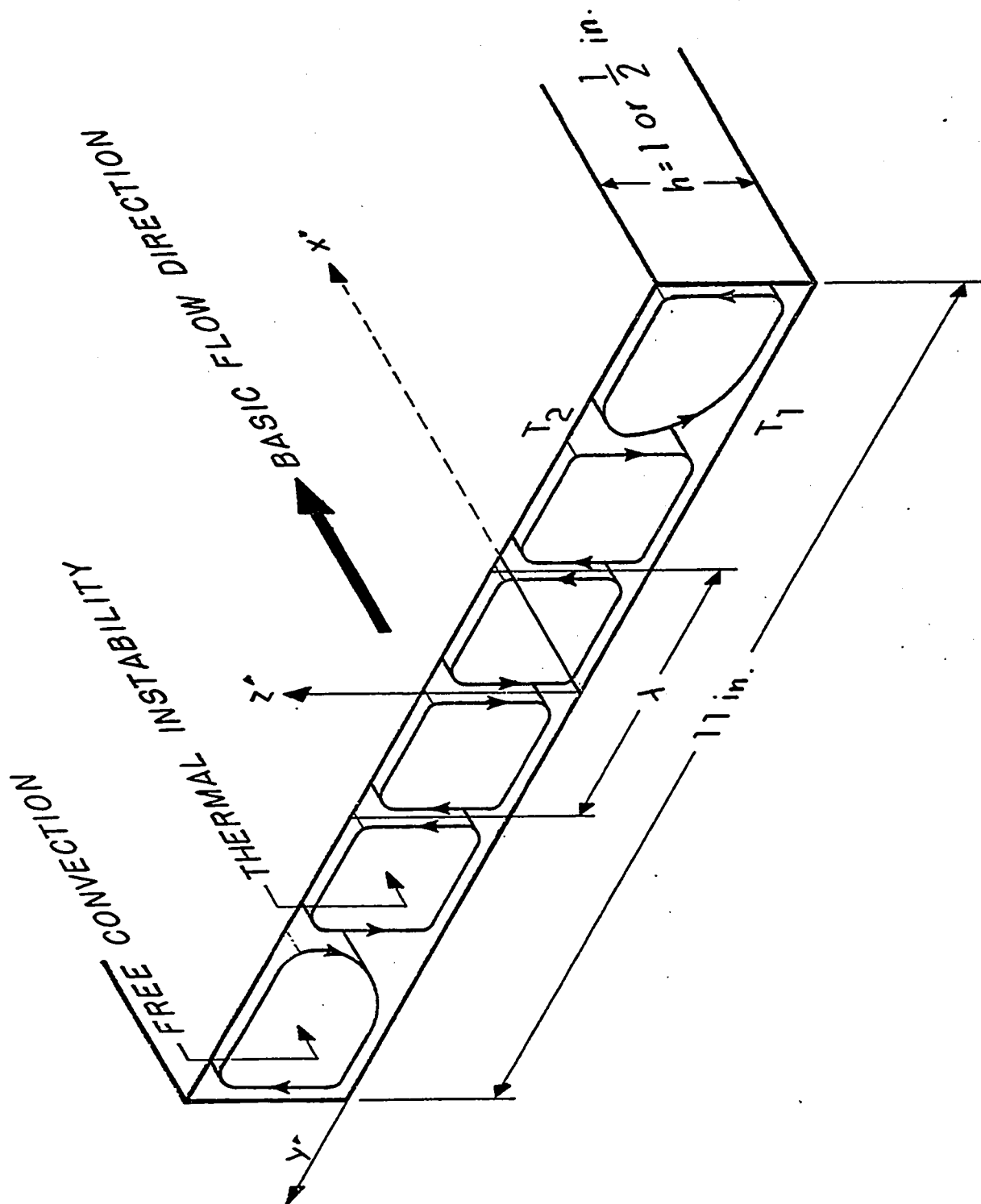


Fig.5.1 Configuration and coordinate system

the case of $T_1 = T_2$, the critical $ReRa_\tau$ depends on Prandtl number only. As shown in Fig. 5.1, the eigenvalue and boundary-value problems may exist side by side for the horizontal rectangular channel with aspect ratio say around 10.

Recently, Mori and Uchida [4.6] carried out a theoretical and experimental study on the effect of longitudinal vortex rolls on forced convective heat transfer between two horizontal plates for the limiting case of vanishing axial temperature gradient $\tau = 0$ where the lower plate is heated isothermally and the upper plate is cooled isothermally. More recently, Sparrow and Husar [5.2] reported an experimental investigation on the occurrence and characteristics of longitudinal vortices superposed upon the natural convection main flow on an inclined plate. Experimentally, the longitudinal vortices were also observed by Terada and Tamano [5.3] in Poiseuille flow, and by Chandra [5.4] and others in Plane Couette flow, all heated from below.

In the present experimental investigation, the onset of longitudinal vortices for the fully developed laminar forced convection between two horizontal flat plates subjected to uniform axial wall temperature gradient with air as a working fluid is studied to verify the theoretical results reported in Chapter IV. The secondary flow in the present problem arises from the destabilizing effects due to the adverse temperature gradient and also the advective motion of the main flow disturbance.

5.2 Experimental Apparatus and Procedure

The schematic diagram of the testing apparatus is shown in Fig. 5.2. Air from a centrifugal blower or air tap passes through a settling chamber and enters a horizontal rectangular channel (cross section 11" x 1" or 1/2"). The test section is constructed by two mirror-like smooth brass plates (6' x 1' x 1/8") with side walls made of marinite insulator and reinforced by steel bars for accurate dimension. In order to insure uniform heating, the heating elements and the brass plates are separated by a 3/16" thick aluminum plate. The heating elements consist of 0.008" x 1/8" Nikrothal tape wound around 1/16" thick mica sheet with a pitch of 3/8" and the electrical insulation is provided by 1/16" thick mica sheets. The heaters for each plate were subdivided into thirteen segments in the direction of the main flow with each segment consisting of one main heater and two guard heaters, one on each side. Each heater can be controlled individually by a voltage controller and two large capacity voltage controllers were used to regulate the temperature difference between the upper and lower plates. The surface temperature of the flat plates is measured by iron-constantan thermocouples (0.01" dia.) embedded in the brass plates and electrically insulated to minimize the electrical noise on the temperature recording system.

The flow rate of the air is measured by providing a metering orifice as shown in Fig. 5.2 where the pressure

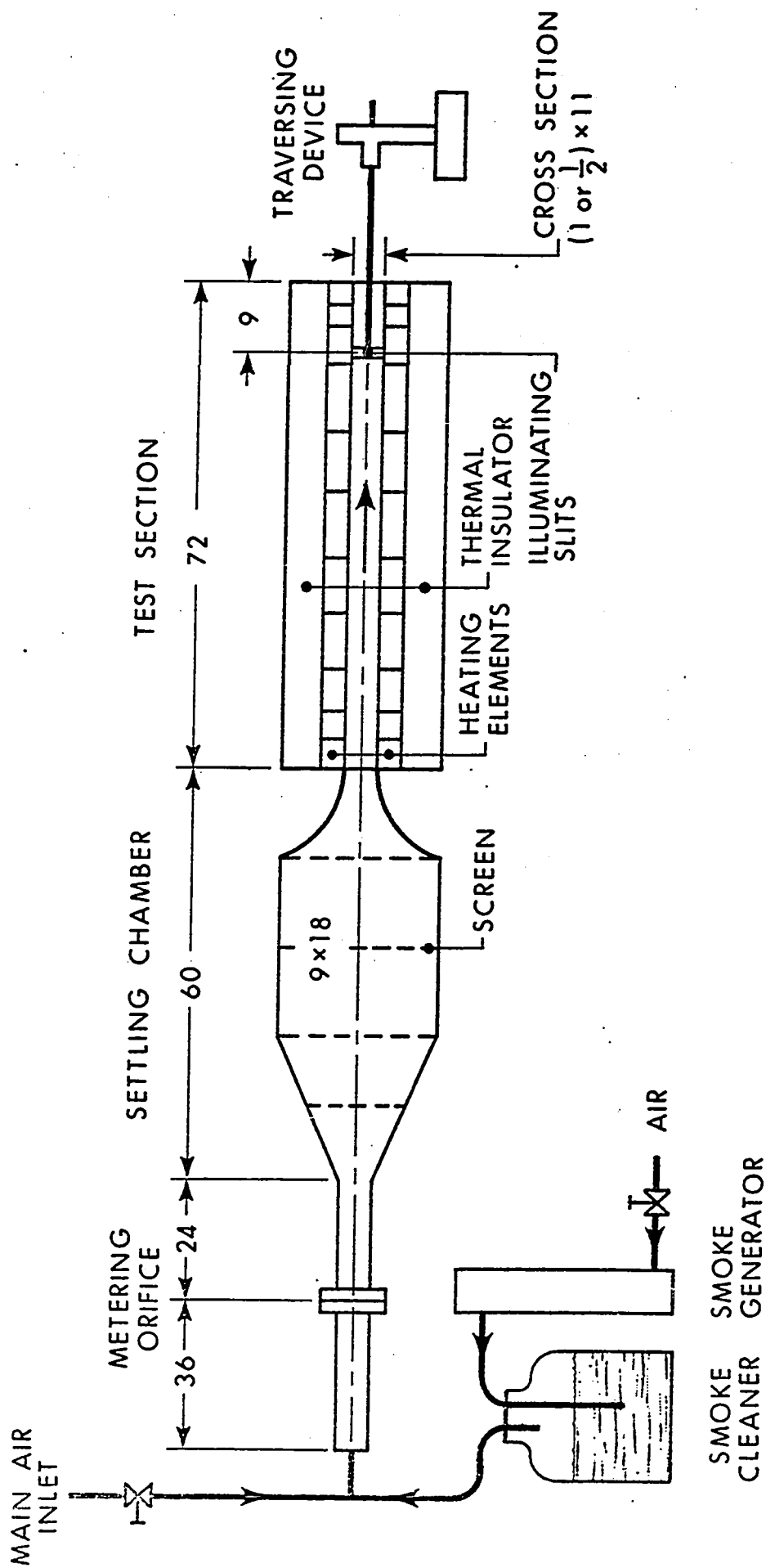


Fig.5.2 Schematic diagram of experimental apparatus (unit:inch)

difference is measured by Chattock type manometer. The metering system is calibrated by a rotary type gas meter with an error of approximately 0.5 per cent. Throughout the experiment, the Reynolds number is kept below 100 in order to eliminate the growth of any undesirable hydrodynamic disturbances which may be caused by any irregularity of the flow passage.

Smoke generator is located at some distance ahead of the metering orifice as shown in Fig. 5.2. This arrangement yields a fairly uniform smoke distribution in the test section. The flow visualization technique is confirmed by the experimental verification of the well known critical Rayleigh number of 1708 for the limiting case $\mu = 0$ and the determination of the critical $ReRa_T$ by transverse temperature measurement for the case $|\mu| \rightarrow \infty$ which will be described later. It may also be of interest to note that the cigarette smoke is selected for this experiment because of its smallest particle size among the many smoke sources available.

Two types of test section are used for the experiment. In one series of tests, the channel height is kept at $h = 1/2$ " with the upper plate having either heating elements or water cooling system. The latter consists of nine independently controlled segments arranged in the direction of main flow [5.1]. For a given value of the Reynolds number and a channel height h , an examination of the characteristic parameter $\mu = ReTh/\Delta T$ shows that the parameter μ can be increased

by adjusting either the axial temperature gradient τ or the temperature difference ΔT . However, there is an upper limit to the value of the temperature gradient τ to be imposed since in the theoretical analysis (see Chapter IV), the physical properties are all considered to be constant except for the density in the buoyancy term. We also note that for a given channel height h and the type of fluid such as air the only way one can raise the Rayleigh number is by increasing the temperature difference ΔT between the two plates. Consequently, it is found that the value of the characteristic parameter μ can not exceed around 10 with $h = 1/2$ ". This channel is found to be quite satisfactory for the experiment with $\mu = 0$ and the positive Rayleigh number for $\mu < 10$.

In another series of tests, the channel height is raised to $h = 1$ " with the upper plate having heating element only [5.1]. This modification enables us to carry out the experiment at higher values of the characteristic parameter μ and is found to be very satisfactory for the case of $\mu = 0$ and the case of negative Rayleigh number.

5.3 Experimental Results and Discussion

In order to confirm fully developed laminar flow at the test section, measurements for the velocity profile in the vertical direction through the center of the channel are made at several axial stations. The typical results for the measurements made at the distance $x' = 57$ in., 62 in., and 67 in., respectively, from the entrance of the channel without heating are shown in Fig. 5.3 with comparison made against the theoretical plane Poiseuille profile. It is found that there is no difference between the Poiseuille profile for the parallel-plate channel and the theoretical result for the rectangular channel (11 in. x 1 in.) through the center. Since a flow between two infinite horizontal parallel plates is simulated by a horizontal rectangular channel with finite aspect ratio, the extent of the influence of the two side walls must be ascertained. For this purpose, the transverse velocity profile through the center of the channel is also measured with a typical result compared against the theoretical curve for the rectangular channel in Fig. 5.4. Figs. 5.3 and 5.4 show clearly that the velocity distribution is fully developed at the measuring stations even at relatively high Reynolds number of 160. Consequently, with lower Reynolds number, we are further assured of the fully developed flow regime. It is also seen that a considerably wide central region of around $7h$ ($h = 1$ in.) may be considered as fully developed Poiseuille profile for the parallel-plate channel.

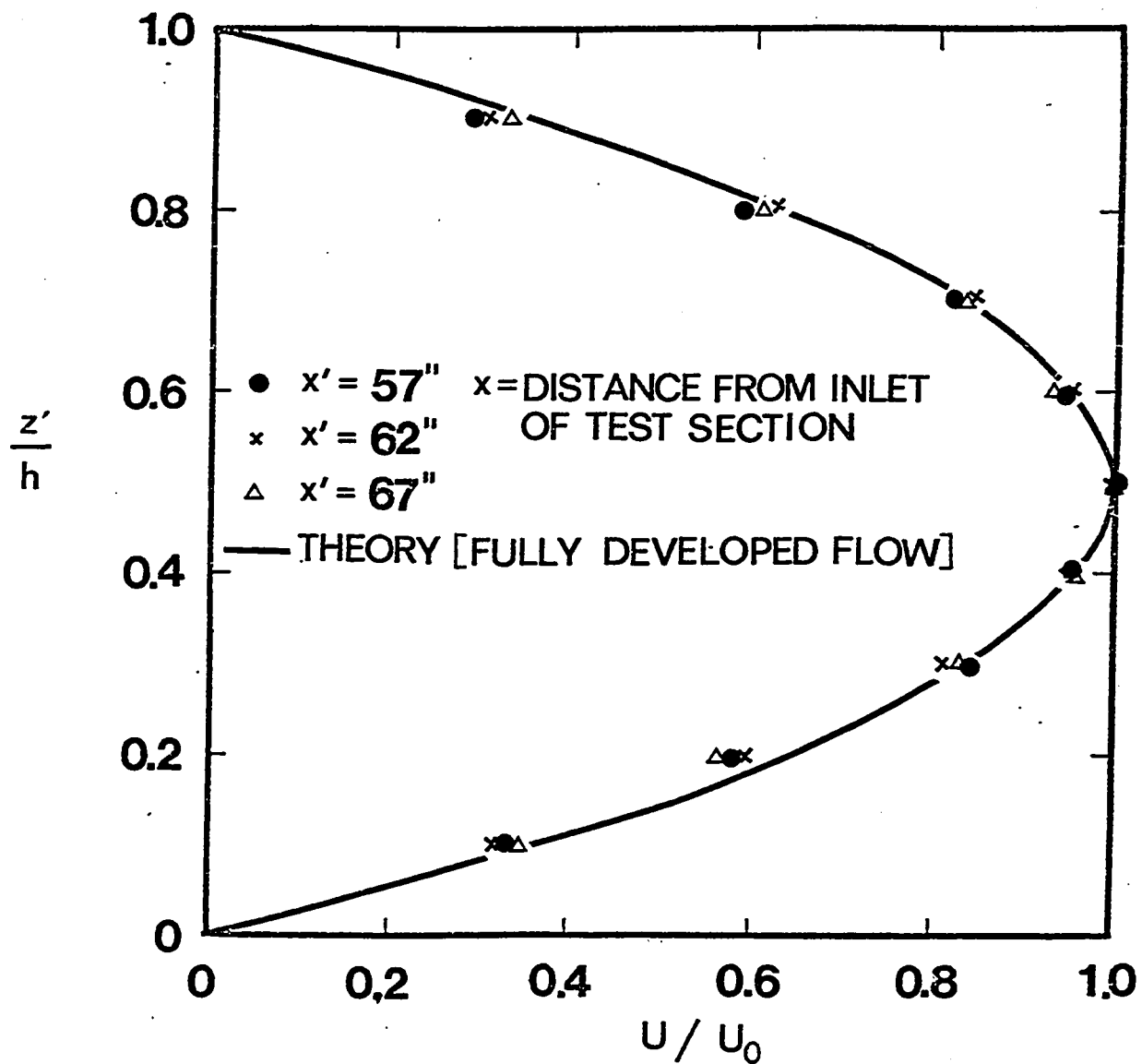


Fig. 5.3 Comparison of experimental data with theoretical velocity distribution at $y' = 0$ with $h = 1$ inch and $Re = 160$

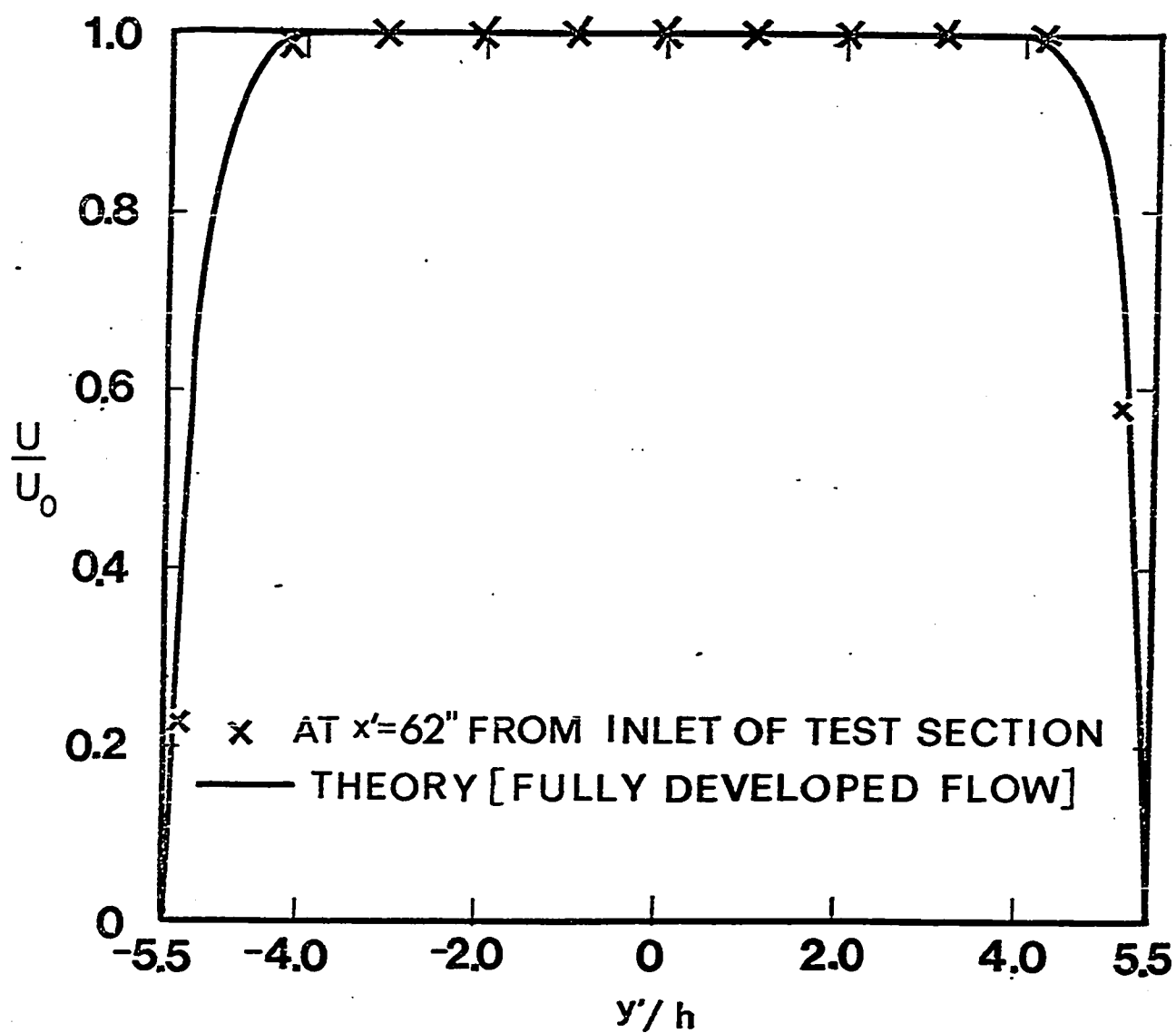


Fig.5.4 Comparison of experimental data with theoretical velocity distribution along transverse direction y' at $z'/h = 0.5$ with $h = 1$ inch and $Re = 160$.

We can conclude that the aspect ratios of the rectangular channel used are sufficiently large to simulate plane Poiseuille flow in the central region of the channel.

In addition to the confirmation of hydrodynamically fully developed laminar flow, thermally fully developed temperature field is also ascertained by temperature measurements at several axial stations and typical results of the temperature measurements in the vertical direction through the center of the channel are shown in Fig. 5.5 for the thermal boundary conditions of $T_1 = T_2$ and uniform temperature gradient ($1.85^\circ\text{F}/\text{in.}$) in the axial direction. The solid curve in Fig. 5.5 represents the theoretical plane Poiseuille flow profile and we can see that the agreement is good. We may add that the linear temperature distributions in the axial direction for both upper and lower plate are quite satisfactory.

The primary purpose of this investigation is the experimental determination of the critical Rayleigh number for the onset of the longitudinal vortex rolls and the comparison with the theoretical neutral stability curves presented in Chapter IV. The onset of the columnar vortices is determined by flow visualization and confirmed also by transverse temperature profile measurement for the case of $|\mu| \rightarrow \infty$. Based on the theoretical result for isothermals of perturbation temperature reported in Fig. 4.8 of Chapter IV, transverse temperature measurements are made at $z' = h/4$ from the bottom plate surface in the central region of the channel

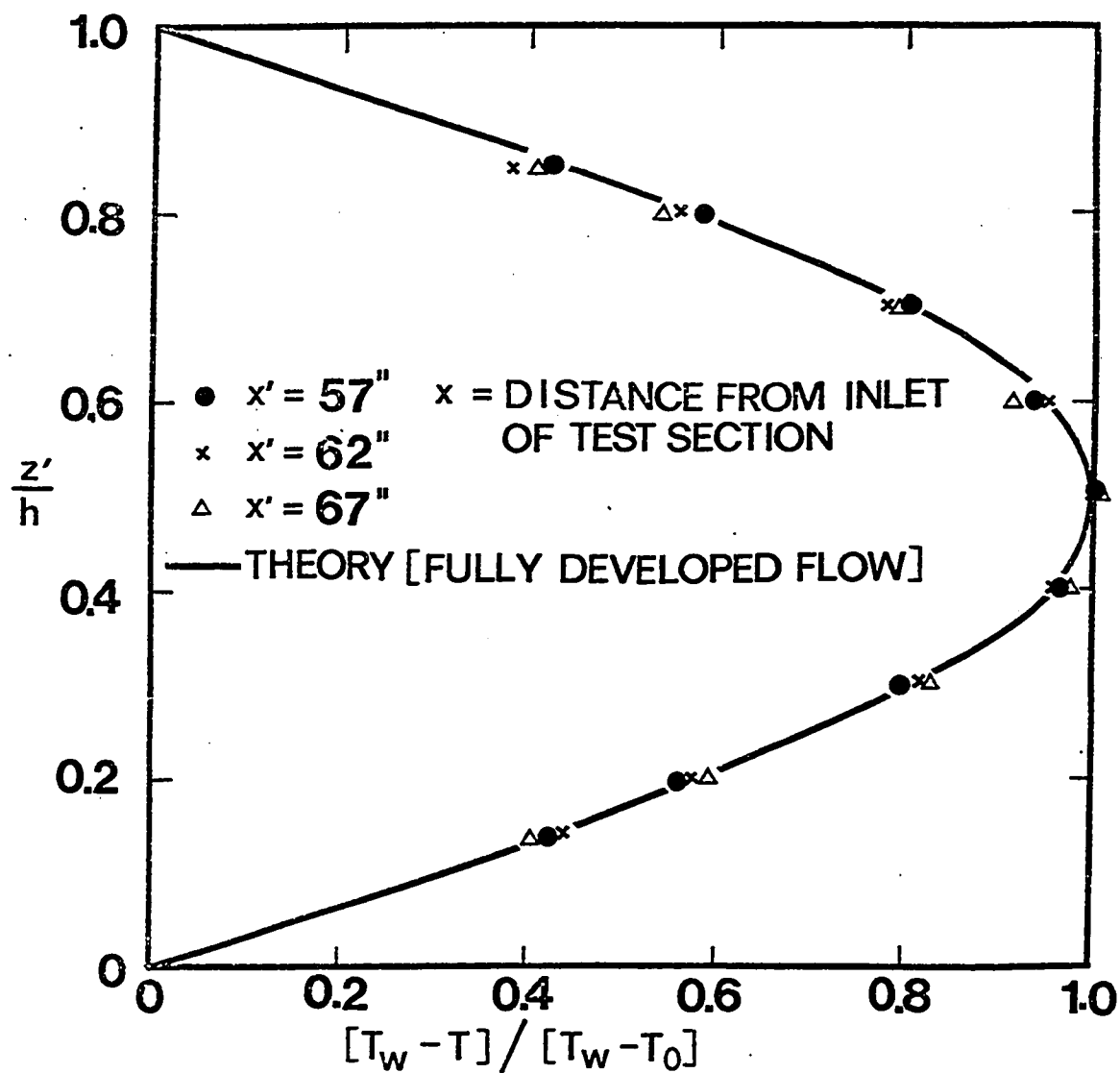


Fig.5.5 Comparison of experimental data with theoretical temperature distribution at $y' = 0$ with $Re = 140$, $h = 1$ inch, $\tau = 1.85^\circ\text{F/in.}$ and $T_w = 85.6^\circ\text{F}$ at $x' = 62$ inches

in order to obtain approximately maximum temperature fluctuation. For the purpose of flow visualization and photographing the flow pattern from the exit of the channel, the channel is illuminated by two light sources through two side slits of 1/8 in. width located at 9 in. from the exit as illustrated in Fig. 5.2. Temperature measurement is made using two-dimensional traversing mechanism for a thermocouple under smoke free condition.

In this investigation, the experiment is done for the following four cases:

(a) The characteristic parameter $\mu = Re\tau h/\Delta T = 0$ or $\tau = 0$, $T_1 > T_2$ and $Re \neq 0$. This case is specifically designed to check the accuracy of the testing apparatus by utilizing the well known critical Rayleigh number of 1708 regardless of the presence of forced flow. We note that the variation of Reynolds number has no effect on the onset of the secondary flow. However, at extremely low Reynolds number, the longitudinal vortices may disappear.

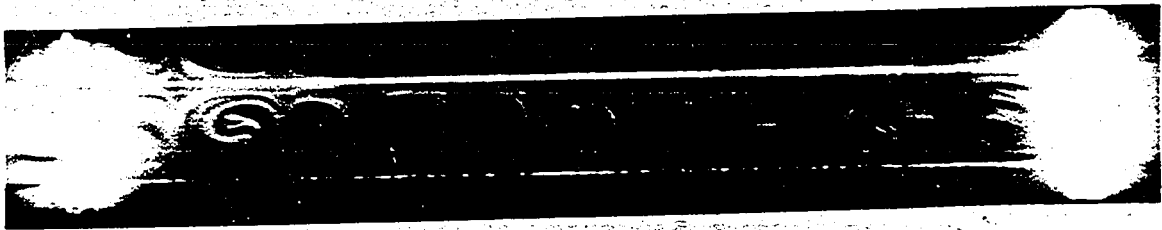
(b) The case of $\mu > 0$, $Ra > 0$ ($T_1 > T_2$), and $\tau = \text{constant}$. The data for this case are obtained from the channel with height $h = 1/2$ in. and the magnitude of the parameter μ is limited to around 7 because of the limitation imposed by the height of the channel as explained earlier.

(c) The Rayleigh number is negative ($T_2 > T_1$) and $\tau = \text{constant}$. The range of the characteristic parameter used is $-6 > \mu > -60$. This case of negative Rayleigh number

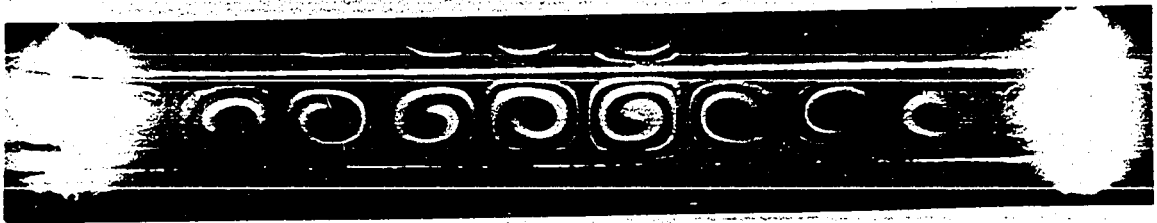
allows us to traverse the stable, neutral and unstable regions by simply varying the Reynolds number. The data for this case are obtained from the channel with $h = 1$ in.

(d) The limiting case of $|\mu| \rightarrow \infty$ where the top and bottom plates are kept at the same temperature with the uniform axial wall temperature gradient. This case is of interest in practical application.

The experimental results on the determination of the critical Rayleigh number for the above four cases will be explained next. For case (a) with vanishing axial temperature gradient, the eigenvalue problem concerning with the onset of the vortex rolls is independent of the fully developed velocity profile and the problem is identical to that solved by Pellew and Southwell [4.7]. The instability of the problem is solely due to the adverse temperature gradient in the vertical direction. The flow patterns of the vortex rolls at $Ra = 4160$ for the channel with $h = 1$ in. are shown in Fig. 5.6 for several different Reynolds numbers. For a given Rayleigh number, the number of closed streamlines increases as the Reynolds number decreases. This is clearly seen in Fig. 5.6. For the cases with $Ra > 1708$, the flow pattern is very regular and the pitch of the vortex rolls does not seem to change appreciably. Mori and Uchida [4.6] note that the wavelength predicted by the linearized theory agrees with the experimental results only up to $h = 15$ mm and the wavelength remains constant if $h > 15$ mm. However, the



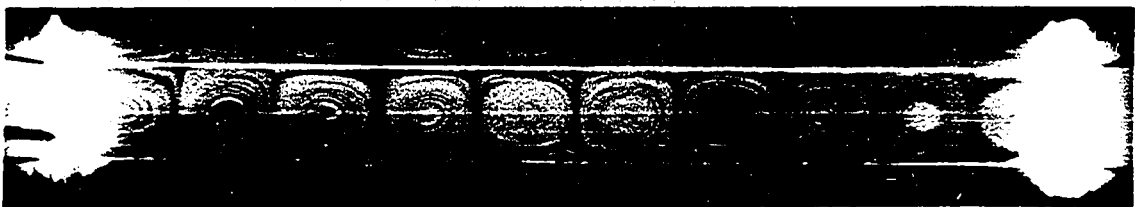
$Ra = 4,160$, $Re = 46.9$, and $a = 3.31$



$Ra = 4,160$, $Re = 18.8$, and $a = 3.00$

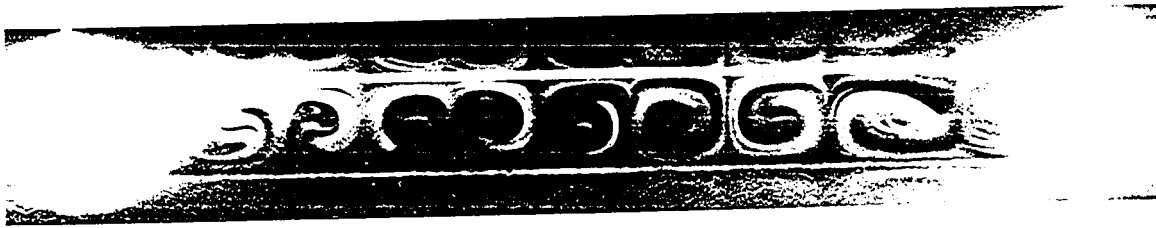


$Ra = 4,160$, $Re = 8.3$, and $a = 3.00$



$Ra = 4,160$, $Re = 4.7$, and $a = 3.00$

Fig.5.6 Secondary flow patterns for the case $\mu = 0$ and $h = 1$ inch



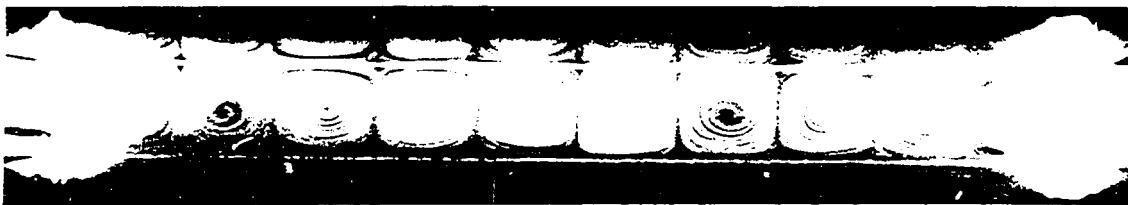
$Ra = 4,160$, $Re = 46.9$, and $a = 3.31$



$Ra = 4,160$, $Re = 18.8$, and $a = 3.00$



$Ra = 4,160$, $Re = 8.3$, and $a = 3.00$



$Ra = 4,160$, $Re = 4.7$, and $a = 3.00$

Fig.5.6 Secondary flow patterns for the case $\mu = 0$ and $h = 1$ inch

result of the present study for the case $h = 1$ in. clearly contradicts with their result. It is believed that as long as the flow is fully developed and the temperature difference ΔT remains small enough so that Bousinnesq approximation is valid, the linearized theory can be applied even for the case when $h > 15$ mm. The results of flow visualization for this case with $\mu = 0$ are plotted in Fig. 5.7 where a cross means no detectable secondary flow, a triangle means uncertain situation and a circle means definitely observable secondary motion. Since the experimental data confirm well the well-known critical Rayleigh number of 1708, we may conclude that the testing apparatus yields sufficiently accurate data.

For the reasons explained earlier, the channel with height $h = 1/2$ in. is not suitable for the experiments involving the case when $|\mu| > 8$. Case (b) of the experiment is conducted using this channel. For this case the instability is caused by the presence of both the adverse temperature gradient in the vertical direction and the product of axial temperature gradient τ and the main flow velocity disturbance. An examination of the neutral stability curve for the case of positive Rayleigh number ($T_1 > T_2$) for the air (see Fig. 5.7) shows that the slope of the curve is rather small for the value of μ ranging from 1 to 10. Consequently, in order to obtain a series of data crossing the theoretical stability curve, we must adjust the temperature difference ΔT between the two plates and this requires quite a long time. For this

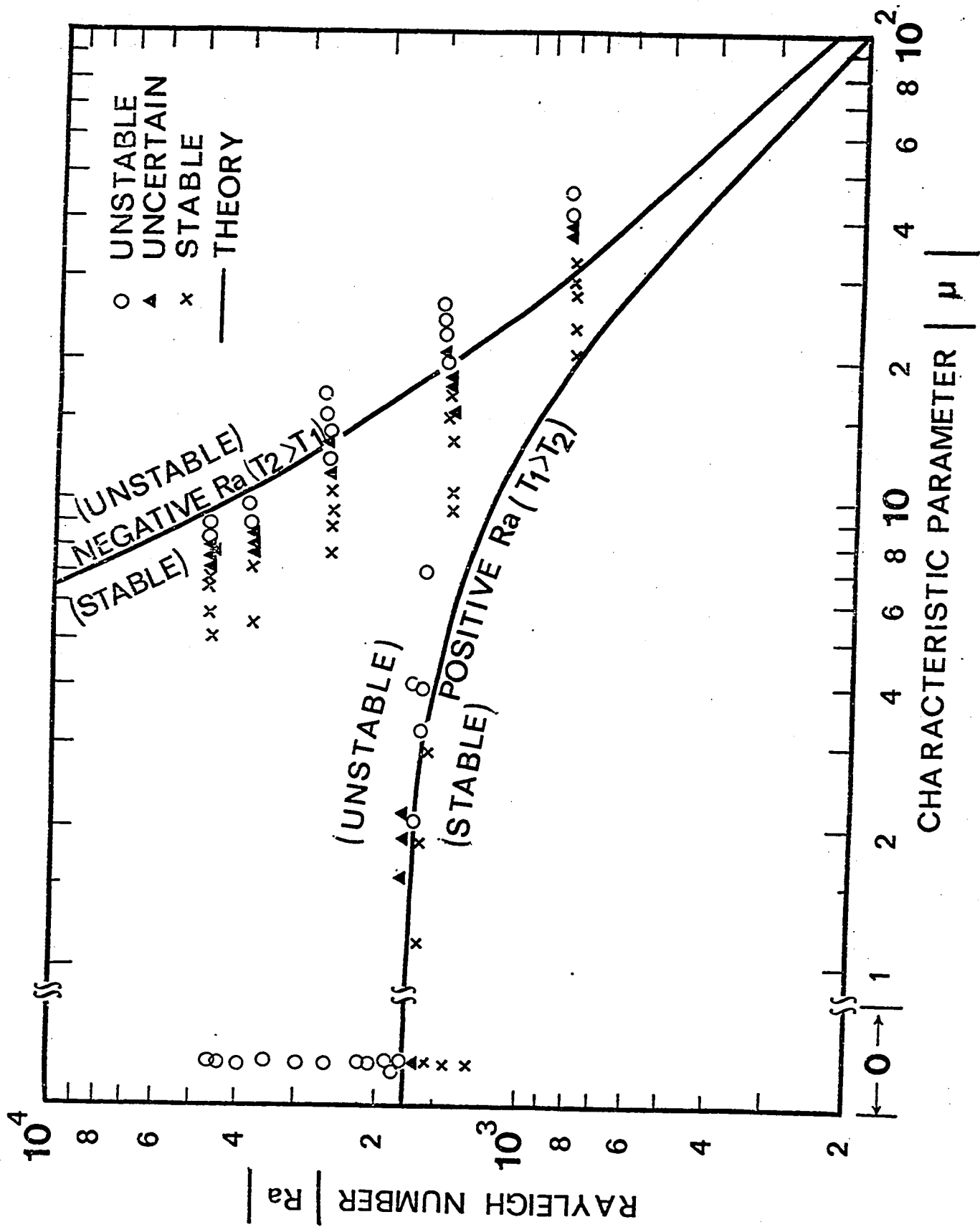


Fig.5.7 Comparison of experimental data with theoretical stability curves for longitudinal vortex rolls.

series of experiment, the temperature difference ΔT ranges from 20 to 35°F and the axial temperature gradient τ ranges from 1.5 to 4.0°F/in. The experimental data from flow visualization are plotted in Fig. 5.7. The difficulties encountered by the channel with $h = 1/2$ in. can be overcome readily by increasing the channel height to $h = 1$ inch.

The experimental data for the case of negative Rayleigh number ($T_2 > T_1$) using channel height $h = 1$ in. will be discussed next. It will be recalled that for the horizontal fluid layer with main flow but with vanishing axial temperature gradient, the flow is theoretically always stable. With main flow and axial temperature gradient, the instability is again caused by the adverse temperature gradient which exists near the lower plate and the product of axial temperature gradient τ and the main flow velocity disturbance u' . An examination of the theoretical neutral stability curve for this case (see Fig. 5.7) shows that it is convenient to cross the neutral stability curve by changing the value of μ (or Reynolds number). For this series of tests, the temperature difference ΔT between the two plates is kept generally between a few degrees to less than 10°F and the axial temperature gradient τ is kept constant in each case with the value ranging from 0.81 to 0.96°F/inch.

The experimental data from flow visualization for the case of negative Rayleigh number are compared against the theoretical neutral stability curve in Fig. 5.7. Fig. 5.8

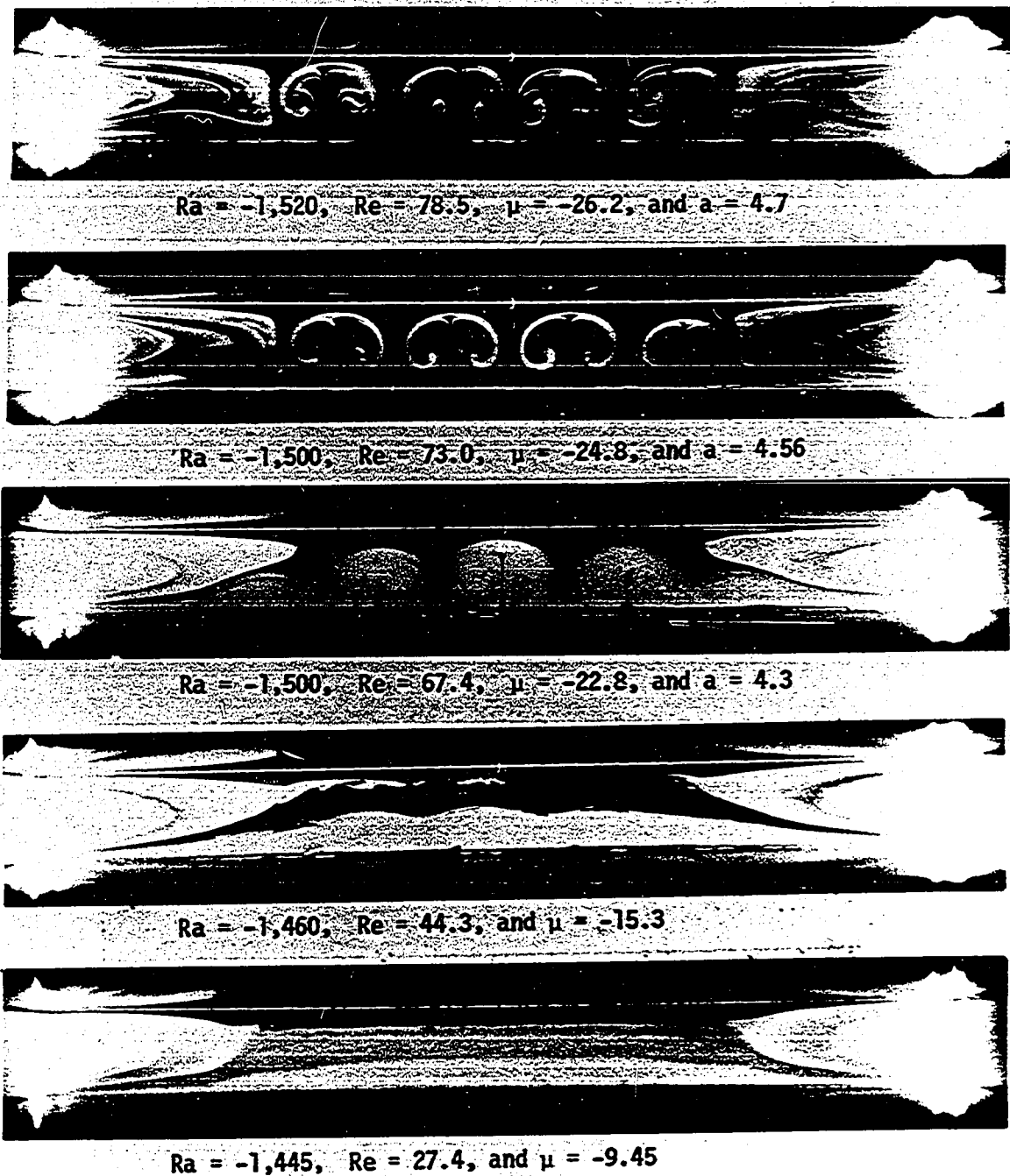


Fig.5.8 Formation of secondary flow patterns with free convection effect for the case of negative μ and $h = 1$ inch

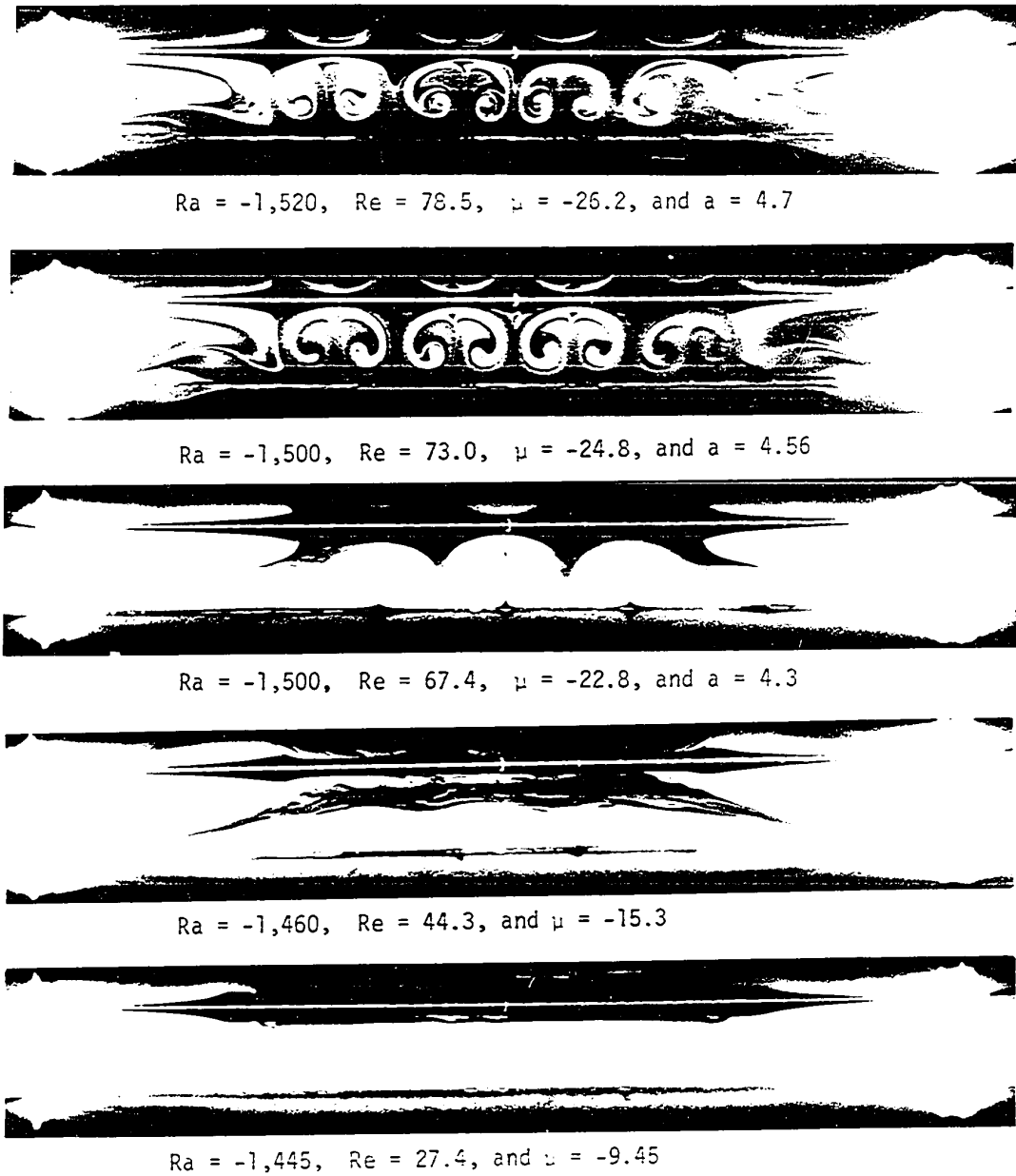


Fig.5.8 Formation of secondary flow patterns with free convection effect for the case of negative μ and $h = 1$ inch

illustrates a series of flow pattern starting from stable state to post-critical regime. At $\mu = -9.45$ and $Ra = -1445$, we can see that laminar free convection from heated vertical side wall extends to about $3h$ in the horizontal direction. Noting that the channel width is $11h$ in this case, we conclude that the side wall effect is considerable. We can see the distribution of smoke particles in the central region which is still stable. This situation is marked as a cross in Fig. 5.7. At $\mu = -15.3$ and $Ra = -1460$, we can barely detect the motion of smoke particles in the horizontal direction and the extent of free convection effect due to side walls increases slightly. This situation is marked as a triangle in Fig. 5.7 indicating the uncertain situation. It is seen that the smoke particles occupy the lower half of the central region of the channel. At $\mu = -22.8$ and $Ra = -1500$, three pairs of longitudinal vortices appear clearly and this situation is marked as a circle in Fig. 5.7 indicating definite instability. The deviation from the theoretical stability curve for the two sets of experimental data at higher values of Rayleigh number can be attributed to the free convection effect due to side walls and variable property effect. The remaining three sets of experimental data at lower values of Rayleigh number are considered to be quite satisfactory and in particular at $Ra = -800$ the agreement with theory is excellent.

The experimental data from flow visualization and

transverse temperature measurement for the limiting case of $|\mu| \rightarrow \infty$ are compared against the theoretical critical value of $\text{ReRa}_\tau = 2.13 \times 10^4$ in Fig. 5.9. One set of flow patterns illustrating the gradual development of secondary flow starting from completely stable state to the post-critical state is shown in Fig. 5.10. The general situation is similar to the ones discussed earlier. In addition to the photographic results, experimental data from the transverse temperature profile measurement made at a distance $z' = h/4$ from the lower plate surface are presented in Fig. 5.11 and these correspond to the test run number 2 in Fig. 5.9. Referring to Fig. 5.11, at $\text{ReRa}_\tau = 1.23 \times 10^4$, we can detect slight variation of transverse temperature distribution but this result is marked as a cross in Fig. 5.9 indicating stability because of its rather uniform distribution and uncertain nature of disturbances. At $\text{ReRa}_\tau = 2.65 \times 10^4$, we can see definite fluctuation of transverse temperature profile around mean temperature but this result is considered to be uncertain in Fig. 5.9 since the pitch is not clearly defined yet. At $\text{ReRa}_\tau = 3.37 \times 10^4$, we can see the periodic distribution indicating the definite establishment of the secondary flow. With further increase of ReRa_τ , the amplitude of the periodic temperature distribution increases further indicating stronger secondary flow intensity. For the limiting case of $|\mu| \rightarrow \infty$, the experimental data from visualization and transverse temperature measurement confirm each other serving to demonstrate

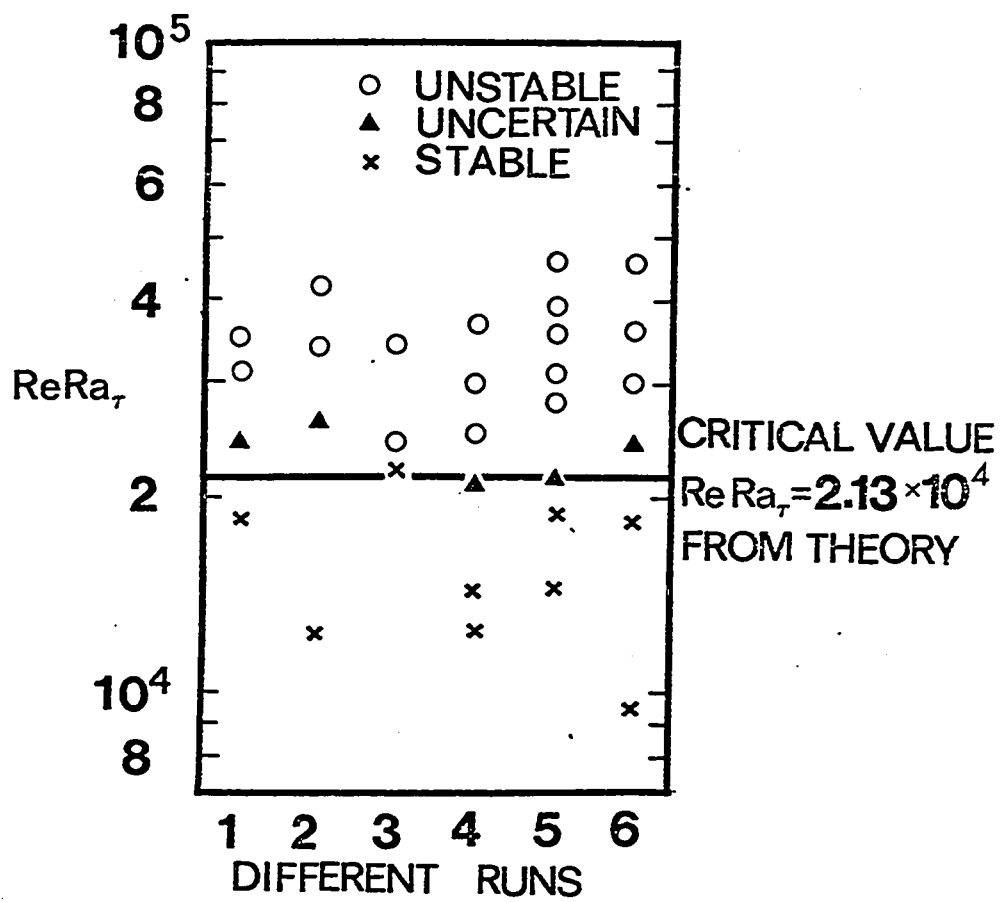


Fig.5.9 Comparison of experimental data with critical $ReRa_\tau$ for the case $|\mu| \rightarrow \infty$.

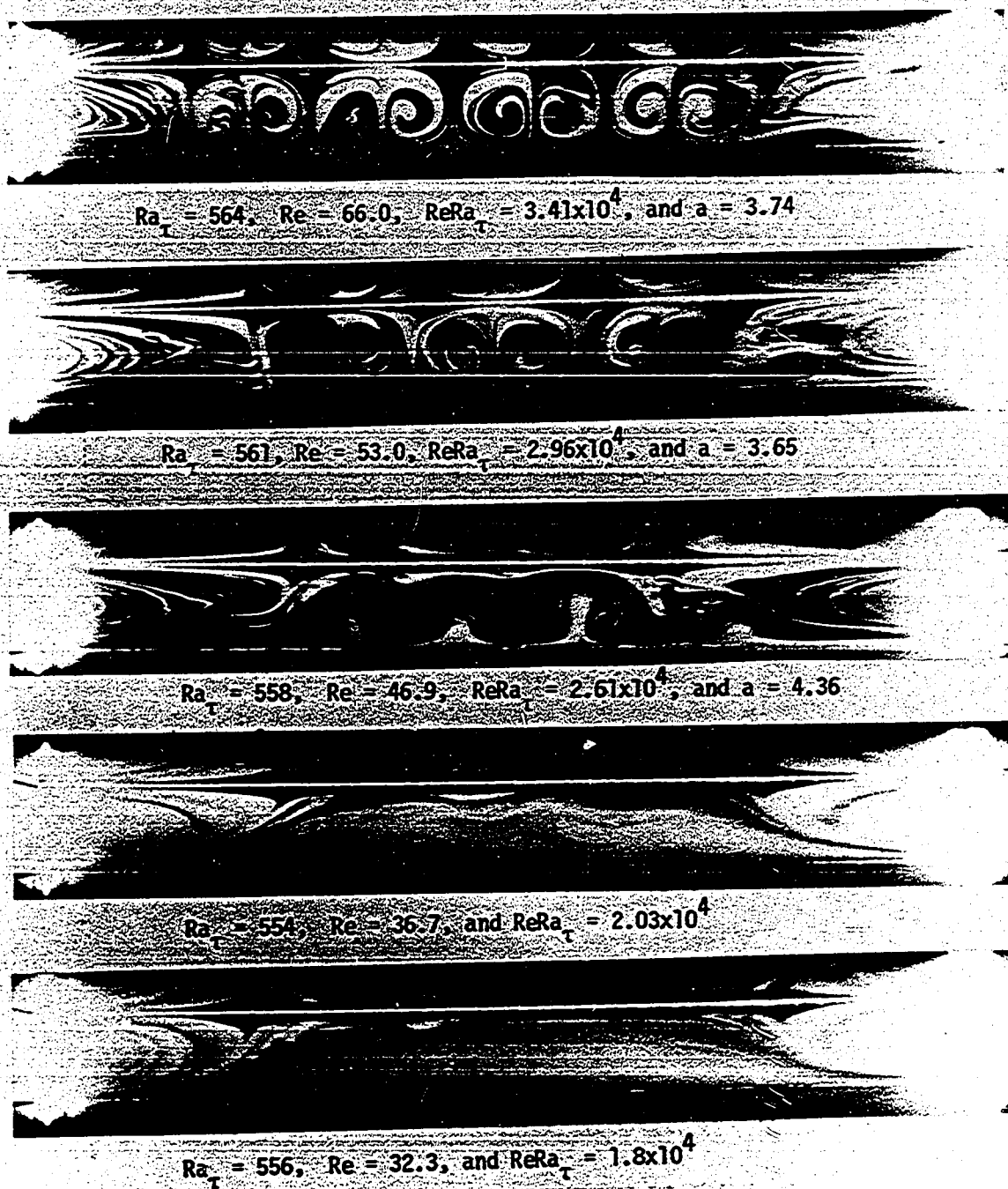


Fig.5.10 Formation of secondary flow patterns with free convection effect for the case $|\mu| \rightarrow \infty$ and $h = 1$ inch



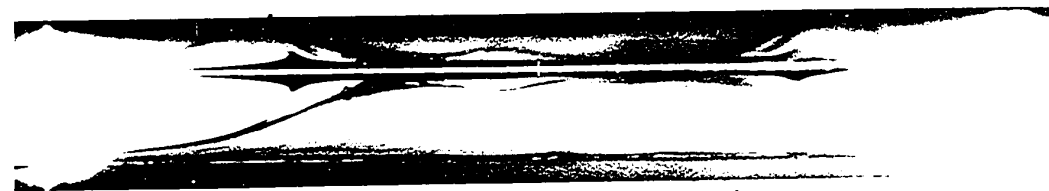
$$Ra_\tau = 564, Re = 66.0, ReRa_\tau = 3.41 \times 10^4, \text{ and } a = 3.74$$



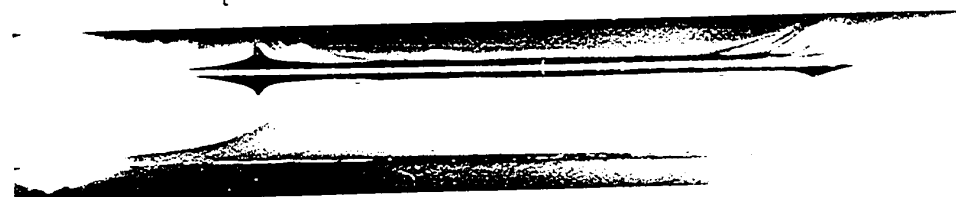
$$Ra_\tau = 561, Re = 53.0, ReRa_\tau = 2.96 \times 10^4, \text{ and } a = 3.65$$



$$Ra_\tau = 558, Re = 46.9, ReRa_\tau = 2.61 \times 10^4, \text{ and } a = 4.36$$



$$Ra_\tau = 554, Re = 36.7, \text{ and } ReRa_\tau = 2.03 \times 10^4$$



$$Ra_\tau = 556, Re = 32.3, \text{ and } ReRa_\tau = 1.8 \times 10^4$$

Fig.5.10 Formation of secondary flow patterns with free collector effect for the case $|\psi| \rightarrow \infty$ and $h = 1$ inch

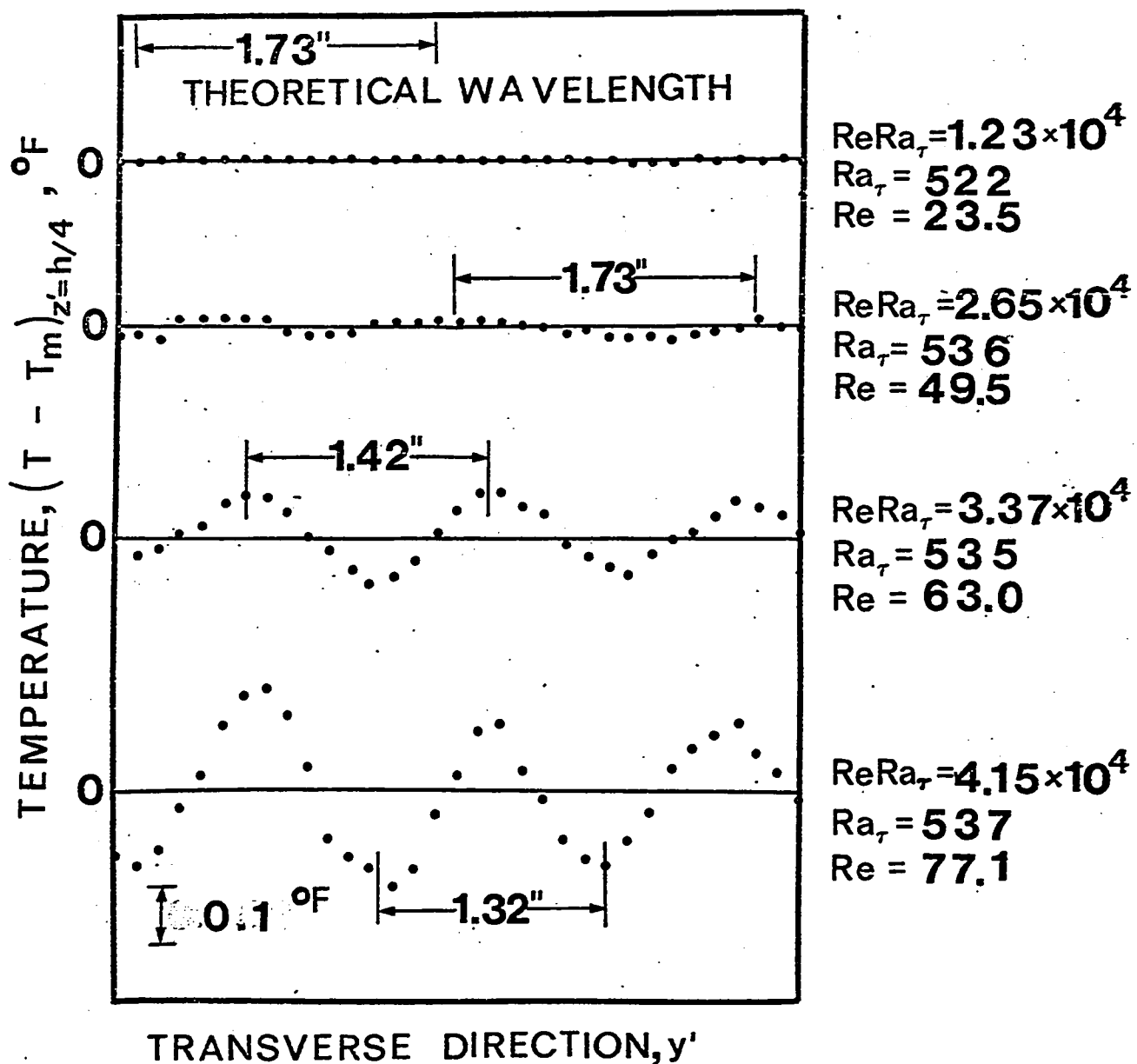


Fig.5.11 Transverse temperature measurement data for $|\mu| \rightarrow \infty$

the adequacy of the flow visualization technique.

Fig. 5.12 summarizes the data for the variation of wave number $a = 2\pi h/(\text{wave length})$ with the characteristic parameter $|\mu|$ in the post-critical regime. The curves for critical wave number versus $|\mu|$ from theory are also shown. The results from thermocouple data are shown as square and the solid circle or square represents the closest data point near the theoretical curve for a given series of tests. For the limiting case of $\mu = 0$, the solid circles are seen to be located quite close to the theoretical value of $a = 3.116$. The remaining data also do not deviate very far from the theoretical value of $a = 3.116$. For the case when $|\mu| \rightarrow \infty$, the experimental data show a definite increase of the wave number (or decrease of the wavelength) with the variation of ReRa_τ . The solid circles and squares check very well again with the theoretical value $a = 3.621$. For the case of negative μ (or negative Rayleigh number), the solid circles generally follow the theoretical curve but the other data show some uncertain result. Because of the free convection effect from the side walls, experimental errors and other uncertainties, the above remark must be considered as tentative.

Finally, we note that the case of $|\mu| \rightarrow \infty$ corresponds to the limiting case of infinite aspect ratio for the combined free and forced laminar convection in horizontal rectangular channel reported in reference [2.5]. For the problem dis-

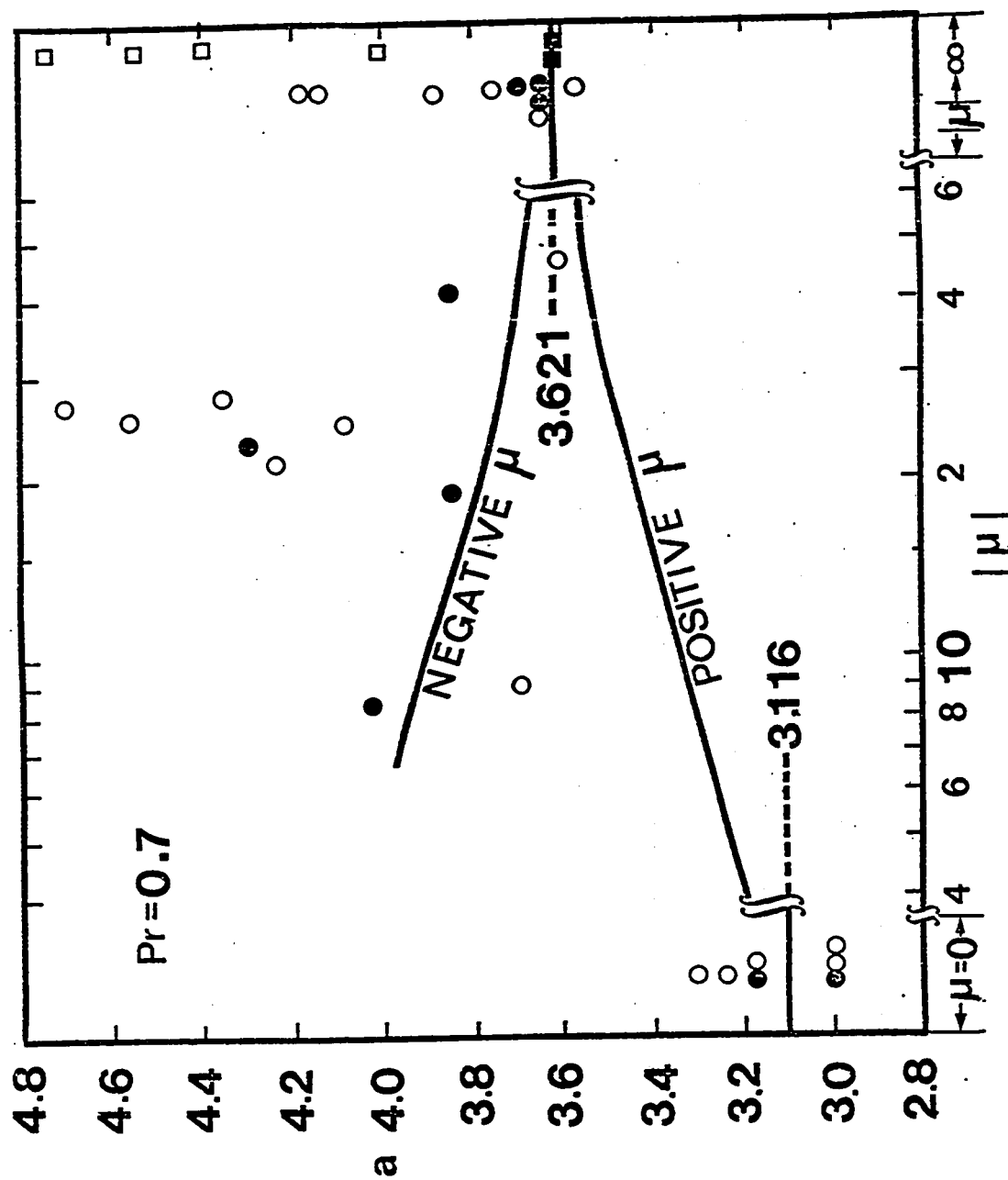


Fig.5.12 Comparison of critical wave number versus $|\mu|$ from theory with experimental data from post-critical regime.

cussed in reference [2.5], secondary motion exists only near the side walls. Theoretical analysis in Chapter IV reveals the possibility of secondary flow even in the case of infinite aspect ratio. The present experimental study (see Fig. 5.10) reveals further that with the aspect ratio of 11 used in the experiment, another type of secondary flow in the form of longitudinal vortices due to thermal instability will appear at a certain critical $ReRa_T$ depending on Prandtl number in addition to the known secondary motion due to free convection near the side walls. The practical implication of Fig. 5.10 is significant since it reveals that with the aspect ratio of around 10 for the horizontal rectangular channel, the flow and heat transfer characteristics cannot be predicted with the existing theory after reaching a certain critical $ReRa_T$. For example, according to reference [2.5], for the horizontal rectangular channel with infinite aspect ratio, the secondary flow has no effect on flow and heat transfer results. However, as confirmed by the present experimental study thermal instability problem appears in practice. This also means that the known Nusselt number of 8.235 for fully developed laminar flow between two parallel plates with uniform wall heat flux cannot be applied when the $ReRa_T$ reaches a certain critical value.

5.4 Concluding Remarks

(a) Experimental data on the onset of longitudinal vortices for fully developed laminar forced convection between two horizontal plates are compared with theory and the agreement is found to be good. The accuracy of the testing apparatus is ascertained by considering the limiting case of vanishing axial temperature gradient and heating from below which has a known critical Rayleigh number of 1708. The adequacy of the flow visualization technique used is confirmed by the transverse temperature measurement at a distance of $h/4$ from the bottom surface for limiting case of $|\mu| \rightarrow \infty$.

(b) For the negative Rayleigh number case, the free convection effect due to side walls is appreciable. The exact reasons for the deviation of experimental data from theory at higher Rayleigh numbers are difficult to assess. However, free convection effect due to side walls and variable property effect are believed to be the contributing factors.

(c) The flow visualization technique developed is satisfactory for the present investigation and reasonably good flow patterns are obtained for the secondary flow. Based on photographic results, we can see the extent of free convection effect due to side walls. The flow visualization technique is expected to be effective particularly for the experimental study dealing with post-critical regime. For example, the measurement of the pitch of vortex rolls can be

made readily.

(d) The practical implication of the present photographic results is believed to be significant since it reveals that for a horizontal rectangular channel with large aspect ratio, say near the order of 10, the effect of longitudinal vortices due to thermal instability must be considered in addition to free convection effect near the side walls for the evaluation of flow and heat transfer results after reaching a certain critical value of the characteristic parameter. Under this condition, we have boundary-value problem near the side walls and thermal instability problem in the central region of the channel. At present theoretical study in this area does not seem to be available in the literature.

References

- 5.1 Akiyama, M., Hwang, G.J., and Cheng, K.C., "Experiments on the Onset of Longitudinal Vortices in Laminar Forced Convection Between Horizontal Plates," Submitted to Journal of Heat Transfer for publication.
- 5.2 Sparrow, E.M., and Husar, R.B., "Longitudinal Vortices in Natural Convection Flow on Inclined Plates," Journal of Fluid Mechanics, Vol. 37, 1969, pp. 251-255.
- 5.3 Terada, T., and Tamano, M., "Further Researches on Periodic Columnar Vortices Produced by Convection," Report of the Aeronautical Research Institute, Tokyo University, Vol. IV, 12, No. 53, December, 1929.
- 5.4 Chandra, K., "Instability of Fluids Heated from Below," Proceedings Royal Society, London, Series A, Vol. 164, 1938, pp. 231-242.

CHAPTER VI

FINITE AMPLITUDE CONVECTION IN PLANE

POISEUILLE FLOW

6.1 Introduction

It is shown theoretically in Chapter IV and confirmed experimentally in Chapter V that for fully developed laminar forced convection between two finite horizontal flat plates, longitudinal vortices (vortices with axis in the main flow direction) occur if the destabilization due to buoyancy is large enough to overcome the stabilizing effects of viscous and thermal diffusion.

Several deficiencies or restrictions may be observed in the application of the results of the linearized theory for the thermal instability problem discussed in Chapter IV. Specifically they are:

(a) Physical properties are assumed to be constant and independent of temperature. The variation of density with temperature is ignored except in association with gravity (Boussinesq approximation). The variable property effect may be significant for some fluids. This may limit the range of applicability of the numerical results.

(b) The basic velocity and temperature fields are assumed to be fully developed. As pointed out in Chapter IV, the instability of flow in the entrance region may be significant under certain circumstances.

(c) The disturbances may not be considered to be infinitesimally small. This can be discussed from two points of view. Firstly, some type of finite amplitude disturbance may occur before the appearance of the infinitesimal disturbance. In other words, the flow may be disturbed by a finite amplitude disturbance with characteristic parameter below a certain critical value. Secondly, in the post-critical regime, the amplitude of the small disturbance may grow and the inertia and advective terms in the governing equations may no longer be considered to be relatively small.

(d) The wavelength and preferred mode shape of the longitudinal vortices may change in the post-critical regime, but they cannot be predicted by using the linearized theory. Similarly, with the linearized theory the amplitude of the disturbance is unknown and the disturbance may grow exponentially without limit.

(e) The flow and heat transfer characteristics cannot be determined.

In order to overcome the above difficulties (c), (d) and (e) due to linearized stability theory, many researchers have considered finite amplitude problems for nonlinear processes involving, for example, Taylor vortices between rotating cylinders and the Bénard cells of thermal convection. In 1923, Taylor [4.3] observed the vortex instability in flow between rotating cylinders. He observed that a moderate increase in the speed of the cylinders merely increases the

intensity of the circulation in the vortices without altering appreciably their spacing or position. In 1958, Malkus and Veronis [6.1] made the first attempt to predict the heat transfer rates for finite amplitude cellular convection. The quasi-linear equations describing the fields of motion and temperature are expanded in a sequence of inhomogeneous linear equations dependent upon the solutions of the linear stability problem. An infinite number of steady state finite amplitude solutions which formally satisfy the basic equations are found to exist. A criterion for "relative stability" is deduced which selects as the realized solution that one which has the maximum mean-square temperature gradient. In 1958, Stuart [6.2] described finite disturbances under subcritical and supercritical conditions by using an energy method and the shape of the amplitude functions obtained from the linearized theory. In 1965, Roberts [6.3] considered the non-linear Bénard convection by using an approximate procedure. By employing the concept of local potential, Roberts shows the behavior of the preferred wave number as a function of the Rayleigh number. The wave number a varies from 0 to 1% for Rayleigh numbers ranging from 1708 to 4000. However, the small variation of the wave number may not have significant effect on the heat transfer result. In the same year, Fromm [6.4] obtained numerical solutions of the quasi-linear equation for a horizontal fluid layer heated from below for both free-free and rigid-rigid boundary conditions. The solutions

are obtained for values of the Rayleigh number ranging from the critical value to 10^7 . In 1966, Mori and Uchida [4.6] applied Stuart's approximate energy method for nonlinear mechanics of hydrodynamic stability [6.2] to fully developed laminar forced convection between two infinite horizontal flat plates where the lower plate is heated isothermally and the upper plate is cooled isothermally. Mori and Uchida studied the problem in post-critical regime with Rayleigh numbers ranging from the critical value up to nine times the critical value and compared with experimental work. It is noted that Stuart's method represents an approximation to a perturbation theory about the critical characteristic number and so the energy-balance method cannot be expected to be valid for a large range of Rayleigh number above the critical value. For the analogous problem of rotating-cylinder flow, it is estimated that for a Taylor number up to ten times the critical value the largest error is about 7% for the torque. It is significant to note that the problem treated by Mori and Uchida [4.6] is identical to steady laminar Bénard convection with two-dimensional rolls. It is also of interest to note that Stuart's integral theory was applied by Mori and Uchida [6.5] in 1967 to forced convection heat transfer in a curved rectangular channel with large aspect ratio (height/width) where the vortex rolls are caused by an instability phenomenon due to centrifugal forces. In the same year, Samuels and Churchill [6.6] applied finite-difference

methods to compute hydrodynamic instability due to natural convection in an enclosed horizontal rectangular region heated from below. Critical Rayleigh numbers were determined for a series of Prandtl numbers and length-to-height ratios. For Rayleigh number greater than the critical value, the Nusselt number, temperature and velocity fields were determined. In 1968, Plows [6.7] presented numerical results for two-dimensional steady laminar Bénard convection. An iterative numerical technique was used to calculate the Nusselt number and the structure of the roll for Rayleigh numbers ranging from 2000 to 22000 for the various Prandtl numbers of 0.5, 1, 2, 6, 8 and 200. In these calculations, the roll width was taken to be π/a where $a = 3.117$ corresponds to the primary mode predicted by linear perturbation analysis. It is noted that the literature on the classical problem of the Bénard convection is too extensive to be reviewed here; only a brief review of some references which are related to the present study is attempted.

The purpose of this chapter is to study the effects of longitudinal vortex rolls in the post-critical regime on flow and heat transfer characteristics for fully developed laminar forced convection between two infinite horizontal parallel plates subjected to the same thermal boundary conditions as those described in Chapter IV for linear stability analysis. The physical problem of interest here is the finite amplitude thermal convection in plane Poiseuille flow

considering the nonlinear effect on the flow structure and temperature field. Because of uncertainty and the absence of accurate theory, the wave number a for the post-critical regime in this study will be taken to be the one which is predicted by the linear stability analysis discussed in Chapter IV for the primary mode. It is believed that the above assumption on the wave number a provides a good approximation at least for the parameter near the critical value. In view of the fact that Stuart's method is a perturbation approach and leads to appreciable error for thermal convection at high Rayleigh numbers, a numerical solution is employed for the present problem. Specifically, the boundary vorticity method is used in the numerical computation for the case of $\mu = 0$ and $Pr = 0.7$ and an improved iterative scheme discussed in Section 2.3(c) of Chapter II is also applied in the calculations for the cases of $\mu = \text{finite}$, $Pr = 0.7$ and $|\mu| \rightarrow \infty$ with various Prandtl numbers.

6.2 Theoretical Analysis

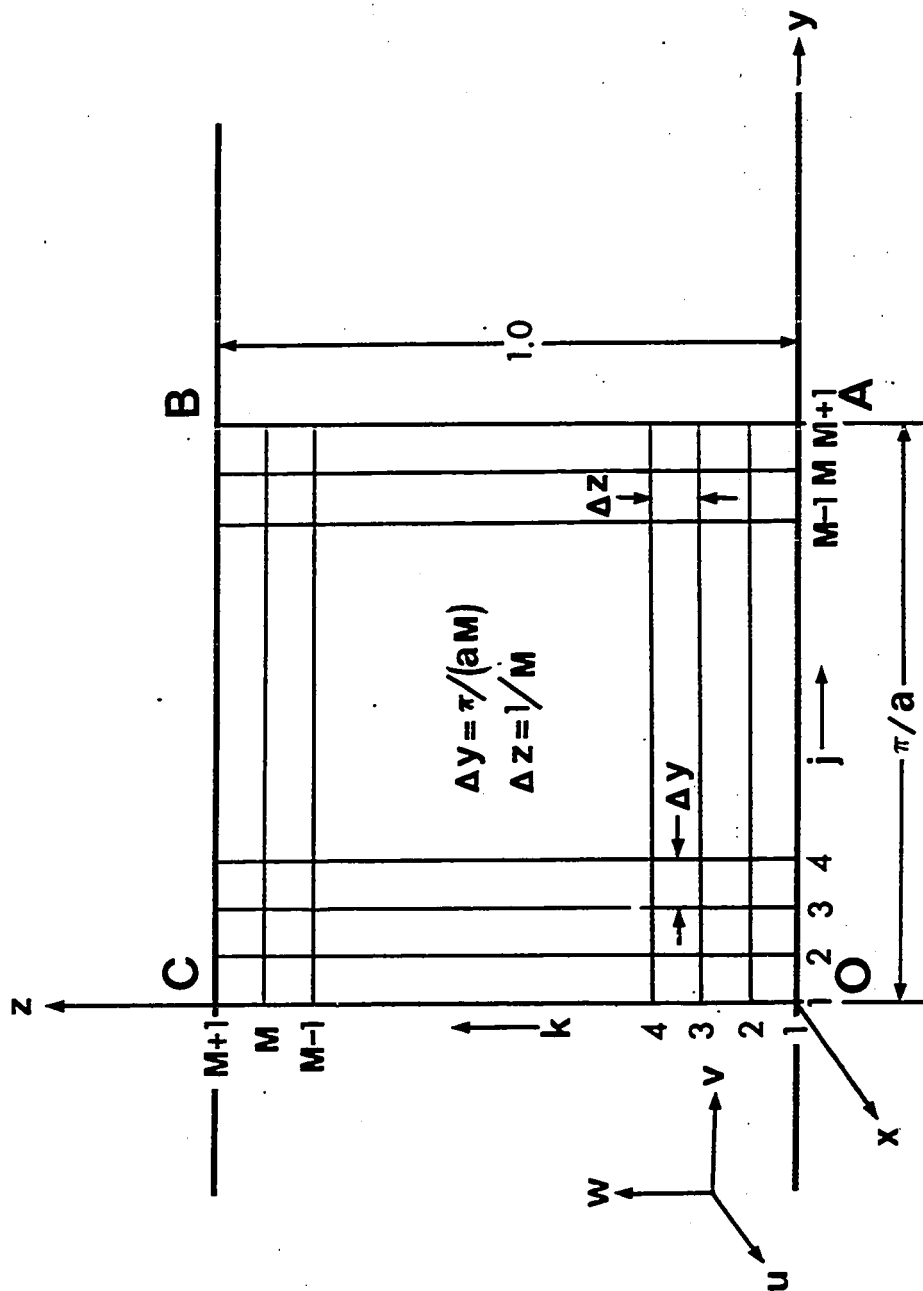
Consider a steady fully developed laminar forced convection in the post-critical regime between two infinite horizontal plates where the walls are subjected to the same uniform axial temperature gradient but possibly differing in temperature at any axial position. The onset of longitudinal columnar vortices due to buoyant forces was the subject of investigation in Chapter IV. The subject of interest here is the study of flow and heat transfer characteristics after the longitudinal vortex rolls set in.

In the formulation of the present problem, the following basic assumptions are made:

- (a) Velocity and temperature fields are fully developed, that is, all the first derivatives in the axial direction are either constant or zero.
- (b) Physical properties are constant and the Boussinesq approximation is valid.
- (c) Only the steady state solution is considered.
- (d) The wave number a for the post-critical regime is taken to be the one which is predicted by the linear stability analysis presented in Chapter IV.

The coordinate system employed here is similar to that shown in Fig. 4.1 except that the coordinate origin $y' = 0$ is now shifted horizontally by one-half wavelength to take advantage of the symmetry (see also Fig. 6.1).

In order to investigate the flow structure and tempera-



Along the lines DA and BC $u = \theta = \psi = \partial\psi/\partial z = 0$
 Along the lines AB and OC $\partial u/\partial y = \partial\theta/\partial y = \psi = \xi = 0$

Fig. 6.1 Coordinate system and numerical grid

ture field for the post-critical regime, perturbation quantities are superimposed on the basic flow quantities as,

$$U = U_b + u', V = v', W = w', T = T_b + \theta' \text{ and } P = P_b + p' \quad (6.1)$$

where the basic flow quantities U_b , T_b and P_b satisfy the well-known equations for plane Poiseuille flow. The solutions for the unperturbed state are:

$$U_b = 4U_0(z - z^2) = U_0\phi_u/2$$

$$T_b = T_1 - (U_0\tau h/\kappa)(z - 2z^3 + z^4)/3 - z\Delta T$$

$$= T_1 - \text{Pr Re}\tau h \phi_\theta - z\Delta T \quad (6.2)$$

$$\phi_u = 8(z - z^2)$$

$$\phi_\theta = (2/3)(z - 2z^3 + z^4)$$

where $z = z'/h$, U_0 is the maximum velocity in the unperturbed state, $\tau = \partial T/\partial x'$ is a constant axial temperature gradient and $\text{Re} = U_0 h/(2\nu)$.

Applying the assumptions (a) to (d) and equation (6.1) to the Navier-Stokes equations and the energy equation, and subtracting the equations for plane Poiseuille flow from

the respective Navier-Stokes equations and the energy equation then we obtain the equations for the perturbation quantities after eliminating pressure terms between y' - and z' -direction momentum equations. The perturbation equations are:

Axial momentum equation

$$v' \frac{\partial u'}{\partial y'} + w' \frac{\partial u'}{\partial z'} + w' \frac{\partial u_b}{\partial z'} = \nu \nabla_1^2 u' \quad (6.3)$$

Vorticity transport equation for secondary flow

$$v' \frac{\partial \xi'}{\partial y'} + w' \frac{\partial \xi'}{\partial z'} = \nu \nabla_1^2 \xi' - \beta g \frac{\partial \theta'}{\partial y'} \quad (6.4)$$

where the vorticity function is defined by

$$\xi' = \nabla_1^2 \psi' \quad (6.5)$$

and the stream function ψ' is defined by

$$v' = \frac{\partial \psi'}{\partial z'}, \quad w' = - \frac{\partial \psi'}{\partial y'}, \quad (6.6)$$

Energy equation

$$u' \tau + v' \frac{\partial \theta'}{\partial y'} + w' \frac{\partial T_b}{\partial z'} + w' \frac{\partial \theta'}{\partial z'} = \kappa \nabla_1^2 \theta' \quad (6.7)$$

where $\nabla_1^2 = \partial^2/\partial y'^2 + \partial^2/\partial z'^2$

Note that the vorticity function is introduced here to apply the boundary vorticity method. The boundary conditions are:

At the top and bottom plates $u' = \psi' = \partial\psi'/\partial z' = \theta' = 0$ (6.8)

Along the vertical lines $y' = 0$, $0 < z' < h$ and $y' = \pi h/a = \text{one-Half wave length}$, $0 < z' < h$ $\partial u'/\partial y' = \psi' = \xi' = \partial\theta'/\partial y' = 0$

For the purpose of simplification and convenience, the above equations (6.3) to (6.7) and the boundary conditions (6.8) are reduced to non-dimensional forms by using the following transformations,

$(y', z') = (y, z)h$, $(u', v', w') = (Re\ u, v, w)v/h$, $\theta' = \Delta T\theta$,

$\xi' = \xi v/h^2$, $\psi' = v\psi$, and the parameters $Re = U_0 h/(2v)$, (6.9)

$Gr = g\beta\Delta T h^3/v^2$, $Ra = PrGr$ $\mu = Re\eta h/\Delta T$.

The results are:

Axial momentum equation

$$v \frac{\partial u}{\partial y} + w \frac{\partial u}{\partial z} + w \frac{\partial \phi_u}{\partial z} = \nabla^2 u \quad (6.10)$$

Vorticity transport equation for secondary flow

$$v \frac{\partial \xi}{\partial y} + w \frac{\partial \xi}{\partial z} = \nabla^2 \xi - \frac{Ra}{Pr} \frac{\partial \theta}{\partial y} \quad (6.11)$$

where the dimensionless vorticity function is

$$\xi = \nabla^2 \psi \quad (6.12)$$

and the dimensionless stream function ψ is defined by

$$v = \frac{\partial \psi}{\partial z}, \quad w = -\frac{\partial \psi}{\partial y} \quad (6.13)$$

Energy equation

$$\mu u + v \frac{\partial \theta}{\partial y} + w \frac{\partial \theta}{\partial z} - w(Pr \mu \frac{\partial \phi_\theta}{\partial z} + 1) = \frac{1}{Pr} \nabla^2 \theta \quad (6.14)$$

where $\nabla^2 = \partial^2/\partial y^2 + \partial^2/\partial z^2$

The boundary conditions are:

At the top and bottom plates $u = \psi = \partial \psi / \partial z = \theta = 0$

Along the vertical lines $y = 0, 0 < z < 1$ (6.15)

and $y = \pi/a, 0 < z < 1 \quad \partial u / \partial y = \psi = \xi = \partial \theta / \partial y = 0$

At this point, it is noted that the no-slip boundary conditions $\partial \psi / \partial z = 0$ at the top and bottom plates cannot be applied directly but the boundary vorticity method discussed in

Chapter II is found to be quite effective. The boundary vorticity method is subsequently improved and a detailed comparison of the boundary vorticity method with the improved iterative scheme is made in a later section.

For the case when $|\mu| \rightarrow \infty$, it is not proper to employ ΔT as a characteristic temperature difference. The modified non-dimensional quantities and the governing equations for this case are given as:

$$\theta' = \text{Pr Re} \tau h \theta_{\tau}, \quad \text{Gr}_{\tau} = g \beta \tau h^4 / \nu^2, \quad \text{Ra}_{\tau} = \text{Pr Gr}_{\tau} \quad (6.16)$$

$$v \frac{\partial u}{\partial y} + w \frac{\partial u}{\partial z} + w \frac{\partial \phi_u}{\partial z} = \nabla^2 u, \quad (6.17)$$

$$v \frac{\partial \xi}{\partial y} + w \frac{\partial \xi}{\partial z} = \nabla^2 \xi - \text{Re Ra}_{\tau} \frac{\partial \theta_{\tau}}{\partial y}, \quad (6.18)$$

$$\xi = \nabla^2 \psi, \quad (6.19)$$

$$v = \partial \psi / \partial z, \quad w = - \partial \psi / \partial y \quad (6.20)$$

and

$$u + \text{Pr} \left(v \frac{\partial \theta_{\tau}}{\partial y} + w \frac{\partial \theta_{\tau}}{\partial z} \right) - \text{Pr} w \frac{\partial \phi_{\theta}}{\partial z} = \nabla^2 \theta_{\tau} \quad (6.21)$$

For the case when $\mu = 0$, two parameters Pr and Ra appear in equations (6.10) to (6.14). This case corresponds to the forced convection problem between two horizontal flat plates studied by Mori and Uchida [4.6] and equations (6.11) to (6.14) are seen to be identical to the governing equations for the two-dimensional Bénard convection problem solved, for example, by Plows [6.6]. For the case when μ is finite, three parameters Pr , μ and Ra appear in equations (6.10) to (6.14). On the other hand, when $|\mu| \rightarrow \infty$, two parameters Pr and $ReRa_\tau$ appear in equation (6.17) to (6.21).

In equations (6.10) and (6.17), we see that the axial direction disturbance is caused mainly by the product of the vertical direction disturbance, w , and the main flow velocity gradient, $\partial\phi_u/\partial z$. This product is balanced by the remaining inertia terms, $v \partial u/\partial y$ and $w \partial u/\partial z$, and also by the viscous term $\nabla^2 u$. In equations (6.11) and (6.18), the secondary motion is seen to be driven by the unbalanced buoyant force terms $(Ra/Pr) \partial\theta/\partial y$ and $ReRa_\tau \partial\theta_\tau/\partial y$, respectively. In the energy equation (6.14), the thermal disturbance is seen to come from three sources for the case when μ is finite;

- (a) the term due to the convective motion of the main flow disturbance, μu ,
- (b) the term due to the vertical direction convection through linear basic temperature distribution, w ,
- (c) the term due to the vertical direction convection through the nonlinear basic temperature distribution, $w Pr \mu \cdot \partial\phi_\theta/\partial z$.

For the case when $\mu = 0$, the sources (a) and (c) vanish and the thermal disturbance comes solely from source (b). In equation (6.21) for the case when $|\mu| \rightarrow \infty$, we see that the thermal disturbance comes from the convective motion of the main flow disturbance, u , and the vertical direction convection through the nonlinear basic temperature distribution, $Pr w \frac{\partial \phi_\theta}{\partial z}$.

When $|\mu| \rightarrow \infty$ and $Pr \rightarrow \infty$ and $ReRa_\tau$ is still very close to the critical value (see Chapter IV, Appendix 4.2 for the case when $|\mu| \rightarrow \infty$), the inertia terms, $v \partial \xi / \partial y$ and $w \partial \xi / \partial z$ in equation (6.18) and the term representing the convective motion due to the main flow disturbance u , in equation (6.21) may be neglected as compared with the remaining terms in the respective equations. By transforming (v, w) into $(v, w)ReRa_\tau$, only one parameter $PrReRa_\tau$ is left in the governing equations. This observation for large Prandtl number effect is also confirmed by numerical results to be presented later.

6.3 Finite-Difference Approximations

In view of the complexity of equations (6.10) to (6.14) or equations (6.17) to (6.21) and the fact that appreciable error is observed by applying Stuart's approximate method to the analogous problem of rotating-cylinder flow for a high Taylor number, the finite-difference technique and boundary vorticity method described in Chapter II will be applied to the present rather complicated problem.

Referring to Fig. 6.1, the main flow direction momentum equation (6.10) and the energy equation (6.14) can be approximated by the following finite-difference form.

$$\begin{aligned} \sigma(v_{j,k}^0 \frac{f_{j+1,k} - f_{j-1,k}}{2\Delta y} + w_{j,k}^0 \frac{f_{j,k+1} - f_{j,k-1}}{2\Delta z}) \\ = \frac{f_{j+1,k} - 2f_{j,k} + f_{j-1,k}}{(\Delta y)^2} \quad (6.22) \\ + \frac{f_{j,k+1} - 2f_{j,k} + f_{j,k-1}}{(\Delta z)^2} + G_{j,k} \end{aligned}$$

where $\sigma = 1$, $G_{j,k} = -w_{j,k}^0 \left(\frac{\partial \phi_u}{\partial z} \right)_{j,k}$ when $f_{j,k} = u_{j,k}$ and

$\sigma = \text{Pr}$, $G_{j,k} = \text{Pr } w_{j,k}^0 \left(\text{Pr } \mu \frac{\partial \phi_\theta}{\partial z} + 1 \right)_{j,k} - \text{Pr } \mu u_{j,k}$ when

$f_{j,k} = \theta_{j,k}$.

The superscript o stands for the value obtained at the previous step and $j, k=2, 3, \dots, M$. The vorticity transport equation (6.11) and equation (6.12) for the stream function can also be approximated in the form of equation (6.22) with the following replacement.

$$\sigma = 1, G_{j,k} = -\frac{Ra}{Pr} \left(\frac{\partial \theta}{\partial y}\right)_{j,k} \text{ when } f_{j,k} = \xi_{j,k}$$

$$\text{and } \sigma = 0, G_{j,k} = -\xi_{j,k} \text{ when } f_{j,k} = \psi_{j,k}$$

where $j=1, 2, \dots, M+1, k=2, 3, \dots, M$.

For the case when $|\mu| \rightarrow \infty$, equations (6.17) to (6.19) and equation (6.21) can similarly be approximated in the form of equation (6.22) with the following substitution for $G_{j,k}$.

$$G_{j,k} = -ReRa_{\tau} \left(\frac{\partial \theta}{\partial y}\right)_{j,k} \text{ when } f_{j,k} = \xi_{j,k} \text{ for equation (6.18)}$$

$$G_{j,k} = Pr w_{j,k}^o \left(\frac{\partial \phi_{\theta}}{\partial z}\right)_{j,k} - u_{j,k} \text{ when } f_{j,k} = \theta_{j,k} \text{ for equation (6.21).}$$

6.3.1 Properties of Matrices and the Relaxation Factor

Rearranging equation (6.22), we have

$$\begin{aligned}
& (1 + \sigma \frac{\Delta z}{2} w_{j,k}^0) f_{j,k-1} - 2[1 + (\frac{\Delta z}{\Delta y})^2] f_{j,k} + (1 - \sigma \frac{\Delta z}{2} w_{j,k}^0) f_{j,k+1} \\
& = - (\frac{\Delta z}{\Delta y})^2 [(1 + \sigma \frac{\Delta y}{2} v_{j,k}^0) f_{j-1,k} \quad (6.23) \\
& + (1 - \sigma \frac{\Delta y}{2} v_{j,k}^0) f_{j+1,k}] - (\Delta z)^2 G_{j,k}
\end{aligned}$$

With the existence of the nonlinear terms, the properties of the coefficient matrix for equation (6.23) are:

- (a) real,
- (b) non-symmetric,
- (c) diagonally dominant, if and only if

$$|\sigma \frac{\Delta z}{2} w_{j,k}^0| \leq 1$$

for all j's and k's. (6.24)

$$|\sigma \frac{\Delta y}{2} v_{j,k}^0| \leq 1$$

Since the matrices are not symmetric and their eigenvalues vary from step to step during iteration, the determination of the optimal relaxation factor is very difficult. For most of the computations in the present problem, a relaxation factor of unity is used. An under-relaxation factor of 0.5 is often used to stabilize the numerical computation.

6.3.2 The Application of the Boundary Vorticity Method and Its Improved Iterative Scheme

The application of the boundary vorticity method and its improved iterative scheme for solving equations (6.11) and (6.12) without inertia terms and the associated boundary conditions (6.15) were discussed clearly in Chapter II. The appearance of the nonlinear terms $v \partial \xi / \partial y$ and $w \partial \xi / \partial z$ in equation (6.12) does not make any essential difference in the application of the boundary vorticity method and its improved iterative scheme. Thus the detailed algorithm is not repeated here. A comparison of the method of unsteady state solution employed in [6.7], the present boundary vorticity method, and its improved iterative scheme is made in subsection 6.3.4.

6.3.3 Errors and Mesh Sizes

In the process of computation, errors may arise from the following sources:

- (a) finite-difference approximation,
- (b) errors due to the convergence of elliptic equations and nonlinear terms,
- (c) round-off errors.

These factors were discussed clearly in subsection 3.3.3 and are not repeated here. The prescribed error is kept to be the order of 10^{-5} .

Fig. 6.2 shows the convergence of the flow and heat transfer results for the case of $\mu = 0$ and $Ra = 8010.52$ with

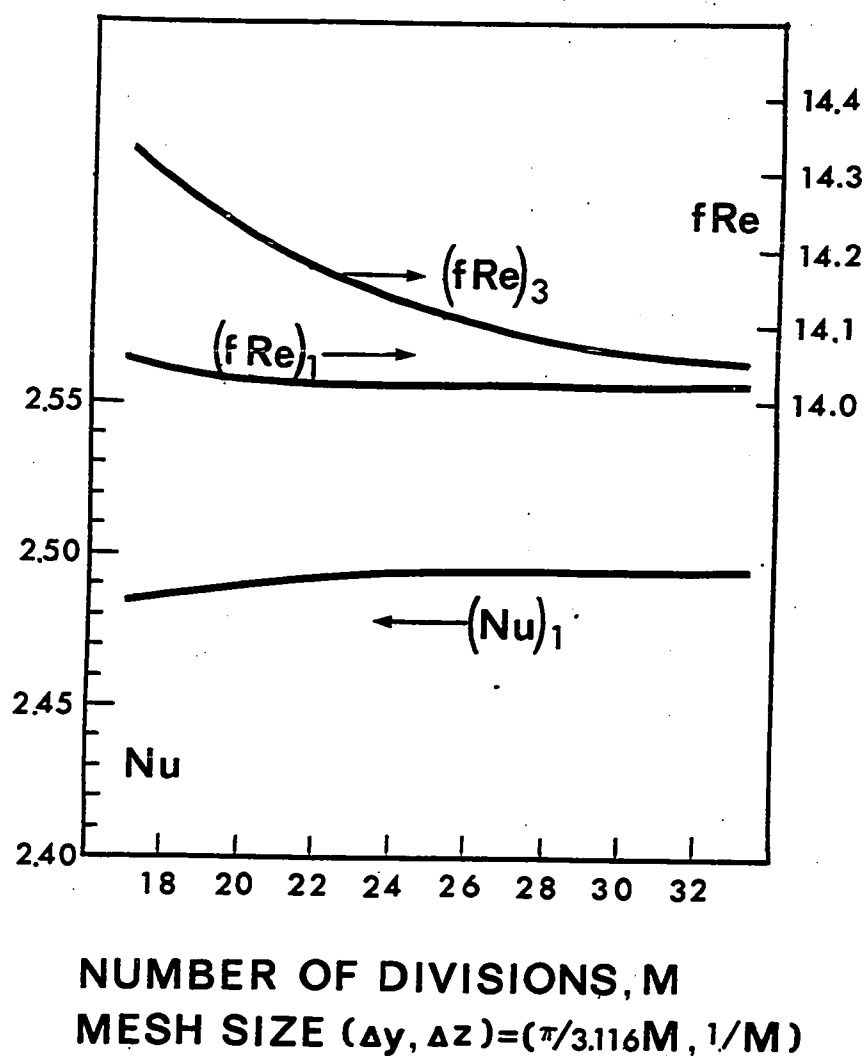


Fig. 6.2 Effect of grid size on the convergence of the flow and heat transfer results for the case of $Pr = 0.7$, $\mu = 0$ and $Ra = 8010.52$

respect to the number of divisions M for both y - and z -directions. The definitions of the flow parameter, fRe , and the heat transfer parameter, Nu , are given later. Here the subscript 1 denotes the value evaluated at the lower plate and the subscript 3 denotes the value obtained from an overall force balance. It is seen that with the number of divisions at $M = 24$, the value of $(Nu)_1$ already remains unchanged and the difference between $(fRe)_1$ and $(fRe)_3$ is less than one per cent for further increase of M . This indicates that the numerical solution gives quite reliable results if the number of divisions M greater than say 24. In the present work, values of $M = 24, 28$ and 40 , are used for various orders of magnitude of Rayleigh number for the case $\mu = 0$. For the cases $\mu \neq 0$ and $|\mu| \rightarrow \infty$, $M = 28$ is used. The number of divisions, $M = 40$, is employed to extend the range of Ra for the computation involving the case $\mu = 0$. However, the Rayleigh number is extended only slightly from 10^5 to 3×10^5 but the computing time increases substantially from around 10 minutes for $M = 28$ to about 45 minutes for $M = 40$ on an IBM 360/67. Because of the excessive computing time requirement, the number of divisions, $M = 40$, is not employed for other cases such as $\mu = \text{finite}$ and $|\mu| \rightarrow \infty$.

6.3.4 A Comparison of the Method of Unsteady State Solution, Boundary Vorticity Method, and Its Improved Iterative Scheme

Samuels and Churchill [6.6] employed a finite-difference technique to solve the thermal instability problem in an enclosed horizontal rectangular region. By using explicit forward integration and the value of the boundary vorticity evaluated at the previous time step, a time dependent solution is obtained and consequently a steady state solution is reached after a sufficiently large number of time steps. The method of unsteady state solution is also applied to the present problem in an attempt to compare the boundary vorticity method and its improved iterative scheme with the method used in reference [6.6]. However, the computations are made only at $Ra/Ra^* = 4.69$ for the case $\mu = 0$ using the number of divisions $M = 10$ and 20 . Table 6.1 shows the results from these three methods. It can be stated that the method of unsteady state solution requires longer computing time, a larger number of outer iterations and one additional storage step than the present steady state solutions. In the computation for the unsteady solution using the explicit forward integration technique, the time increment is restricted by the size of the mesh because of numerical stability and furthermore it requires a complete solution for the stream function at each time step. Thus, it is believed that for a problem where the transient (or unsteady) solution is not of interest, the steady state

Table 6.1 A comparison of the method of unsteady state solution, boundary vorticity method, and its improved iterative scheme for the case of $\mu = 0$ and $Ra/Ra^* = 4.69$

	Method of Unsteady State Solution*1		Steady State Solution *2		
			Boundary Vorticity Method	Improved Iterative Scheme	
M x M	10 x 10	20 x 20	10 x 10	10 x 10	20 x 20
Computing time*3 for each outer iteration (sec.)	0.35~ 0.4	2.3	0.2	0.82	0.62
Total number of outer iterations	191	764 (estimated)	126	356	124
Dimensions	3		2	2	
Number of iteration steps stored	2		1	1	
Solution obtained	unsteady and steady		steady	steady	steady

*1 A point successive over-relaxation method is employed to obtain the stream function at each time step.

*2 A relaxation factor of unity is used for both boundary vorticity method and its improved iterative scheme.

*3 The computing time shown is based on the program without optimization.

solution is much more economical from the viewpoint of computing time and storage space. The results for the improved iterative scheme listed in Table 6.1 show some improvement in terms of computing time (with savings up to 1/4 of the computing time) over the boundary vorticity method since the repeated iteration is not required for finding the value of boundary vorticity. The improved iterative scheme was conceived only after all the computations for the case of $\mu = 0$ had been completed. Thus, the improved iterative scheme is employed only in the computations for the cases of $\mu = \text{finite}$ and $|\mu| \rightarrow \infty$. Finally, we should note that the above comparison does not imply that the improved scheme is always better than the boundary vorticity method since the comparison is based only on the present problem formulated in Cartesian coordinates and the iteration is carried out with a relaxation factor of unity. The question of whether or not the improved iterative scheme is advantageous in problems formulated in polar coordinates cannot be answered without further numerical experiments using various relaxation factors. Consequently, the improved iterative scheme must be interpreted only within the scope of the present study.

6.4 Results and Discussion

For the problem under consideration, three cases result depending on the magnitude of the characteristic parameter μ , namely, $\mu = 0$, $\mu = \text{finite}$ (negative or positive) and $|\mu| \rightarrow \infty$. The limiting case of $\mu = 0$ is analogous mathematically to the classical steady laminar Bénard convection with two-dimensional rolls whose heat transfer characteristics in the post-critical regime has been studied very extensively in recent years. The analytical and experimental works for this problem have been carried out notably to explain the nature of turbulence using the mechanism of convective cells due to buoyancy.

In order to carry out the detailed quantitative measurements, Mori and Uchida [4.6] superimposed the fully developed main flow to the steady laminar Bénard convection between the two infinite horizontal rigid boundaries. They presented the detailed comparisons between the experimental data and the results from the approximate analytical method which is a modification of the Stuart's method [6.2] for the flow between rotating concentric cylinders with Taylor vortex rolls. Since the problem treated by Mori and Uchida represents the limiting case of $\mu = 0$ for the present problem, it is possible to compare the results from the present numerical solution with the analytical and experimental results of Mori and Uchida. The other limiting case of $|\mu| \rightarrow \infty$ is also of considerable practical importance since it corresponds

to the fully developed laminar flow without buoyancy effect between two parallel plates subjected to the uniform wall heat flux with the well-known Nusselt number of 8.235.

Before proceeding to the presentation of flow and heat transfer results, we should note that all the results reported here are based on the assumption that the wave number is taken to be the one which is predicted by the linear stability analysis reported in Chapter IV. Only a Prandtl number of 0.7 (air) is considered for the cases of $\mu = 0$ and $\mu = \text{finite}$. The Prandtl number effect is studied only for the case of $|\mu| \rightarrow \infty$.

As noted earlier, the case of $\mu = 0$ affords detailed comparison of the present numerical results with those of Mori and Uchida [4.6]. For this purpose, the axial velocity and temperature distributions along three vertical lines from the numerical solution are compared with those of Mori and Uchida based on approximate analytical solution and experimental measurements in Figs. 6.3 and 6.4, respectively, for the case of $Pr = 0.7$, $\mu = 0$ and $Ra = 8010.52 = 4.69 (Ra^*)$.

For the velocity profiles shown in Fig. 6.3, it is seen that the experimental data generally lie between the present numerical predictions and Mori and Uchida's analytical results. In particular, we note that the analytical method apparently predicts the wrong trend for the velocity profile along the vertical line 2 near the central region ($z = 0.5$) exhibiting a saddle shape velocity profile. This phenomenon

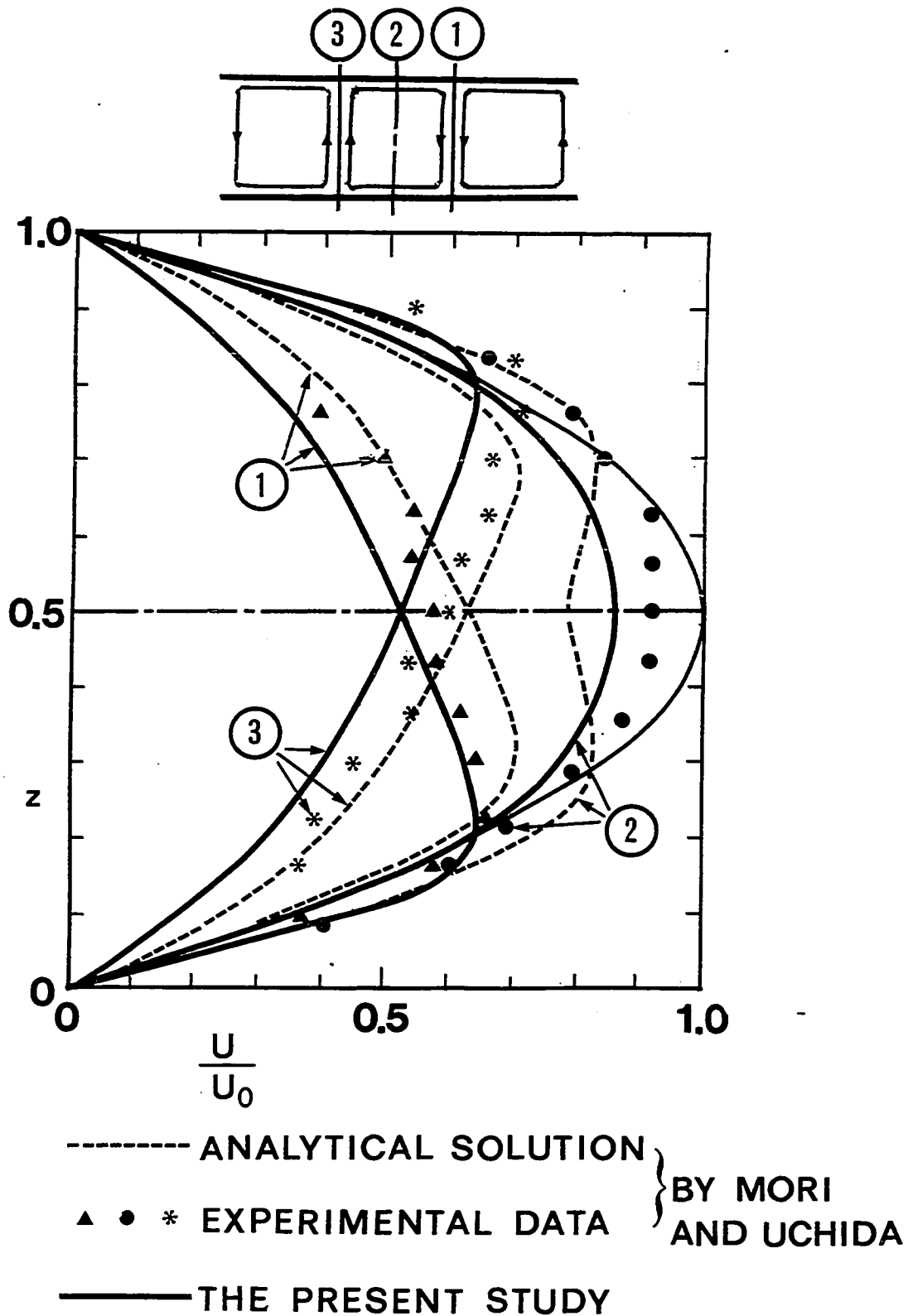


Fig. 6.3 Comparison of velocity profiles from this investigation with the approximate analytical results of Mori and Uchida and their experimental data for the case of $Pr = 0.7$, $\mu = 0$ and $Ra = 8010.52$

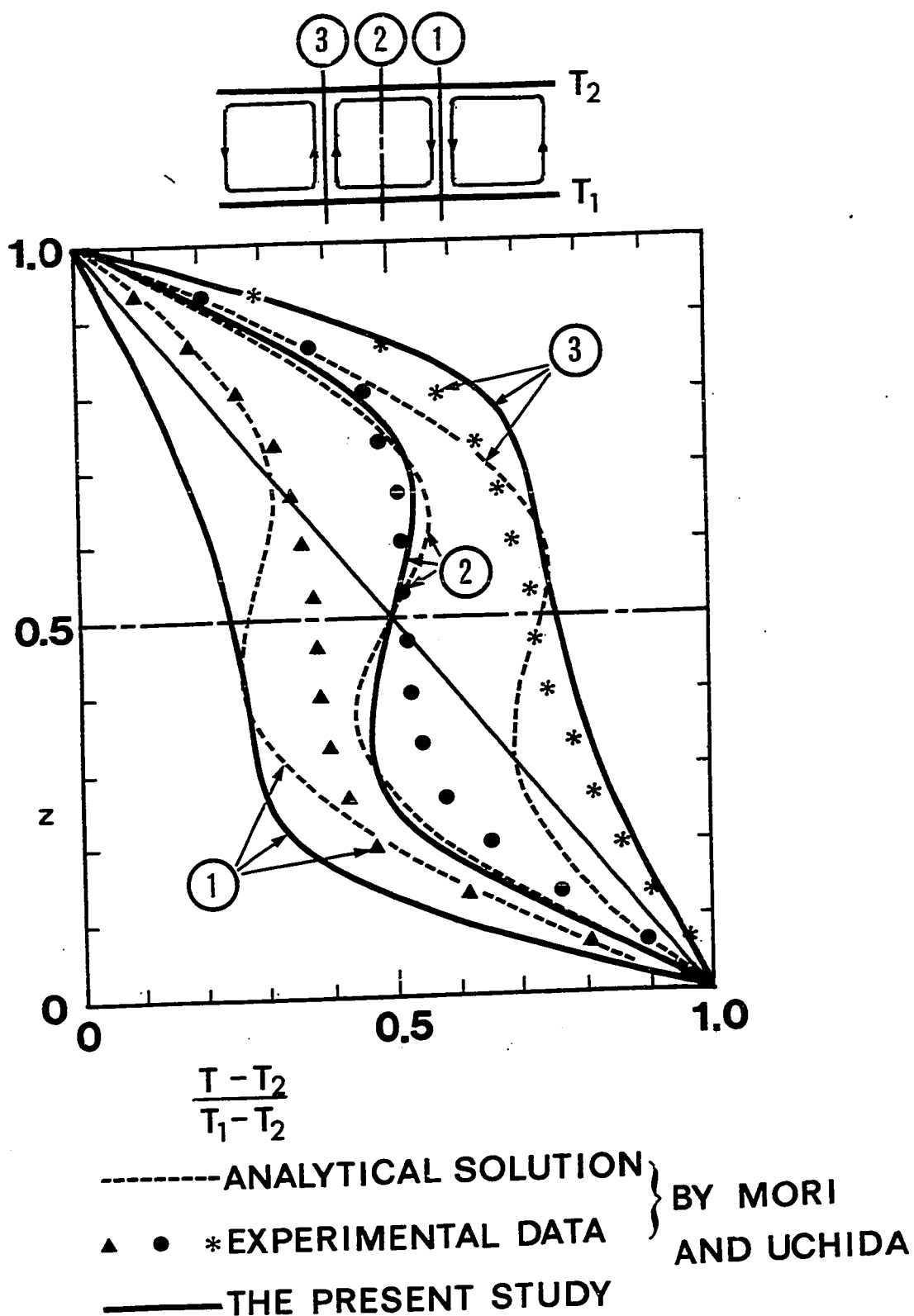


Fig. 6.4 Comparison of temperature profiles from this investigation with the approximate analytical results of Mori and Uchida and their experimental data for the case of $Pr = 0.7$, $\mu = 0$ and $Ra = 8010.52$.

contradicts with both experimental data and numerical solution and cannot be explained physically. It is further noted that the numerical result agrees better with experimental data for $z < 0.2$ along the vertical line 1 and $z > 0.8$ along the vertical line 3 than the analytical result. We clearly see the distortion of the axial velocity profile from the parabolic distribution due to longitudinal vortex rolls.

As shown in Fig. 6.4, the temperature profile along the vertical line 3 from the numerical solution agrees very well with the experimental data as compared with the analytical result. In particular, along the lines 1 and 3 the analytical result predicts positive vertical temperature gradient in the central region in contrast to the negative one demonstrated by both the experimental data and the numerical solution. For the temperature profile along the line 2, both the analytical solution and the numerical solution exhibit positive vertical temperature gradient near the central region with the point of inflection located at $z = 0.5$. In contrast, the experimental data do not appear to show this trend. The result of the present numerical solution shows that along the line 2 the vertical temperature gradient reverses its sign approximately from $z = 0.3$ to $z = 0.7$ indicating that heat is conducted from the upper part to the lower part in this region. We also note that in the same region along line 2 the secondary flow is relatively weak and at $z = 0.5$ secondary flow vanishes completely. Furthermore, this region of reversed

vertical temperature gradient disappears at least along the lines 1 and 3 as shown in Fig. 6.4. Noting that for steady state the heat flow rate from the lower plate to the upper plate is constant, we see that rather strong convection motion due to secondary flow exists in the region near $y = 0$ (line 1), $z = 0.5$ and $y = 1.008$ (line 3), $z = 0.5$ to compensate for the reversed heat flow. We can also gain some insight about this situation by examining the isotherms which will be presented next.

It is instructive to examine the distributions of constant axial velocity lines, isothermals, constant vorticity lines and secondary flow streamlines for the case of $Pr = 0.7$ and $\mu = 0$ at two different values of Rayleigh number, namely, $Ra = 8010.52$ and 4×10^4 . Fig. 6.5 shows the constant axial velocity lines. We note that without secondary motion the constant axial velocity lines are straight and horizontal but with the secondary motion the constant velocity lines are distorted. We can gain better understanding of the profiles shown in Fig. 6.3 by considering the distributions of constant axial velocity lines along the lines $y = 0$, 0.504 and 1.008 , respectively. It is clearly seen that the saddle-shape velocity profile shown in Fig. 6.3 along the line 2 based on approximate analytical prediction [4.6] is unreasonable. Fig. 6.5 shows that the higher constant velocity lines are displaced from the lines of symmetry $y = 0$ and 1.008 and form a series of closed curves near the central

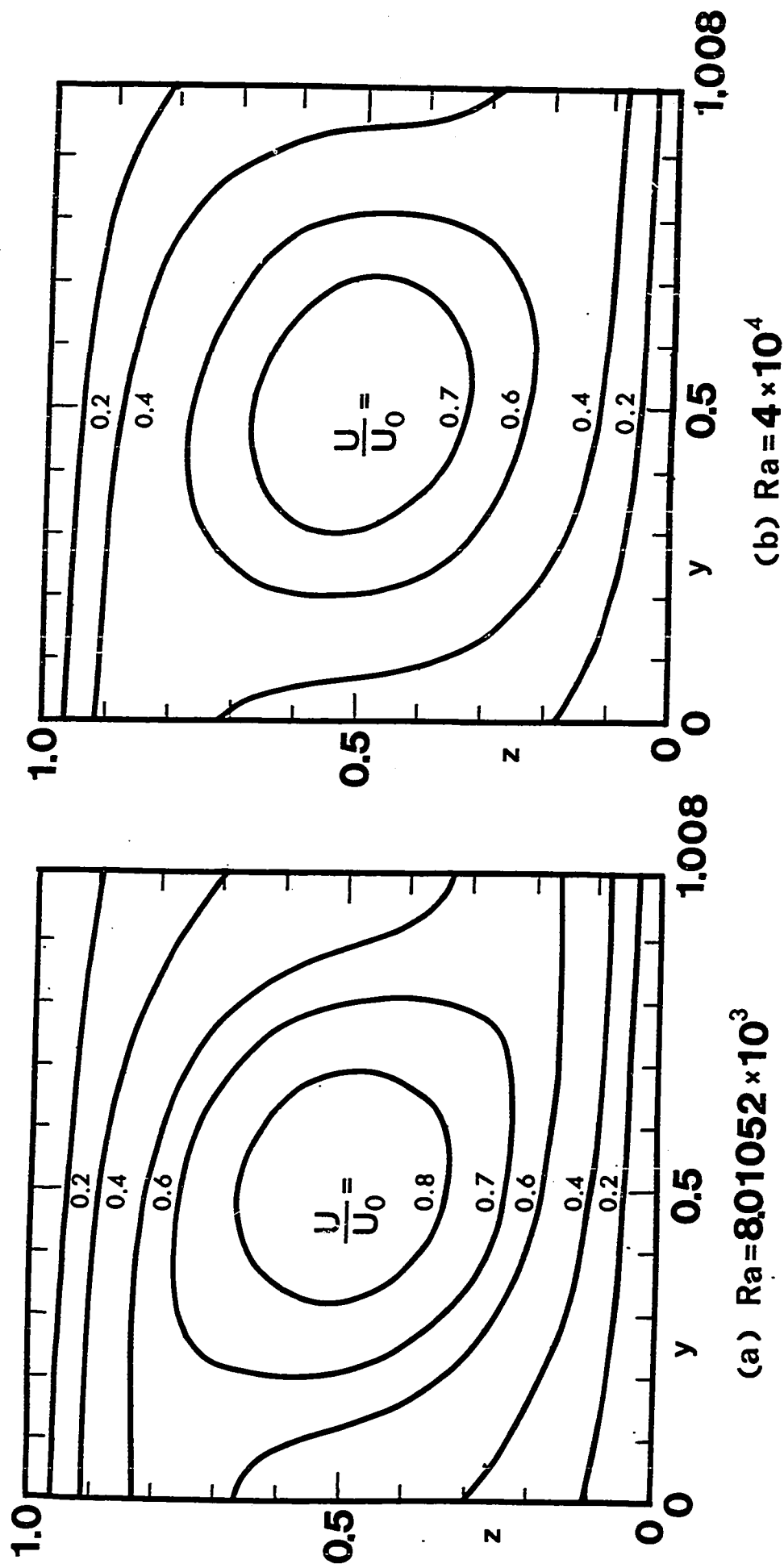


Fig. 6.5 Lines of constant axial velocity for the case of $Pr = 0.7$ and $\mu = 0$

region at $y = 0.504$. At higher value of Rayleigh number $Ra = 4 \times 10^4$, the value of the maximum axial velocity is seen to decrease as compared with that at $Ra = 8010.52$. Fig. 6.5 also shows that the stronger secondary flow effect manifests itself by the larger distance between two constant axial velocity lines.

Figs. 6.6(a) and (b) show the distribution of isothermals for the case of $Pr = 0.7$, $\mu = 0$ at $Ra = 8010.52$ and 4×10^4 , respectively, based on the dimensionless temperature difference $(T - T_1)/(T_1 - T_2)$. Without the secondary motion, the isothermals are horizontal straight lines but with the secondary flow effect the isothermals are distorted. As the Rayleigh number increases, so is the distortion of the isothermals. It is noted that the distance between two isothermals in some region is larger than that in the other region indicating that the advective term in the energy equation is dominant in that region. On the other hand, in the vicinity of the stagnation points $y = 0$, $z = 1.0$ and $y = 1.008$, $z = 0$ the conduction term is dominant. By looking at Fig. 6.6, we can clearly distinguish the hot and cold regions by noting the isothermal line for $(T - T_1)/(T_1 - T_2) = -0.5$. We can also clearly see that plumes of warm (cool) current impinge strongly upon the cool (warm) plate indicating the strong effect due to nonlinear advection caused by the buoyancy forces. We can gain further insight into the mechanism of conduction heat transfer by considering the heat flow lines

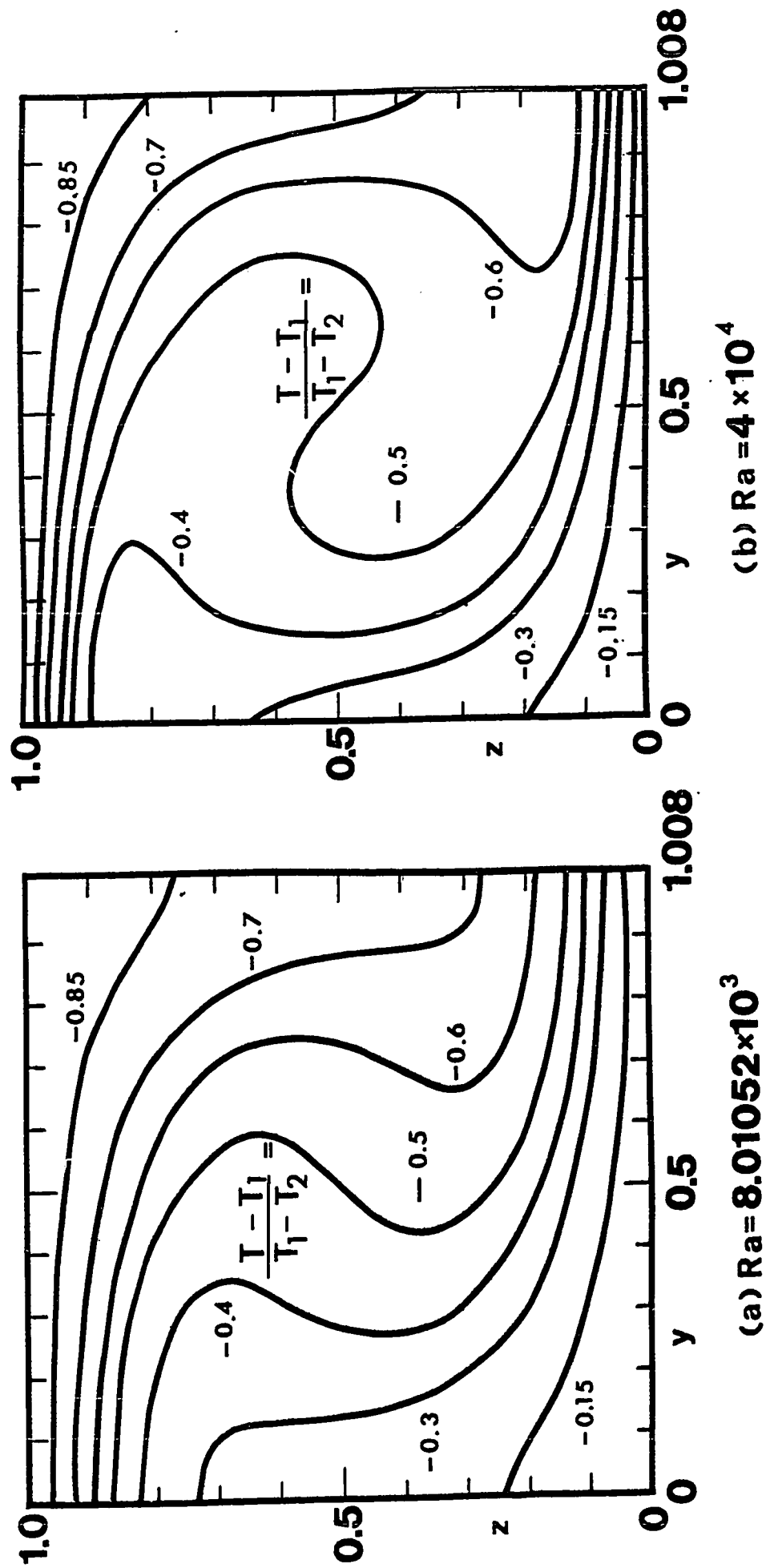


Fig. 6.6 Isotherms for the case of $Pr = 0.7$ and $\mu = 0$

which are normal to the isothermal lines. The temperature profiles along the lines 1, 2, and 3 shown in Fig. 6.4 correspond to the distributions of the isothermals at $y = 1.008$, 0.504 and 0 , respectively. Fig. 6.6 clearly indicates that the reversal of the sign for the vertical temperature gradient does not exist along the lines $y = 0$ and 1.008 contradicting with the prediction of the approximate analytical solution [4.6]. On the other hand, the reversal of the temperature gradient does indeed exist along the line $y = 0.504$.

The distributions of the constant vorticity lines for the case of $Pr = 0.7$ and $\mu = 0$ at $Ra = 8010.52$ and 4×10^4 are shown in Figs. 6.7(a) and (b), respectively. It is seen that along the line of symmetry $y = 0$ and 1.008 , the vorticity function ξ vanishes. We know that the solid boundary represents the source of the vorticity function and the vorticity function is generated at the top and bottom plates (with negative sign) and dissipated into the central region as a sink of the vorticity function (with positive sign). At $Ra = 4 \times 10^4$, we see that there are two sinks with $\xi = 520$ in the central region for the two strong sources of vorticity function located near $y = 0.65$, $z = 0$ and $y = 0.35$, $z = 1.0$, respectively, on the rigid boundaries. This is in contrast to the one sink and two sources for $Ra = 8010.52$. We are particularly impressed with the drastic change of pattern for the vorticity as the value of the Rayleigh number increases

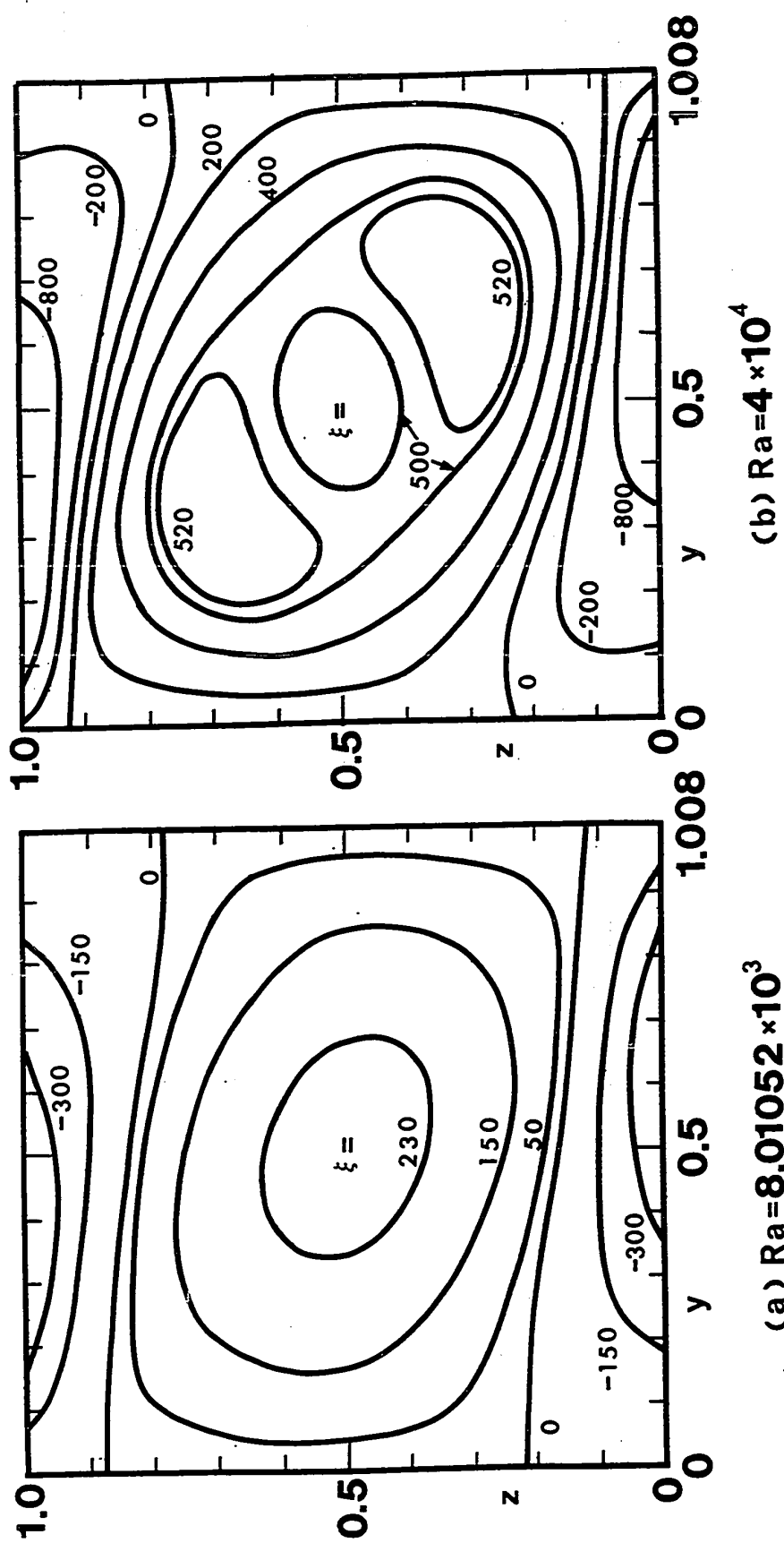


Fig. 6.7 Lines of constant vorticity for the case of $Pr = 0.7$ and $\mu = 0$

from 8010.52 to 4×10^4 . It is interesting to note that the maxima of the absolute vorticity occur right at the boundaries because here the horizontal shear stress is greatest. The pattern for vorticity at $Ra = 4 \times 10^4$ is rather complex.

Fig. 6.8 illustrates the streamlines for the case of $\mu = 0$ at $Ra = 8010.52$ and 4×10^4 . For this case of $\mu = 0$, we can see that the two diagonal lines are lines of symmetry by substituting $(u, -v, -w, -\theta, \psi, \xi, -y$ and $-z)$ for $(u, v, w, \theta, \psi, \xi, y$ and $z)$ into equations (6.10) to (6.14). For the Rayleigh number near the critical value, the streamlines are seen to be almost symmetric with respect to the lines $y = 1.008/2$ and $z = 0.5$. However, Fig. 6.8 shows that as the value of Ra increases, the streamlines are seen to be compressed in the direction of the line $y = 0, z = 0$ and $y = 1.008, z = 1.0$ representing slight distortion into an oblong shape. It is interesting to note that the distributions of the stream function are much more smoother than those of the vorticity function due to the fact that the stream function is a twice-integrated version of the vorticity.

All the illustrations shown in Figs. 6.5 to 6.8 are for the case $\mu = 0$ at $Ra = 8010.52$ and 4×10^4 to indicate the build-up of the secondary flow intensity with the increase of the Rayleigh number for $Pr = 0.7$. The profiles for axial velocity and temperature shown in Figs. 6.3 and 6.4, respectively, can be contrasted with the distributions shown in Figs. 6.5(a) to 6.8(b) along the vertical lines

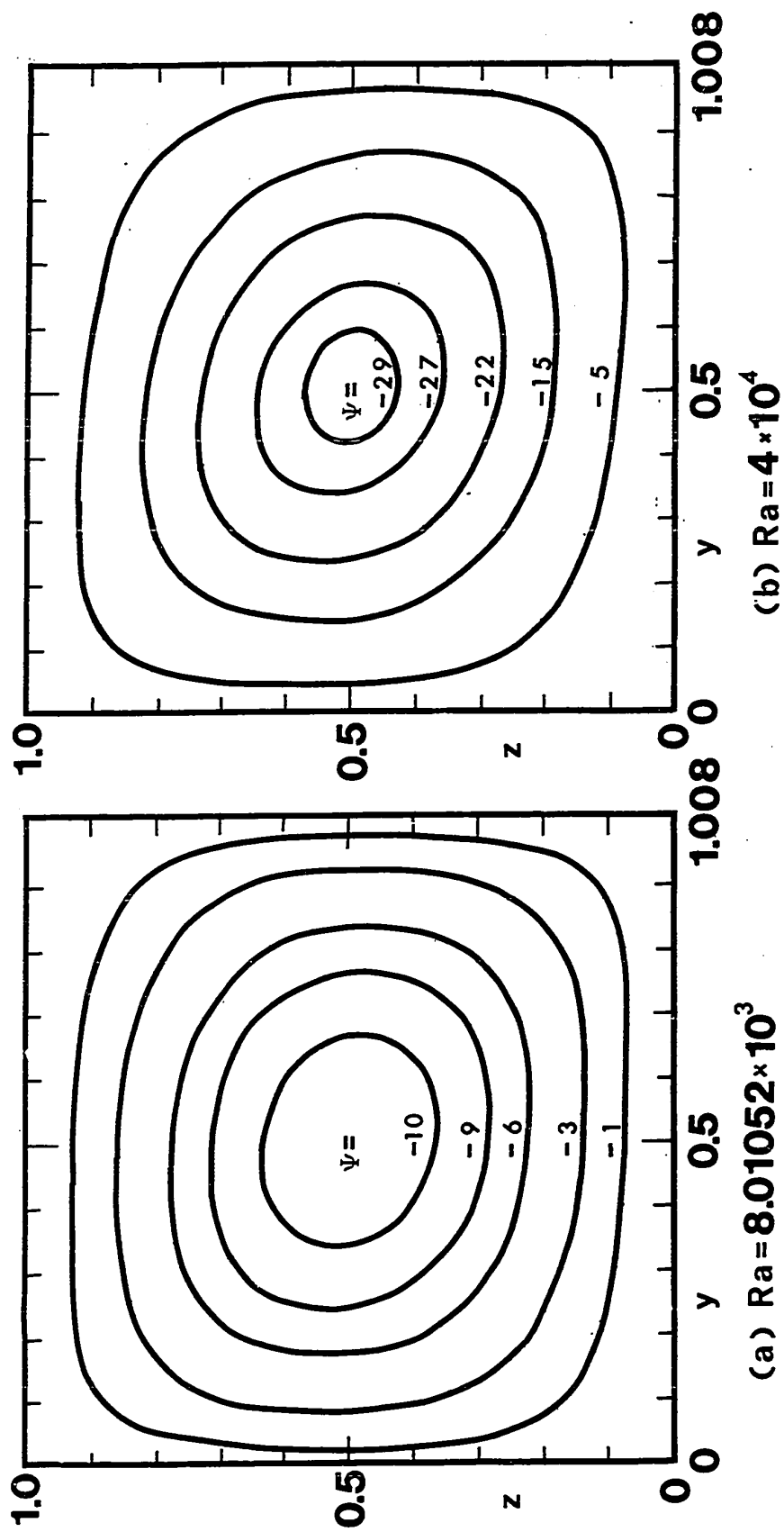


Fig. 6.8 Secondary flow streamlines for the case of $Pr = 0.7$ and $\mu = 0$

$y = 0, 0.504$ and 1.008 . The numerical solution clearly yields the detailed flow structure and sheds the light on the detailed heat transfer mechanism. Before proceeding on presenting the over-all flow and heat transfer results for the limiting case of $\mu = 0$, some features on the flow structure in the form of streamlines for the cases of $\mu = \text{finite}$ and $|\mu| \rightarrow \infty$ will be considered next.

Three typical secondary flow streamlines for the case of $\mu = -30$ with $a = 3.735$ and $Pr = 0.7$ at three different values of the Rayleigh number are shown in Fig. 6.9 indicate the gradual development of the streamline patterns. It is noted that the value of $Ra = -1000$ (see Fig. 6.9(a)) is not too far from the critical value of $Ra^* = -884.47$ (see Appendix 4.2 in Chapter IV). Since the unstable region is confined further to lower part of the channel for the case of negative μ in comparison with the case of positive μ , the intensity of the secondary motion is seen to be much stronger in the lower part than that in the upper part. This is also reflected in the location of the minimum stream function (the eye of streamlines) being situated in the lower part of the channel and also to the left of the central vertical line ($y = 0.8411/2$) of a vortex roll. Consequently, the upward stream is much stronger than the downward stream. Fig. 6.9(b) shows that at $Ra = -3000$, the eye of the streamlines is further shifted toward the vertical line $y = 0$ in the region of the upward stream. The secondary motion is seen

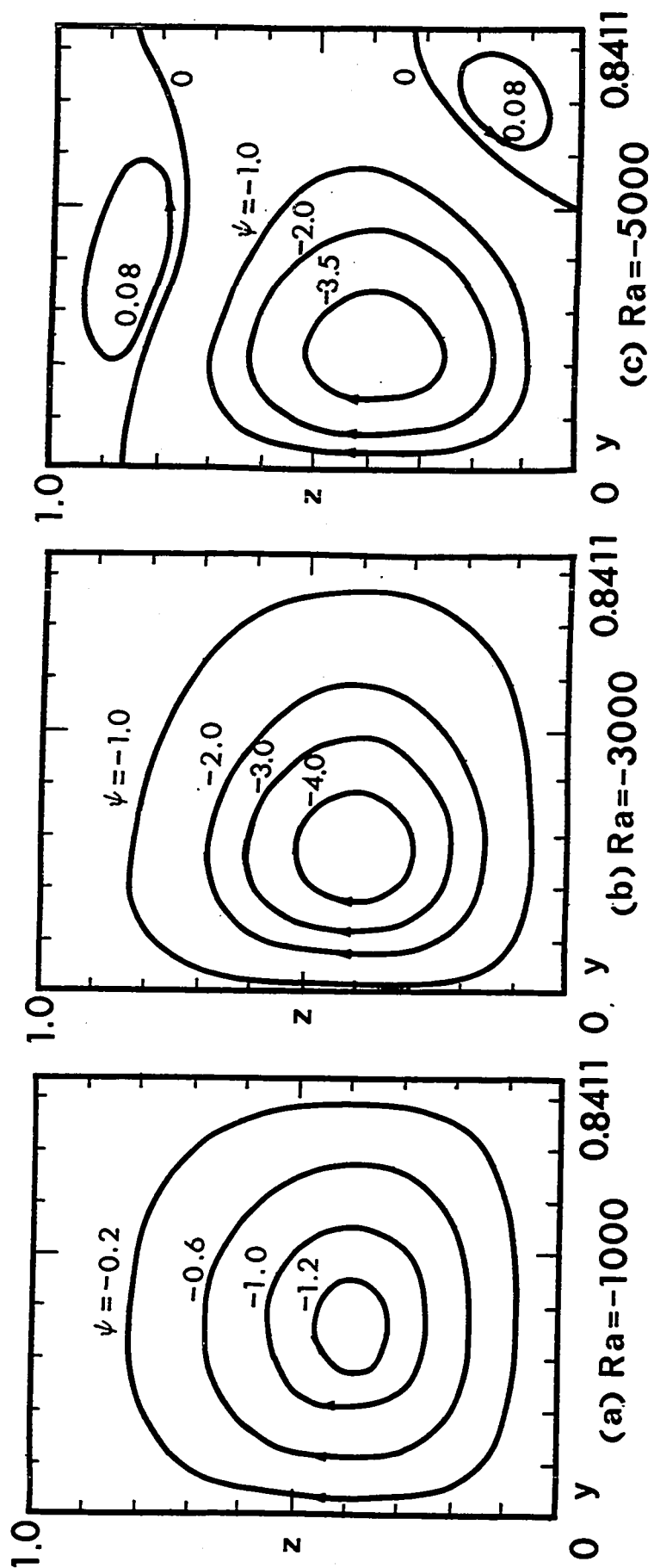


Fig. 6.9 Secondary flow streamlines for the case $Pr = 0.7$ and $\mu = -30$

to be very weak near the upper right-hand corner and rather weak near the lower right-hand corner as compared with the secondary flow near the lower left-hand corner. At $Ra = -5000$, the numerical technique fails to yield a convergent solution with an error of $O(10^{-5})$ but numerical solution is obtained with a larger error of $O(10^{-3})$ and the resulting secondary flow streamlines are shown in Fig. 6.9(c). As a result of the weaker secondary motion in the upper part of the channel and near the lower right-hand corner, two secondary vortices with flow opposite to that of the primary vortex appear. Although the numerical solution cannot be considered to be sufficiently convergent at $Ra = -5000$, it is known that single eye secondary motion is not always stable in the region of the channel where the basic temperature distribution is stable. At $Ra = -5000$, we see that the upward stream is much stronger and the eye of the primary vortex is moved further toward the vertical line $y = 0$.

For the case $|\mu| \rightarrow \infty$, three typical secondary flow streamlines at different values of the parameter $ReRa_\tau$ are shown in Fig. 6.10 for $Pr = 0.7$ and $a = 3.621$. The patterns for the streamlines shown in Fig. 6.10(a) and (b) are more or less similar to those shown in Fig. 6.9(a) and (b), respectively. At $ReRa_\tau = 1.5 \times 10^5$, the numerical technique again yields a solution only with a relatively large error of $O(10^{-3})$ and the situation is very similar to the case shown in Fig. 6.9(c). In contrast to the case shown in

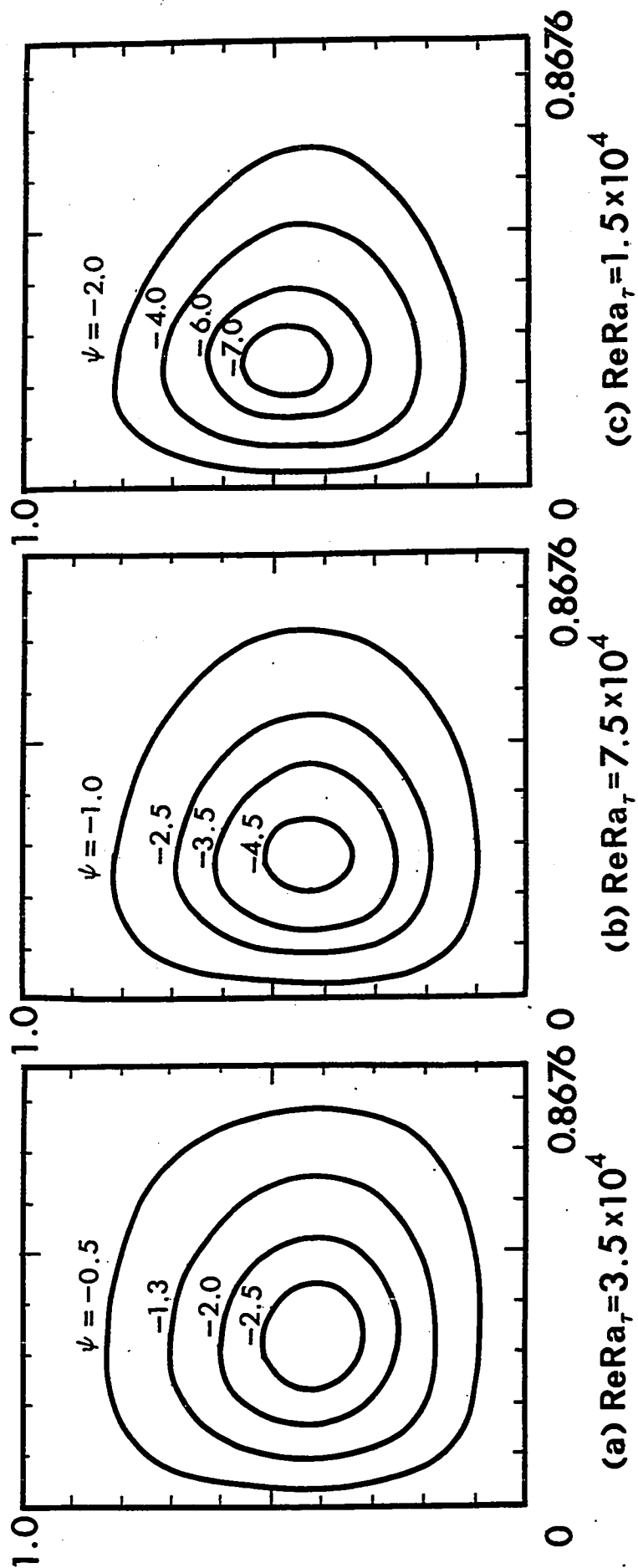


Fig. 6.10 Secondary flow streamlines for the case of $\text{Pr} = 0.7$ and $|\mu| \rightarrow \infty$

Fig. 6.9(c), we cannot detect any secondary vortices in the form of reversed flow for the case shown in Fig. 6.10(c). We can conclude that within the range of the present investigation the weaker secondary vortices in the form of reversed flow do not exist for the case of $|\mu| \rightarrow \infty$ up to at least $\text{ReRa}_\tau = 1.5 \times 10^5$. In making the above comparison between the cases of negative μ and $|\mu| \rightarrow \infty$, we must recognize the fact that for the case $|\mu| \rightarrow \infty$, the region in exactly the upper half of the channel is completely stable and only the lower half is unstable whereas for the case of negative μ the unstable region occupies only part of the lower half of the channel. This observation can be seen from the basic temperature distributions. For the case shown in Fig. 6.10(c), the secondary motion is seen to be rather weak in the regions near the upper and lower right-hand corners. We may speculate that with the further increase of the value of ReRa_τ the region of reversed flow may appear eventually. In view of the above observations for Figs. 6.9 and 6.10, the structure of the secondary motion is still quite uncertain beyond the range of the parameter Ra or ReRa_τ studied in this investigation.

As noted earlier in Figs. 6.9(a) and (b) and also Figs. 6.10(a) and (b), the intensity of the upward stream is much stronger than that of the downward stream. It may be of interest to see the effects of the strong upward stream and weak downward stream for secondary flow on the axial

velocity and temperature distributions. Figs. 6.11 and 6.12 show the distributions of the axial velocity and temperature, respectively, along the lines $y = 0$ and 0.8411 for the case of $Pr = 0.7$, $\mu = -30$ at $Ra = -1000$ and -3000 . In both Figs. 6.11 and 6.12, solid lines represent the distribution in the unperturbed state, dashed lines represent the distributions along $y = 0$ (upward stream) and broken lines represent the distributions along $y = 0.8411$ (downward stream). For the case of $Ra = -1000$, both Figs. 6.11 and 6.12 show that the deviations of the axial velocity and temperature profiles from the unperturbed state are greater along the line $y = 0$ than along the line $y = 0.8411$. For the case of $Ra = -3000$, this trend is more pronounced. It is also interesting to note that for the case of $Ra = -1000$ shown in Fig. 6.11, the dimensionless axial velocity U/U_0 is even slightly greater than 1 near $y = 0.8411$ and $z = 0.43$.

For the finite amplitude thermal convection problem under consideration, such overall quantities as resistance coefficient and Nusselt number are usually of interest in design. In view of the complexity of the present problem, the product of the friction factor and Reynolds number, fRe , and the Nusselt number, Nu , are defined in several different ways as follows:

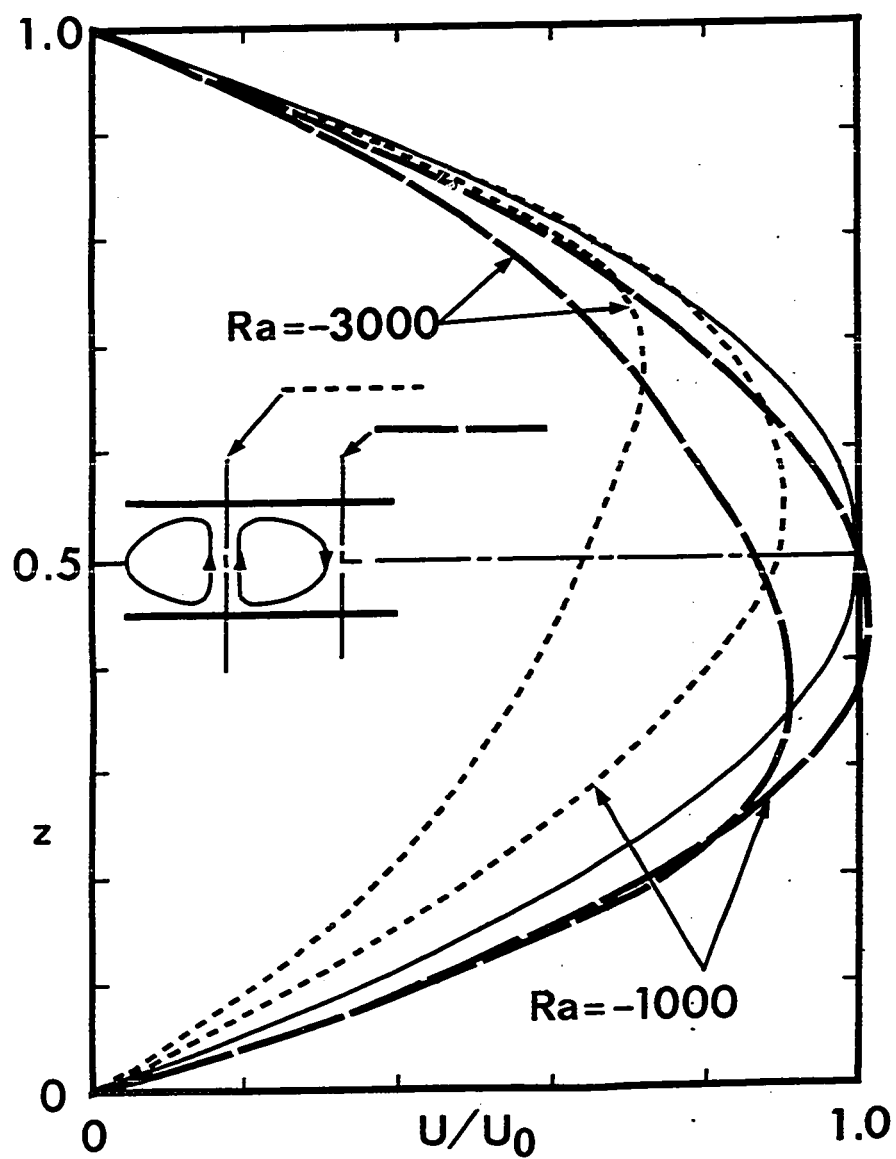


Fig. 6.11 Axial velocity distributions for the case of $Pr = 0.7$ and $|\mu| \rightarrow \infty$

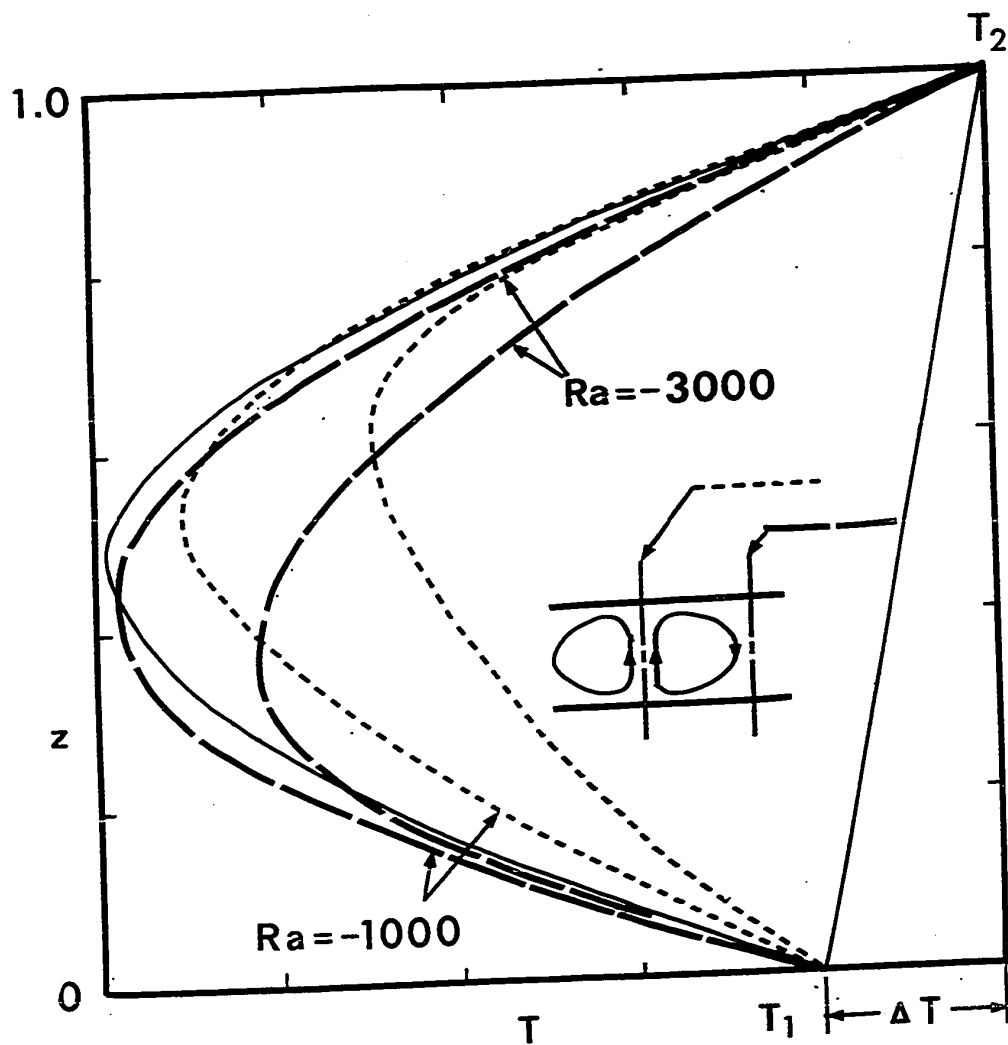


Fig. 6.12 Temperature distributions for the case of $Pr = 0.7$ and $\mu = -30$

$$(fRe)_1 = \frac{\left| 4 + \frac{1}{2} \left(\frac{\partial u}{\partial z} \right)_{z=0} \right|}{\left[4(z-z^2) + \frac{u}{2} \right]^2}, \text{ at lower plate} \quad (6.25)$$

$$(fRe)_2 = \frac{\left| -4 + \frac{1}{2} \left(\frac{\partial u}{\partial z} \right)_{z=1} \right|}{\left[4(z-z^2) + \frac{u}{2} \right]^2}, \text{ at upper plate} \quad (6.26)$$

$$(fRe)_3 = [(fRe)_1 + (fRe)_2]/2 = 4/\left[4(z-z^2) + \frac{u}{2} \right]^2,$$

$$\text{from overall force balance} \quad (6.27)$$

$$\text{where } f_1 = 2\mu \left| \frac{\partial U}{\partial z} \right|_{z'=0} / \rho \bar{U}^2, \quad f_2 = 2\mu \left| \frac{\partial U}{\partial z} \right|_{z'=h} / \rho \bar{U}^2,$$

$$f_3 = (\partial P / \partial x') h / \rho \bar{U}^2 \quad \text{and } Re = U_0 h / (2\nu).$$

The above definitions for the parameter fRe apply to all the cases considered in this investigation, namely, $\mu = 0$, $\mu = \text{finite}$ and $|\mu| \rightarrow \infty$ and the physical meaning of each definition is obvious.

$$(Nu)_1 = \frac{q_1 h}{\Delta T k} = (2/3) \cdot Pr \mu + 1 - \left(\frac{\partial \theta}{\partial z} \right)_{z=0} \quad (6.28)$$

$$(Nu)_2 = \frac{q_2 h}{\Delta T_k} = (2/3) \cdot Pr \mu - 1 + \left(\frac{\partial \theta}{\partial z} \right)_{z=1} \quad (6.29)$$

$$(Nu)_3 = \frac{q_3 h}{\Delta T_k} = [(Nu)_1 + (Nu)_2]/2 = Pr \mu (2/3 + \bar{u}/2) \quad (6.30)$$

where q_1 and q_2 are the amount of heat conducted from the lower and upper plates, respectively, to the fluid per unit time per unit area and q_3 is the net energy increase in the fluid per unit time per unit cross-sectional area.

The above expressions for the Nusselt number are based on the temperature difference between the two horizontal plates and applicable to the cases of $\mu = 0$ and $\mu = \text{finite}$ only. We note that for the case of $\mu = 0$, the definition $(Nu)_1$ represents the total heat transported by the system in the steady state and is given by the mean temperature gradient evaluated at the lower boundary. Accordingly, the expression $(Nu)_1$ is identical to the Nusselt number usually used in the Bénard convection problem and direct comparison is possible. It is instructive to note that for the case of finite μ , $(Nu)_1$ and $(Nu)_2$ represent the average heat transfer rate at the lower and upper plates, respectively, whereas $(Nu)_3$ represents the heat transfer rate in the main flow direction by convection.

The case of $|\mu| \rightarrow \infty$ corresponds to the well-known case of fully developed laminar flow between two parallel

plates without secondary flow for the uniform wall heat flux boundary conditions at the upper and lower plates. Consequently, for this case of $|\mu| \rightarrow \infty$ (or $T_1 = T_2 = T_w$), the expressions for the Nusselt number are defined by using the mixed mean temperature difference in accordance with the current practice as follows:

$$\begin{aligned} T_w - T_M &= \text{PrRe}\tau h \int_0^1 \int_0^{\pi/a} (\phi_\theta - \theta_\tau) U dy dz / (\bar{U} \cdot \pi/a) \\ &= \text{PrRe}\tau h (\phi_\theta - \theta_\tau)_M \end{aligned} \quad (6.31)$$

$$(Nu)_1 = \frac{q_1 h}{(T_w - T_M) k} = \frac{\frac{2}{3} - \left(\frac{\partial \theta_\tau}{\partial z}\right)_{z=0}}{(\phi_\theta - \theta_\tau)_M} \quad (6.32)$$

$$(Nu)_2 = \frac{q_2 h}{(T_w - T_M) k} = \frac{\frac{2}{3} - \left(\frac{\partial \theta_\tau}{\partial z}\right)_{z=1}}{(\phi_\theta - \theta_\tau)_M} \quad (6.33)$$

$$(Nu)_3 = \frac{q_3 h}{(T_w - T_M) k} = \frac{(Nu)_1 + (Nu)_2}{2} = \frac{\frac{2}{3} + \frac{\bar{u}}{2}}{(\phi_\theta - \theta_\tau)_M} \quad (6.34)$$

where ϕ_θ and θ_τ are defined in equations (6.2) and (6.16), respectively, and q_i , ($i=1,2,3$) has the same meaning as in the cases of $\mu = 0$ and $\mu = \text{finite}$. It is noted that all the average velocity and temperature gradients contained in the above definitions (6.25) to (6.34) are evaluated by using non-central five-point finite-difference formula and all integrations are carried out by using Simpson's rule. The expressions $(Nu)_1$ and $(Nu)_2$ represent the average heat transfer rate at the lower and upper plates, respectively, and Nu_3 represents the overall heat transfer rate in the main flow direction by convection which can be compared directly with the usual definition in forced convection without secondary flow. After defining the expressions for fRe and Nu , the flow and heat transfer results for the present problem will be considered next.

Fig. 6.13 shows the flow result in the form of the ratio $(fRe)_3/(fRe)_0$ versus Ra for the cases of $\mu = 0$ and $\mu = \text{finite}$ (negative or positive) with $Pr = 0.7$. We note that $(fRe)_0 = 9.0$ for the case without free convection effect. It is interesting to note that for a given value of Ra , the value of $(fRe)_3/(fRe)_0$ is larger for the positive μ as compared with the negative μ of the same value. Similarly, Fig. 6.14 illustrates the variation of $(fRe)_3/(fRe)_0$ with the parameter $PrReRa_\tau$ for the case of $|\mu| \rightarrow \infty$ with various Prandtl numbers. The reason for using the product of Pr and $ReRa_\tau$ as one parameter was explained earlier in section

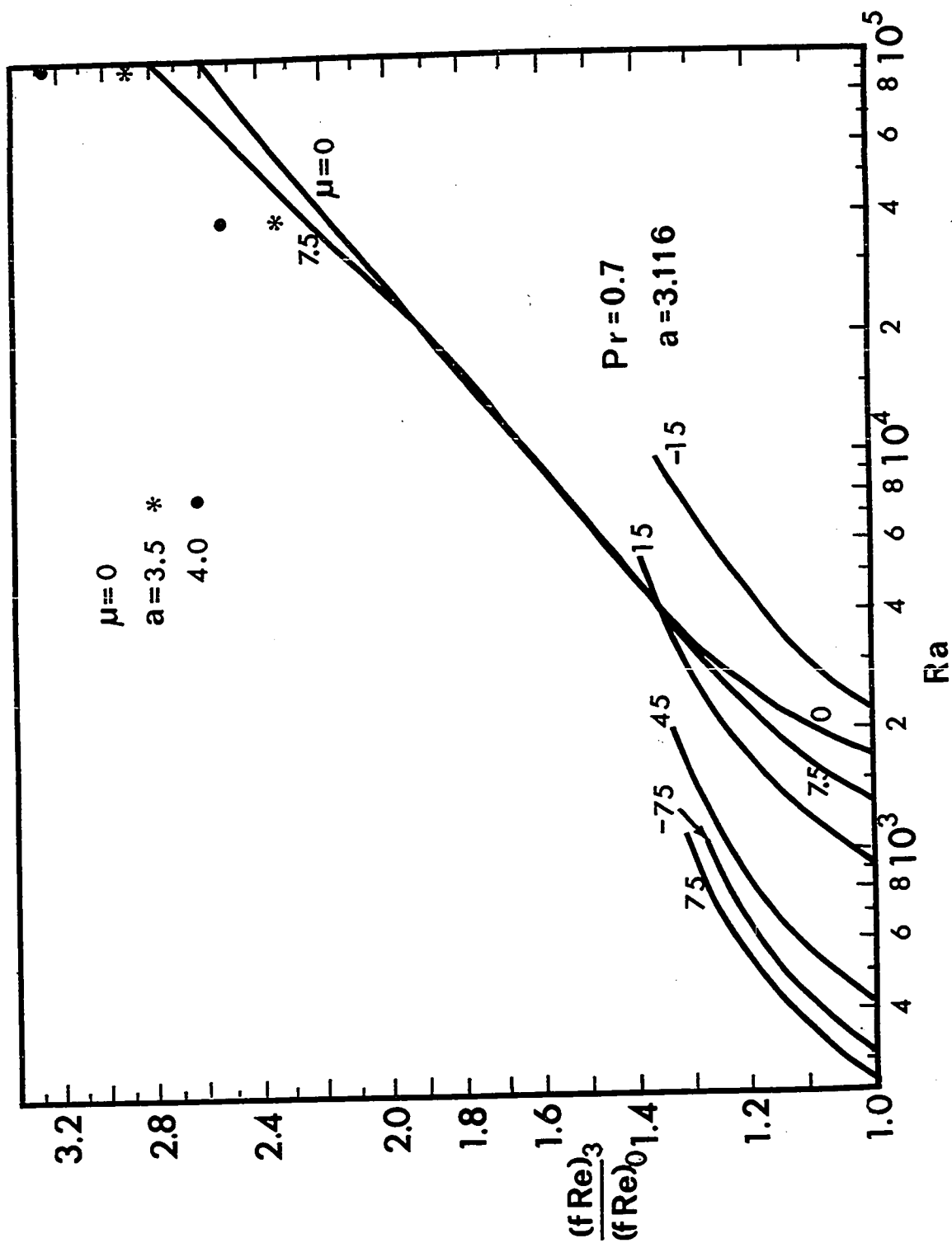


Fig. 6.13 $(fRe)_3/(fRe)_0$ versus Ra for the cases of $\mu = 0$ and $\mu = \text{finite}$ with $Pr = 0.7$

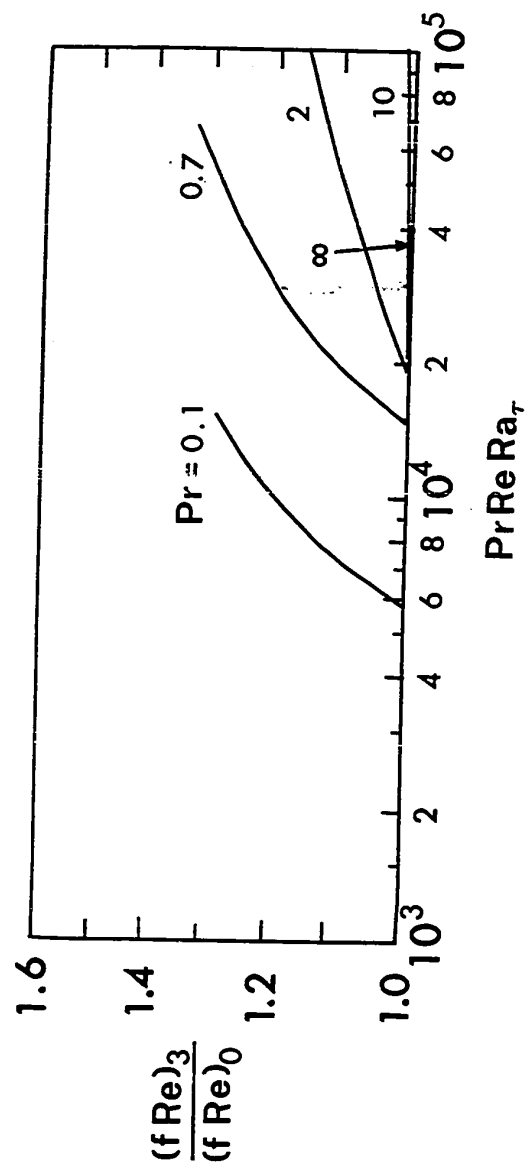


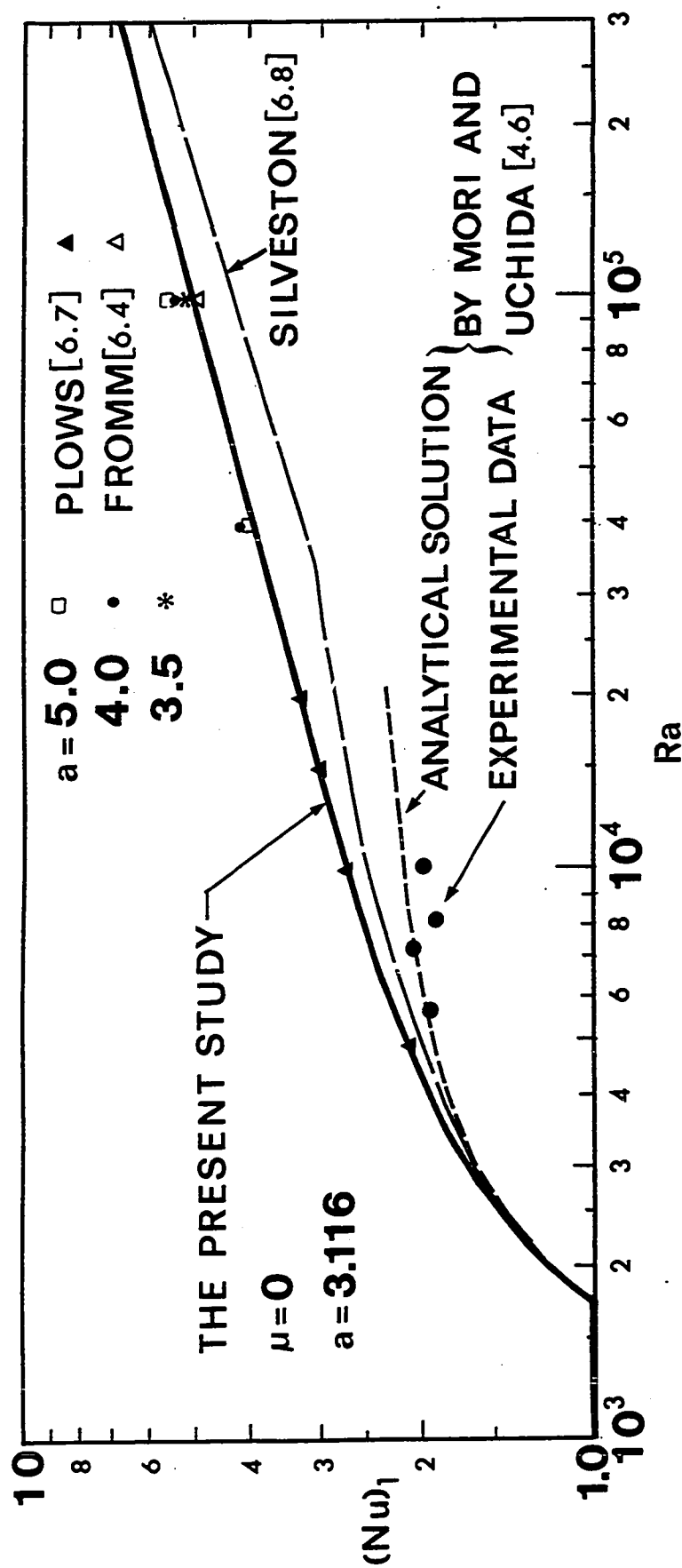
Fig. 6.14. $(fRe)_3/(fRe)_0$ versus $PrReRa_\tau$ for the case of $|\mu| \rightarrow \infty$

6.2. For the range of $Ra(\mu = \text{finite})$ or $PrReRa_\tau(|\mu| \rightarrow \infty)$ beyond the one shown in the figure, the present numerical technique fails to yield a convergent solution. However, for the case of $\mu = 0$, the present result clearly indicates an asymptotic behavior for the large Ra . For the case of $|\mu| \rightarrow \infty$ with large Prandtl number, the effect of the secondary flow on friction factor is seen to be negligible. This observation can also be seen by examining equations (6.18) and (6.21). For a given finite value of $PrReRa_\tau$ with large Pr , the value of $ReRa_\tau$ is small and the intensity of secondary flow is weak. Consequently, the increment of the value of $(fRe)_3$ indicating the effect of secondary motion on flow result is not significant. Furthermore, Fig. 6.14 indicates that at $PrReRa_\tau = 10^5$ (about five times the critical $PrReRa_\tau$), the friction factor increases by about 15 per cent only for $Pr = 2$ as compared with the case without secondary flow. Unfortunately, theoretical or experimental data for flow are not available in the literature for comparison with the present results shown in Fig. 6.13 and 6.14. A numerical experiment is also made to evaluate the wave number effect. For the case of $\mu = 0$, at $Ra = 10^5$ the difference of about 10% and 25% for the flow result is observed as the wave number is varied from 3.116 to 3.5 and 4.0, respectively.

In order to assess the accuracy of the present numerical solution, comparison of the result of this investigation for the case of $\mu = 0$ with the analytical result of Mori and

Uchida, their experimental data [4.6] and Plows' numerical result [6.7] for two-dimensional steady laminar Bénard convection is made in Fig. 6.15. Plows [6.7] considered the effect at Prandtl number for the Rayleigh number ranging from 2000 to 20000. However, only the curve for $Pr = 0.5 \sim 1$ is taken for comparison here. It is not surprising that the result of the present numerical solution and Plows' numerical result coincide exactly since the governing equations and the boundary conditions are identical for the Bénard problem with two-dimensional rolls between two rigid surfaces and the present fully developed laminar forced convection between two horizontal plates with longitudinal vortex rolls for the case $\mu = 0$. The agreement of the two results serves to confirm the accuracy of the present numerical technique.

Mori and Uchida's result from analytical solution based on Stuart's method starts deviation at $Ra = 3000$ from the results of the two numerical solutions and considerable difference is seen at higher Rayleigh number. At $Ra/Ra^* = 9.0$, Mori and Uchida's result is seen to have about 25 per cent error as compared with the numerical result. Mori and Uchida's experimental data are also seen to lie below the two numerical solutions. As mentioned in the Introduction, the solution of the analogous problem of flow between rotating cylinders by Stuart's energy-balance method is estimated to have a largest error of about 7 per cent for the torque at a Taylor number up to ten times the critical value. Although similar energy-

Fig. 6.15 $(Nu)_1$ versus Ra for the case of $\mu = 0$

balance method due to Stuart is used, the error of 25 per cent in heat transfer result for the present problem with $\mu = 0$ and the error of 7 per cent in flow result for Taylor's problem represent quite a contrast. A comparison with Fromm's numerical solution for Bénard's problem [6.4] is also possible. Since his graphical result cannot be read accurately, only one datum point at $Ra = 10^5$ is plotted in Fig. 6.15 for comparison and an excellent agreement is again observed. Although the present problem for $\mu = 0$ is not exactly identical to the Bénard problem except for the case of two-dimensional rolls, nevertheless, the heat transfer results for the two problems are known to be similar and a comparison of numerical solution with experimental data [6.8] for Bénard convection is also made in Fig. 6.15. A largest difference of 20 per cent based on numerical solution is observed at $Ra = 3.5 \times 10^4$ for the experimental data.

A numerical experiment is also made to study the effect of variable wave number. As shown in Fig. 6.15, only a few per cent difference is found for a rather wide range of wave number from $a = 3.116$ to 5.0 at a high Rayleigh number of $Ra = 10^5$. For smaller variation of wave number and at lower Rayleigh numbers, the difference is found to be even smaller. Consequently, we can conclude that the present assumption on wave number is a reasonable approximation for the heat transfer result at least for the case of $\mu = 0$.

Heat transfer results for $Pr = 0.7$ in the form of

$(Nu)_i/(Pr\mu)$ ($i=1,2,3$) versus Rayleigh number with μ ($=$ finite) as a parameter are shown in Fig. 6.16. By examining equations (6.28) to (6.30), it is not difficult to see the reason for taking $(Nu)_i/(Pr\mu)$ ($i=1,2,3$) as a coordinate. Based on the temperature difference, ΔT , for the definition of Nusselt number we see that the effect of secondary flow does not necessarily lead to increased heat transfer rate. The value of $(Nu)_1/(Pr\mu)$ represents the average heat transfer rate at the lower plate and is seen to increase as Ra increases for positive $\mu \leq 15$ and decrease for the other values of μ . The value of $(Nu)_2/(Pr\mu)$ represents the average heat transfer rate at the upper plate and is seen to decrease as Ra increases for all μ 's. The value of $(Nu)_3/(Pr\mu)$ represents the overall heat transfer rate for fluid and is seen to decrease as Ra increases for all μ 's. The reason for a decreased overall heat transfer rate can be explained easily by examining the term $(2/3 + \bar{u}/2)$ in the expression for $(Nu)_3/(Pr\mu)$. It is noted that the mean velocity for perturbed flow is always negative and its value decreases further as the intensity of secondary flow (or Ra) increases. For $\mu = 7.5$, the behavior for heat transfer results shown in Fig. 6.16 is rather complex, For example, the value of $(Nu)_2/(Pr\mu)$ becomes zero at some value of Rayleigh number and from thereon the value for $(Nu)_1/(Pr\mu)$ increases at higher rate with the further increase of Ra . For $\mu = 7.5$, it is seen that the present configurations is effective in removing heat from the lower plate but

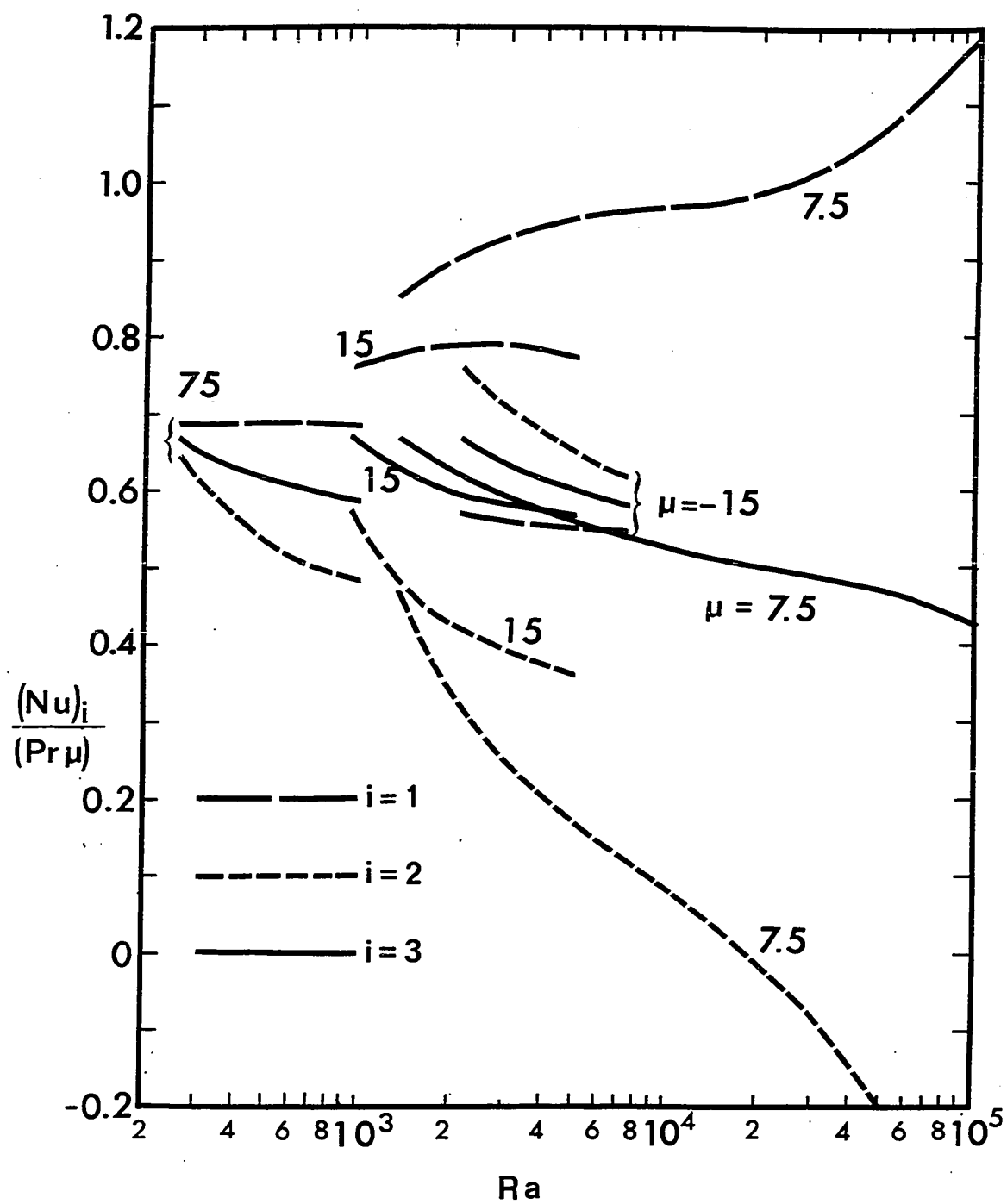


Fig. 6.16 $(Nu)_i / (Pr \mu)$ ($i=1,2,3$) versus Ra with μ (= finite) as a parameter for $Pr = 0.7$

rather poor from the viewpoint of heating the fluid. In general, it can be stated that the case of finite μ is not efficient for heating fluid and this observation is believed to be significant in a design problem.

Fig. 6.17 shows the results for Nusselt number ratio $(Nu)_i/(Nu)_0$ ($i=1,2,3$) versus $PrReRa_\tau$ for the case of $|\mu| \rightarrow \infty$ with various Prandtl numbers. The reason for taking the product of Pr and $ReRa_\tau$ as a parameter is based on the observation that for a given value of $PrReRa_\tau$, the value of $(Nu)_i/(Nu)_0$ ($i=1,2,3$) for $Pr \geq 2$ is seen to approach the asymptotic solution for $Pr \rightarrow \infty$ with a maximum difference of about 3 per cent. This observation on asymptotic behavior for Prandtl number effect suggests that for the case of $|\mu| \rightarrow \infty$ only one computation is required to predict the heat transfer result for a Prandtl number ranging from say 2 to ∞ . It is also seen in Fig. 6.17 that the value of $(Nu)_2/(Nu)_0$ for various Prandtl numbers is found to be approximately one. This may be caused by the fact that the heat transfer rate is not affected by the weak secondary motion near the plate as shown in Fig. 6.10.

A brief outline on the order of magnitude analysis for the governing equations is given in Appendix 6.1 and numerical results for flow and heat transfer are tabulated in Appendix 6.2 for possible future reference.

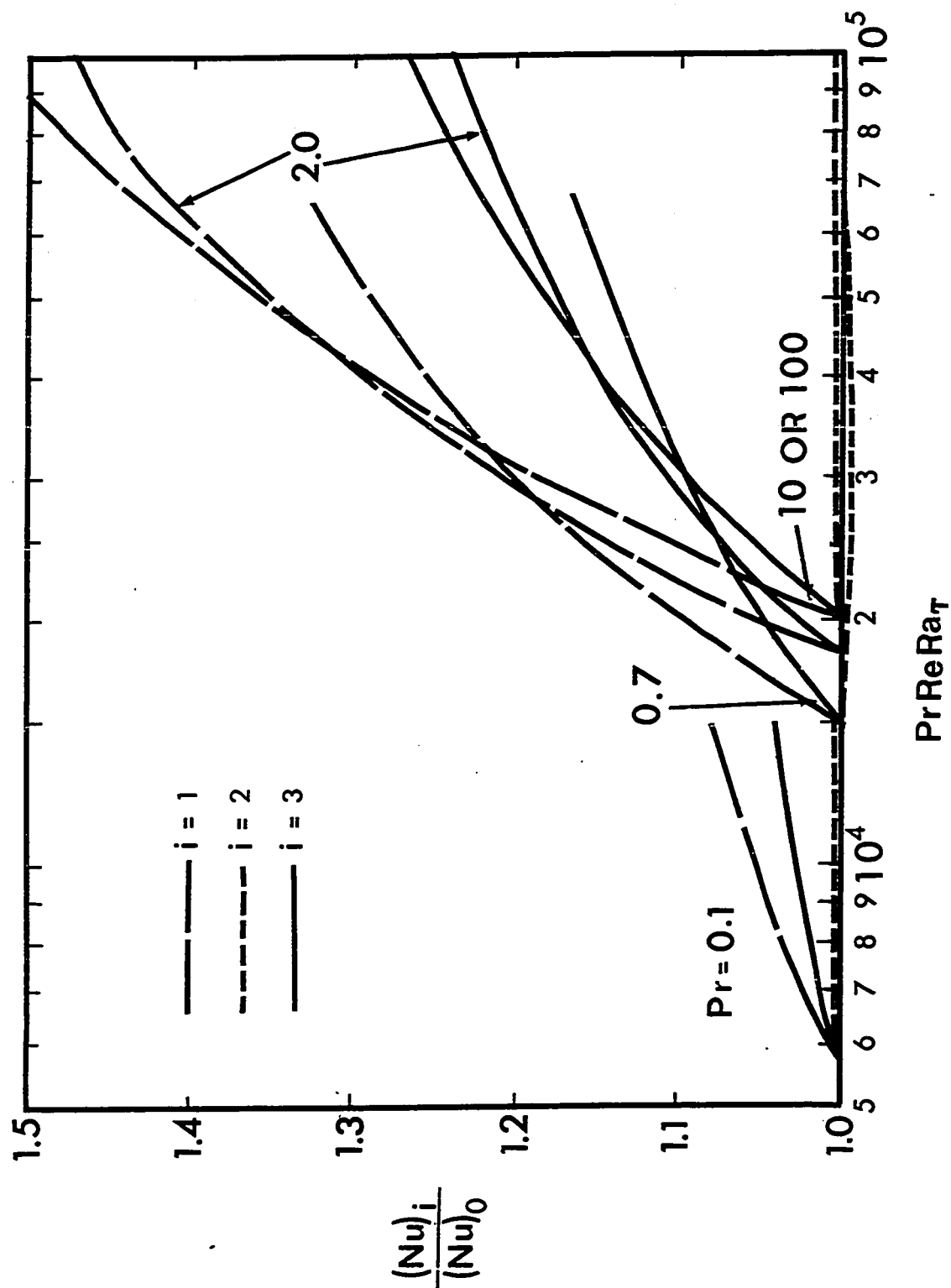


Fig. 6.17 $(Nu)_i / (Nu)_0$ ($i=1,2,3$) versus $Pr Re Ra_\tau$ for the case of $|\mu| \rightarrow \infty$

6.5 Concluding Remarks

(a) The boundary vorticity method and its improved iterative scheme (within the scope of the present study) have been shown to be quite effective for the numerical solution of the present rather complicated problem. With respect to the determination of the boundary vorticity, the method of unsteady state solution employed in [6.6] requires a longer computing time and one additional step than the present techniques. The numerical experiment shows that up to about one-quarter of computing time can be saved by using the improved (or modified) iterative scheme as compared with the boundary vorticity method using a relaxation factor of unity. This does not imply that the improved iterative scheme is always better than the boundary vorticity method if the relaxation factor is other than one or for a problem formulated in polar coordinates.

(b) The heat transfer result from the present numerical study for the case of $\mu = 0$ agrees exactly with the numerical result reported in [6.7] for the Bénard convection problem. This agreement serves to confirm the accuracy of the present numerical technique. Mori and Uchida's approximate analytical result [4.6] starts deviation from the present numerical result at $Ra = 3000$, and about 25 per cent error is observed at $Ra = 9.0 Ra^*$. Thus, we can conclude that Stuart's method is valid only for Rayleigh number ranging up to say $Ra = 3.0 Ra^*$ with a maximum error of about 10 per cent.

Besides the present problem, the boundary vorticity method and its improved (or modified) iterative scheme are believed to be equally effective for the numerical solution of a host of other similar finite amplitude convection problems in the post-critical regime.

(c) The asymptotic behavior of the flow and heat transfer results for $Pr \geq 0(1)$ observed in both the combined free and forced convection problem (Chapter III) and the thermal instability problem (Chapter IV) is also observed in the present finite amplitude convection problem. Fig. 6.14 shows that the effect of secondary motion on the flow result is negligible for $Pr \geq 2$ for the parameter $PrReRa_T$ within the range of present investigation. Fig. 6.17 also shows that for $Pr \geq 2$, the heat transfer result already approaches the solution for the large Prandtl number with a maximum error of less than 3 per cent. This observation suggests that computations for all the Prandtl numbers between 2 and ∞ are not required to study the Prandtl number effect.

(d) The assumption that the wave number in the post-critical regime does not deviate from the critical value determined by the linear stability analysis discussed in Chapter IV is found to be a fairly good approximation for the heat transfer result but a rather poor approximation for the flow result in the case of $\mu = 0$. Due to considerable computing time requirement, the numerical experiment was not carried out for the other cases. However, it is suggested

that the wave number in the post-critical regime should be determined from a study in the entrance region instead of the fully developed region considered in this study. From the viewpoint of physical reasoning, we have no reasons to expect that the size and structure of the vortex roll should be determined in the fully developed region alone. It is believed that a study in the thermal entrance region will shed some light regarding the variation of the wave number in the post-critical regime.

References

- 6.1 Malkus, W.V.R., and Veronis, G., "Finite Amplitude Cellular Convection," *Journal of Fluid Mechanics*, Vol. 4, 1958, pp. 225-260.
- 6.2 Stuart, J.T., "On the Nonlinear Mechanics of Hydrodynamic Stability." *Journal of Fluid Mechanics*, Vol. 4, 1958, pp. 1-21.
- 6.3 Roberts, P.H., "On Nonlinear Bénard Convection," *Non-Equilibrium Thermodynamics, Variational Techniques and Stability*, Donnelly, R.J., Herman, R., and Prigogine, I., eds., (Proceedings of a Symposium Held at the University of Chicago, May 17-19, 1965), The University of Chicago Press, Chicago and London, 1966.
- 6.4 Fromm, J.E., "Numerical Solutions of the Nonlinear Equations for a Heated Fluid Layer," *The Physics of Fluids*, Vol. 8, 1965, pp. 1757-1774.
- 6.5 Mori, Y., and Uchida, Y., "Forced Convective Heat Transfer in a Curved Channel," *JSME Semi-International Symposium, Heat and Mass Transfer, Thermal Stress*, JSME, Vol. 1, 1967, pp. 181-190.
- 6.6 Samuels, M.R., and Churchill, S.W., "Stability of a Fluid in a Rectangular Region Heated from Below," *AIChE Journal*, Vol. 13, No. 1, 1967, pp. 77-85.

- 6.7 Plows, W.H., "Some Numerical Results for Two-Dimensional Steady Laminar Bénard Convection," The Physics of Fluids, Vol. 11, 1968, pp. 1593-1599.
- 6.8 Silveston, P.L., "Wärmedurchgang in Waagerechten Flüssigkeitsschichten," Part 1, Forsch, Ing. Wes. Vol. 24, 1958, pp. 29-32 and pp. 59-60.

Appendix 6.1 Order of Magnitude Analysis for Governing Equations

For the sake of simplicity, the discussion on the orders of magnitude of the terms representing compression work, viscous dissipation and variable property effects will not be made here. Referring to Fig. 6.1, the dependent variables describing the steady state velocity, pressure and temperature fields are written as,

$$\begin{aligned} U &= U_b + u', \quad V = v', \quad W = w', \quad P = P_b + p' \quad \text{and} \\ T &= T_b + \theta' \end{aligned} \quad (6.1.1)$$

It is noted that the basic quantities U_b and T_b in the unperturbed state are given in equation (6.2) for the steady fully developed plane Poiseuille flow and the perturbation quantities u' , v' , w' , p' and θ' are functions of space variables x' , y' and z' only.

To normalize the perturbation equations, we introduce the following dimensionless quantities for dependent and independent variables,

$$\begin{aligned} u' &= u_c u, \quad v' = v_c v, \quad w' = w_c w, \quad p' = p_c p, \quad \theta' = \theta_c \theta, \\ x' &= Lx, \quad y' = \frac{\pi h}{2a} y \quad \text{and} \quad z' = \frac{h}{2} z \end{aligned} \quad (6.1.2)$$

where h is a distance between the two parallel plates and the length $\frac{\pi h}{2a}$ is one-quarter of a wavelength. Observing the governing equations and the physical character of longitudinal vortex rolls, we find that

$$\text{continuity equation } 0(\partial v'/\partial y') = 0(v' \partial w'/\partial z')$$

$$x'\text{-direction momentum equation } 0(v' \partial^2 u'/\partial z'^2) = 0(w' \partial u'/\partial z')$$

$$y'\text{-direction momentum equation } 0(\partial p'/\partial y') = 0(v' \partial^2 v'/\partial z'^2)$$

$$z'\text{-direction momentum equation } 0(\beta g \theta') = 0(v' \partial^2 w'/\partial z'^2).$$

Using the above relations, the relationships between the characteristic quantities are obtained as,

$$v_c = w_c \pi/a, w_c = u_c/Re, p_c = v_c 2\rho v \pi/(ah) \text{ and}$$

$$w_c = \theta_c \beta g h^2/(4v) \quad (6.1.3)$$

Substituting equations (6.1.1), (6.1.2) and (6.1.3) into the continuity, momentum, and energy equations, the equations for the perturbation quantities can be shown as:

$$\epsilon_1 \frac{\partial u}{\partial x} + \frac{\partial v}{\partial y} + \frac{\partial w}{\partial z} = 0 \quad (6.1.4)$$

$$\begin{aligned}
& \epsilon_1 \left(\frac{\phi_u}{2} \frac{\partial u}{\partial x} + B_1 u \frac{\partial u}{\partial x} \right) + B_1 \left(u \frac{\partial u}{\partial y} + w \frac{\partial u}{\partial z} \right) + \frac{w}{2} \frac{\partial \phi_u}{\partial z} \\
& = B_2 \epsilon_1 \frac{\partial p}{\partial x} + \epsilon_2 \frac{\partial^2 u}{\partial x^2} + \frac{1}{B_2} \frac{\partial^2 u}{\partial y^2} + \frac{\partial^2 u}{\partial z^2}
\end{aligned} \tag{6.1.5}$$

$$\begin{aligned}
& \epsilon_1 \left(\frac{\phi_u}{2} \frac{\partial v}{\partial x} + B_1 u \frac{\partial v}{\partial x} \right) + B_1 \left(v \frac{\partial v}{\partial y} + w \frac{\partial v}{\partial z} \right) = - \frac{\partial p}{\partial y} \\
& + \epsilon_2 \frac{\partial^2 v}{\partial x^2} + \frac{1}{B_2} \frac{\partial^2 v}{\partial y^2} + \frac{\partial^2 v}{\partial z^2}
\end{aligned} \tag{6.1.6}$$

$$\begin{aligned}
& \epsilon_1 \left(\frac{\phi_u}{2} \frac{\partial w}{\partial x} + B_1 u \frac{\partial w}{\partial x} \right) + B_1 \left(v \frac{\partial w}{\partial y} + w \frac{\partial w}{\partial z} \right) = - B_2 \frac{\partial p}{\partial z} \\
& + \epsilon_2 \frac{\partial^2 w}{\partial x^2} + \frac{1}{B_2} \frac{\partial^2 w}{\partial y^2} + \frac{\partial^2 w}{\partial z^2} + \theta
\end{aligned} \tag{6.1.7}$$

$$\begin{aligned}
& \text{Pr} \epsilon_1 \left(\frac{\phi_u}{2} \frac{\partial \theta}{\partial x} + B_1 u \frac{\partial \theta}{\partial x} \right) + \text{Pr} B_1 \left(v \frac{\partial \theta}{\partial y} + w \frac{\partial \theta}{\partial z} \right) + \text{Ra} \left(\frac{\mu}{16} u \right. \\
& \left. - \frac{\text{Pr} \mu}{8} w \frac{\partial \phi_\theta}{\partial z} - \frac{\text{Ra}}{16} w \right) = \epsilon_2 \frac{\partial^2 \theta}{\partial x^2} + \frac{1}{B_2} \frac{\partial^2 \theta}{\partial y^2} + \frac{\partial^2 \theta}{\partial z^2}
\end{aligned} \tag{6.1.8}$$

where $\epsilon_1 = \text{Re}h/(2L)$, $\epsilon_2 = h^2/(4L^2)$, $B_1 = u_c/U_0$ and $B_2 = (\frac{\pi}{a})^2$.

Equations (6.1.4) to (6.1.8) can be reduced to equa-

tions (6.3) to (6.5) and (6.7) by setting $L \rightarrow \infty$ for fully developed flow provided that Pr , B_1 , Re and h are finite.

In addition to the fully developed flow assumption, by setting $B_1 = \frac{u_c}{U_0} \rightarrow 0$ for infinitesimal disturbance, equations (6.1.4) to (6.1.8) can be further reduced to the linearized equations discussed in Chapter IV.

Appendix 6.2 Numerical Results

$Pr = 0.7, \mu = 0, a = 3.116$

$Ra \times 10^{-3}$	$(fRe)_1$	$(fRe)_2$	$(fRe)_3$	$(Nu)_1$	$(Nu)_2$	$(Nu)_3$
≤ 1.7087	9.0	9.0	9.0	1.0	-1.0	0
2.5	10.75	10.75	10.76	1.485	-1.485	0
3.5	11.82	11.82	11.85	1.820	-1.820	0
5.5	13.04	13.04	13.11	2.201	-2.201	0
8.0105	14.02	14.02	14.14	2.493	-2.493	0
10.0	14.61	14.61	14.77	2.664	-2.664	0
15.0	15.34	15.34	15.56	2.872	-2.872	0
17.08	16.15	16.15	16.44	3.096	-3.096	0
40.0	19.24	19.24	19.51	3.912	-3.912	0
100.0	23.50	23.50	23.00	5.083	-5.083	0
300.0	26.67	26.67	25.89	6.643	-6.643	0

$Pr = 0.7, \mu = 0, Ra = 4 \times 10^4$

a	$(fRe)_1$	$(fRe)_2$	$(fRe)_3$	$(Nu)_1$	$(Nu)_2$	$(Nu)_3$
3.5	20.93	20.93	21.20	4.001	-4.001	0
4.0	22.46	22.46	23.02	4.047	-4.047	0
5.0	25.69	25.69	26.37	4.038	-4.038	0

$Pr = 0.7, \mu = 0, Ra = 1 \times 10^5$

a	$(fRe)_1$	$(fRe)_2$	$(fRe)_3$	$(Nu)_1$	$(Nu)_2$	$(Nu)_3$
3.5	2.626	2.626	2.553	5.249	-5.249	0
4.0	2.984	2.984	2.875	5.408	-5.408	0
5.0	3.505	3.505	3.273	5.517	-5.517	0

$$Pr = 0.7, \mu = 7.5, a = 3.284$$

$Ra \times 10^{-3}$	$(fRe)_1$	$(fRe)_2$	$(fRe)_3$	$(Nu)_1$	$(Nu)_2$	$(Nu)_3$
≤ 1.3290	9.0	9.0	9.0	4.5	2.5	3.5
2.5	11.41	10.66	11.04	4.837	1.479	3.160
5.0	12.98	12.38	12.71	5.005	0.8834	2.946
10.0	14.40	14.56	14.55	5.064	0.4405	2.752
20.0	16.21	17.53	17.06	5.167	-0.0812	2.542
30.0	17.51	19.72	18.88	5.318	-0.4729	2.417
60.0	20.00	25.07	22.38	5.760	-1.326	2.220
100.0	21.96	32.11	25.20	6.205	-2.247	2.091

$$Pr = 0.7, \mu = 15, a = 3.415$$

$Ra \times 10^{-3}$	$(fRe)_1$	$(fRe)_2$	$(fRe)_3$	$(Nu)_1$	$(Nu)_2$	$(Nu)_3$
≤ 0.94366	9.0	9.0	9.0	8.0	6.0	7.0
1.5	10.84	9.982	10.42	8.194	4.810	6.507
3.0	12.42	11.09	11.76	8.272	3.964	6.123
4.5	12.95	11.66	12.33	8.195	3.756	5.982
5.0	12.94	11.70	12.35	8.126	3.790	5.976

$$Pr = 0.7, \mu = 45, a = 3.546$$

$Ra \times 10^{-2}$	$(fRe)_1$	$(fRe)_2$	$(fRe)_3$	$(Nu)_1$	$(Nu)_2$	$(Nu)_3$
≤ 4.1098	9.0	9.0	9.0	22.0	20.0	21.0
6.0	10.56	9.685	10.13	22.15	17.43	19.80
8.0	11.40	10.04	10.72	22.23	16.24	19.24
10.0	11.92	10.28	11.11	22.23	15.56	18.90
15.0	12.65	10.71	11.71	22.12	14.72	18.41

$$Pr = 0.7, \mu = 75, a = 3.576$$

$Ra \times 10^{-2}$	$(fRe)_1$	$(fRe)_2$	$(fRe)_3$	$(Nu)_1$	$(Nu)_2$	$(Nu)_3$
≤ 2.6081	9.0	9.0	9.0	36.0	34.0	35.0
4.0	10.72	9.722	10.23	36.17	29.48	32.84
6.0	11.81	10.17	11.0	36.23	27.06	31.67
8.0	12.40	10.43	11.42	36.16	25.92	31.07
10.0	12.73	10.60	11.70	35.92	25.28	30.70

$$Pr = 0.7, \mu = -7.5, a = 3.962$$

$Ra \times 10^{-3}$	$(fRe)_1$	$(fRe)_2$	$(fRe)_3$	$(Nu)_1$	$(Nu)_2$	$(Nu)_3$
≥ -7.2236	9.0	9.0	9.0	-2.5	-4.5	-3.5
-8.0	9.371	9.116	9.229	-2.495	-4.440	-3.456
-9.0	9.999	9.334	9.674	-2.440	-4.306	-3.376
-10.0	10.40	9.455	9.930	-2.421	-4.239	-3.332
-15.0	11.93	9.899	10.91	-2.352	-4.014	-3.179

$$Pr = 0.7, \mu = -15, a = 3.836$$

$Ra \times 10^{-3}$	$(fRe)_1$	$(fRe)_2$	$(fRe)_3$	$(Nu)_1$	$(Nu)_2$	$(Nu)_3$
≥ -2.2204	9.0	9.0	9.0	-6.0	-8.0	-7.0
-3.0	10.33	9.440	9.888	-5.924	-7.438	-6.678
-3.5	10.90	9.603	10.25	-5.893	-7.223	-6.558
-4.0	11.37	9.729	10.55	-5.869	-7.059	-6.464
-4.5	11.75	9.829	10.80	-5.847	-6.931	-6.391
-5.0	12.08	9.913	11.0	-5.830	-6.827	-6.331
-6.0	12.61	10.05	11.34	-5.799	-6.664	-6.236
-7.0	13.03	10.15	11.60	-5.773	-6.544	-6.165

$$Pr = 0.7, \mu = -30, a = 3.735$$

$Ra \times 10^{-3}$	$(fRe)_1$	$(fRe)_2$	$(fRe)_3$	$(Nu)_1$	$(Nu)_2$	$(Nu)_3$
≥ -0.88447	9.0	9.0	9.0	-13.0	-15.0	-14.0
-1.0	9.623	9.236	9.430	-12.96	-14.40	-13.68
-2.0	11.96	9.955	10.96	-12.85	-12.53	-12.69
-3.0	12.96	10.23	11.59	-12.80	-11.90	-12.33
-3.5	13.30	10.35	11.84	-12.75	-11.72	-12.20

$$Pr = 0.7, \mu = -75, a = 3.667$$

$Ra \times 10^{-2}$	$(fRe)_1$	$(fRe)_2$	$(fRe)_3$	$(Nu)_1$	$(Nu)_2$	$(Nu)_3$
≥ -3.0983	9.0	9.0	9.0	-34.0	-36.0	-35.0
-4.0	10.14	9.443	9.795	-33.93	-33.17	-33.55
-6.0	11.45	9.883	10.67	-33.89	-30.38	-32.14
-8.0	12.18	10.12	11.16	-33.82	-29.01	-31.43
-10.0	12.66	10.28	11.48	-33.74	-28.20	-30.99

$$Pr = 0.1, |\mu| \rightarrow \infty, a = 3.192$$

$ReRa_\tau \times 10^{-4}$	$(fRe)_1$	$(fRe)_2$	$(fRe)_3$	$(Nu)_1$	$(Nu)_2$	$(Nu)_3$
≤ 5.6319	9.0	9.0	9.0	8.235	8.235	8.235
6.5	9.768	9.359	9.564	8.372	8.245	8.308
7.5	10.34	9.602	9.975	8.478	8.246	8.363
8.5	10.80	9.782	10.29	8.564	8.246	8.404
10.0	11.34	9.993	10.67	8.666	8.245	8.455
15.0	12.55	10.46	11.51	8.892	8.252	8.571

$$\text{Pr} = 0.7, |\mu| \rightarrow \infty, a = 3.621$$

	$\text{ReRa}_\tau \times 10^{-4}$	$(f\text{Re})_1$	$(f\text{Re})_2$	$(f\text{Re})_3$	$(\text{Nu})_1$	$(\text{Nu})_2$	$(\text{Nu})_3$
\leq	2.1305	9.0	9.0	9.0	8.235	8.235	8.235
	3.0	10.44	9.577	10.01	9.154	8.188	8.673
	3.5	10.94	9.761	10.36	9.485	8.172	8.832
	4.0	11.33	9.90	10.62	9.745	8.164	8.959
	4.5	11.65	10.02	10.84	9.962	8.161	9.064
	6.0	12.30	10.26	11.29	10.41	8.169	9.293
	7.5	12.68	10.41	11.57	10.64	8.181	9.443
	9.0	12.97	10.58	11.81	10.85	8.231	9.549

$$\text{Pr} = 2, |\mu| \rightarrow \infty, a = 3.826$$

	$\text{ReRa}_\tau \times 10^{-4}$	$(f\text{Re})_1$	$(f\text{Re})_2$	$(f\text{Re})_3$	$(\text{Nu})_1$	$(\text{Nu})_2$	$(\text{Nu})_3$
\leq	0.90473	9.0	9.0	9.0	8.235	8.235	8.235
	1.0	9.137	9.057	9.097	8.691	8.234	8.460
	1.5	9.624	9.246	9.436	9.960	8.192	9.080
	2.0	9.983	9.370	9.680	10.66	8.167	9.419
	3.0	10.52	9.532	10.02	11.46	8.156	9.810
	4.0	10.87	9.632	10.26	11.89	8.159	10.04
	5.0	11.08	9.686	10.39	12.09	8.177	10.15

$$\text{Pr} = 10, |\mu| \rightarrow \infty, a = 3.955$$

	$\text{ReRa}_\tau \times 10^{-3}$	$(f\text{Re})_1$	$(f\text{Re})_2$	$(f\text{Re})_3$	$(\text{Nu})_1$	$(\text{Nu})_2$	$(\text{Nu})_3$
\leq	1.9885	9.0	9.0	9.0	8.235	8.235	8.235
	3.0	9.026	9.011	9.019	9.803	8.258	9.036
	5.0	9.069	9.028	9.049	11.16	8.244	9.717
	7.0	9.108	9.043	9.076	11.89	8.246	10.09
	8.0	9.126	9.049	9.088	12.14	8.250	10.21
	9.0	9.142	9.055	9.099	12.34	8.254	10.32

$$Pr = 100, |\mu| \rightarrow \infty, a = 3.989$$

	$ReRa_\tau \times 10^{-2}$	$(fRe)_1$	$(fRe)_2$	$(fRe)_3$	$(Nu)_1$	$(Nu)_2$	$(Nu)_3$
\leq	2.0332	9.0	9.0	9.0	8.235	8.235	8.235
	3.0	9.0	9.0	9.0	9.747	8.275	9.013
	5.0	9.001	9.0	9.001	11.16	8.272	9.722
	7.0	9.001	9.001	9.001	11.90	8.280	10.10
	9.0	9.002	9.001	9.001	12.35	8.284	10.34
	10.0	9.002	9.001	9.001	12.47	8.292	10.40

CHAPTER VII

GENERAL CONCLUDING REMARKS

Boundary vorticity method is developed for the numerical solution of the fully developed laminar forced convection heat transfer with secondary flow. Mathematically, forced convective heat transfer problems with secondary flow can be classified into two categories. When the critical characteristic parameter depicting the onset of secondary flow is zero, the problem is a boundary-value problem. If the secondary flow appears discretely only after a critical value of the characteristic parameter is reached, then the problem is an eigenvalue problem for thermal instability.

At present no theoretical method of solution is available for the whole range of the parameter characterizing the intensity of secondary flow for the boundary-value problem. The reason is clear from the consideration of the physical situation. For the characteristic parameter up to intermediate range, the viscosity and heat conduction are important throughout the whole region of the channel cross-section. In the high parameter range, the viscosity and heat conduction are negligibly small in the core region which occupies the substantial part of the cross-section. It is noted that the viscous and heat conduction terms represent the highest order terms in the governing equations. By its very nature the perturbation method is valid only for the very

small parameter region. On the other hand, boundary-layer technique is an approximate method and is valid only for the high parameter range. Besides closing the gap between the perturbation method and the boundary-layer technique, the numerical solution using boundary vorticity method is valid up to a reasonably high value of the parameter where the asymptotic behavior for flow and heat transfer results already appears and further results for the high parameter region can be obtained by linear extrapolation.

In general, secondary flows, superposed on the main axial flow in a tube, are found to increase the friction factor and heat transfer coefficient. This fact can be utilized in design problems.

As an application of the boundary vorticity method to the boundary-value problem, the important practical problem of fully developed combined free and forced laminar convection in uniformly heated horizontal tubes is solved numerically and the results are compared with those available in the literature.

After solving the thermal instability problem for fully developed laminar convection between two infinite horizontal plates subjected to various thermal boundary conditions with consideration also for Prandtl number effect, the boundary vorticity method and its modified version are applied to the finite amplitude thermal convection in the post-critical regime with success.

Eventually the boundary vorticity method diverges at a certain high value of the characteristic parameter and this is believed to be associated with the change of the physical character. For example, for the boundary-value problem at high parameter, the viscous and conduction terms representing the highest order terms can probably be neglected in the central core region of the channel and yet the numerical scheme is still based on the elliptic type equation. It appears that a special method of treating the viscous and conduction terms must be developed such that the difference equations remain "well-behaved" in the high parameter range in order to overcome the difficulty.

From the results of present investigation, the following general conclusions and suggestions for future work may be made:

- (1) The new algorithm for the numerical determination of the boundary vorticity is believed to be sufficiently general and have wide applicability to various forced convective heat transfer problems with secondary flow caused by various body forces. The algorithm utilizes the Gaussian elimination method and the iterative technique by linearizing the nonlinear terms. The method eliminates the need of solving a linearized biharmonic equation involving stream function. The numerical solution of the biharmonic equation in polar coordinates is known to converge very slowly. The method has the advantage of solving two second order partial

differential equations instead of the fourth order one.

(2) The improved or modified method discussed in the last section of Chapter II is utilized in Chapter VI for the cases of $|\mu| \neq 0$ and $|\mu| \rightarrow \infty$. The modified method is shown to be more efficient than the boundary vorticity method at least for the problem treated. It can be stated that the computing time required by the non-steady state solution method employed by Samuels and Churchill [6.6] in obtaining the steady state solution is much longer than the direct steady state solution method employed in this investigation. It is believed that the non-steady state solution method may be applied only for the transient problems in view of the availability of the boundary vorticity method.

(3) The variation of wave number with the characteristic parameter for fully developed laminar forced convection in the post-critical regime between two infinite horizontal plates needs further investigation. It is suggested that the wave number for the vortex roll may not be determined by consideration in the fully developed region alone. It is expected that secondary flow is already formed somewhere in the thermal entrance region. The pitch of the vortex roll in the entrance region may remain constant and only the intensity of the secondary flow increases along the main flow direction up to the point where the fully developed condition prevails. From the physical reasoning, there is no reason to expect that the size and structure of the vortex roll should

be determined in the fully developed region alone. In this connection, the present experimental facilities for thermal instability in plane Poiseuille flow are believed to be capable of shedding some light on the above speculation about the wave number variation.

(4) If the speculation stated in (3) proves to be true, then the thermal instability problem in the thermal entrance region is of considerable practical importance. The above observation also reveals that another series of thermal instability problems for external flow such as Blasius problem involving longitudinal vortex rolls may exist.

(5) The observation of the asymptotic behavior in flow and heat transfer results for Prandtl number effect is noteworthy and significant. For example, by using a suitable parameter the heat transfer results for the two secondary flow problems studied in this thesis can be correlated such that the results for a Prandtl number of order one already approach the asymptotic results for $Pr \rightarrow \infty$. It is to be expected that the asymptotic behavior for Prandtl number effect exists also for all the forced convective heat transfer problems with secondary flow regardless of the source of body forces. Furthermore, for large Prandtl number fluids, the inertia terms in the momentum equations can be neglected. This leads to a considerable simplification in the solution of Graetz problem (thermal entrance problem) with significant buoyancy effect. The asymptotic behavior for Prandtl number

effect is also clearly observed in neutral stability curves and the critical wave number for the thermal instability problem in plane Poiseuille flow.

(6) The results of present investigation suggest that forced and/or free laminar convection from heated horizontal cylinders or spheres may be solved numerically by transforming the external region into a unit circle without using the usual boundary-layer approximation. However, this possibility remains to be explored in future.

(7) Besides the laminar convection problems with secondary flow, the boundary vorticity method can be applied to biharmonic boundary-value problems in solid mechanics. This possibility will provide a new alternative approach to the numerical solution of a class of engineering problems in solid mechanics governed by biharmonic equation.

(8) The methods used in this thesis can also be applied to mass transfer and chemical reaction phenomena where the secondary flow arises due to the body forces acting in the cross section normal to the main flow.

 LIST OF FORTRAN IV PROGRAMMING

 PROGRAMS FOR THE PROBLEMS STUDIED IN CHAPTERS III, IV AND VI

 '*' IN COL. 6: THIS LINE IS A PART OF PREVIOUS CARD

```

C
C
C   THIS IS A PROGRAM FOR CHAP. III
C   COMBINED CONVECTION IN HORI. CIRCULAR TUBES
C
C
C   DIMENSION R(33),PHI(33),ZA(33),ZB(33),ZC(33),AA(33),BB
C   * (33),
C   ICC(33),DF(33,33),W(33,33),T(33,33),VO(33,33),S(33,33),
C   * U(33,33),
C   2V(33,33),A(33,33),B(33,33),C(33,33),AP(33,33),BP(33,33
C   * ),
C   3CP(33,33),WR2(33,33),RCT(33,33)
C   COMMON MI,M,M1,N1,N,N1,OME1,OME2,OME3,HI,HI2,HJ,HJ2,
C   IZA,ZB,ZC,R,PHI
C   COMMON MT1,MT2
C   PI=3.1415927
C   READ(5,60) M,MT1,MT2,MT3,ACC
C   M: NO. OF DIVS. IN R-DIR.
C   MT1: NO. OF INNER ITERATIONS IN SUBWT
C   MT2: NO. OF INNER ITERATIONS IN SUBVS
C   MT3: NO. OF OUTER ITERATIONS
C   ACC: A PRESCRIBED ERROR
C   READ(5,60) IREAD
C   MI=M-1
C   M1=M+1
C   N=M
C   N: NO. OF DIVS. IN PHI-DIR.
C   NC=N/2
C   NI=N-1
C   N1=N+1
C   DO 2 I=1,M1
C   DO 2 J=1,N1
C   W(I,J)=0.0
C   T(I,J)=0.0
C   VO(I,J)=0.0
C   S(I,J)=0.0

```

```

      U(I,J)=0.0
2    V(I,J)=0.0
      IF(IREAD.EQ.0) GO TO 14
C    READ INITIAL VALUES
      READ(5,56) ((W(I,J),I=1,M1,2),J=1,N1,2)
      READ(5,56) ((T(I,J),I=1,M1,2),J=1,N1,2)
      READ(5,56) ((VO(I,J),I=1,M1,2),J=1,N1,2)
      READ(5,56) ((S(I,J),I=1,M1,2),J=1,N1,2)
      READ(5,56) ((U(I,J),I=1,M1,2),J=1,N1,2)
      READ(5,56) ((V(I,J),I=1,M1,2),J=1,N1,2)
      DO 100 I=2,M,2
      II=I+1
      II=I-1
      DO 100 J=1,N1,2
      W(I,J)=0.5*(W(II,J)+W(II,J))
      T(I,J)=0.5*(T(II,J)+T(II,J))
      VO(I,J)=0.5*(VO(II,J)+VO(II,J))
      S(I,J)=0.5*(S(II,J)+S(II,J))
      U(I,J)=0.5*(U(II,J)+U(II,J))
      V(I,J)=0.5*(V(II,J)+V(II,J))
100  CONTINUE
      DO 101 J=2,N,2
      J1=J+1
      J1=J-1
      DO 101 I=1,M1
      W(I,J)=0.5*(W(I,J1)+W(I,J1))
      T(I,J)=0.5*(T(I,J1)+T(I,J1))
      S(I,J)=0.5*(S(I,J1)+S(I,J1))
      U(I,J)=0.5*(U(I,J1)+U(I,J1))
      V(I,J)=0.5*(V(I,J1)+V(I,J1))
      VO(I,J)=0.5*(VO(I,J1)+VO(I,J1))
101  CONTINUE
      14 HI=1.0/M
      HI2=HI**2
      HJ=PI/N
      HJ2=HJ**2
      PHI(1)=0.0
      DO 15 J=2,N1
15    PHI(J)=PHI(J-1)+HJ
      R(1)=0.0
C    DEFINE ELEMENTS OF MATRICES
      DO 1 I=2,M
      R(I)=R(I-1)+HI
      ZA(I)=0.5*HI/R(I)
      ZB(I)=(HI/(R(I)*HJ))**2
      ZC(I)=HI2/(R(I)*HJ)
      BB(I)=2*(1.0+ZB(I))
      CC(I)=1.0+ZA(I)
      AA(I)=1.0-ZA(I)
1    CONTINUE
      BB(M1)=1.0
      AA(M1)= 1.0

```



```

      CC(M1)=0.0
      DO 22 I=1,M
      DO 22 J=1,N1
22  DF(I,J)=4*HI2
13  READ(5,50) PR,RAC,OME1,OME2,OME3
      WRITE(6,50) PR,RAC,OME1,OME2,OME3
      PRHI=C.5*PR*HI
      IT=1
      IIT=1
12  CONTINUE
      DO 3 I=2,M
      DO 3 J=1,N1
      A(I,J)=AA(I)+0.5*HI*U(I,J)
      B(I,J)=BB(I)
      C(I,J)=CC(I)-0.5*HI*U(I,J)
3   CONTINUE
      B(1,1)=4.0
      C(1,1)=1.0-0.5*HI*V(1,1)
C   SOLVE FOR AXIAL VEL. W
      CALL SUBKT(1.0,A,B,C,V,W,DF)
      DO 6 I=2,M
      DO 6 J=1,N1
      AP(I,J)=AA(I)+PRHI*U(I,J)
      BP(I,J)=BB(I)
      CP(I,J)=CC(I)-PRHI*U(I,J)
6   CONTINUE
      BP(1,1)=4.0
      CP(1,1)=1.0-PRHI*V(1,1)
      DO 9 I=1,M1
      DO 9 J=1,N1
9   WR2(I,J)=HI2*W(I,J)
C   SOLVE FOR TEMPERATURE T
      CALL SUBWT(PR,AP,BP,CP,V,T,WR2)
C   FINE TEMP. GRADS.
      CALL SUBGT(RAC,T,RCT)
C   APPLY BOUNDARY VORTICITY METHOD AND SOLVE FOR
C   VORTICITY AND STREAM FUNCTION
      CALL SUBVS(AA,BB,CC,A,B,C,RCT,VC,S,V)
C   FIND SECONDARY FLOW VEL. COMPONENTS
      CALL SUBUV(S,U,V,ERROR)
      WRITE(6,51) IT,ERROR
      IF(IT.GE.MT3.OR.ERROR.LE.ACC ) GO TO 10
      IT=IT+1
      GO TO 12
C   FIND FRE AND NU
10  CALL FRENU(W,T,RAC)
      WRITE(6,52)
      WRITE(6,53) ((W(I,J),I=1,M),J=1,N1)
      WRITE(6,54)
      WRITE(6,53) ((T(I,J),I=1,M),J=1,N1)
      WRITE(6,55)
      WRITE(6,53)((VC(I,J),I=2,M1),J=1,N1)

```

```
WRITE(6,53) ((S(I,J),I=2,M1),J=1,N1)
WRITE(6,53) ((U(I,J),I=1,M),J=1,N1)
WRITE(6,53) ((V(I,J),I=1,M),J=1,N1)
WRITE(7,56) ((W(I,J),I=1,M1,2),J=1,N1,2)
WRITE(7,56) ((T(I,J),I=1,M1,2),J=1,N1,2)
WRITE(7,56) ((VC(I,J),I=1,M1,2),J=1,N1,2)
WRITE(7,56) ((S(I,J),I=1,M1,2),J=1,N1,2)
WRITE(7,56) ((U(I,J),I=1,M1,2),J=1,N1,2)
WRITE(7,56) ((V(I,J),I=1,M1,2),J=1,N1,2)
GO TO 13
50 FORMAT(5E10.3)
51 FORMAT(5X,3HIT=,I4,5X,6HERROR=,E10.3)
52 FORMAT(5X,5HWWWWW,5X,8HI=1 TO M,5X,9HJ=1,NC,N1)
53 FORMAT(10E13.4)
54 FORMAT(5X,5HTTTTTT,5X,8HI=1 TO M,5X,9HJ=1,NC,N1)
55 FORMAT(5X,5HSSSSSS,5X,9HI=2 TO M1,5X,9HJ=1 TO N1)
56 FORMAT(20A4)
60 FORMAT(4I5,E10.2)
END
```

```

C
C   A SUBROUTINE FOR SOLVING W AND T
C
      SUBROUTINE SUBWT(PR,A,B,C,V,F,DF)
      DIMENSION A(33,33),B(33,33),C(33,33),V(33,33),F(33,33)
      * ,
      1DF(33,33),ZA(33),ZB(33),ZC(33),H(33,33),HP(33,33),PZV(
      * 33,33),
      2FK(33),P(33),Y(200),R(33),PHI(33)
      COMMON MI,M,M1,NI,N,N1,OME1,OME2,OME3,HI,HI2,HJ,HJ2,
      1ZA,ZB,ZC,R,PHI
      COMMON MT1,MT2
      OMEGA=OME2
      IF(PR.GT.0.8) OMEGA=OME1
      IM=2
      DO 1 J=1,N1
      IF(J.NE.1) IM=3
      IMI=IM-1
      H(IMI,J)=C(IMI,J)/B(IMI,J)
      DO 1I=IM,M
      HP(I,J)=B(I,J)-A(I,J)*H(I-1,J)
      1 H(I,J)=C(I,J)/HP(I,J)
      DO 5 I=2,M
      DO 5 J=2,N
      5 PZV(I,J)=PR*ZC(I)*V(I,J)*0.5
      IT=1
      15 J=1
      SF=0.0
      SD=0.0
      IM=2
      FK(1)=2*F(2,N/2+1)+DF(1,1)+(PR*0.5*HI*V(1,1)+1.0)*F(2,
      * N1)
      DO 2 I=2,M
      2 FK(I)=2*ZB(I)*F(I,2)+DF(I,1)
      GO TO 3
      12 FK(2)=A(2,N1)*F(1,1)+2*ZB(2)*F(2,N)+DF(2,N1)
      DO 4 I=3,M
      4 FK(I)=2*ZB(I)*F(I,N )+DF(I,N1)
      GO TO 3
      11 DO 6 I=2,M
      FK(I)=(ZB(I)+PZV(I,J))*F(I,J-1)+(ZB(I)-PZV(I,J))*F(I,J
      * +1)+DF(I,J)
      IF(I.GT.2) GO TO 6
      FK(2)=FK(2)+A(2,J)*F(1,1)
      6 CONTINUE
      3 IF(J.NE.1) IM=3
      IMI=IM-1
      P(IMI)=FK(IMI)/B(IMI,J)
      DO 9 I=IM,M
      9 P(I)=(FK(I)+A(I,J)*P(I-1))/HP(I,J)
      FN=P(M)
      DI=OMEGA*(FN-F(M,J))

```

```
F(M,J)=F(M,J)+DI
SF=ABS(F(M,J))+SF
SC=ABS(DI)+SD
I=MI
10 FN=P(I)+H(I,J)*FN
DI=OMEGA*(FN-F(I,J))
F(I,J)=F(I,J)+DI
SF=SF+ABS(F(I,J))
SD=SC+ABS(DI)
IF(I.LE.IMI) GO TO 20
I=I-1
GO TO 10
20 J=J+1
IF(J-N1) 11,12,13
13 ERR=SC/SF
IF(ERR.LE.1E-5.CR.IT.GE.MT1)GO TO 14
IT=IT+1
GO TO 15
14 CONTINUE
DO 16 J=2,N1
16 F(1,J)=F(1,1)
RETURN
END
```

```

C
C      A SUBROUTINE FOR FINDING TEMP. GRADS.
C
      SUBROUTINE SUBGT(RAC,I,RCT)
      DIMENSION T(33,33),RCT(33,33),ZA(33),ZB(33),ZC(33),R(3
* 3),
      I PHI(33),TR(33,33),TPHI(33,33)
      COMMON MI,M,M1,NI,N,N1,OME1,OME2,OME3,HI,HI2,HJ,HJ2,
      IZA,ZB,ZC,R,PHI
      COMMON MT1,MT2
      HIP=HI*12
      HJP=HJ*12
      DO 6 J=2,N1
6 T(1,J)=T(1,1)
      DO 1 J=2,N
      TR(2,J)=(T(5,J)-6*T(4,J)+18*T(3,J)-10*T(2,J)-3*T(1,1))
* /HIP
1 TR(M,J)=-(T(M-3,J)-6*T(M-2,J)+18*T(MI,J)-10*T(M,J))/HI
* P
      DO 2 I=3,MI
      DO 2 J=2,N
2 TR(I,J)=(T(I-2,J)-8*T(I-1,J)+8*T(I+1,J)-T(I+2,J))/HIP
      DO 3 I=2,M
      T PHI(I,2)=(T(I,5)-6*T(I,4)+18*T(I,3)-10*T(I,2)-3*T(I,
* 1))/HJP
3 T PHI(I,N)=-(T(I,N-3)-6*T(I,N-2)+18*T(I,N-1)
1-10*T(I,N)-3*T(I,N1))/HJP
      DO 4 I=2,M
      DO 4 J=3,NI
4 T PHI(I,J)=(T(I,J-2)-8*T(I,J-1)+8*T(I,J+1)-T(I,J+2))/HJ
* P
      DO 5 I=2,M
      DO 5 J=2,N
5 RCT(I,J)=RAC*(TR(I,J)*SIN(PHI(J))+T PHI(I,J)*COS(PHI(J)
* )
      1/R(I))*HI2
      RETURN
      END

```

```

C
C   A SUBROUTINE FOR SOLVING VO. AND STREAM FUNCTION
C   (AN APPLICATION OF BOUNDARY VORTICITY METHOD)
C
      SUBROUTINE SUBVS(AA,BB,CC,A,B,C,RCT,VO,S,V)
      DIMENSION AA(33),BB(33),CC(33),A(33,33),B(33,33),C(33,
* 33),
      1RCT(33,33),VO(33,33),S(33,33),ZA(33),ZB(33),ZC(33),
      2R(33),PHI(33),H(33,33),HP(33,33),HH(33),HHP(33),FKK(33
* ),
      3ZV(33,33),FK(33),P(33),PP(33),VOP(33,3),SP(33,3),V(33,
* 33)
      COMMON MI,M,M1,NI,N,N1,OME1,OME2,OME3,HI,HI2,HJ,HJ2,
      1ZA,ZB,ZC,R,PHI
      COMMON MT1,MT2
      DO 1 J=2,N
      H(2,J)=C(2,J)/B(2,J)
      DO 2 I=3,M
      HP(I,J)=B(I,J)-A(I,J)*H(I-1,J)
      2 H(I,J)=C(I,J)/HP(I,J)
      HH(2)=CC(2)/BB(2)
      DO 31 I=3,M1
      HHP(I)=BB(I)-AA(I)*HH(I-1)
      31 HH(I)=CC(I)/HHP(I)
      1 CONTINUE
      DO 32 I=2,M
      DO 32 J=2,N
      32 ZV(I,J)=ZC(I)*V(I,J)*0.5
      IT=1
      19 SD=0.0
      SS=0.0
      DO 3 J=2,N
      DO 4 I=2,M1
      FK(I)=(ZB(I)+ZV(I,J))*VO(I,J-1)+(ZB(I)-ZV(I,J))*VO(I,J
* +1)-RCT(I,J)
      4 CONTINUE
      P(2)=FK(2)/B(2,J)
      DO 7 I=3,M1
      7 P(I)=(FK(I)+A(I,J)*P(I-1))/HP(I,J)
      K=0
      VOP(M1,1)=0.0
      16 K=K+1
      FK(M)=(ZB(M)+ZV(M,J))*VO(M,J-1)+(ZB(M)-ZV(M,J))*VO(M,J
* +1)
      1+C(M,J)*VOP(M1,K)-RCT(M,J)
      9 P(M)=(FK(M)+A(M,J)*P(M1))/HP(M,J)
      VOP(M,K)=P(M)
      DO 11 II=2,M1
      I=M1-II
      11 VOP(I,K)=P(I)+H(I,J)*VOP(I+1,K)
      DO 33 I=2,M
      33 FKK(I)=ZB(I)*(S(I,J-1)+S(I,J+1))-VOP(I,K)*HI2

```

```
FKK(M1)=-VOP(M1,K)*HI2/2
PP(2)=FKK(2)/BB(2)
DO 12 I=3,M1
12 PP(I)=(FKK(I)+AA(I)*PP(I-1))/HHP(I)
   SP(M1,K)=PP(M1)
   IF(K-2) 13,14,15
13 VOP(M1,2)=-100
   GO TO 16
14 VOP(M1,3)=100*SP(M1,1)/(SP(M1,2)-SP(M1,1))
   GO TO 16
15 DO 17 II=1,M1
   I=M1-II
17 SP(I,3)=PP(I)+HH(I)*SP(I+1,3)
   S(M1,J)=SP(M1,3)
   VO(M1,J)=VOP(M1,3)
   DO 3 I=2,M
   VO(I,J)=VOP(I,3)
   DI=OME3*(SP(I,3)-S(I,J))
   S(I,J)=S(I,J)+DI
   SS=SS+ABS(S(I,J))
3 SD=SD+ABS(DI)
ERR=SD/SS
IF(ERR.LE.1E-5.OR.IT.GE.MT2)GO TO 18
IT=IT+1
GO TO 19
18 CONTINUE
RETURN
END
```

```

C
C      A SUBROUTINE FOR FINDING U AND V FROM STREAM FUNCTION
C
      SUBROUTINE SUBUV(S,U,V,ERR)
      DIMENSION S(33,33),U(33,33),V(33,33),UU(33,33),VV(33,3
* 3),
      IZA(33),ZB(33),ZC(33),R(33),PHI(33)
      COMMON MI,M,M1,NI,N,N1,OME1,OME2,OME3,HI,HI2,HJ,HJ2,
      IZA,ZB,ZC,R,PHI
      COMMON MT1,MT2
      DO 1 I=2,M
      RH6=R(I)*HJ*6
      RH12=RH6*2
      UU(I,1)=(8*S(I,2)-S(I,3))/RH6
      UU(I,2)=(-S(I,2)+8*S(I,3)-S(I,4))/RH12
      UU(I,N1)=(S(I,N1)-8*S(I,N))/RH6
      UU(I,N)=(S(I,N-2)-8*S(I,N1)+S(I,N))/RH12
      DO 1 J=3 NI
1 UU(I,J)= (S(I,J-2)-8*S(I,J-1)+8*S(I,J+1)-S(I,J+2))/RH12
      HI12=HI*12
      DO 2 J=2,N
      VV(2,J)=(10*S(2,J)-18*S(3,J)+6*S(4,J)-S(5,J))/HI12
      VV(M,J)=(S(M-3,J)-6*S(M-2,J)+18*S(M-1,J)-10*S(M,J))/HI
* 12
      DO 2 I=3,MI
2 VV(I,J)=(S(I+2,J)-8*S(I+1,J)+8*S(I-1,J)-S(I-2,J))/HI12
      VV(1,1)=(S(3,N/2+1)-8*S(2,N/2+1))/(6*HI)*(-1)
      DO 4 J=1,N1
      UU(1,J)=0.0
4 VV(1,J)=VV(1,1)
      DO 5 I=2,M
      VV(I,1)=0.0
5 VV(I,N1)=0.0
      SD=0.0
      SUV=0.0
      DO 3 I=1,M
      DO 3 J=1,N1
      DU=UU(I,J)-U(I,J)
      DV=VV(I,J)-V(I,J)
      SD=SD+ABS(DU)+ABS(DV)
      SUV=SUV+ABS(UU(I,J))+ABS(VV(I,J))
      U(I,J)=UU(I,J)
3 V(I,J)=VV(I,J)
      ERR=SD/SUV
      RETURN
      END

```



```

C
C      A SUBROUTINE FOR EVALUATING FRE AND NU
C
      SUBROUTINE FRENu(W,T,RAC)
      REAL MGT,MGW,MWT,MW,NU1,NU2
      DIMENSION W(33,33),T(33,33),GT(33),GW(33),WTP(33),WP(3
* 3),
      IZA(33),ZB(33),ZC(33),R(33),PHI(33)
      COMMON MI,M,MI,NI,N,N1,OME1,OME2,OME3,HI,HI2,HJ,HJ2,
      IZA,ZB,ZC,R,PHI
      COMMON MT1,MT2
      PI=3.1415927
      DO 1 J=1,N1
      GT(J)=-{T(M-3,J)/4-4*T(M-2,J)/3+3*T(M-1,J)-4*T(M,J)}/H
* I
1  GW(J)=-{W(M-3,J)/4-4*W(M-2,J)/3+3*W(M-1,J)-4*W(M,J)}/H
* I
      MGT=GT(1)+GT(N1)
      MGW=GW(1)+GW(N1)
      DO 2 J=2,N,2
      MGT=MGT+GT(J)*4
      MGW=MGW+GW(J)*4
2  CONTINUE
      DO 3 J=3,NI,2
      MGT=MGT+GT(J)*2
3  MGW=MGW+GW(J)*2
      MGT=FJ*MGT/3*1.0/PI
      MGW=HJ*MGW/3*1.0/PI
      DO 4 I=2,M
      WTP(I)=W(I,1)*T(I,1)+W(I,N1)*T(I,N1)
      WP(I)=W(I,1)+W(I,N1)
      DO 5 J=2,N,2
      WTP(I)=WTP(I)+W(I,J)*T(I,J)*4
5  WP(I)=WP(I)+W(I,J)*4
      DO 6 J=3,NI,2
      WTP(I)=WTP(I)+W(I,J)*T(I,J)*2
6  WP(I)=WP(I)+W(I,J)*2
      WTP(I)=HJ*WTP(I)/3
4  WP(I)=HJ*WP(I)/3
      MWT=0.0
      MW=0.0
      DO 7 I=2,M,2
      MWT=MWT+WTP(I)*R(I)*4
7  MW=MW+WP(I)*R(I)*4
      DO 8 I=3,MI,2
      MWT=MWT+WTP(I)*R(I)*2
8  MW=MW+WP(I)*R(I)*2
      MWT=HI*MWT/3*2.0/PI
      MW=HI*MW/3*2.0/PI
      FRE1=4*MGW/MW
      NU1=2*MW*MGT/MWT
      FRE2=8.0/MW

```

```
NU2=Mh**2/MWT
RERA=2*MW*RAC
WRITE(6,53) RERA
WRITE(6,50)
WRITE(6,52) MGW,MGT,MW,MWT
WRITE(6,51)
WRITE(6,52) FRE1,FRE2,NU1,NU2
RETURN
50 FORMAT(1X,30HTHESE ARE MGW, MGT, MW AND MWT)
51 FORMAT(1X,22HFRE1,FRE2, NU1 AND NU2)
52 FORMAT(4E15.5)
53 FORMAT(10X,5HRERA=,E15.5)
END
```

```

C
C
C   THIS IS A PROGRAM FOR CHAP. IV
C   THERMAL INSTABILITY
C   (FOR THE NONLINEARITY APPROACHING INFINITE ONLY)
C
C
      DOUBLE PRECISION F(80),P,U,A,R,PU,A2,A4,A6,A8,B(80,7),
      1C1,C2,C3,C4(80),C5(80),C6(80),C7(80),FK(4,7),C(4,4),
      2FM1,FM2,D,HA,DR,DA(11),RA(11),SIR(11),AA(21),RT(21),
      3SIA,RO,RI,DI
      F(1)=1D0
      DO 6 I=1,54
        6 F(I+1)=F(I)/(I+1)
      14 READ(5,50) P,A,RO
      READ(5,51) MM,DR
      WRITE(6,53) P,A,RO,DR,MM
C     P: PRANDTL NO.
C     A: WAVE NO.
C     RO: INITIAL RAYLEIGH NO.
C     DR: INCREMENT OF RAYLEIGH NO.
C     MM: NO. OF TERMS IN SERIES EXPANSION
      INA=1
      23 DO 15 IA=1,21
        R=RO
        A2=A*A
        A4=A2*A2
        A6=A2*A4
        A8=A2*A6
        DO 1 I=1,7
          DO 1 J=1,7
            IF(I.EQ.J) GO TO 2
            B(I,J)=0
            GO TO 1
          2 B(I,J)=1D0
        1 CONTINUE
        B(4,2)=2*A2
        B(6,2)=3*A4
        C1=4*A2
        C2=-6*A4
        INR=1
      19 DO 16 IR=1,11
        C3=4*A6-0.5*P*R*A2
        MM1=MM+8
        DO 4 M=2,MM
          FM1=M*(M-1)
          FM2=M*(M-1)*(M-2)
          C4(M)=-A8+12*P*R*A2*(0.5+M+A2/24+0.25*FM1)+6*R*A2
          C5(M)=-12*P*R*A2*(M*M+FM2/6)-12*A2*M*R
          C6(M)=-3*P*A4*R*FM1
        4 C7(M)=2*P*A4*R*FM2
        N=2

```

```

11 B(8,N)=C1*B(6,N)+C2*B(4,N)+C3*B(2,N)
    B(9,N)=C1*B(7,N)+C2*B(5,N)+C3*B(3,N)
    B(10,N)=C1*B(8,N)+C2*B(6,N)+C3*B(4,N)+C4(2)*B(2,N)
    B(11,N)=C1*B(9,N)+C2*B(7,N)+C3*B(5,N)+C4(3)*B(3,N)+
1C5(3)*B(2,N)
    DC 5 N=4,MM
5 B(M+8,N)=C1*B(M+6,N)+C2*B(M+4,N)+C3*B(M+2,N)+C4(M)*
1B(M,N)+C5(M)*B(M-1,N)+C6(M)*B(M-2,N)+C7(M)*B(M-3,N)
    FK(1,N)=OD0
    FK(2,N)=OD0
    FK(3,N)=OD0
    FK(4,N)=OD0
    DO 7 I=8,MM1
    FK(1,N)=FK(1,N)+F(I)*B(I,N)
    FK(2,N)=FK(2,N)+F(I-1)*B(I,N)
    F(3,N)=FK(3,N)+(F(I-4)-A2*2*F(I-2))*B(I,N)
7 FK(4,N)=FK(4,N)+(F(I-6)-3*A2*F(I-4)+3*A4*F(I-2))*B(I,N
* )
    IF(N.LT.3) GO TO 8
    IF(N.LT.5) GO TO 9
    IF(N.LT.7) GO TO 10
    GO TO 12
8 N=3
    GO TO 11
9 N=5
    GO TO 11
10 N=7
    GO TO 11
C FIND ELEMENTS OF MATRIX
12 C(1,1)=0.5+F(4)*B(4,2)+F(6)*B(6,2)+FK(1,2)
    C(1,2)=F(3)+FK(1,3)
    C(1,3)=F(5)+FK(1,5)
    C(1,4)=F(7)+FK(1,7)
    C(2,1)=1+F(3)*B(4,2)+F(5)*B(6,2)+FK(2,2)
    C(2,2)=0.5+FK(2,3)
    C(2,3)=F(4)+FK(2,5)
    C(2,4)=F(6)+FK(2,7)
    C(3,1)=-2*A2+B(4,2)*(1-A2)+B(6,2)*(0.5-A2/12)+FK(3,2)
    C(3,2)=-2*A2+FK(3,3)
    C(3,3)=1-A2/3+FK(3,5)
    C(3,4)=F(3)-A2/6C+FK(3,7)
    C(4,1)=3*A4+B(4,2)*(1.5*A4-3*A2)+B(6,2)*(1-1.5*
1A2+A4/8)+FK(4,2)
    C(4,2)=3*A4+FK(4,3)
    C(4,3)=-3*A2+0.5*A4+FK(4,5)
    C(4,4)=1-0.5*A2+A4/40+FK(4,7)
C EVALUATE THE DETERMINANT
    CALL TRIM(4,C,D)
    DA(IR)=D
    RA(IR)=R
    IF(IR.EQ.1) GO TO 17
    DI=CA(IR-1)

```

```

      RI=RA(IR-1)
      SIR(IR)=DA(IR)*DA(IR-1)
      IF(SIR(IR).LT.0C0) GO TO 18
C     CHANGE RAYLEIGH NO.
      17 R=RA(IR)+DR/INR
      16 CONTINUE
      18 IF(INR.GE.10000C0) GO TO 20
      R=R-DR/INR
      INR=INR*10
      GO TO 19
      20 WRITE(6,52) A,R,D,RI,DI
      AA(IA)=A
      RT(IA)=R
      IF(IA.LE.2.OR.INA.GT.10) GO TO 21
      SIA=(RT(IA)-RT(IA-1))*(RT(IA-1)-RT(IA-2))
      IF (SIA.LE.0D0) GO TO 22
C     CHANGE WAVE NO.
      21 A=A+0.1/INA
      15 CONTINUE
      22 IF(INA.GE.100) GO TO 14
      A=A-2*0.1/INA
      INA=INA*10
      GO TO 23
      50 FORMAT(D15.2,2D15.4)
      51 FORMAT(5X,I5,D15.4)
      52 FORMAT(5X,D15.5,4D20.9)
      53 FORMAT(D15.2,3D15.4,I5)
      END

```

```
C
C   A SUBROUTINE FOR EVALUATING A DETERMINANT
C
SUBROUTINE TRIM(ISIZE,A,Y)
DCUBLE PRECISION A(4,4),Y
DO 71 M=2,ISIZE
DO 71 I=M,ISIZE
DO 71 J=M,ISIZE
N=M-1
71 A(I,J)=A(I,J)-A(I,N)*A(N,J)/A(N,N)
Y=1D0
DO 72 I=1,ISIZE
72 Y=Y*A(I,I)
RETURN
END
```

```

C
C
C   THIS IS A PROGRAM FOR CHAP. VI
C   FINITE AMPLITUDE CONVECTION
C
C
C   DIMENSION GU(41),GT(41),U(41,41),V(41,41),W(41,41),T(4
*   1,41),
IS(41,41),VO(41,41),A(41,41),AA(41,41),C(41,41),CC(41,4
*   1),
2DF(41,41),F1(41,41),F2(41,41),FF1(41,41),FF2(41,41),
3BS(41),HBS(41),SMA1(41)
COMMON B,OMEGA,RCZY2,RDZY,DCZ,DZ,DY
COMMON MI,M,M1
PI=3.141593
READ(5,50) ITO,M,ACC,OMEGA
READ(5,51) PR,FMU,RA,A1,IW1,IW2
READ(5,50) IREAD
C   ITO: NO. OF CUTER ITERATIONS
C   M: NO. OF DIVS. IN Y- AND Z-DIR.
C   ACC: A PRESCRIBED ERROR
C   OMEGA: RELAXATION FACTOR
C   PR: PRANDTL NO.
C   FMU: NONLINEARITY
C   RA: RAYLEIGH NO.
C   A1: WAVE NO.
M1=M+1
M1=M-1
IF(IREAD.EQ.0) GO TO 100
READ(5,57) ((U (J,K),J=1,M1,2),K=1,M1,2)
C   READ INITIAL VALUES
READ(5,57) ((V (J,K),J=1,M1,2),K=1,M1,2)
READ(5,57) ((W (J,K),J=1,M1,2),K=1,M1,2)
READ(5,57) ((T (J,K),J=1,M1,2),K=1,M1,2)
READ(5,57) ((S (J,K),J=1,M1,2),K=1,M1,2)
READ(5,57) ((VO(J,K),J=1,M1,2),K=1,M1,2)
DO 101 K=2,M,2
K1=K+1
K1=K-1
DO 101 J=1,M1,2
U (J,K)=0.5*(U (J,K1)+U (J,K1))
V (J,K)=0.5*(V (J,K1)+V (J,K1))
W (J,K)=0.5*(W (J,K1)+W (J,K1))
T (J,K)=0.5*(T (J,K1)+T (J,K1))
S (J,K)=0.5*(S (J,K1)+S (J,K1))
VO(J,K)=0.5*(VO(J,K1)+VO(J,K1))
101 CONTINUE
DO 102 J=2,M,2
J1=J+1
J1=J-1
DO 102 K=1,M1
U (J,K)=0.5*(U (J1,K)+U (J1,K))

```

```

      V (J,K)=0.5*(V (J1,K)+V (JI,K))
      W (J,K)=0.5*(W (J1,K)+W (JI,K))
      T (J,K)=0.5*(T (J1,K)+T (JI,K))
      S (J,K)=0.5*(S (J1,K)+S (JI,K))
      VO(J,K)=0.5*(VO(J1,K)+VO(JI,K))
102  CONTINUE
      GO TO 30
100  CONTINUE
      DO 1 I=1,M1
      U(I,1)=0.0
      V(I,1)=0.0
      W(I,1)=0.0
      T(I,1)=0.0
      S(I,1)=0.0
      VO(I,1)=0.0
      U(I,M1)=0.0
      V(I,M1)=0.0
      W(I,M1)=0.0
      T(I,M1)=0.0
      S(I,M1)=0.0
      VO(I,M1)=0.0
      V (1,I)=0.0
      S (1,I)=0.0
      VO(1,I)=0.0
      V (M1,I)=0.0
      S (M1,I)=0.0
      VO(M1,I)=0.0
      1  CCNTINUE
C      INITIAL DISTURBANCE
      CALL DIST(S,U,T,PI,A1)
C      FIND SECNDARY FLOW
      CALL SUBVW(V,W,S)
      DDY=(PI/(A1*M))**2
      DDZ=(1.0/M)**2
      DO 21 K=2,M
      K1=K+1
      K1=K-1
      DO 31 J=2,M
      VO(J,K)=(S(J+1,K)+S(J-1,K)-2*S(J,K))/DDY+(S(J,K1)+
1S(J,K1 )-2*S(J,K))/DDZ
31  CONTINUE
30  CONTINUE
      MH=M/2
      M1Q=M/4
      M3Q=3*M/4
      DY=PI/(A1*M)
      DZ=1.0/M
      DDY=DY**2
      DDZ=DZ**2
      DDZ8=4*DDZ/DY
      DZ4Y=DZ/(4*DY)
      RDZY=DDZ/DDY

```



```

PRDZ4Y=PR*DZ4Y
PRUDZ=PR*FMU*DDZ
PR2UDZ=PR**2*FMU*DDZ/(DY*2)
PRDDZ=PR*DDZ/(DY*2)
GRZ2Y=RA*DDZ/(2*PR*DY)
RDZY2=2*RDZY
B=-2*(1+RDZY)
DO 2 K=2,M
KI=K+1
KI=K-1
FKI=KI
Z=FKI/M
GU(K)=DDZ8*(1.0-2*Z)
GT(K)=PR2UDZ*(8*Z**3/3-4*Z**2+2.0/3)+PRDDZ
2 CONTINUE
BS(2)=1.0/B
DO 21 K=3,M
HBS(K)=B-BS(K-1)
21 BS(K)=1.0/HBS(K)
IT=0
9 CONTINUE
C DEFINE ELEMENTS OF MATRICES
DO 3 J=1,M1
DO 3 K=2,M
HA=DZ4Y*W(J,K)
HB=PRDZ4Y*W(J,K)
C(J,K)=1.0-HA
CC(J,K)=1.0-HB
A(J,K)=1.0+HA
AA(J,K)=1.0+HB
HA=DZ4Y*V(J,K)
HB=PRDZ4Y*V(J,K)
F1(J,K)=-HA-RDZY
F2(J,K)=HA-RDZY
FF1(J,K)=-HB-RDZY
FF2(J,K)=HB-RDZY
DF(J,K)=GU(K)*W(J,K)
3 CONTINUE
SIGN=1
C SOLVE FOR U
CALL SUBUT(A,C,F1,F2,U,DF,ERR1,SIGN)
DO 7 J=1,M1
DO 7 K=2,M
DF(J,K)=PRUDZ*U(J,K)-W(J,K)*GT(K)
7 CONTINUE
SIGN=-1
C SOLVE FOR T
CALL SUBUT(AA,CC,FF1,FF2,T,DF,ERR2,SIGN)
DO 11 J=2,M
J1=J+1
J1=J-1
DO 11 K=2,M

```

```

11 DF(J,K)=GRZ2Y*(T(J1,K)-T(JI,K))
C   SOLVE FOR VO. AND STREAM FUNCTION
C   FIND FRE AND NU
   CALL SUBVOS(A,C,F1,F2,DF,VO,S,BS,HBS)
C   FIND SECONDARY FLOW
   CALL SUBVW(V,W,S)
   IT=IT+1
   WRITE(6,52) IT,ERR1,ERR2
   IF(IT.GE.IT0.OR.ERR1.LT.ACC) GO TO 8
   GO TO 9
8  CONTINUE
   VWMAX=0.0
   DO 41 J=1,M1
   DO 41 K=2,M
   HA=ABS(V(J,K))/DZ
   HB=ABS(W(J,K))/DY
   VWMAX=AMAX1(VWMAX,HA,HB)
41  VWMAX=VWMAX/2
   WRITE(6,58) VWMAX
   WRITE(6,53) M,ACC
   WRITE(6,54) PR,FMU,RA,A1
   CALL FRENUS(U,T,PR,FMU,GT,A1,SM)
   IF(IW1.NE.1) GO TO 33
   WRITE(6,55) ((U(J,K),K=1,M1),J=1,M1,MH)
   WRITE(6,55) ((T(J,K),K=1,M1),J=1,M1,MH)
   WRITE(6,55) ((U(J,K),J=1,M1),K=M1Q,M3Q,M1Q)
   WRITE(6,55) ((T(J,K),J=1,M1),K=M1Q,M3Q,M1Q)
33  IF(IW2.NE.1) GO TO 34
   WRITE(6,55) ((U(J,K),J=1,M1,4),K=1,M1,4)
   WRITE(6,55) ((T(J,K),J=1,M1,4),K=1,M1,4)
   WRITE(6,55) ((S(J,K),J=1,M1,4),K=1,M1,4)
   WRITE(6,55) ((VO(J,K),J=1,M1,4),K=1,M1,4)
   WRITE(7,57) ((U(J,K),J=1,M1,2),K=1,M1,2)
   WRITE(7,57) ((V(J,K),J=1,M1,2),K=1,M1,2)
   WRITE(7,57) ((W(J,K),J=1,M1,2),K=1,M1,2)
   WRITE(7,57) ((T(J,K),J=1,M1,2),K=1,M1,2)
   WRITE(7,57) ((S(J,K),J=1,M1,2),K=1,M1,2)
   WRITE(7,57) ((VO(J,K),J=1,M1,2),K=1,M1,2)
34  CONTINUE
50  FORMAT(2I5,2E10.3)
51  FORMAT(2E10.3,2E15.7,2I5)
52  FORMAT(5X,3HIT=,I5,5X,7HERRORS=,2E10.3)
53  FORMAT(5X,13HNO. OF. DIV.=,I3,5X,11HPRE. FRROR=,E10.3)
54  FORMAT(5X,3HPR=,E10.3,5X,14HNON-LINEARITY=,E10.3,
   13HRA=,E15.7,9HWAVE NO.=E15.7)
55  FORMAT(11E12.4)
56  FORMAT(5X,E15.4,2I5)
57  FORMAT(20A4)
58  FORMAT(5X,6HMAXVW=E10.3)
   STOP
   END

```

```

C
C   A SUBROUTINE FOR READING INITIAL DISTURBANCE
C
      SUBROUTINE DIST(S,U,T,PI,A1)
      DIMENSION SO(21),UO(21),TO(21),S1(41),U1(41),T1(41),
1U(41,41),T(41,41),S(41,41)
      COMMON B,OMEGA,RCZY2,RDZY,DDZ,DZ,DY
      COMMON MI,M,M1
      READ(5,50)(SO(K),K=1,20)
      READ(5,50)(UO(K),K=1,20)
      READ(5,50)(TO(K),K=1,20)
      SO(21)=0.0
      UO(21)=0.0
      TO(21)=0.0
      K=1
      DO 1 KK=2,21
      KKI=KK-1
5 FM=KKI-K*20.0/M
  IF(FM) 1,3,3
3 FM1=1.0-FM
  K=K+1
  S1(K)=FM*SO(KKI)+FM1*SO(KK)
  U1(K)=FM*UO(KKI)+FM1*UO(KK)
  T1(K)=FM*TO(KKI)+FM1*TO(KK)
  IF(FM.GT.0.0) GO TO 5
1 CONTINUE
  DO 2 J=2,M
  AY=(J-1)*PI/M
  SA=-SIN(AY)/A1
  CO=-COS(AY)
  DO 2 K=2,M
  S(J,K)=S1(K)*SA
  U(J,K)=U1(K)*CO*(-1)
  T(J,K)=T1(K)*CO
2 CONTINUE
  DO 4 K=2,M
  U(1,K)=-U1(K)*(-1)
  U(M1,K)=U1(K)*(-1)
  T(1,K)=-T1(K)
  T(M1,K)=T1(K)
4 CCNTINUE
  RETURN
50 FORMAT(20A4)
  END

```

```

C
C   A SUBROUTINE FOR SOLVING U AND T
C
SUBROUTINE SUBUT(A,C,F1,F2,F,DE,ERROR,SIGN)
  DIMENSION A(41,41),C(41,41),F1(41,41),F2(41,41),F(41,4
  * 1),
  IDF(41,41),D(41),BP(41),Q(41)
  COMMON B,OMEGA,RCZY2,RDZY,DCZ,DZ,DY
  COMMON MI,M,M1
  M2=M1+1
  SFD=0.0
  SF=0.0
  DO 1 J=1,M1
    IF(J.EQ.1) GO TO 2
    IF(J.EQ.M1) GO TO 3
    JI=J-1
    J1=J+1
    DO 4 K=2,M
      4 D(K)=F1(J,K)*F(JI,K)+F2(J,K)*F(J1,K)+DE(J,K)
      GO TO 5
    2 DO 6 K=2,M
      6 D(K)=-RCZY2*F(2,K)+DE(1,K)
      GO TO 5
    3 DO 7 K=2,M
      7 D(K)=-RDZY2*F(M,K)+DE(M1,K)
    5 CONTINUE
    BP(2)=C(J,2)/B
    Q(2)=D(2)/B
    DO 8 K=3,MI
      KI=K-1
      HA=B-A(J,K)*BP(KI)
      BP(K)=C(J,K)/HA
    8 Q(K)=(D(K)-A(J,K)*Q(KI))/HA
      FN=(D(M)-A(J,M)*Q(MI))/(B-A(J,M)*BP(MI))
      FD=FN-F(J,M)
      SFD=SFD+ABS(FD)
      SF=SF+ABS(FN)
      F(J,M)=F(J,M)+OMEGA*FD
      DO 11 KK=2,MI
        K=M1-KK
        FN=Q(K)-BP(K)*FN
        FD=FN-F(J,K)
        SFD=SFD+ABS(FD)
        SF=SF+ABS(FN)
        F(J,K)=F(J,K)+OMEGA*FD
    11 CONTINUE
    1 CONTINUE
    ERRCR=SFD/SF
    RETURN
  END

```

```

C
C   A SUBROUTINE FOR SOLVING VO. AND STREAM FUNCTION
C   AN IMPROVED (MODIFIED) ITERATIVE SCHEME
C
SUBROUTINE SUBVCS(A,C,F1,F2,GTY,VO,S,BS,HBS)
DIMENSION A(41,41),C(41,41),F1(41,41),F2(41,41),
1GTY(41,41),VO(41,41),S(41,41),BS(41),HBS(41),TVO(41),
2BVO(41),TS(41),HA(41),DVO(41),DS(41),QS(41),QVO(41)
COMMON B,OMEGA,RDZY2,RDZY,DDZ,DZ,DY
COMMON MI,M,MI
TS(1)=0.0
TS(MI)=0.0
DO 2 J=2,M
JI=J-1
J1=J+1
DO 16 K=2,M
16 DS(K)=-RDZY*(S(JI,K)+S(J1,K))+DDZ*VO(J,K)
QS(2)=DS(2)/B
DO 7 K=3,M
7 QS(K)=(DS(K)-QS(K-1))/HBS(K)
TS(M)=QS(M)
DO 8 KK=2,MI
K=M1-KK
8 TS(K)=QS(K)-BS(K)*TS(K+1)
DO 15 K=2,M
15 S(J,K)=S(J,K)+OMEGA*(TS(K)-S(J,K))
BVO(2)=C(J,2)/B
DO 3 K=3,MI
HA(K)=B-A(J,K)*BVO(K-1)
BVO(K)=C(J,K)/HA(K)
DVO(K)=F1(J,K)*VO(J-1,K)+F2(J,K)*VO(J+1,K)+GTY(J,K)
3 CONTINUE
DVO(2)=-2*S(J,2)*A(J,2)/DDZ
1+ F1(J,2)*VO(J-1,2)+F2(J,2)*VO(J+1,2)+GTY(J,2)
DVO(M)=-2*S(J,M)*C(J,M)/DDZ
1+ F1(J,M)*VO(J-1,M)+F2(J,M)*VO(J+1,M)+GTY(J,M)
QVO(2)=DVO(2)/B
DO 4 K=3,MI
4 QVO(K)=(DVO(K)-A(J,K)*QVO(K-1))/HA(K)
TVO(M)=(DVO(M)-A(J,M)*QVO(MI))/(B-A(J,M)*BVO(MI))
DO 5 KK=2,MI
K=M1-KK
5 TVO(K)=QVO(K)-BVO(K)*TVO(K+1)
DO 2 K=2,M
VC(J,K)=VO(J,K)+OMEGA*(TVO(K)-VO(J,K))
2 CONTINUE
RETURN
END

```

```
C
C   A SUBROUTINE FOR FINDING V AND W
C
  SUBROUTINE SUBVW(V,W,S)
  DIMENSION V(41,41),W(41,41),S(41,41)
  COMMON B,OMEGA,RDZY2,RDZY,DDZ,DZ,DY
  COMMON M1,M,M1
C   V,W:Y,Z DIR VEL *2(DZ,DY)
  DO 1 K=2,M
  W(1,K)=-2*S(2,K)
  W(M1,K)=2*S(M,K)
  DO 1 J=2,M
  V(J,K)=S(J,K+1)-S(J,K-1)
  W(J,K)=S(J-1,K)-S(J+1,K)
1  CONTINUE
  RETURN
  END
```

```

C
C      A SUBROUTINE FOR FINDING FRE ABD NU
C
      SUBROUTINE FRENUS(U,T,PR,FMU,GT,A1,SM)
      DIMENSION U(41,41),T(41,41),GU1(41),GU2(41),GT1(41),
      1GT2(41),GT(41),TUA(41,41),UA(41,41),SA(41,41),
      2UMK(41),TUMK(41),SMK(41),GTY(41,41),GTZ(41,41),
      3PMUT(41),UP(41),Q1L(41),Q2L(41)
      COMMON B,OMEGA,RDZY2,RDZY,CDZ,DZ,DY
      COMMON MI,M,M1
      PI=3.141593
      DYA=DY*A1/(3*PI)
      DO 1 J=1,M1
      GU1(J)=(-U(J,5)/4+4*U(J,4)/3-3*U(J,3)+4*U(J,2))/DZ
      GT1(J)=(-T(J,5)/4+4*T(J,4)/3-3*T(J,3)+4*T(J,2))/DZ
      GU2(J)=(U(J,M-3)/4-4*U(J,M-2)/3+3*U(J,M1)-4*U(J,M))/DZ
      GT2(J)=(T(J,M-3)/4-4*T(J,M-2)/3+3*T(J,M1)-4*T(J,M))/DZ
1 CONTINUE
      DY22=2*DY
      DZ22=2*DZ
      DO 2 K=2,M
      DO 2 J=2,M
      GTY(J,K)=(T(J+1,K)-T(J-1,K))/DY22
2 GTZ(J,K)=(T(J,K+1)-T(J,K-1))/DZ22
      DO 3 I=1,M1
      GTY(I,I)=0
      GTY(M1,I)=0
      GTZ(I,1)=GT1(I)
      GTZ(I,M1)=GT2(I)
      GTY(I,1)=0
3 GTY(I,M1)=0
      DO 4 K=2,M
      GTZ(1,K)=(T(1,K+1)-T(1,K-1))/DZ22
4 GTZ(M1,K)=(T(M1,K+1)-T(M1,K-1))/DZ22
      DO 5 K=1,M1
      FKI=K-1
      Z=FKI/M
      PMUT(K)=PR*FMU*(2*Z**4/3-4*Z**3/3+2*Z/3)+Z
      UP(K)=4*(Z-Z**2)
      DO 5 J=1,M1
      UA(J,K)=UP(K)+U(J,K)/2
      TUA(J,K)=(T(J,K)-PMUT(K))*UA(J,K)
5 CONTINUE
      GU1M=GU1(1)+GU1(M1)+4*GU1(M)
      GT1M=GT1(1)+GT1(M1)+4*GT1(M)
      GT2M=GT2(1)+GT2(M1)+4*GT2(M)
      GU2M=GU2(1)+GU2(M1)+4*GU2(M)
      DO 6 J=3,M1,2
      JI=J-1
      GU1M=GU1M+GU1(JI)*4+GU1(J)*2
      GU2M=GU2M+GU2(JI)*4+GU2(J)*2
      GT1M=GT1M+GT1(JI)*4+GT1(J)*2

```

```

6 GT2M=GT2M+GT2(JI)*4+GT2(J)*2
  GU1M=GU1M*DYA
  GU2M=GU2M*DYA
  GT1M=GT1M*DYA
  GT2M=GT2M*DYA
  DO 7 J=1,M1
    UMK(J)=UA(J,1)+UA(J,M1)+4*UA(J,M)
    TUMK(J)=TUA(J,1)+TUA(J,M1)+4*TUA(J,M)
  DO 8 K=3,M1,2
    KI=K-1
    UMK(J)=UMK(J)+UA(J,KI)*4+UA(J,K)*2
    TUMK(J)=TUMK(J)+TUA(J,KI)*4+TUA(J,K)*2
8 CONTINUE
  UMK(J)=UMK(J)*DZ/3
  TUMK(J)=TUMK(J)*DZ/3
7 CONTINUE
  UM=UMK(1)+UMK(M1)+UMK(M)*4
  TUM=TUMK(1)+TUMK(M1)+TUMK(M)*4
  SM=SMK(1)+SMK(M1)+SMK(M)*4
  DO 9 J=3,M1,2
    JI=J-1
    UM=UM+UMK(JI)*4+UMK(J)*2
    TUM=TUM+TUMK(JI)*4+TUMK(J)*2
9 CONTINUE
  UM=UM*DYA
  TUM=TUM*DYA
  SM=0.0
  HA=PR*FMU*2/3
  Q1=HA+1-GT1M
  Q2=HA-1+GT2M
  Q3=UM*PR*FMU
  TM1=TUM/UM
  TM2=TM1+1
  FRE1=ABS(4+GU1M/2)/UM**2
  FRE2=ABS(-4+GU2M/2)/UM**2
  FRE3=4/UM**2
  DO 10 J=1,M1
    Q1L(J)=HA+1-GT1(J)
10 Q2L(J)=HA-1+GT2(J)
    WRITE(6,54)
    WRITE(6,55) (Q1L(J),J=1,M1)
    WRITE(6,55) (Q2L(J),J=1,M1)
    WRITE(6,53)
    WRITE(6,51) GU1M,GU2M,GT1M,GT2M
    WRITE(6,50)
    WRITE(6,51) Q1,Q2,Q3,TM1,TM2
    WRITE(6,52)
    WRITE(6,51) FRE1,FRE2,FRE3,SM,UM
50 FORMAT(2X,26HTHESE ARE Q1,Q2,Q3,TM1,TM2)
51 FORMAT(2X,5E15.7)
52 FORMAT(2X,33HTHESE ARE FRE1,FRE2,FRE3,M.S.G,UM)
53 FORMAT(2X,29HTHESE ARE GU1M,GU2M,GT1M,GT2M)

```

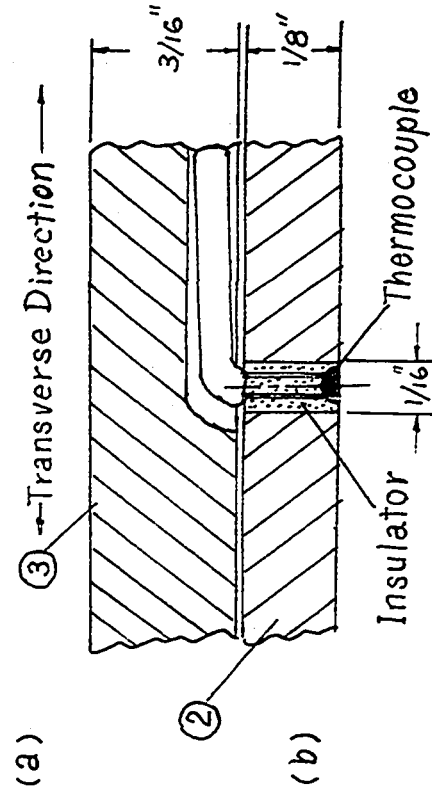
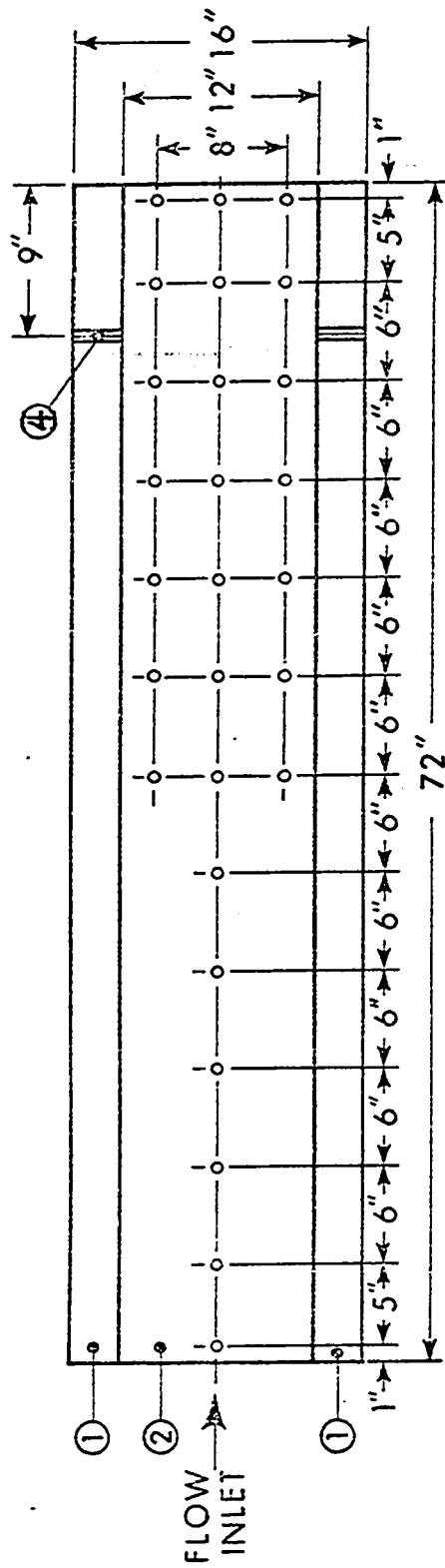


```
54 FORMAT(2X,48HTHESE ARE LOCAL H.T.RATE AT BOTTOM AND TO  
  * P PLATE)  
55 FORMAT(11E12.4)  
  RETURN  
  END
```

ADDENDUM

After the thesis was submitted to the examining committee, the author received comments from Professor E.M. Sparrow of the University of Minnesota regarding Chapters V and VI. He suggested that detailed experimental details such as the installation and arrangement of thermocouples, measurements of velocity and temperature, and axial wall temperature variation data should be reported for possible future reference. In addition, he pointed out that for the finite amplitude convection in plane Poiseuille flow discussed in Chapter VI, the maximum velocity U_0 in the unperturbed flow is no longer a physical quantity known a priori and consequently a correlation between the maximum axial velocity U_0 in the unperturbed state and the mean axial velocity \bar{U} must be provided in order to utilize the flow and heat transfer results presented in Chapter VI. This addendum was prepared in order to accommodate Professor Sparrow's valuable suggestions which materially contributed to the completeness of the thesis.

1. The locations of the embedded thermocouples are shown in Fig.A1(a) and the installation of a thermocouple is illustrated in Fig.A1(b). After drilling a hole with 1/16 inch diameter, a thermocouple was embedded using electrical insulator and a thermocouple wire was led in the transverse direction outside the channel plate in order to avoid undesirable temperature gradient along the wire.

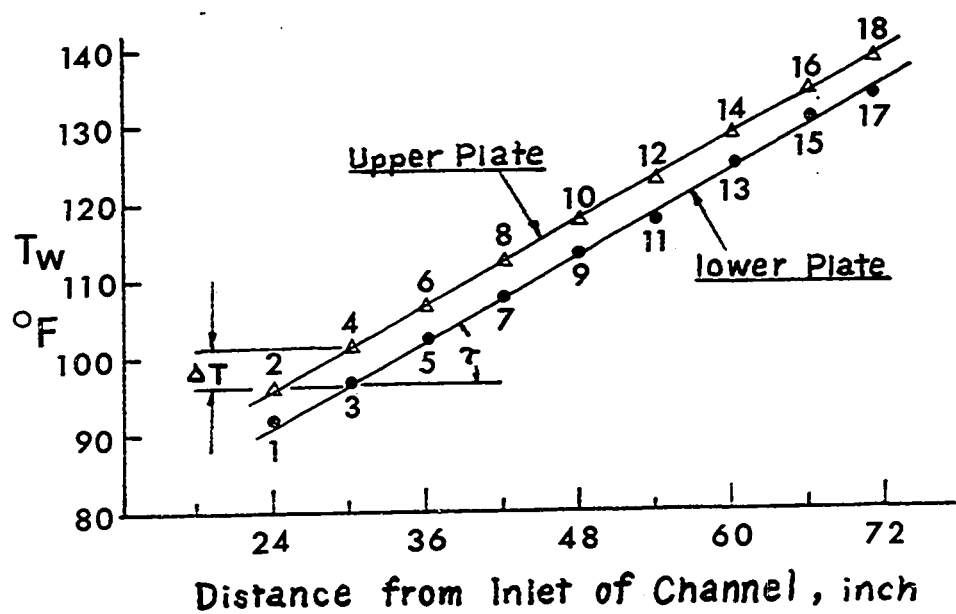


1. Heat insulator (Marinite board)
2. Brass plate (1/8 in.)
3. Aluminum plate (3/16 in.)
4. 1/8 inch illuminating slits

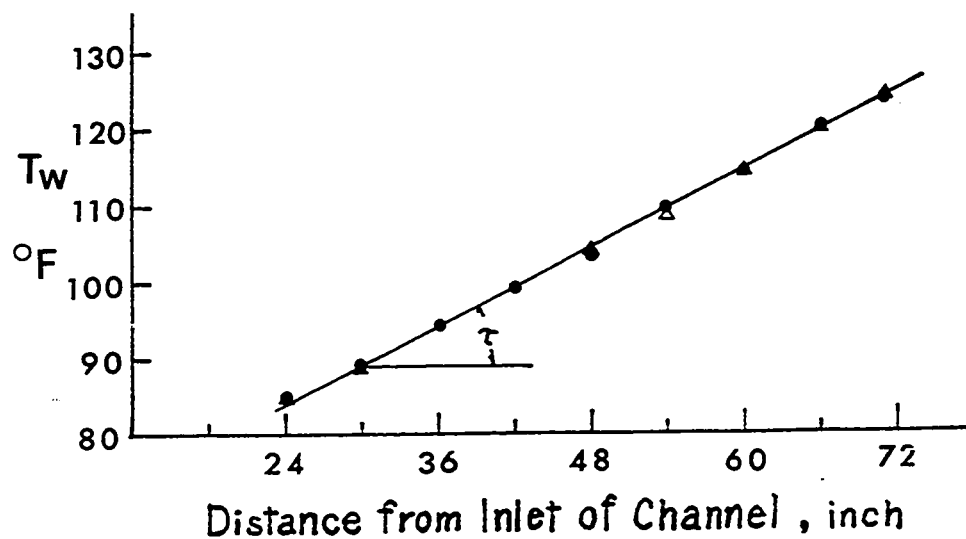
Fig.A1 Location of embedded thermocouples(plan view) and installation of a thermocouple

2. The surface temperature of the flat plate was measured by using iron-constantan thermocouples with a diameter of 0.01 inch. These thermocouples were connected to a Speedomax G, Model S, 60000 Series temperature recorder (Leeds & Northrup Company). Two typical data for the axial variation of wall temperature for the cases of negative μ and $|\mu| \rightarrow \infty$ are shown in Fig. A2(a) and (b), respectively. In the experimental study, the axial temperature gradient was determined by taking the mean value for the axial temperature gradients at the lower and upper plates. The axial temperature gradient at the lower plate was based on the temperature difference and distance between the thermocouples Nos. 3 and 15. Similarly for the axial temperature gradient at the upper plate, the temperature indicated by the thermocouples Nos. 4 and 16 were used. It is noted that the linear variation of the axial wall temperature is very satisfactory for both upper and lower plates. Regarding the uniformity of the temperature distributions in the transverse direction, it is noted that the variation of the temperature at 4 inches from the axial center line (see Fig. A1(a)) was generally found to be less than 0.5°F as compared with the wall temperature at the center of the plate.

3. Temperature and velocity measurements were made by using two-dimensional traversing mechanism for a thermocouple and a hot-wire probe under smoke-free conditions. The traversing



(a) $\mu = \text{negative}$, $\Delta T = -4.5^\circ\text{F}$ and $\tau = 0.945^\circ\text{F/in.}$



(b) $|\mu| \rightarrow \infty$ and $\tau = 0.847^\circ\text{F/in.}$

Fig.A2 Typical data for the axial variation of wall temperature along center line

direction of this device was adjusted carefully to be parallel to the edge of the lower plate of the channel. Distance between the location of measurement and the exit edge of the channel was also carefully checked. A block with a known height was used at several transverse locations of the test section to establish the reference height and adjust the final leveling of the traversing device. This adjustment was repeated before each series of tests. The temperature measurement was made by using a Leeds & Northrup 7555 type K-5 potentiometer which is capable of detecting a voltage variation up to 0.1 microvolt which corresponds to a temperature difference of about 0.003 °F. The velocity measurement was done by using a Flow Corporation hot-wire anemometer probe W3 and a constant temperature anemometer Model 900-A. The hot-wire was not calibrated and a linear relationship between voltage and velocity was used. As can be seen in Figs. 5.3 and 5.4, the velocity ratio which represents the voltage ratio shows reasonably good agreement with theoretical curve. This observation confirms the applicability of the linear relationship between voltage and velocity for the range of velocities investigated.

4. The definition of the Reynolds number $Re = U_0 h / (2\nu)$ in Chapter VI is based on the maximum velocity U_0 for the unperturbed flow. The Reynolds number Re also appears in the expression for the characteristic parameter $\mu = Re \tau h / \Delta T$.

For the practical utilization of the flow and heat transfer results presented in Chapter VI, it is required to determine U_0 from the average axial velocity \bar{U} . Fig.A3 shows the ratio $3\bar{U}/(2U_0)$ versus $|Ra|$ for the cases of $\mu=0$ and $\mu=\text{finite}$. By using this figure, the parameter μ used in Figs.6.13 and 6.16 can be transformed into a new parameter $\mu' = Re \tau h / \Delta T$ where $Re = \bar{U}h/(2\nu)$. Similarly, Fig.A4 shows the ratio $3\bar{U}/(2U_0)$ versus the parameter $PrReRa_\tau$ for the case with $|\mu| \rightarrow \infty$. By using Fig.A4, the parameter $PrReRa_\tau$ used in Figs.6.14 and 6.17 can be transformed into a parameter where Re is based on the mean axial velocity. It is well to note that the problems treated in Chapters III and VI are basically similar except the geometrical shape. In Chapter III, the parameter $PrRaC$ is finally transformed into $PrReRa$ where Re is based on the mean axial velocity.

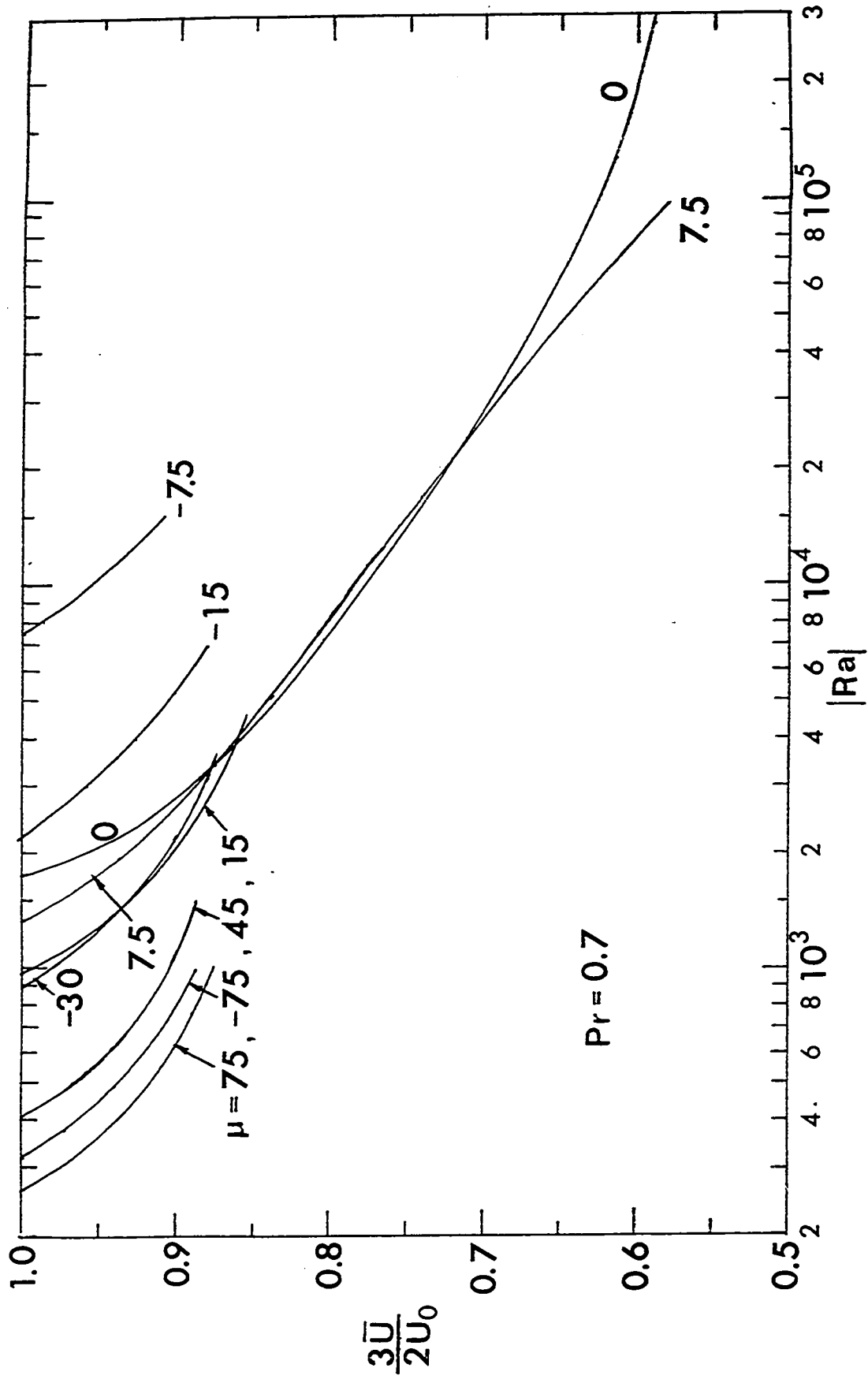


Fig.A3 $3\bar{U}/(2U_0)$ versus $|Ra|$ for $Pr=0.7$ with μ as a parameter

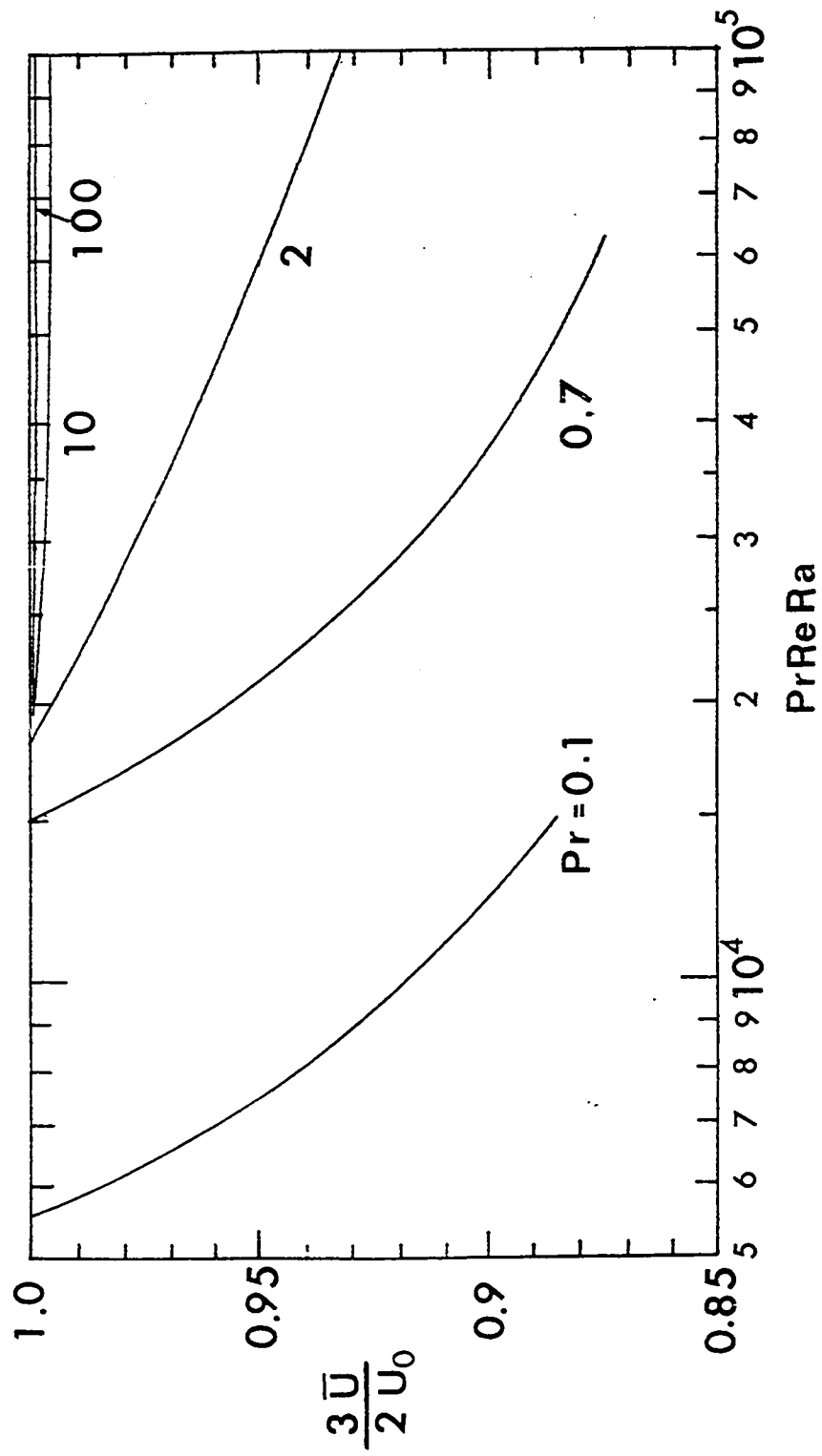


Fig.A4 $\frac{3\bar{U}}{2U_0}$ versus $PrReRa_\tau$ for $|\mu| \rightarrow \infty$ with Pr as a parameter